A DAMAGE MODEL FOR THE DUCTILE FAILURE ANALYSIS OF PLASTIC COMPONENTS

UNIVERSIDADE FEDERAL DE SANTA CATARINA
PROGRAMA DE PÓS – GRADUAÇÃO EM ENGENHARIA MECÂNICA

WESLEY NOVAES MASCARENHAS

A DAMAGE MODEL FOR THE DUCTILE FAILURE ANALYSIS OF PLASTIC COMPONENTS

Tese submetida ao Programa de Pós-Graduação em Engenharia Mecânica da Universidade Federal de Santa Catarina para a obtenção do grau de DOUTOR em Engenharia Mecânica.

Orientador: Prof. Marcelo Krajnc Alves, Ph.D.
Co-orientador: Prof. Kristofer Gamstedt, Ph.D. (KTH – Suécia)

Florianópolis, SC

Fevereiro de 2011

Catalogação na fonte pela Biblioteca Universitária
da
Universidade Federal de Santa Catarina

M395d Mascarenhas, Wesley Novaes
A damage model for the ductile failure analysis of plastic components [tese] / Wesley Novaes Mascarenhas ; orientador, Marcelo Krajnc Alves ; co- orientador, Kristofer Gamstedt. - Florianópolis, SC, 2011.
230 p.: il., grafs., tabs.

Tese (doutorado) - Universidade Federal de Santa Catarina, Centro Tecnológico. Programa de Pós-Graduação em Engenharia Mecânica.

Inclui referências

1. Engenharia mecânica. 2. Termoplásticos. 3. Viscoplasticidade. 4. Variáveis (Matemática). 5. Termodinâmica. I. Alves, Marcelo Krajnc. II. Gamstedt, Kristofer. III. Universidade Federal de Santa Catarina. Programa de Pós-Graduação em Engenharia Mecânica. IV. Título.

CDU 621

WESLEY NOVAES MASCARENHAS

A DAMAGE MODEL FOR THE DUCTILE FAILURE ANALYSIS OF PLASTIC COMPONENTS

Esta tese foi julgada adequada para a obtenção do título de DOUTOR em Engenharia Mecânica e aprovada na sua forma final pelo Programa de Pós-Graduação em Engenharia Mecânica.

Florianópolis, 18 de Fevereiro de 2011.

_____

Prof. Marcelo Krajnc Alves, Ph. D. – UFSC
Orientador

_____

Prof. E. Kristofer Gamstedt, Ph. D. – KTH (Suécia)
Co-Orientador

_____

Prof. Eduardo Alberto Fancello, D. Sc. – UFSC
Coordenador do Programa de Pós-Graduação em Engenharia Mecânica

BANCA EXAMINADORA

_____

Prof. Marcelo Krajnc Alves, Ph. D. – UFSC
Presidente da Banca Examinadora

_____

Prof. Heraldo Silva da Costa Mattos, Dr. – UFF
Relator

_____

Prof. Guilherme Mariz de Oliveira Barra, Dr. – UFSC

_____

Prof. Júlio Apolinário Cordioli, Dr. Eng. – UFSC

_____

Prof. Rodrigo Rossi, Dr. Eng. – UFRGS

This work is dedicated to those (relatives and friends) who, by some means, have contributed to its accomplishment. I especially dedicate this work to my parents, Antônio Paulírio and Yvone Genelhu, who have always supplied me with all the necessary tools, so that I could get this achievement; to my grandmother Edésia Mascarenhas, who has molded the man I have been presently and to the great man Antônio Genelhu (in memoriam), whose yield of his years of hard work has been, once, extremely important. Wherever you are now, thank you very much!

Este trabalho é dedicado a todos (parentes e amigos) que, de alguma forma, contribuíram com a sua realização. Eu dedico especialmente este trabalho aos meus pais, Antônio Paulírio e Yvone Genelhu, que sempre me forneceram as ferramentas necessárias para que eu conseguisse atingir este objetivo; a minha avó Edésia Mascarenhas, que moldou o homem que eu sou atualmente e ao grande homem Antônio Genelhu (in memoriam), cujo fruto de seus longos anos de trabalho árduo foi, mais uma vez, extremamente importante. Onde quer que você esteja neste momento, muito obrigado!

ACKNOWLEDGEMENTS

This is the end of a four years journey and the beginning of the long journey for the rest of a life. As usual, the finishing of another stage in our lives is extremely rewarding and when looking back to the way we have gone through over the last four years, it is unavoidable to feel a sense of satisfaction and mission accomplished.

For more technical and pretentious that this kind of work seems to be, its accomplishment, although it seems typically solitary, definitively it is not. The way that leads to the conclusion of a doctorate thesis is generally tortuous, full of obstacles and difficulties which, certainly, are beyond the capacity of a single person to overcome them alone. This could not be different with me, because if I could get this achievement, this is the great evidence that I have had an invaluable and precious contribution, dedication and encouragement of many people, which deserve to be remembered here, so it would be extremely unfair to give all the merit of this work only to that who has done it.

The greatest thanks to our celestial **father** for the life gift awarded to me and for being the inexhaustible source of faith and strength to track the way I have gone through, in order to overcome all obstacles met during the accomplishment of this work.

The silent and, sometimes, active contribution from those, even so far, have taken part in my anguishes, have listened my lamentations and have given me support, comprehension and consolation. To my **parents**, **relatives** and **friends** who have always supported me and have always kept the expectation to see this work finished.

An academic work of this nature is not feasible to be performed without an idea and, consequently, without an idealizer. Once, I have counted on the intervention of the great friend **Cajuhi**. I wish I said thank him, not only for having become the genuine idealizer of this work, but also for the exceptional contribution and support that he has given to my professional life.

In order that the defined idea is executed efficiently, it is important to keep a good relationship with our advisors, so that we can achieve the desired objectives. The better this relationship is, the quicker and better the results will be. And I have no doubt that we really have cultivated a good relationship; because our objectives have been achieved and a good work has been produced in the end. For my advisors **Marcelo Krajnc Alves** and **Kristofer Gamstedt**, to say only thank you very much is too little to demonstrate all my gratitude for everything you have done, in order to make this work come true.

During this four years journey, many people have appeared in my life. Some of them just came and left, while others have become good friends. Either way, all of them have left their personal contribution and, unintentionally, have made this tough journey more pleasant. Thus, I wish I said thank you to my colleagues from GMAC: **Maura**, **Fábio**, **Ivan**, **Miguel**, **Maldaner**, **Hilbert**, **Lindaura**, **Guilherme**, **Marcus** and **Fernanda**; from Grante: **Pedrão** and **Enildo** and everyone from the **Biocomposites group** at KTH, specially **Ingela Bjurhager**, for her precious support on the DSP and density tests. In addition, I wish I said thank you to **Bruska Azhdar** and **Thomas Blomfeldt**, both from Polymeric Materials Group at KTH, for their assistance on the manufacturing of the specimens and on the tensile tests, respectively. In sum, I am very happy for having met all of you, for the good moments we have spent together and for the precious contribution and support that you have given to this work.

I could not also forget to express all my gratitude to **CNPq** for the financial support granted to me over these four years, including the abroad fellowship program; to **Prof. Cristiano Mascarenhas** and the **Exact Science Department** from Feira de Santana State University (UEFS) for having made available a computer, so that I could run some numerical examples; to **Geovani Bresolin** for his great support in the completion of this work and to **PosMec** for having given me this valuable opportunity to grow a little bit more as a person and professionally.

Finally, I would really like to express all my gratitude to **everyone** who has been cited here and also to those who have not, but they have not been forgotten. I dedicate them the hope that the efforts put in this work will not be in vain and that it can be profitable or can offer even a minimal contribution on what it is of any service to improve a little bit this world which we live in.

To everybody, my sincere thank you very much!

AGRADECIMENTOS

Este é o final de uma jornada de quatro anos e o início da longa jornada do resto de uma vida. Como de costume, a conclusão de mais uma etapa nas nossas vidas é extremamente gratificante e quando olhamos para o caminho que trilhamos, é inevitável sentir a sensação de satisfação e de dever cumprido.

Por mais técnico e pretensioso que este tipo de trabalho pareça ser, sua realização, apesar de ser tipicamente solitária, definitivamente, não é. O caminho que conduz à conclusão de uma tese de doutorado é geralmente crivado de obstáculos e dificuldades que, certamente, estão além da capacidade humana de superá-los sozinho. Não poderia ser diferente comigo, pois se consegui chegar até aqui é porque eu tive uma inestimável e valiosa contribuição de várias pessoas, que merecem ser lembradas aqui, pois seria extremamente injusto dar todo o mérito deste trabalho apenas àquele que o fez.

O maior agradecimento ao nosso **pai** celestial pelo dom da vida concedida a mim e por ser uma inesgotável fonte de fé e força para que eu conseguisse trilhar o caminho percorrido até aqui, a fim de que eu pudesse superar todos os obstáculos encontrados durante a realização deste trabalho.

A contribuição silenciosa e, às vezes, ativa de quem, mesmo distante, participou das minhas angústias, ouviu minhas lamúrias e me deu apoio, compreensão e conforto. Aos meus **pais**, **parentes** e **amigos**, que sempre me deram força e sempre mantiveram a expectativa de ver este trabalho concluído.

Um trabalho acadêmico desta natureza não é possível de ser realizado sem uma idéia e, consequentemente, sem um idealizador. Mais uma vez, pude contar com a participação do grande amigo **Cajuhi**. Eu gostaria de agradecê-lo, não apenas por se tornar o idealizador deste trabalho, mas também pela excepcional contribuição e apoio que ele tem dado a minha vida profissional.

A fim de que a idéia definida seja executada eficientemente, é importante manter um bom relacionamento com os nossos orientadores, para que consigamos alcançar os objetivos desejados. Quanto melhor este relacionamento, melhor serão os resultados. E eu não tenho dúvidas de que nós realmente cultivamos um bom relacionamento, pois nossos objetivos foram alcançados e um bom trabalho foi produzido no final. Para os meus orientadores **Marcelo Krajnc Alves** e **Kristofer Gamstedt**, dizer muito obrigado é pouco para demonstrar toda a minha gratidão por tudo que vocês fizeram, a fim de tornar este trabalho uma realidade.

Durante esta jornada de quatro anos, muitas pessoas apareceram na minha vida. Algumas apenas vieram e se foram, enquanto outros se tornaram bons amigos. De qualquer forma, todos eles deixaram sua contribuição pessoal e, sem querer, fizeram esta jornada ser mais prazerosa. Assim, eu gostaria de agradecer os meus colegas do GMAC: **Maura**, **Fábio**, **Ivan**, **Miguel**, **Maldaner**, **Hilbert**, **Lindaura**, **Guilherme**, **Marcus** e **Fernanda**; do Grante: **Pedrão** e **Enildo**, e todos do **grupo de Biocompostos** do KTH, em especial **Ingela Bjurhager**, por seu precioso apoio nos ensaios de DSP e de densidade. Além disso, eu gostaria de agradecer ao **Bruska Azhdar** e ao **Thomas Blomfeldt**, ambos do Grupo de Materiais Poliméricos do KTH, pela assistência na fabricação dos corpos de prova e na realização dos ensaios de tração, respectivamente. Enfim, estou muito feliz por ter encontrado todos vocês, pelos bons momentos que passamos juntos e pela preciosa contribuição e apoio que vocês deram a este trabalho.

Eu não poderia esquecer de expressar toda a minha gratidão ao **CNPq** pelo apoio financeiro oferecido a mim durante estes quatro anos, incluindo a bolsa de doutorado sanduíche, ao **Prof. Cristiano Mascarenhas** e ao **Departamento de Ciências Exatas** da Universidade Estadual de Feira de Santana (UEFS), que disponibilizaram um computador para que eu pudesse executar alguns exemplos numéricos; ao **Geovani Bresolin** pelo seu apoio na finalização do trabalho e ao **PosMec** por ter me proporcionado essa valiosa oportunidade de poder crescer um pouco mais como pessoa e como profissional.

Enfim, eu gostaria de expressar toda a minha gratidão a **todos** estes e também àqueles que não foram citados aqui, mas não foram esquecidos. Dedico a esperança de que os esforços colocados neste trabalho não serão em vão e que ele possa ser útil ou possa oferecer uma mínima contribuição no que lhe servir para ajudar a melhorar um pouquinho este mundo em que vivemos.

A todos, meu sincero Muito Obrigado!

"The roots of education are bitter, but the fruit is sweet".

Aristotle

"A educação tem raízes amargas, mas seus frutos são doces".

Aristóteles

THE AUTHOR

Wesley Novaes Mascarenhas was born in September, 1974 in Salvador city, Bahia state. In 1978, he moved to Feira de Santana city, Bahia, where he has attended his elementary and high school education and served the army at the 35° Infantry Battalion, in 1994. In 1995, he began to pursue his undergraduation degree in mechanical engineering from Federal University of Bahia (UFBA), where he majored in 1999. The following year, he begun to pursue his master degree in mechanical engineering from Federal University of Santa Catarina (UFSC) on manufacturing field and presented his master degree dissertation on May 28, 2002. Following, he was hired by Trilogy International of Brazil Company as a consultant engineer to work at the product development (PD) center of the Ford Motor Company plant in Camaçari city, Bahia. Initially, he started working with heat transfer analyses of under hood and underbody automotive components and, following, with nonlinear stress and strain analyses of body components, from August 2002 to March 2005, when, then, he decided to leave the company to pursue his doctorate degree at UFSC again, where he presented his doctorate thesis on February 18, 2011. He has worked again at the product development center of the Ford Motor Company plant in Camaçari city with durability and nonlinear stress and strain analyses of chassis and body components for two years. Presently, he has been working at MFX do Brasil with design of umbilical cables for offshore oil and natural gas industries.

O AUTOR

Wesley Novaes Mascarenhas nasceu em Setembro de 1974, na cidade do Salvador, estado da Bahia. Em 1978, mudou-se pra a cidade de Feira de Santana, Bahia, onde realizou seu período escolar fundamental e médio e serviu o Exército no 35° Batalhão de Infantaria, em 1994. Em 1995, iniciou seu curso de graduação em engenharia mecânica na Universidade Federal da Bahia (UFBA), onde se graduou em 1999. No ano seguinte, iniciou seu curso de mestrado em engenharia mecânica na Universidade Federal de Santa Catarina (UFSC), na área de fabricação, e apresentou sua dissertação no dia 28 de Maio de 2002. Logo em seguida, foi contratado pela Trilogy International do Brasil, como engenheiro consultor, para trabalhar no centro de desenvolvimento de produtos (PD) da planta da Ford na cidade de Camaçari, Bahia. Inicialmente, ele começou a trabalhar com análises de transferência de calor em componentes do motor e de chassi e, em seguida, com análises não-lineares de tensões e deformações em componentes de carroceria, de Agosto de 2002 a Março de 2005, quando, então, ele decidiu desligar-se da empresa e iniciar seu curso de doutorado na UFSC novamente, onde apresentou sua tese no dia 18 de Fevereiro de 2011. Trabalhou novamente no centro de desenvolvimento de produtos da planta da Ford em Camaçari com análises de durabilidade e análises não-lineares de tensões e deformações de componentes de chassi e carroceria por dois anos. Atualmente, atua na MFX do Brasil com projeto de cabos umbilicais para a indústria do petróleo e gás natural.

NOTA DE ESCLARECIMENTO

Devido às regras da universidade onde este trabalho foi apresentado, o documento escrito não pode ser redigido em língua estrangeira. Como grande parte deste trabalho foi desenvolvida em parceria com o Departamento de Tecnologia de Fibras e Polímeros do Instituto Real de Tecnologia (KTH), em Estocolmo, Suécia, sob a supervisão de pessoas que não compreendem a língua portuguesa, o mesmo foi escrito em sua totalidade na língua inglesa, que é a *lingua franca* da comunidade de pesquisa internacional. Para suprir as regras da universidade, ao final deste trabalho de tese, o resumo estendido, redigido em português, é apresentado (Chapter 9). O autor e seus orientadores compreendem a necessidade de crescimento da produção científica nacional, no entanto, para que a mesma seja reconhecida pela comunidade científica internacional, o trabalho deve ser de fácil acesso, o que é garantido pela sua redação em língua inglesa, meio de comunicação comum entre os pesquisadores, cientistas e engenheiros do mundo inteiro.

NOTE OF EXPLANATION

Due to the rules of the university where this work has been presented, the final document can not be written in a foreign language. However, since a considerable part of this work has been developed in association with the Department of Fibre and Polymer Technology of the Royal Institute of Technology (KTH), in Stockholm, Sweden, under supervision of people who do not understand the Portuguese language, it has been entirely written in English, which is the *lingua franca* of the international research community. In order to fulfill the requirements of the origin university, at the end of this thesis work, the extended summary, written in Portuguese, is presented (Chapter 9). The author and his advisors understand that it is necessary to increase the national scientific production, however, in order that this work is also accepted by the international research community, it must be easily accessible, what is guaranteed by its writing in English, which has been the most common means of communication among researchers, scientists and engineers of the whole world.

CONTENTS

LIST OF FIGURES

LIST OF TABLES

ABBREVIATIONS

ABS	Acrylonitryle – Butadiene – Styrene.
ADSC	Alternating Differential Scanning Calorimetry.
ASTM	American Society for Testing and Materials.
CAD	Computer Aided Design.
CAE	Computer Aided Engineering.
CD	Compact Disc.
CRR	Cooperatively Rearranging Regions.
DIC	Digital Image Correlation.
DVD	Digital Versatile Disc or Digital Video Disc.
DMA	Dynamic Mechanical Analysis.
DSC	Differential Scanning Calorimeter.
DSP	Digital Speckle Photography.
HDPE	High Density Polyethylene.
HIPS	High Impact Polystyrene.
ISO	International Organization for Standardization.
KTH	*Kungliga Tekniska Högskolan* (Royal Institute of Technology).
LDPE	Low Density Polyethylene.
PA	Polyamide.
PC	Polycarbonate.
PE	Polyethylene.
PEEK	Polyaryletherketone.
PET	Polyethylene Terephthalate.
PMMA	Polymethyl Methacrylate.
PP	Polypropylene.
PPO	Polyphenylene Oxide
PPS	Polyphenylene Sulfide.
PS	Polystyrene.
PTFE	Polytetrafluoroethylene.
PVC	Polyvinyl Chloride.
RAL	***R**eichs**a**usschuß für **L**ieferbedingungen und Gütesicherung* (State Commission for Delivery Terms and Quality Assurance).
SAN	Styrene – Acrylonitryle.
SAE	Society of American Engineers.
SI	*Systéme International d'Unités* (International System of Units).
TMA	Thermomechanical Analyzer.
UL	Underwriters Laboratories.
UV	Ultraviolet.
VBO	Viscoplasticity Based on Overstress.
VBOP	Viscoplasticity Based on Overstress for Polymers.

LIST OF SYMBOLS

The symbols and notations adopted in this work are commonly used in the Continuum and Damage Mechanics literatures, i.e., one has tried to be as classical and uniform as possible. In this regard, either Latin or Greek letters have been used to represent the physical and mathematical variables of the phenomena studied and modeled in this work. In some cases, it has been unavoidable to use the same letter to represent different variables. In general, the symbols can be organized as follow:

- **Scalars and Scalar-Valued Functions**: *Latin and Greek italic light-face letters* (*a,b,c,… or A,B,C,… or α,β,γ,… or Γ,Δ,Ξ,…*).
- **Vectors and Vector-Valued Functions**: *Latin italic light-face letters with an arrow above* ($\vec{a},\vec{b},\vec{c},...$ or $\vec{A},\vec{B},\vec{C},...$). *Latin italic light-face letters with Latin italic index* ($a_i,b_j,c_k,...$ or $A_i,B_j,C_k,...$) *for Cartesian components*.
- **Matrices**: *Upright bold-face Latin capital letters* ($\mathbf{A},\mathbf{B},\mathbf{C},...$). *Upright light-face with Latin italic indexes* ($\mathrm{A}_{ij},\mathrm{B}_{kl},\mathrm{C}_{rs},...$) *for Cartesian components.*
- **Tensors and Tensor-Valued Functions**: *Latin italic bold-face capital letters* ($\boldsymbol{A},\boldsymbol{B},\boldsymbol{C},...$) *and Greek italic bold-face letters* ($\boldsymbol{\alpha},\boldsymbol{\beta},\boldsymbol{\gamma},...$) *for second-order tensors. Italic light-face with Latin italic indexes* ($A_{ij},B_{kl},C_{rs},...$ or $\alpha_{ij},\beta_{kl},\gamma_{rs},...$) *for Cartesian components. Latin Euclid Math Two bold-face upright capital letters* ($\mathbb{A},\mathbb{B},\mathbb{C},...$) *for fourth-order tensors. Latin Euclid Math Two upright capital letters with Latin italic indexes* ($\mathbb{A}_{ijkl},\mathbb{B}_{mnrs},\mathbb{C}_{pqrs},...$) *for Cartesian components*.
- **Sets**: *Latin calligraphy capital letters* ($\mathcal{A},\mathcal{B},\mathcal{C},...$).
- **Domain and Boundary**: *Greek upright light-face capital letters* (*Γ, Δ, Ξ,…*).

The meaning of the symbols will be described in the following items.

SCALARS

A_v	Volumetric external source of damage work.
A_s	Surface external source of damage work.
D	Isotropic damage variable.
D_{cd}	Critical damage.
e	Specific internal energy.
e_{ef}^{vp}	Effective viscoplastic strain.
$e_{ef_{th}}^{vp}$	Threshold effective viscoplastic strain.
$e_{ef_{adm}}^{vp}$	Admissible effective viscoplastic strain.
$\dot{e}_{ef}^{vp}$	Effective viscoplastic strain ratio.
$e_{H_{n+1}}^{e\ trial}$	Hydrostatic part of the trial elastic strain tensor at t_{n+1}.
E	Modulus of elasticity – Young's modulus.
E^*	Complex modulus.
E'	Storage modulus.
E''	Loss modulus.
E_{int}	Internal energy.
$f(\bullet)$	Yield function.
F	Internal work of damage.
F^{reac}	Reaction force of damage.
F^r	State variable associated with β.
F^i	State variable associated with $\dot{\beta}$.
G	Shear modulus.
$\bar{H}$	Heaviside function.
I_1	First invariant of the stress tensor.
I_k	Indicator function.
$I_K^{\bar{\eta}}$	Regularized indicator function.
J	Determinant of the Jacobian matrix.
J_2	Second invariant of the deviatoric stress tensor.
J_3	Third invariant of the deviatoric stress tensor.
$\acute{k}$	Parameter that measures the influence of the damage at a material point on the damage of its neighborhood.
k	Number of iterations of the Newton method.
k	Number of internal variable.

k_b	Number of cyclic loading blocks.
K	Kinetic energy.
K_r	Material parameter of the model proposed by Riand *et al.* [5].
K_n	Creep material parameter of the Norton law.
K_∞	Viscosity material parameter of the Benallal model.
M	Viscosity material exponent of Benallal's model.
n	Number of cycles of a specific loading block.
N	Norton creep material exponent.
N	Number of cycles associated with failure at the stress level of the loading block obtained from *S-N* diagram.
N_i	Interpolation functions.
P_{ext}	Power of external loads.
P_a	Virtual power of the acceleration forces.
P_i	Virtual power of the internal forces.
P_e	Virtual power of the external forces.
p_{n+1}^{trial}	Trial hydrostatic part of the Cauchy stress tensor.
q	Deviatoric part of the Cauchy stress tensor.
q_{n+1}^{trial}	Trial deviatoric part of the Cauchy stress tensor.
r	Accumulated viscoplastic strain.
r	Radial coordinate in a cylindrical coordinate system.
r_{n+1}^{trial}	Trial accumulated plastic strain at t_{n+1}.
$\overline{r}$	Volumetric density of the material heat production.
R	Isotropic strain hardening variable.
$\overline{R}$	Residual error.
R_v	Triaxiality function.
s	Specific entropy.
S	Entropy.
S_f	Safety factor.
S_o	Parameter that measures the damage strength of the material.
t	Time.
t_f	Final time of the analysis.
Tol	Global convergence tolerance.
T	Temperature.
T_g	Glass transition temperature.

T_m Melting temperature.

T_c Crystallization temperature.

$\overline{u}_x$ Tensile prescribed displacement in the *x*-direction.

$\overline{u}_r$ Tensile prescribed displacement in the radial direction.

u_r Radial displacement component.

u_z Axial displacement component.

u_θ Circumferential displacement component.

V_k *k*-th internal variable.

V Volume.

x Cartesian coordinate of material points.

X_c Degree of crystallinity.

$\dot{W}^{vp}$ Effective inelastic work rate.

z Axial coordinate in a cylindrical coordinate system.

β Cohesion variable.

δ Kronecker delta.

σ_{oy} Initial yield stress.

σ_y Yield stress.

σ_{eq}^{vm} Von Mises equivalent stress.

σ_{ef} Effective stress measure.

σ^* Complex stress.

ε^{vp} Uniaxial viscoplastic strain.

ε_x Longitudinal strain.

ε_y Transverse strain.

ε_y Strain at yielding.

ε_{zz} Strain in the longitudinal direction.

ξ Axis of the natural coordinate system.

γ Velocity of the microscopic links.

γ_{xz} Shear strain in the *xz* plane.

γ_{yz} Shear strain in the *yz* plane.

ϕ Specific heat flow of the DSC equipment.

$\dot{\lambda}$ Viscoplastic multiplier.

$\overline{\lambda}$ Lamé constant.

μ Variable that incorporates the effect of the hydrostatic stress.
$\bar{\mu}$ Lamé constant.
η Axis of the natural coordinate system.
$\bar{\eta}$ Penalty parameter.
ν Poisson ratio.
ρ Specific mass.
ω Frequency of excitation.
Δ Dissipation.
ΔH_m Specific heat absorbed during melting.
ΔH_c Specific heat released for the crystallization.
ΔH_{fus} Specific heat absorbed during melting, when the material is fully crystalline.
Δt Variation of time.
τ Local variable employed in the parametrization of the boundary.
Ψ Helmholtz free energy potential.
Ψ^{vp} Helmholtz free energy potential for viscoplasticity.
θ Angular coordinate in a cylindrical coordinate system.
σ_H Hydrostatic part of the Cauchy stress tensor.
φ Dissipation potential.
φ^* Dual dissipation potential.
φ^*_{vp} Viscoelastoplastic dissipation potential.
φ^*_{vp} Thermal dissipation potential.
φ^*_D Damage dissipation potential.

VECTORS

$\vec{b}$ Body force per unit mass vector.
$\vec{F}^G$ Global nodal force vector.
$\vec{H}$ Flux vector of internal work of damage.
$\vec{n}$ Outward unit vector.
$\vec{q}$ Heat Flux vector.
$\vec{q}_e$ Finite element degree of freedom vector.
$\vec{t}$ Traction prescribed on the boundary.
$\vec{u}$ Displacement field vector.
$\vec{u}_o$ Displacement vector of the body at instant $t = 0$.

$\ddot{\vec{u}}$ Acceleration field vector.

$\vec{U}$ Vector of all nodal degree of freedom.

$\hat{\vec{v}}$ Virtual displacement field vector.

$\vec{v}$ Velocity field vector.

$\vec{v}_o$ Velocity vector of the body at instant $t = 0$.

$\vec{V}$ Array of internal variables.

$\vec{V}_{n+1}^{trial}$ Array of trial internal variables at t_{n+1}.

$\vec{x}$ Position vector of material points.

$\Delta\vec{U}_{n+1}$ Vector of global nodal degree of freedom at t_{n+1}.

MATRICES

$\mathbf{B}^u$ Strain-displacement matrix.

$\mathbf{B}^d$ Damage-displacement matrix.

$\mathbf{K}^T$ Local tangent stiffness matrix.

$\mathbf{K}^G$ Global consistent tangent stiffness matrix.

$\mathbf{N}^u$ Interpolation function matrix for displacement degree of freedom.

$\mathbf{N}^d$ Interpolation function matrix for damage degree of freedom.

SECOND AND FOURTH ORDER TENSORS

$\breve{\boldsymbol{D}}_{uu}^{ep}$ Compact form of the consistent displacement tangent modulus.

$\boldsymbol{D}_{n+1}^{ud}$ Consistent displacement-damage tangent modulus at t_{n+1}.

$\boldsymbol{I}$ Second order identity tensor.

$\boldsymbol{\sigma}$ Cauchy stress tensor.

$\boldsymbol{\sigma}^D$ Deviatoric part of the Cauchy stress tensor.

$\boldsymbol{\sigma}_{n+1}^{D\ trial}$ Deviatoric part of the trial stress tensor at t_{n+1}.

$\boldsymbol{\sigma}_o$ Initial residual stress tensor.

$\tilde{\boldsymbol{\sigma}}$ Effective Cauchy stress tensor.

$\boldsymbol{\varepsilon}$ Total strain tensor.

$\dot{\boldsymbol{\varepsilon}}$ Total strain rate tensor.

$\boldsymbol{\varepsilon}^D$ Deviatoric part of the total strain tensor.

$\boldsymbol{\varepsilon}^e$ Elastic strain tensor.

$\dot{\boldsymbol{\varepsilon}}^e$ Elastic strain rate tensor.

$\boldsymbol{\varepsilon}_{n+1}^{e\ trial}$	Trial elastic strain tensor at t_{n+1}.
$\boldsymbol{\varepsilon}^{vp}$	Viscoplastic strain tensor.
$\dot{\boldsymbol{\varepsilon}}^{vp}$	Viscoplastic strain rate tensor.
$\dot{\boldsymbol{\varepsilon}}^{vp\,D}$	Deviatoric part of the viscoplastic strain rate tensor.
$\boldsymbol{\varepsilon}_{n}^{vp}$	Viscoplastic strain at t_n.
$\boldsymbol{\varepsilon}^{in}$	Inelastic strain tensor.
$\boldsymbol{\vartheta}$	Back strain tensor to account for kinematic hardening.
$\boldsymbol{\chi}$	Back stress tensor.
$\Delta\boldsymbol{\varepsilon}^{vp}$	Variation of the viscoplastic strain tensor.
$\mathbb{D}$	Fourth order elasticity tensor.
$\mathbb{D}_{n+1}^{uu}$	Consistent displacement tangent modulus at t_{n+1}.
$\mathbb{I}$	Fourth order identity tensor.

SETS

$\bar{\mathcal{K}}$	Set of admissible displacements and damage.
$\bar{\mathcal{K}}_u$	Set of admissible displacement.
$\bar{\mathcal{K}}_D$	Set of admissible damage.
$\mathcal{R}$	Set of real numbers.
$\mathcal{V}$	Set of admissible variations.
$\mathcal{V}_u$	Set of admissible displacement variations.
$\mathcal{V}_D$	Set of admissible damage variations.

DOMAIN AND BOUNDARY

Ω	Domain of the body.
Ω_e	Finite element domain.
$\partial\Omega$	Boundary of the domain.
Γ_t	Region of the boundary with prescribed traction.
Γ_u	Region of the boundary with prescribed displacement.

INDICIAL NOTATION, SUBSCRIPTS AND SUPERSCRIPTS

When indicial notation is used, one has adopted *italic subscripts i*, *j*, *k*, *l*,…, ranging from 1 to 3 and they will mean Cartesian components of the variable. But, subscripts are not employed exclusively in association

with indicial notation. Different connotations are assigned to subscripts throughout the text and their meanings should be clear from the context. A relevant example is the context of incremental numerical procedures. In this case, subscripts indicate the relevant increment number. Thus, in the expression $\Delta(\bullet) = (\bullet)_{n+1} - (\bullet)_n$, the subscripts n and $n + 1$ refer to the value of the variable $(\bullet)$ at the end of increments n and $n + 1$, respectively. Superscripts are also used in the text. Their meanings will be stated the first time it appears in the text and should be clear from the context thereafter.

MATHEMATICAL OPERATORS

$div(\bullet)$	Divergence of $(\bullet)$.
$\ln(\bullet)$	Natural logarithm of $(\bullet)$.
$tr(\bullet)$	Trace of $(\bullet)$.
$\Delta(\bullet)$	Increment of $(\bullet)$. In other words, $\Delta(\bullet) = (\bullet)_{n+1} - (\bullet)_n$.
$\vec{\nabla}(\bullet)$	Gradient of $(\bullet)$.
$\partial(\bullet)$	Boundary of the domain $(\bullet)$.
$\dot{(\bullet)}$	Time derivative of $(\bullet)$.
$\partial^{loc}(\bullet)$	Sub differential of $(\bullet)$.
$\frac{d(\bullet)}{dy}$	Total derivative of $(\bullet)$ with respect to y.
$\frac{\partial(\bullet)}{\partial y}$	Partial derivative of $(\bullet)$ with respect to y.
$(\bullet)_{,y}$	Derivative of $(\bullet)$ with respect to y.
$(\bullet)_{,yy}$	Second derivative of $(\bullet)$ with respect to y.
$\partial_{yy}(\bullet)$	Second partial derivative of $(\bullet)$ with respect to y.
$(\bullet)^T$	The transpose of $(\bullet)$.
$\boldsymbol{A} \cdot \boldsymbol{B}$ $\vec{u} \cdot \vec{v}$	Scalar product of tensors or vectors.
$\boldsymbol{A} \otimes \boldsymbol{B}$ $\vec{u} \otimes \vec{v}$	Tensor product of tensors or vectors.
$\lVert(\bullet)\rVert$	Norm of tensors and vectors.
$\langle(\bullet)\rangle$	Macaulay operator.

$a \equiv b$	Means a is defined as b. This symbol is used to emphasize that the expression in question is a definition.
$\bigcup$	Finite element assembly operator.
$\sup_{a}\{\bullet\}$	Supremum limit or least upper bound of the set $(\bullet)$ of real numbers.

TÍTULO & RESUMO

UM MODELO DE DANO PARA A ANÁLISE DA FALHA DÚCTIL DE COMPONENTES DE PLÁSTICO

O objetivo deste trabalho é propor um modelo matemático e um sistema computacional, baseado no método dos elementos finitos, capaz de auxiliar a atividade de análise estrutural de componentes de plástico submetidos à falha dúctil. Basicamente, este sistema computacional será composto por um modelo elasto-viscoplástico acoplado ao dano, a fim de ser possível descrever a evolução das deformações inelásticas e os processos degradativos que conduzirão à falha e, assim, auxiliar no dimensionamento de componentes. O referido modelo foi desenvolvido sob as teorias propostas por Lemaitre [1], Fremond e Nedjar [2] e sob as abordagens da termodinâmica dos meios contínuos e do método do estado local, onde foram introduzidos os conceitos de potenciais termodinâmicos e de variáveis de estado. Ao se utilizar estas abordagens, assegura-se que os modelos produzirão resultados termodinamicamente consistentes. A fim de certificar o modelo proposto e validar o sistema numérico, realizou-se um ensaio uniaxial, em que o corpo de provas foi deformado até a sua fratura. Os dados obtidos do referido ensaio e de outros ensaios complementares foram utilizados na identificação das propriedades e constantes materiais, que definem o modelo proposto. Os procedimentos experimentais foram realizados no Departamento de Fibras e Tecnologia de Polímeros do Instituto Real de Tecnologia (KTH), em Estocolmo, Suécia.

Palavras – chave: termoplásticos, elasto-viscoplasticidade, dano, variáveis internas, potencial termodinâmico.

ABSTRACT

The objective of this work is to propose a mathematical model and a numerical scheme, based on the finite element method, to be used to analyze mechanical components manufactured with plastic material, subjected to monotonic loading conditions that undergo a ductile failure. Basically, this numerical scheme will be composed by an elasto-viscoplastic model coupled with a nonlocal damage theory, in order to describe the evolution of the inelastic strains and the damaging processes of the material, which will consequently lead to the failure of the component. The cited model has been developed by means of the theories proposed by Lemaitre [1], Fremond and Nedjar [2], among others, and makes use of the method of local state variables and is derived within the scope of the consistent thermodynamics of the continuum medium. The main advantage of using these approaches is the confidence they give that the models can not produce thermodynamically unreasonable results. In order to attest the proposed model and to validate the numerical scheme, one considers an experimental uniaxial test, in which the specimen is deformed up to its ductile fracture. The data obtained from the given experimental uniaxial test and from other complementary experimental tests is then employed for the identification of the material properties and parameters, which define the proposed damage model. The experimental procedures have been performed at the Fibre and Polymer Technology Department of the Royal Institute of Technology (KTH), in Stockholm, Sweden.

Key-words: thermoplastics, elasto-viscoplasticity, damage, state variables, thermodynamic potentials.

CHAPTER 1

INTRODUCTION

In this introductory chapter, one will be defined and outlined the main directions of this work. Initially, one will be presented the focus, in order that the objective of the work is clearly established and understood. Following, one will be discussed the main reasons, which has motivated its accomplishment, its objectives and a bibliographical review. In addition, the main assumptions and hypotheses, which have supported the development of this work, will also be stated. At last, one will be presented the content of the work.

1.1. FOCUS OF THE WORK

This work starts by wondering why is important to model engineering materials. Why so many researchers around the world have concentrated their efforts on the study and modeling of engineering materials. During the last decades, there has been an increasing demand for high quality industrial products, followed by the development and application of new nonmetallic materials. As a consequence, material modeling has become an important research area in Applied Mathematics, because one has required capturing the behavior of these materials as close as possible of reality. In order that these models are able to be applied in practice, they are normally solved numerically, implemented on commercial softwares, commonly known as CAE[1] systems, and, then, used to assist the development process of industrial products, so that they are designed as reliable as possible and can fulfill their durability and quality requirements.

One must emphasize that the reliability of the numerical results strongly depends on the ability of the designer engineer to choose the correct constitutive model, apply the correct material parameters and boundary conditions and understand the underlying numerical procedures of the numerical package, in which the constitutive models are implemented. Otherwise, the numerical simulations on commercial softwares might not be representative, what might lead to a poor evaluation and, consequently, to the design of an unsuccessful product.

During the last decades, plastic materials have been one of the most commonly used materials in engineering, because plastic

[1] CAE stands for **Computer Aided Engineering**. According to Lee [3], CAE systems are computational tools used to analyze, virtually, the geometry of a component or system, allowing the designer to simulate and study how this component or system will behave, so that their designs can be refined and optimized.

components have been extensively applied as structural elements or as replacement of metallic components of industrial products in many engineering fields, due to their cost, great versatility, lightness and durability. Although the application of plastic materials in engineering has been increasing, some aspects of their utilization have not been totally established. One of these aspects refers to the analysis of plastic components subjected to ductile failure. In this case, the component will be prone to fail and become useless prematurely.

Currently, one has noticed that few works on modeling of the degradation processes and failure of plastic components have been developed. These works are necessary because plastic components have been widely used in industrial applications; so, one expects that these components also exhibit the same reliability as metallic components. Thus, based on these considerations, this work is focused on the study and on the mathematical modeling of the inelastic and damaging processes of plastic components, due to mechanical loading.

1.2. MOTIVATIONS

The determination of irreversible deformation mechanisms and the modeling of the damaging processes of plastic materials have recently required considerable attention, due to the increasing use of these materials to manufacture structural elements or as replacement of metallic materials in many load bearing industrial applications. As a consequence, one has expected that plastics also exhibit the same reliability as metallic materials. Thus, in order to ensure this requirement, the components, which will be submitted to severe loading conditions and environment, will require a lifetime analysis before production. The first step of this analysis is the inelastic evaluation, which will provide information about stresses and strains as a function of displacement and time, during manufacturing and service.

In practice, the design of plastic components is performed empirically, i.e., one applies the same approach used to analyze metallic components: one accomplishes a static stress analysis and one tries to keep the maximum von Mises stress below an equivalent stress, which is obtained by dividing the yield stress of the plastic material (σ_y) by a safety factor (S_f). For components under fatigue regime, one uses to take 75% of the yield stress of the material, in order to compensate the uncertainties associated with the methods used to determined the yield stress of the material, and divide it by three. At last, an equivalent stress is, then, calculated, using the result of this operation and one tries to keep the maximum von Mises stress less than this equivalent stress.

In many cases, the empiric way in which the design of a plastic component is performed may lead to the production of over-dimensioned components with, consequently, high cost and weight. Thus, one considers that the motivations of this work are based on the empiricism in which the design of plastic components is performed and on the absence of consistent numerical tools capable of simulating the damaging processes of plastic materials, when submitted to mechanical loading. Thus, this work may be specially useful to assist the structural analysis of industrial components, in order to prevent them from premature failure[2].

1.3. OBJECTIVES OF THE WORK

Based on the focus and on the motivations presented previously, the main objectives of this work are:

- Propose a theoretical model and a numerical scheme based on the Galerkin Finite Element Method, which can be used for the analysis of mechanical components manufactured with plastic materials, submitted to monotonic mechanical loadings up to its ductile failure[3]. The proposed mathematical model is composed by an elasto-viscoplastic model coupled with a nonlocal damage theory. The usage of a nonlocal damage model is fundamental for reducing the mesh sensitivity that occurs when local theories are employed. As a consequence, one may obtain a better prediction of the material degradation behavior and a good prediction of the structural size effect, which is particularly important in mechanical engineering.
- Describe and perform a set of experimental tests, which are necessary in order to identify the required material parameters employed in the description of the proposed model.

One of the main advantages of this work is the possibility of implementing the proposed model on commercial codes, like Abaqus, Ansys and LS-Dyna. As a consequence, this work may be employed to analyze industrial components in more general setting of loading, geometry and boundary conditions, as currently most commercial codes are not able to predict properly the ductile damage process of plastic materials, such as the cold drawing phenomenon, which will be defined later.

---

[2] One considers that a component has failed precociously when it exhibits damage or malfunctioning before the time established as its lifetime.

[3] In this work, **ductile failure** means that there will be extensive inelastic deformation before fracture.

1.4. BASIC ASSUMPTIONS AND HYPOTHESES

According to Lemaitre [1], despite their different physical structure, the engineering materials have similar mechanical behavior, at the mesoscale, qualitatively speaking. All exhibit elastic behavior, yielding, irreversible strain, cyclic hysteresis loops, damage due to monotonic or fatigue loading and crack growth. This means that the common mesoscopic properties can be explained by a few energy mechanisms that are similar for all these materials. Thus, based on these considerations, the mathematical model of this work has been developed by **assuming that the inelastic behavior and the damaging processes of plastic materials can also be treated within the standard generalized material framework**. The development used is identical to that applied to model metals and their alloys with modifications, making possible to describe some phenomena specific to plastics. In this regard, the most noticeable differences come from the expression of the yield criterion and the locking strategy for the damaged material behavior, discussed in section 4.6. In addition to this assumption, some hypotheses have also been considered, which, basically, are:

- **Infinitesimal Strain Regime :** One assumes that, at any time instant t, the total strain tensor, $\boldsymbol{\varepsilon}$, is additively decomposed into an elastic (reversible), $\boldsymbol{\varepsilon}^{e}$, and an inelastic (irreversible) part, $\boldsymbol{\varepsilon}^{vp}$, also known as viscoplastic strain, because of its dependence on time. Presently, there is not a consensual limit value of applicability of this hypothesis, but, according to Ghorbel [4] and Riand *et al*. [5], strains up to 5% can be considered as infinitesimal.
- **Thermodynamic Variables:** The classical thermodynamic formalism considered in this work is based on the hypothesis of the local state variables, which requires the knowledge of the state variables of the material. These variables are decomposed into observable and internal variables.
- **Free Energy Potential (Ψ):** The thermodynamic formalism is also based on the hypothesis of the existence of a free energy potential, Ψ, from which the state laws of viscoplasticity are derived. In addition, decoupling between the elastic and viscoplastic behavior is also assumed.
- **Dissipation Potential (φ):** One assumes the existence of a dissipation potential expressed as a continuous and convex scalar function, null at the origin of the flux variables. From the dissipation potential, one derives the complementary laws, necessary for describing the dissipative processes, by applying the normal dissipation criterion. In

this work, the dissipation potential is also decomposed into two potentials: elastic and viscoplastic potentials.

- **Normality Hypothesis:** The normality hypothesis considers that the viscoplastic flow vector ($\dot{\boldsymbol{\varepsilon}}^{vp}$) is normal to the yield surface. The generalized normality hypothesis associated with the dissipative phenomena is also assumed, allowing expressing the complementary laws of evolution of the internal variables. This hypothesis has supported most (visco)plasticity theories.
- **Isotropy and Homogeneity:** Strictly speaking, plastic materials are neither isotropic nor totally homogeneous. Different arrangements of molecular chains can be obtained (see Figure 2.4), what become the material inhomogeneous and with mechanical and thermal behaviors depending strongly on the direction. In this work, the assumptions of isotropy and homogeneity will be considered. These assumptions have been widely used to model the mechanical and thermal behaviors of plastic materials and, in many cases, one has obtained good results.
- **No Temperature Dependence:** One knows that the mechanical behavior of plastic materials is very sensitive to temperature variations (see section 2.4). For simplicity, one will assume the deformation process to be isothermal. Since the deformation process is dissipative, this assumption requires the loading process to change slowly with time.
- **Quasistatic Process:** A quasistatic process is that, in which a system evolves under a sequence of states that are infinitesimally close to equilibrium. In Solid Mechanics, a process is considered quasistatic when the loading rate is so slow, that the accelerations produced can be neglected. As a consequence, one sets $\ddot{\vec{u}} \approx 0$ and the inertial forces contribution is disregarded.
- **No Residual Stress:** Undesirable molded-in or residual stresses are present in all molded plastic components to some degree and their main causes are uneven cooling and differential shrinkage. According to Lemaitre [1], a residual stress field may be introduced as an initial condition of the problem. In this work, one will consider that the components will be free of molded-in stress.
- **Free of Defects:** Defects, like weld lines and voids (see section 2.5.1), derived from the manufacturing process, are common to happen. In this case, these defects can be considered as an initial damage for the problem, i.e., $D(x,0) \neq 0$. In this work, one will consider that the components will also be free of defects, i.e., one will set $D(x,0) = 0$ as initial condition of the problem, in which D is the damage variable.

- **No Micro Crack Closure Effect:** For most materials under certain conditions of loading, the micro defects may close during compression. This is more often the case for very brittle materials and cyclic load regime. The phenomenon of closure of micro cracks increases the area which effectively carries the load in compression and the stiffness may then be partially or fully recovery [6]. Because this work will deal with the modeling of the ductile failure of plastic material under static loads, then, the micro crack closure effect will not be accounted for.
- **Isotropic Damage:** Due to the anisotropic nature of plastic materials, the damaging process of components, when submitted to mechanical loads, does not evolve isotropically, i.e., the resulting strength, after the nucleation of micro voids and cracks, is direction dependent in general [6]. However, in many practical cases, the anisotropy induced by the damage process may be neglected, resulting in good agreement with experimental data.

1.5. BIBLIOGRAPHICAL REVIEW

In order to improve the understanding of this bibliographical review, this section will be subdivided into three parts. In the first subsection, one will be introduced the existing references related to components design. In the next subsection, one will be introduced the main references related to the viscoplastic modeling of plastic materials proposed in the literature. Lastly, one will introduce the most relevant damage models proposed in the literature to describe the degradation processes of plastic materials.

1.5.1. Design of Plastic Components

Similarly to any industrial product, plastic components also undergo a sequence of processes relating to the stages of their development, which range from their conception up to their launching into the market [7]. Although there are several design methodology proposals, each with its own peculiarities, one notices that all have similar elements and can be summarized according to Figure 1.1, proposed by Ogliari [8].

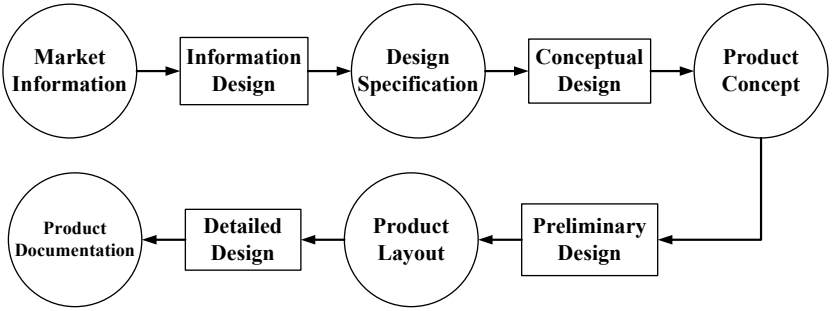

Figure 1.1: Consensual model for design of products [8].

As is illustrated in Figure 1.1, the product design process starts with the **informational design**, in which one defines the customer needs, requirements and design specifications and restrictions. Following, one develops the **conceptual design** phase, in which one defines the conception that best meets the design specifications. Completed the conceptual design phase, the following one is the **preliminary design** phase. The main activities of this phase are: choice of the best solution, defined in the conceptual design phase; mathematical calculations; analyses and numerical simulations; definition of dimensions and tolerances; materials selection; CAD[4] modeling, prototyping and functional tests. As a consequence, the main outcome of this phase is the final drawings of the component, so that it can be materialized in the **detailed design** phase and, then, launched into the market [7].

Within the preliminary design phase, it is introduced the **mechanical design** of the component [7]. This activity is responsible for dimensioning the component, so that it fulfills either its mechanical strength or manufacturing requirements, and it is composed by the following tasks: material selection, CAD modeling and numerical simulations (stress-strain and moldability analyses), by means of commercial softwares. Figure 1.2 illustrates a sequence of steps for the preliminary design phase of plastic components, proposed by Daré [9]. Because this present work is intended to assist the design of plastic components, then, in this context, it will be introduced in the stress-strain analysis step of the preliminary design phase, according to Figure 1.2.

[4] CAD stands for **Computer Aided Design**. CAD systems are computational tool, used to aid the design and drafting (technical or engineering drawings) of a component or system. The design obtained from the CAD tool is usually named **virtual prototype** of a component or system.

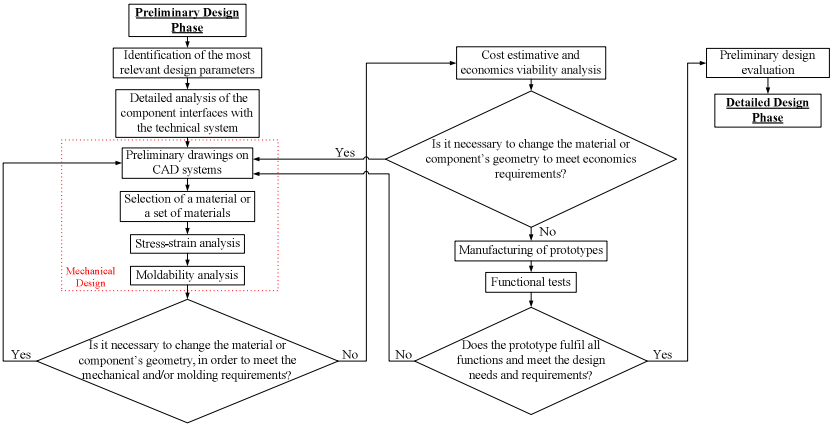

Figure 1.2: Preliminary design phase proposed by Daré [9].

Currently, most references on stress-strain analysis of plastic components are regarded to fatigue failure, because, according to Gotham [10], 70% of premature failures are attributed to the fatigue phenomenon. In general, these references have been based on: design recommendations, empiric practices and proposition of models, based on the fracture mechanics approach. In this case, the residual life of a component is determined by considering the propagation of an existing crack. In practice, this situation is not that unusual, because plastic components are not totally free of defects, mostly originated in the manufacturing process. Thus, these defects may work like an initial damage.

Whatever the approach used to determine fatigue life, the crack nucleation phase, which represents, approximately, 95% of the component life, has been neglected [10]. In this case, one performs an unreliable and poor evaluation about the component life. Due to its importance, one recommends that the crack nucleation phase should not be despised. This may be circumvented by proposing appropriate models, which describe the damaging processes of the material.

In terms of a practical application, Krishna [11] has developed analytical models, based on elastic constitutive relations, for dimensioning plastic automotive instrument panels, submitted to monotonic loads and cyclic variations of temperature. The reliability of the models proposed by Krishna [11] is unknown, since this work does not provide any experimental tests or data that could be used to validate the models and does not account for the viscous behavior of plastic materials.

In contrast with the analytical propositions of Krishna [11], most structural analyses of plastic components have been performed by means of commercial softwares, based on the finite element method, i.e., CAE systems. According to Malloy [12], the main advantages of these tools are the constitutive models available for modeling many different kinds of material behavior, including plastics. This results in a more reliable assessment of the component performance. But, on the other hand, most of these models require the knowledge of unknown material parameters, which, in many cases, must be identified by means of non-standardized tests. Due to this difficulty, one uses to accomplish the analysis empirically, i.e., one uses a trial and error approach: the designer models the components with a non-representative model, one performs a static stress analysis and one tries to keep the maximum von Mises stress less than an equivalent stress, which is obtained by dividing the yield stress of the plastic material by a safety factor, as has been explained previously.

In many cases, the empiric way in which the design of a plastic component is performed leads to the production of over-dimensioned components with, consequently, high cost and weight. It is worth emphasizing that, currently, this is still a very common practice in the main automotive and aeronautics companies, though they have powerful numerical tools.

In engineering designs, the use of safety factors is very common. Informally speaking, Krishnamachari [13] defines safety factors as "factors of ignorance" and they are sized proportional to the fear of the unknown. These safety factors cover the design against the gap between real life and the idealized models of analysis as well as the several non-quantifiable factors of design [14].

According to Krishnamachari [13] and Mascarenhas *et al.* [14], the choice of safety factors should be based on the material behavior, cost concerns, service conditions and the state of the art of design, analysis and processing. These factors may be differently sized for different products, materials, as well as failure modes. Thus, based on these aspects, Mascarenhas *et al.* [14] provide some safety factors recommendations for design of plastic components.

1.5.2. Elasto-Viscoplastic Models

According to Lemaitre and Chaboche [15], elasto-viscoplasticity is the theory responsible for describing the inelastic behavior of strain rate sensitive materials, like plastics. In practice, this theory can be used to calculate permanent deformations and predict plastic collapse of structures, investigate stability or calculate forces required in forming

operations, like thermoforming[5] and vacuum forming[6] processes. In order to apply this theory, one needs to define a yield function, which is responsible for establishing the onset of the inelastic behavior. Usually, the definition of the yield function depends on the material in study.

One knows that plastic materials are much more sensitive to compressive loads than metals. As a consequence, their behavior under tension and compression are distinct. Thus, one recommends using yield functions which take the influence of the hydrostatic part of the stress tensor into account. In this regard, Quinson *et al.* [16], Goldberg *et al.* [17] and Rottler and Robbins [18] have proposed yield functions based on the Drucker-Praguer proposition, also known as modified von Mises yield criterion. Currently, this is the most used proposition.

A new yield function, based on an exponential dependence between the mean stress and the von Mises equivalent stress is proposed by Altenbach and Tushtev [19]. This criterion is expressed as a function of the ratio of failure stresses in uniaxial tension and compression. Two material parameters are also introduced and their identification may be simply determined by means of tensile and compressive tests. The validity of this proposition has been demonstrated by experimental data and one has obtained good agreement. Because the simplicity of the modified von Mises yield criterion, this will be the proposition adopted in this work.

The literature on elasto-viscoplastic models is very extensive. These works have been developed under various considerations or, in some cases, developed to a specific type of material, due to its great demand or importance in the industrial medium. The most common approach is based on a thermodynamic framework with state variables, in which one postulates the existence of a thermodynamic potential, from which the state laws are derived. Other theories, such as viscoplasticity based on overstress (VBO) and cooperatively rearranged regions (CRR) are also used.

The VBO is a rate-dependent unified state variable theory with no yield criterion and no loading/unloading conditions. It consists of two tensor valued state variables: the equilibrium and the kinematic stresses and two scalar valued state variables: isotropic and drag stresses [20]. This approach has been first introduced by Krempl and Ho [20] to model

[5] **Thermoforming** is a manufacturing process, in which a plastic sheet is heated to a malleable forming temperature, formed to a specific shape in a mold and trimmed to create the final product. The sheet is heated in an oven to a high enough temperature, so that it can be stretched on a mold and cooled to the final product shape [12, 21].

[6] **Vacuum forming** is a simplified version of thermoforming process. In this case, the plastic sheet is heated to a forming temperature, stretched on a mold and held on it by applying vacuum between the mold surface and the sheet. This process is usually used to forming plastic components that are rather shallow in depth [12, 21].

metallic materials and, lastly, it has been modified by Krempl and Ho [22] to improve the modeling capabilities of VBO for plastic materials analysis. These authors have specifically named this improved model as **viscoplasticity theory based on overstress for polymers** (VBOP). Thus, under the VBOP approach, one can highlight: Krempl and Ho [22], Colak and Dusunceli [23] and Colak [24].

In the cooperatively rearranged regions theory, the meshing between polymer chain segments limits the rate at which the segments can move under the influence of an externally applied load [25]. In order to illustrate this mechanism, Riesen and Schawe [26] give a practical example. The authors associate this mechanism to a crowded bus. During the trip, the passengers are standing close together and can not move. If someone has to get off at a bus stop and is carrying a large bag, then a number of passengers will have to move together, i.e., cooperatively, to make this possible. A little additional free space is also needed to increase mobility – maybe someone next the door has to leave the bus. Thus, the bus passengers experience a series of cooperative rearrangements. Under this theory, one can highlight: Frank and Brockman [25], Drozdov [27] and [28], Drozdov and Yuan [29] and Drozdov and Gupta [30].

According to Frank and Brockman [25], the CRR approach assumes that the deviatoric part of the viscoplastic strain rate tensor, $\dot{\boldsymbol{\varepsilon}}^{vp\,D}$, is proportional to the deviatoric stress tensor, $\boldsymbol{\sigma}^{D}$, i.e.,

$$\dot{\boldsymbol{\varepsilon}}^{vp\,D} = \bar{\lambda}\boldsymbol{\sigma}^{D} . \tag{1.1}$$

In this case, the factor of proportionality, $\bar{\lambda}$, is defined in terms of the second invariant of the deviatoric stress, J_2, and the flow resistance, Z, i.e.,

$$\bar{\lambda} = \frac{D_o}{\sqrt{J_2}}\left(\frac{3J_2}{Z^2}\right)^n , \tag{1.2}$$

in which, D_o is the limiting viscoplastic deformation and n is a material parameter. High values of n (around 1000 or more) provide nearly rate-independent behavior.

The VBOP theory, proposed by Krempl and Ho [22], consists of a flow law that is easily adapted to cases, in which the strain or the stress is the independent variable and it is given by

$$\dot{\boldsymbol{\varepsilon}} = \dot{\boldsymbol{\varepsilon}}^{e} + \dot{\boldsymbol{\varepsilon}}^{vp} = \frac{(1+\nu)}{CE}\dot{\boldsymbol{\sigma}}^{D} + \frac{3}{2} f\left(\frac{\Gamma}{\bar{D}}\right)\left(\frac{\boldsymbol{\sigma}^{D} - \boldsymbol{g}}{\Gamma}\right), \tag{1.3}$$

in which, $\boldsymbol{\sigma}^{D}$ and $\boldsymbol{g}$ are, respectively, the deviatoric part of the Cauchy stress tensor and the equilibrium stress. Additionally, E and ν are the modulus of elasticity and the Poisson ratio and the variable C is given by

$$C = 1 - \lambda\left(\frac{|\boldsymbol{G} - \boldsymbol{K}|}{A}\right)^{\alpha} \tag{1.4}$$

so that, λ and α are material constants and $\boldsymbol{G}$, $\boldsymbol{K}$ and A are, respectively, the equilibrium, kinematic and isotropic stresses. Moreover, Γ is the invariant of the overstress, given by

$$\Gamma^{2} = \frac{3}{2}\left[\left(\boldsymbol{\sigma}^{D} - \mathbf{g}\right)\cdot\left(\boldsymbol{\sigma}^{D} - \mathbf{g}\right)\right] \tag{1.5}$$

and the function $f\left(\Gamma/\bar{D}\right)$ is given by

$$f\left(\frac{\Gamma}{\bar{D}}\right) = B\left(\frac{\Gamma}{\bar{D}}\right)^{m} \tag{1.6}$$

in which, B and m are material parameters and $\bar{D}$ is the drag stress.

In this approach, the flow law depends on the overstress and the difference between the stress and the equilibrium stress, in which this latter variable is established as one state variable of the problem. The growth law of the equilibrium stress, in turn, contains the kinematic stress and isotropic stress, which are two additional state variables of VBOP. The authors have concluded that VBOP is the most appropriate approach to model the inelastic behavior of most solid polymers.

Colak and Dusunceli [23] have proposed a constitutive model to predict the viscoelastic and viscoplastic behavior of high density polyethylene (HDPE) based on the VBOP approach. In such work, the viscoelastic modeling capabilities are investigated by simulating the behavior of HDPE under uniaxial compression tests at different strain rates. The viscoplastic flow used depends only on the second invariant of the deviatoric part of the stress tensor, i.e., J_2. The simulation results are compared with the experimental data obtained in the literature and a good match has been observed. This proposition seems interesting, but it needs

to identify a large number of material parameters (nearly 13) and it does not account for the influence of the hydrostatic part of the stress tensor. In turn, Colak [24] has applied VBOP theory to model the inelastic behavior of polymeric materials under different loading conditions. In this study, the uniaxial stress-strain diagrams of Polyphenylene Oxide (PPO), obtained in the literature, have been used to identify the material constants of the model. This work has revealed that the nonlinear rate sensitivity, unloading behavior and creep are very well reproduced with VBOP approach.

In recent studies, Frank and Brockman [25] have developed a phenomenological constitutive small strain model, in order to simulate the multi-axial response of glassy polymers. This modeling, based on the cooperatively rearranged regions theory, has combined nonlinear viscoelasticity and viscoplasticity using the general framework of irreversible thermodynamics. The authors have checked the validity of the model by testing glassy thermoplastics, as polycarbonate (PC), and showed that the model accurately predicts the small strain behavior for monotonically increasing strains under tension, but it does not well agree with the experimental results for creep and relaxation tests. Also, under the cooperatively rearranged regions theory, Drozdov and Christiansen [31] have proposed a constitutive model, using the thermodynamic framework approach, to model cyclic viscoplasticity of high density polyethylene (HDPE). According to the authors, this material has been considered, due to its numerous industrial applications.

Developed under a thermodynamic framework with state variables, Ghorbel [4] has proposed a viscoplastic model, based on a new yield criterion. This new proposition is derived from the Drucker-Praguer criterion, in which one includes the first invariant of the stress tensor (I_1) and the second (J_2) and third (J_3) invariants of the deviatoric stress tensor. According to the author, the introduction of J_3 means that the forces needed to activate intermolecular and intramolecular mobility are more important in tension and/or compression than in shear, since the stress, necessary to activate the plastic flow, is lower in shear than in tension and/or compression.

The importance of including J_3 in the yield criterion has been outlined by Lee and Ghosh [32]. These authors have affirmed that if the plastic material is submitted to a twist, then the deformation involves both pure shear and rotation. Hence, three basic deformation mechanism occur: dilatation, characterized by I_1, pure shear, characterized by J_2, and rotation, characterized by J_3. Thus, the authors recommend that these three invariants are introduced in the model.

A thermodynamic framework linked with the VBO theory for anisotropic materials and small strains is presented by Hall [33]. This approach indicates that the stress rate-dependent established in the growth law for the equilibrium stress can not contribute to the dissipation and is, therefore, referred as the elastic equilibrium stress rate. Ghorbel [4] has presented a detailed and very critical review on the main viscoplastic models and yield criteria proposed in the literature. In this study, the proposed modeling has exhibited a good agreement with experimental data from monotonic loading conditions. On the other hand, for cyclic loading, discrepancies have been observed during the unloading path. The author attributes these differences to the experimental process used for the identification of the material parameters, especially those of the hardening law.

1.5.3. Damage Models

According to Fatemi and Yang [34], the damage theories can be classified into six groups: linear damage, nonlinear damage curve, life curve modification methods, approaches based on crack growth concepts, continuum damage mechanics models and energy-based theories. In the industrial medium, the most used damage model is the Palmgren-Miner linear law. This criterion states that if a mechanical component is submitted to a loading spectrum, such that depicted in Figure 1.3, then the accumulated damage (D) can be determined by

$$D = \sum_{i=1}^{k_b} \frac{n_i}{N_i}, \tag{1.7}$$

in which, n_i is the number of cycles of the *i-th* loading block (Figure 1.3), N_i is the total number of cycles associated with failure at the stress level of the *i-th* loading block, obtained from *S-N* diagram and k_b is the number of loading blocks. According to this criterion, the failure will occur when $D = 1$.

Basically, the Palmgren-Miner model has two limitations: it does not recognize the probabilistic nature of the fatigue phenomenon and it is not sensitive to the load sequence effect. In this case, the measure of damage is simply the cycle ratio with basics assumptions of constant work absorption per cycle and characteristic amount of work absorbed at failure [34, 35].

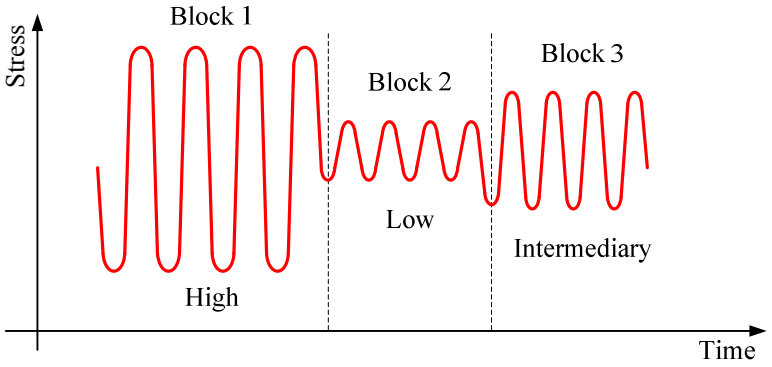

Figure 1.3: Example of a cycling loading spectrum [36].

Despite its limitations, the Palmgren-Miner law has been extensively used as a preliminary orientation. One recommends that this law is used, bearing in mind its limitations and scattering related to the fatigue phenomenon. A very usual recommendation for designs of mechanical components is to adopt $D = 0.3$, for those cases where there is no previous experience [1, 15]. In the automotive industry, one uses to adopt $D = 0.17$ for suspension components and $D = 0.4$ for body components.

The modeling proposed in this work will be based on the continuum damage mechanics approach. According to Lemaitre [1], this approach studies the mechanisms involved in the deterioration of the material, by means of mechanical variables, when it is subjected to external loads. The development of this approach began in 1958, when Kachanov published the first paper on creep failure of metallic materials under uniaxial loads. Since then, damage mechanics has been in development and applied to describe the deterioration processes of various kinds of materials [1].

Currently, most damage models proposed for plastic materials have aimed at describing the degradation processes or determine component life when submitted to fatigue loading, due to its frequent incidence. In this regard, one can highlight the works of Tang and Lee [37], Tang and Plumtree [38], Jie *et al.* [39], Vinogradov and Rassi [40] and Tang *et al.* [41].

In their works, Tang and Lee [37], Tang and Plumtree [38] and Tang *et al.* [41] have proposed both one and two-dimensional damage mechanics based models for describing the decreasing in elastic properties of plastic materials. These authors have performed several tensile tests with Polystyrene (PS) and High Impact Polystyrene (HIPS),

in order to determine the material parameters of the model. In these tests, the authors have noticed that PS has behaved predominantly elastically, whereas HIPS has showed great amount of irreversible strains. The tests have demonstrated good relation with the numerical results and occurrence of anisotropic damage in these materials, even under uniaxial loading.

Vinogradov and Rassi [40] have proposed a damage model to characterize cyclic damage evolution of plastic materials, using a nonlinear constitutive material model. This study is based on the principles of continuum damage mechanics combined with the theory of linear viscoelasticity and the damage evolution law is defined in terms of a linear damage function, which depends on the number of loading cycles.

It is not always possible to obtain plastic components free of defects derived from the manufacturing process. Some of them can even exhibit a high degree of crazing or shear bands. Based on this possibility, Jie *et al.* [39] have presented a model which can predict the evolution of the damage and the energy dissipated in this process. In this work, a mathematical model is proposed by adopting the fibril creep mechanism. Moreover, one considers that the viscoelastic characteristics of the craze fibrils are supposed to obey the Maxwell model and the craze fibrils are assumed to be compressible. Despite the simplicity of the viscoelastic model adopted (Maxwell), the authors have obtained good results, when compared to experimental data.

Zaïri *et al.* [42] have proposed constitutive equations to describe the elasto-viscoplastic damage behavior of polymers. The behavior is well accounted for by a modified Bodner-Partom model, comprising hydrostatic and void evolution terms. Basically, this modeling is mainly based on internal variable inelastic theory supported by phenomenological and micromechanical considerations. According to the authors, successful agreement is obtained between the experimental data and the numerical results obtained with the use of the proposed model.

A damage model developed under the cooperatively rearranged regions theory is proposed by Drozdov [43]. In this work, the damage of the material is modeled as breakage of van der Waals forces between monomeric units. This mechanism takes place when the nominal strain, in a relaxing region, exceeds some threshold level. A good agreement is demonstrated between results of numerical simulations and experimental data for a polycarbonate grade.

As has been assumed in this work, the assumption of isotropic damage is also extensively applied by many authors to model, not only the damaging process of plastics and polymers, but other kind of materials, such as concrete, geomaterials, paper, etc. According to

Isaksson *et al*. [44], isotropic damage means that both the degradation of the elastic stiffness and the damage growth rate depend on a single parameter, D. In turn, for a general anisotropic damage representation, a fourth order damage tensor is required.

One has observed that the main reason why isotropic damage assumption is widely used has been the high number of material parameters involved, when assuming anisotropy. Since these parameters must be identified experimentally, then their identification may become quite difficult. Despite the limitations of this assumption, good agreement with experimental results has been obtained. This peculiarity has been demonstrated by Isaksson and Hägglund [45], Challamel *et al*. [46], Costa Matos and Sampaio [47] and Hägglund and Isaksson [48], among other references.

Isaksson and Hägglund [45] have evaluated and compared the numerical and experimental strain field at a crack-tip of a pre-fabricated crack on a low density paper material. The authors have observed that the experimental measured normal strain is about 60% higher than the computed strain, when using exclusively an elastoplastic J_2 theory coupled with damage. In order to have better predictions, the authors used a nonlocal damage theory and the numerical results have exhibited good agreement with experiments.

A simple time-dependent softening model applied to quasi-brittle materials (rocks and concrete) has been proposed by Challamel *et al*. [46]. This visco-damage model has been developed under a thermodynamic framework and is intended to describe phenomena, such as relaxation, creep and rate-dependent loading effect. According to the authors, one of the most peculiar features of the model is its ability to predict creep failure under high sustained load. A theory for modeling the degradation and fracture of elastic structures is presented by Costa Matos and Sampaio [47]. This theory permits the modeling of different types of materials, such as ceramics, concretes, glasses, etc. The main advantage of this approach is the simplicity in which the material constants of the constitutive equations can be identified experimentally.

Also based on the isotropic damage assumption, Hägglund and Isaksson [48] have developed a damage model for describing the in-plane fracture behavior of embossed low-basis-weight paper. In this work, the assumption of isotropic damage is motivated by that the paper webs produce an approximately uniaxial stress field and, therefore, it is believed that an orthotropic material description does not significantly improve the predictive capability of the model. The authors have observed that the proposed model is capable of capturing the development of damage in rows parallel to the main crack and compares well with experimental results.

The isotropic damage assumption has been widely applied to model different kind of materials. When working with material modeling, one must bearing in mind that a balance between accuracy and practicality must exist. This means that some diversions from a generally correct, but detailed physical model should be tolerated and motivated by the tractability of the model. Therefore, based on these considerations, this work will also assume isotropic damage.

One could also observe that most damage models proposed for plastic materials have been based either on a linear damage law or on the continuum damage mechanics approach. In general, damage is associated with accumulation of inelastic strains in the neighborhood of defects or interfaces. In plastic materials, damage occurs by the breakage of bonds that exist between the long chains of molecules, due to accumulation of viscoplastic strains [1]. This mechanism leads to the formation of shear bands and crazes, which may evolve to a crack. Thus, in order to predict the degradation processes in plastic materials, an elasto-viscoplastic model, with coupled damage must be developed.

This bibliographical review has revealed that most proposed models in the literature do not exhibit the coupling between viscoplasticity and damage and among the few viscoplastic model coupled with damage, none gives especial attention to phenomena, such as cold-drawing and proper ductile failure. In many cases, this may lead to an unreliable evaluation of the degradation processes of the material. In this work, by analyzing the performance of plastic components submitted to monotonic loading up to its ductile failure, one will propose a viscoplastic model coupled with a nonlocal damage. As a consequence, a system with two coupled differential equations will be established, in which one of these equations will describe the evolution of the degradation processes of the material, by means of the damage variable, and the other the equilibrium of the linear momentum equation. In practice, this model may be suitable to assist the structural analysis of real components and, then, to help to produce cheaper and lighter components.

1.5.4. Final Remarks

In the previous sections, one has discussed the main recent studies on the design of plastic components and proposed viscoplastic with damage models, applicable to plastic materials. Some of the most noticeable characteristics of these works are: the empiricism, which has driven the design of plastic components, the decoupling between damage and elasto-viscoplasticity and the assumption of isotropic damage. Additionally, it is very noticeable that due to the lack of appropriate and

consistent constitutive material models, the empiric approach has still been extensively used, for example, in the main automotive and aeronautics companies.

Based on the previous considerations, this work aims at proposing a computational tool, to be used in the structural analysis of plastic mechanical components submitted to ductile failure. Because the damaging process is usually associated with accumulation of inelastic strains, then, this tool will be basically composed by an elasto-viscoplastic with coupled damage model, in order to describe the evolution of the inelastic strains and the damaging processes of the material. As usual, some assumptions and hypotheses have been considered, so that the model equations have been readily obtained, solved and implemented. Moreover, the development of tests, to obtain the material properties and parameters required by the models, will also be part of this objective. One considers that the main motivation of this work is the empiric way, in which the design of a plastic component has been performed, which has led to the production of over-dimensioned components with, consequently, high cost and weight.

1.6. OUTLINE OF THE WORK

In order to better understand the topic studied, this work has been divided into eight chapters, according to the following description.

In **Chapter 1**, this in discussion, one has outlined the main directions of this work. Initially, one has established that this work is focused on the study of mechanical strength analysis of plastic components submitted to ductile failure. Following, one has presented a bibliographical review on this subject, including the currently propositions for predicting the evolution of the inelastic strains and the degradation processes of plastic materials.

Chapter 2 presents a review on the main concepts, characteristics and properties of the plastic materials. This chapter ends with a discussion regarding the main factors which affect the resistance of components and their main mechanism of failure. In **Chapter 3**, one discusses the constitutive laws for damaged media, in which the first and second laws of the thermodynamics will be rewritten to account for the damaged variables. Moreover, the method of local state will also be discussed. **Chapter 4**, presents the proposed viscoplastic coupled with a nonlocal damage model.

In **Chapter 5**, one performs the discretization of the proposed model. One applies the finite element method in the discretization of the geometric domain and employs a fully implicit Euler method, which

consists in the usage of an implicit finite difference method in the discretization of the time domain.

In **Chapter 6**, one discusses the development of the experimental procedures and the results obtained. **Chapter 7** presents the numerical results and addresses with the experimental data. Lastly, in **Chapter 8**, discusses the final considerations of this thesis. This chapter presents also a critical analysis of the models and results obtained previously, a conclusion and some suggestions for future works.

CHAPTER 2

PLASTIC MATERIALS: AN OVERVIEW

The objective of this chapter is to provide nonspecialists in polymers and plastics a general idea on their most important peculiarities. In this regard, this chapter will approach their classifications, main properties, behavior and singular failure modes. The knowledge presented in this chapter is necessary, so that the reader is aware of the considerations upon which the development of the constitutive model described in Chapter 4 will be based. The reading of this chapter may be dispensable for those readers who have been familiar with the topics discussed here.

2.1. DEFINITION OF POLYMERS

Plastic materials belong to the organic materials group named **polymers**. This denomination comes from the union of the Greek words *πολυ* (*polu* - many) and *μέρος* (*meros* – part) and is used to refer to the chemical compounds with high relative molecular weight. In other words, polymers are long-chain molecules of inorganic materials or carbon-based compounds made up of thousands of *meros*, joined together by covalent bonds formed through chemical reactions known as **polymerization**[7] [12, 49]. Figure 2.1 illustrates, for example, the *mero* vinyl chloride from which the Polyvinyl Chloride (PVC) stems. In this figure, *n* represents the degree of polymerization, i.e., the number of repeating unit which forms the long molecule chains of PVC.

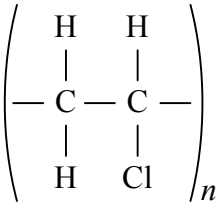

Figure 2.1: *Mero* from which PVC stems [50].

[7] **Polymerization** is a process of reacting monomers molecules together in a chemical reaction to form three-dimensional networks or polymer chains. In turn, **monomers** are small molecules that may become chemically bonded to other monomers to form the long chain molecules of a polymer [12, 21, 49].

Although polymers are soft and moldable materials and behave like a fluid when heated, these materials remain solid in their finished state. As more repeating units (*meros*) are added, the molecular weight of the material increases, what become the molecule heavier. The mechanical and physical properties are directly related to the bonds among molecular chains, as well their length and composition [51].

2.2. CLASSIFICATIONS

There are several different ways to classify polymers. Probably, the classification according to their mechanical characteristics is the most important and the most common way. Actually, this classification originates from the specific configuration of polymer molecules. Under this aspect, polymeric materials can be classified as: **thermoplastics**, **thermosets** and **elastomers**. In practice, one uses to designate thermoplastic as **plastic materials**. This same designation will be considered in this work, from this point on, i.e., every time the term plastic materials is referred, one knows that it is dealing with thermoplastic materials, which will be the material modeled in this work.

Based on the conformation or morphology of the polymeric chains, thermoplastic materials can be classified as: **amorphous**, **crystalline** and **liquid crystalline** [12, 50, 51]. These materials can still contain other materials, known as **additives**, whose main objective is to improve specific characteristics of the matrix material or reduce manufacturing and processing costs [49].

2.2.1. Thermoplastics, Thermosets and Elastomers

Thermoplastics are linear chain polymers, branched[8] or not, which can be repeatedly melted, i.e., they can be repeatedly recycled. Most thermoplastics are soluble in specific solvents and can burn under certain conditions. Softening temperatures, for potential recycling, vary with polymer type and grade[9]. Thermoplastics represent, approximately, 95% of the volume of polymeric material processed worldwide [12, 50, 51]. Some examples of these materials are: Polyamides, usually used to manufacture plastic gears, PVC, very used in pipes of the civil construction, Polypropylene (PP) and Polyethylene (PE), which are very used to manufacture simple household appliances, like pails, basins and electrical appliances covers and Polycarbonate (PC), whose the most

[8] Lateral extensions which can be constituted of the same repeating unit present in the main chain, formed during the polymerization of some bifunctional monomers as resulting of lateral bonds [49].

[9] This term means a specific kind of commercial plastic material.

popular applications are the manufacturing of transparent shields, lenses, CD and DVD media.

Structurally speaking, the thermoplastic molecular chains can be thought of as a series of independent and intertwined strings, resembling spaghetti, as can be observed in Figure 2.2.a. Moreover, these chains can be linear or branched, as can be observed in Figure 2.3.

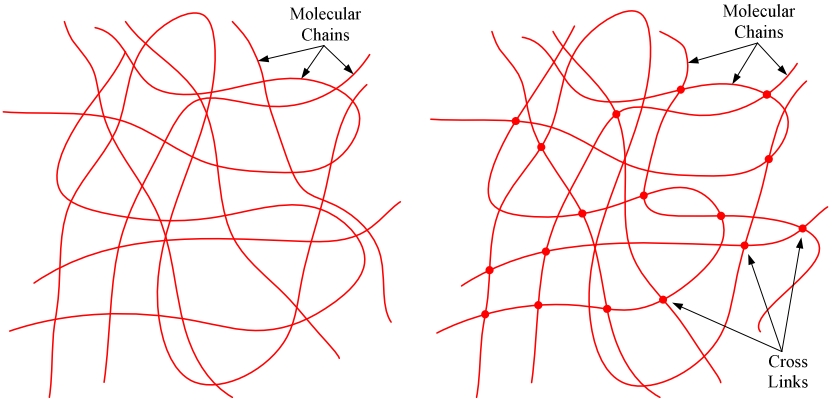

(a) *Thermoplastic* (b) *Thermoset*

Figure 2.2: Thermoplastics and thermosets molecular chains [39].

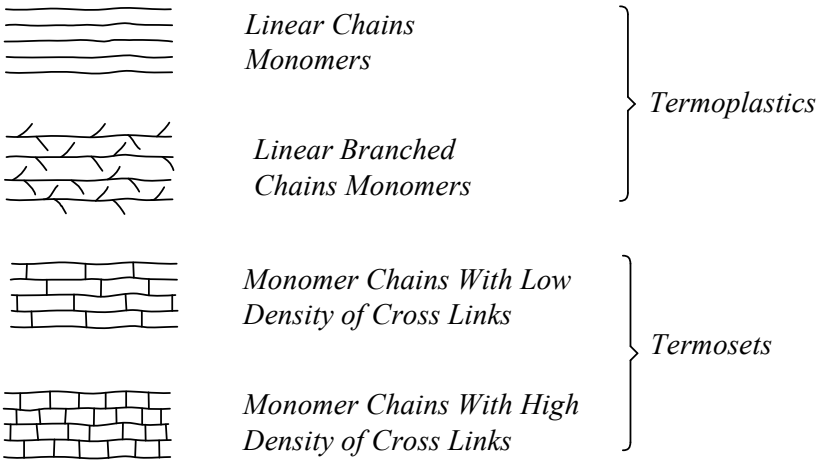

Figure 2.3: Kinds of molecular chains [52].

There still exists another kind of classification assigned to the thermoplastic materials, which has a more commercial connotation. This classification is defined, based on factors like costs, processing, production and thermal and mechanical performance. Thus, based on these concepts, the thermoplastic materials can also be classified as: **commodities**, **specials**, **engineering plastics** and **advanced engineering plastics** [49, 50].

Commodities are those with low cost, high production, easy to process and usually used to manufacture components under low levels of mechanical strength. These materials are equivalent to the low carbon steels of metallurgy (SAE1010, for example). High and Low Density Polyethylene (HDPE and LDPE), Polypropylene (PP), Polystyrene (PS) and Polyvinyl Chloride (PVC) are some examples of commodities. **Specials** distinguish themselves from commodities by the cost slightly higher and better mechanical properties. PTFE, usually used in situations where one demands good chemical and thermal stability, and PMMA and SAN, very used in applications where the main requirement is the transparency, are some examples of special thermoplastics [49, 50].

Engineering plastics are those usually used to manufacture components for applications where one demands excellent mechanical performance (gears and automotive components, for example). High ductility, good dimensional stability and good mechanical performance are the main peculiarities of this kind of material. Examples of engineering thermoplastic are: Polycarbonate (PC), ABS, Polyamides (PA), PET and others. The main characteristic of **advanced engineering plastics** is the great deal of aromatic rings in their molecular chain. This particularity helps to improve the thermal stability of the material, becoming, then, useful for application where one demands the uninterrupted use under very high temperatures. Due to this characteristic, this kind of material is usually applied to manufacture components, whose resistance to high temperatures and to the flame production are the main requirements. PPS and PEEK are some examples of advanced engineering thermoplastics [49, 50].

Thermosets are polymers that, when submitted to temperature and pressure, they soften and flow, taking the shape of the mold. The material reacts chemically in a process of cure, forming an insoluble and infusible three-dimensional molecular structure, physically linked by means of the cross links, as is illustrated in Figure 2.2.b. The main differences between thermosets and thermoplastics are the presence of these links, which join the extensive molecular chains, and their consequent response to thermal loads. Unlike thermoplastics, thermosets are not easily recyclable. When heated, thermosets do not return to its liquid state. In this case, the material is, then, degraded (burned) rather than melted [12, 49 - 52]. This

behavior is somewhat similar to a cooked egg. Further heating does not return the egg to its liquid state, it only burns.

In Figure 2.3, one may also observe that the three-dimensional network, which forms the thermosets molecular chains, can exhibit two configurations: with high and low cross-linking density. This will strongly influence the properties of the material. According to Huang [54], materials with high cross-linking density show very little creep and the impact strength is significantly lower than those of thermoplastics. This is caused by the cross links, which reduce the mobility of the molecular chains, so that the material becomes stiffer and, then, brittle. Bakelite, very used in electrical insulators, unsaturated Polyester, very used to manufacture water reservoirs and pools, and Epoxy resins are some examples of thermosets materials.

According to Canevarolo [49], **elastomers** are polymeric materials with high ductility which, at room temperature, can be extended, at least, twice their initial length. Their original dimensions are quickly retaken after removing the load. To present this characteristic, elastomers, usually, have flexible chains linked with one another, with low cross-linking density.

2.2.2. Amorphous, Crystalline and Liquid Crystalline Thermoplastics

The structure of the solid state in polymers is based on the way how the molecular chains are packed, forming the solid mass. This can be disorganized or organized, regular and repetitive. Thus, the degree of crystallinity in polymers consists in the alignment of segment chains in a perfect three-dimensional arrangement.

A thermoplastic material is named **amorphous**, if its molecular chains are arranged in a disorganized manner or entangled, as is shown in Figure 2.4. In practice, one uses to identify an amorphous polymer, observing if it is transparent. Polycarbonate (PC), Polystyrene (PS) and PMMA are some examples of amorphous materials.

When the polymeric chains of a material are arranged in an organized manner, it is common to name it as **crystalline**. But, one knows that the degree of crystallinity of a material never achieves 100%. Thus, it is more appropriate to name the material as **semicrystalline** or **partially crystalline**, as is shown in Figure 2.4. In this figure, one may observe that part of the polymeric chains is arranged in an organized manner (crystalline phase) and the other part is in a disorganized manner (amorphous phase) [12, 51]. The degree of crystallinity, i.e., the relative percentage of crystalline areas compared to the amorphous ones, is influenced by both the chemical structure of the polymer and by the

manufacturing/processing conditions; particularly the cooling rate of the molten material [12]. Polyethylene (PE), Polypropylene (PP) and Polyamide are some examples of semicrystalline materials.

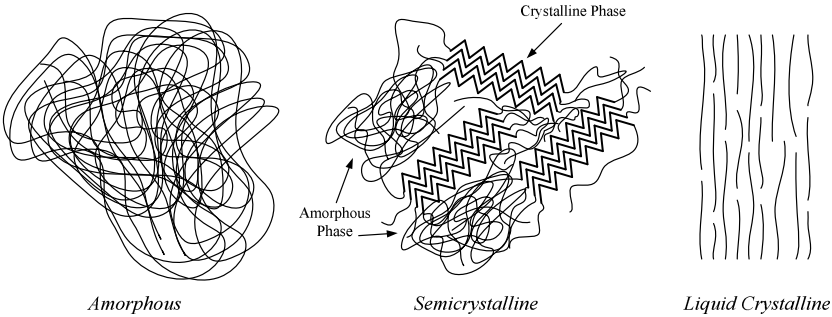

Figure 2.4: Two-dimensional representation of amorphous, crystalline and liquid crystalline structures [12].

Liquid crystalline polymers are characterized by having ordered, stiff and rod like molecular structure that form the parallel arrays or domains, as can be seen in Figure 2.4. These materials have the highest melt temperature among crystalline plastics and the lowest viscosity, warping and shrinkage of all thermoplastics. A good example of liquid crystalline polymer is Kevlar, which is a polyamide with very high tensile strength and is, usually, used to manufacture tire belts, bullet proof jackets and sporting materials [51]. More detailed information regarding these materials can be obtained in McChesney [53].

2.3. MAIN PROPERTIES OF PLASTIC MATERIALS

The properties of plastic materials are influenced by a series of factors, from which are included the kind of material, the processing conditions, chemical composition, morphology and molecular weight of the material. In this section, one will be discussed the main mechanical, thermal, electrical and rheological properties, along with some others, which are also important.

2.3.1. Mechanical Properties

The mechanical properties of a material are characterized by the way, in which these materials respond to the applied mechanical loads, which can either be stresses or strains. Basically, the nature of this

response depends on the chemical structure, temperature, loading time and processing conditions [49].

The mechanical behavior of plastic materials is quite different from that of other more traditional materials used in engineering. According to Huang [54], there are basically two reasons that become difficult the complete understanding on plastic materials behavior. First, engineering plastics are diverse, nowadays. There are, approximately, 70 different basic structures, each of which is available in up to 100 different grades from different suppliers. In addition, plastics can contain additive materials, increasing this number much more. Secondly, the testing methods for mechanical properties, which are generally made under conditions that are intended to be simple and uniform, do not agree with the situations, which the component might be subjected.

The most widely used testing method for obtaining mechanical properties of plastic materials is the tensile test, from which the stress-strain diagram of the material is obtained. Figure 2.5 illustrates two peculiar diagrams of plastic materials with two different behaviors: **brittle** and **ductile**. A ductile plastic material is characterized by exhibiting large strain before failure, which happens due to the relative movement among their molecular chains. On the other hand, a brittle material is characterized by exhibiting low strain before break, which happens due to the breakage of the molecular bonds [49]. Additionally, one also illustrates the evolution of the irreversible strains of the specimen. It is worth emphasizing that the classifications brittle and ductile are regarded to a certain temperature and strain rate, since the behavior of plastic materials is very sensitive to these variables. Properties such as modulus of elasticity, yield stress and strain, Poisson ratio, toughness and rupture stress and strain may be obtained from this diagram, since the toughness represents the area under the diagram up to the rupture of the specimen.

The ductile behavior of Figure 2.5 exhibits two regions: **elastic** and **viscoplastic** regions. In practice, the material exhibits a nonlinear elastic behavior, i.e., the resulting strains do not vary proportionally with the applied stress. When the material extends beyond its yield stress, inelastic strain localization regions appear in the form of micro shear bands, causing a **softening**. These bands multiply and combine, initiating a macroscopic plastic localization zone, commonly called **necking**. Once the neck forms, it extends along the gauge section at a fairly constant rate. The process by which the neck is extended along the specimen is called the **cold drawing** process, in which the polymer chains unravel, aligning themselves parallel to the direction of the applied stress. At point *C*, the molecular chains of the material have reached their maximum extensibility. From this point on, the material exhibits a **hardening**. The

additional strain, up to the failure point *F2*, is due to the growth of the bond distance among carbon atoms. Thus, atomically speaking, the failure happens when the attraction forces among carbon atoms decreases up to the point, in which they can no longer keep themselves together [5, 55].

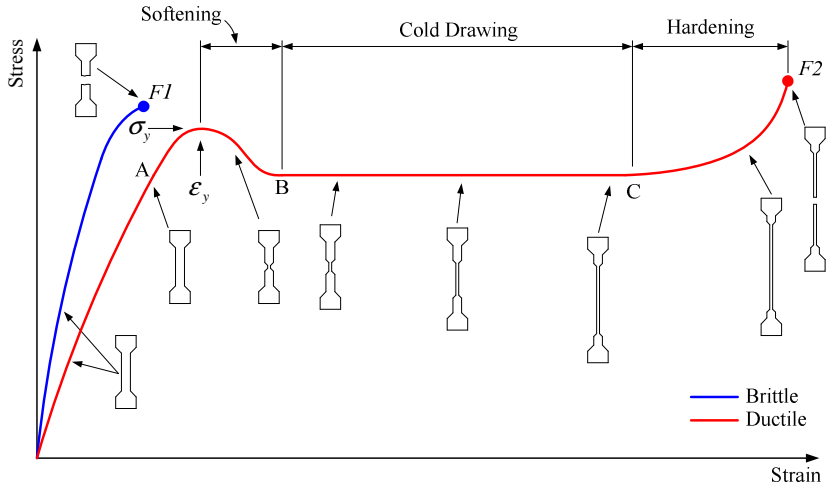

Figure 2.5: Typical nominal stress-strain diagrams for plastic materials [12, 51, 54].

When the plastic material is submitted to very low temperatures or high strain rates, it exhibits a brittle behavior, as can also be seen in Figure 2.5. In this case, the material exhibits little or no evidence of irreversible strains before failure. Figure 2.6 illustrates three specimens tested under different strain rates. As can be seen, at low strain rate, the specimen has exhibited very large irreversible strain, so that its gauge section has been totally stretched. In turn, at high strain rate, there have been no evidence of irreversible strain and the specimen has broken instantaneously. The third specimen has been tested under strain rate recommended by ASTM D 638 standard.

The molecular structure of a polymer gives rise to a viscous behavior, like liquids, superposed with an elastic behavior, like Hookean solids. This well-known phenomenon is called **viscoelasticity** and happens either in thermoplastic or thermosets. Elastomers, particularly, exhibit another phenomenon more peculiar named **rubber elasticity**, which involves large strains [49].

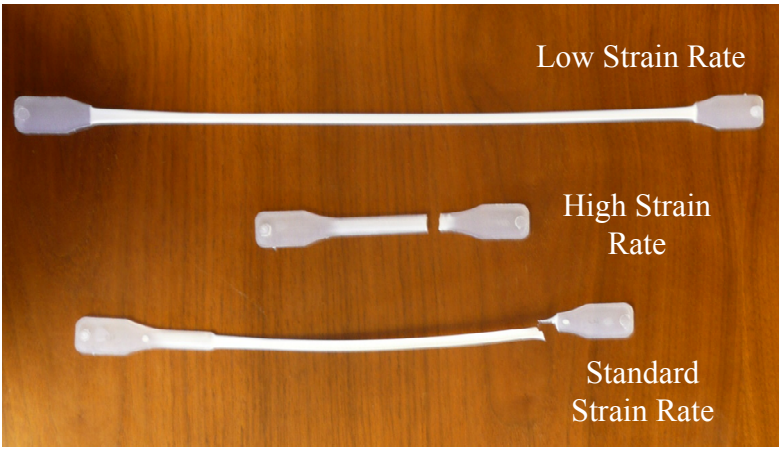

Figure 2.6: Material behavior under different strain rates.

According to Canevarolo [49], viscoelasticity is defined as the phenomenon for which the polymer exhibits characteristics of a fluid and an elastic solid, at the same time. The elastic fraction of the deformation appears due to the change of the angle and bond distance between carbon atoms of the polymeric chain. The viscous part appears due to the friction and the relative sliding of the polymeric molecules. Because of this part of the deformation, the material takes a finite time to respond to the load, generating a phase angle between the load and its response.

In a didactics attempt to represent physically the viscoelastic behavior of a polymer, it has been developed some analytical models, represented by an assembly of mechanical elements, which respond to external loads similar to those expected in the material represented. A spring is used as mechanical element to represent the elastic part of the deformation, since this element obeys Hooke's law. The viscous fraction is usually represented by a dashpot which follows a Newtonian behavior, i.e., the stress is directly proportional to the strain rate. The simplest and most commonly used analytical models are the Maxwell and the Voigt models [49, 56, 57].

As a consequence of the viscoelastic behavior, two phenomena may be identified: **creep** and **stress relaxation**. Creep takes place when a constant load is applied to a plastic component. Initially, it exhibits an initial deformation quite similar to a Hookean solid, i.e., the component deforms elastically. After this initial deformation, the component will keep on deforming and might break after a certain time. On the other hand, stress relaxation is defined as a gradual decay in stress when the component is held under a constant strain [56, 58 - 61].

2.3.2. Thermal Properties

According to Canevarolo [49], the mobility of the molecular chains establishes the physical characteristics of the final product. This mobility is a function of the atomic agitation and it is proportional to the temperature. Hence, in order to understand the thermomechanical performance of a plastic material, it is important to know its physical-chemical characteristics: usually, plastic materials are processed under high temperatures when they behave like a viscous fluid and afterwards they are employed in commercial applications as a solid. Such variability of behavior is a characteristic that is frequently used, when selecting the best material for a specific application.

Generally speaking, plastic materials exhibit, at least, three transition temperatures, which characterize the change in material behavior, which are: **glass transition temperature**, **melt temperature** and **crystallization temperature**. Additionally, other important thermal properties are: coefficient of thermal expansion, thermal conductivity, specific heat and Vicat softening point.

The **glass transition temperature** (T_g) is defined as the approximate midpoint of the temperature range which, during the heating of a plastic material, from a very low temperature to higher values, results in significant molecular mobility of the polymeric chains of the amorphous phase, i.e., possibility of changing their configurations. Below T_g, the material does not have sufficient energy to allow relative movement among its molecular chains. Thus, one says that the material is characterized by being tough, hard and brittle, like glass.

The **melting temperature** (T_m) is defined as the approximate midpoint of the temperature range which, during the heating of the material the crystalline regions disappear, due to the melting of the crystallites. At this point, the energy of the system achieves a necessary level to overcome the secondary intermolecular forces among the chains of the crystalline phase, changing the material behavior from rubbery to viscous state. This transition only happens in the crystalline phase; however, it only makes sense to be applied in semicrystalline polymers.

When a semicrystalline material is cooled from its melted state, i.e., from a temperature over T_m, this material will achieve a state, so that an specific point within the polymeric melted mass, a large number of molecular chains will get organized regularly. This spatial organization allows the formation of a crystalline structure at that specific point. Molecular chains in other points will also be able to get organized, forming new crystals. This phenomenon happens in the whole polymeric mass, in which one produces the crystallization of the melted mass. The

crystallization may occur by two means: isothermically, when the temperature is quickly lowered up to a certain value, usually up to T_g, then it is held constant until the crystallization occurs totally. Besides that one, the crystallization may occur dynamically. In this one, the temperature is continuously reduced, usually under a constant rate, and the crystallization will occur within a temperature range. In this last case, one usually defines the **crystallization temperature** (T_c) as that, in which one obtains the maximum rate of crystallization. The isothermal crystallization is the most studied, but, in practice, the most important is the dynamic, because it is closer to the industrial processes [49].

Additionally to the three transition temperatures discussed previously, other thermal properties, like: **coefficient of thermal expansion**, **thermal conductivity**, **specific heat** and **Vicat softening point** are also used to characterize a plastic material.

2.3.3. Electrical Properties

Plastic materials have certain electrical properties that make them ideal for many electrical and electronic applications, like insulators components. But, these materials are not perfect insulators. Under some conditions, plastic materials may pass significant leakage current, either through the bulk of the material or across its surface [62]. The main electrical properties, used to characterize a plastic material are: **volume** and **surface resistivity**, **dielectric strength**, **dielectric constant**, **dissipation factor** and **arc resistance**.

Presently, most plastic components have been submitted to several kinds of external influence, at the same time. Mobile phones are typical applications, in which the plastic pieces are submitted either to mechanical loads, electrical currents or electromagnetic fields or temperature gradients. Specifically, in this application, besides the aesthetics and mechanical requirements, the plastic material must be selected to fulfill the electromagnetic and thermal requirements, as well. This is only one of the several examples, which demonstrate how important is to know and also to account for the thermal and electromagnetic properties of the material.

2.3.4. Rheological Properties

Rheology is the name given to the science, which studies the mechanics of deformable materials, enclosing either the noncompletely solid materials or the almost liquid ones [14]. The rheological properties are usually measured by means of apparatus known as **rheometers** or

alike and they are mainly used to provide some information on the material behavior during the filling and packing[10] phase, when the material is injected into the mold. Usually, the tests performed to obtain the rheological properties of plastic materials are performed under low shear rates, which do not agree with those rates produced during the injection molding process. Thus, these properties should be used carefully. The main rheological properties of a plastic material are: **viscosity**, **melt flow rate index** and **spiral flow**.

2.3.5. Other Properties

There are a variety of other properties that the designers should concern, when selecting a material for a certain application. In this regard, one can highlight: density, specific gravity, specific volume and flammability. Biological properties are also relevant in certain applications, as will be discussed later.

Density is the mass per unit volume of a material, whereas the **specific volume** is its reciprocal. **Specific gravity** is the density of a material divide by the density of water at 23 °C. In practice, these information are useful to determine weight and costs of a plastic component [51, 59, 60]. These properties may be determined by means of ASTM D 792 standard.

All plastic materials contract during a temperature transition from a molten state to room temperature as they cool down and solidify after being plasticized. As a result of this process, when designing a mold, it is necessary to make the core and cavity slightly larger, in dimension, than the finished component size. The difference in dimensions which exist between the mold and component is known as the **volumetric shrinkage**. Volumetric shrinkage can vary considerably, depending on mold geometry and processing conditions. For example, thin walled components exhibit less shrinkage than those with thicker walls. Usually, amorphous and liquid crystalline materials shrink less than semicrystalline materials [58].

Flammability of a plastic material defines its burning characteristics after ignition has started. According to Malloy [12] and Ticona [51], this characteristic is related to three distinct properties: combustibility, smoke generation and ignition temperature. These properties are important in electrical applications and other situations, where the material constitutes a significant percentage of the exposed

[10] In the injection molding process, after the cavity is totally filled, the material keeps cooling and turning into solid. Due to this cooling, the component shrinks. In order to compensate this shrinkage, more material is pushed into the cavity until the injection channel is totally frozen. This phase of the process is named **packing** or **compensation** phase and the pressure applied to push more material into the cavity is named **packing pressure** [63].

area of a defined enclosed space, like plastic panels used in the interior of an aircraft cabin [51]. The flammability resistance of most plastic materials can be improved using specific additives for this objective, known as **flame retardants**.

According to Michaeli [64], natural polymers, such as cellulose, are subjected to severe attack by microorganisms and can be easily degraded by them. On the other hand, synthetic polymers impose difficult to be degraded biologically. The resistance to microorganisms must be taken into account when selecting, for example, a material for manufacturing pipes, for civil construction or components for military use. In order to improve the resistance to microorganism and delay its biological degradation, one uses products known as **biostabilizers** or **biocides** [65, 64]. Data related to biological degradation of plastic materials should be provided by the material supplier.

2.4. THERMO-MECHANICAL BEHAVIOR OF PLASTIC MATERIALS

Compared to most metals, plastic materials properties tend to be very sensitive to temperature variations. A specific material can have performance totally distinct under different ranges of temperature. According to Malloy [12], plastic materials with good thermal stability are those with a low coefficient of thermal expansion and good mechanical performance over the range of temperatures associated with the application, i.e., they are able to maintain their dimensions tolerances when thermically loaded and exhibit little variations of their mechanical properties.

This is a very important concern, which demands total attention of designers, mainly when selecting a material for an application which involves properties change, due to temperature variations. One of the greatest consequences assigned to this behavior was the space shuttle Challenger disaster in 1986, which exploded 73 seconds into its flight. Before the liftoff, the ambient temperature was below rubber O-rings T_g, what made that they could not flex adequately to form proper seals between sections of the two solid fuel rocket boosters. Consequently, in its liftoff, the fuel leaked, causing the disaster [21].

Temperature affects mechanical properties by means of its influence on intermolecular interactions [54]. According to Huang [54], the effect of temperature on mechanical properties can be understood by examining the relationship between elastic modulus and temperature. Diagram *A* of Figure 2.7 shows a typical diagram of this relation. This diagram, in particular, is typical of amorphous material and one can notice that at temperatures below T_g, the material is rigid and glassy and

has a brittle behavior. At a critical temperature, or more appropriately over a narrow temperature range, the material starts to become flexible or leathery. This temperature is known as the glass transition temperature. When exceeding this temperature, the material becomes more ductile and with lower elastic modulus. At temperatures closer to T_m, its modulus drops and it behaves like a viscous fluid, flowing like a high viscosity liquid [12, 54].

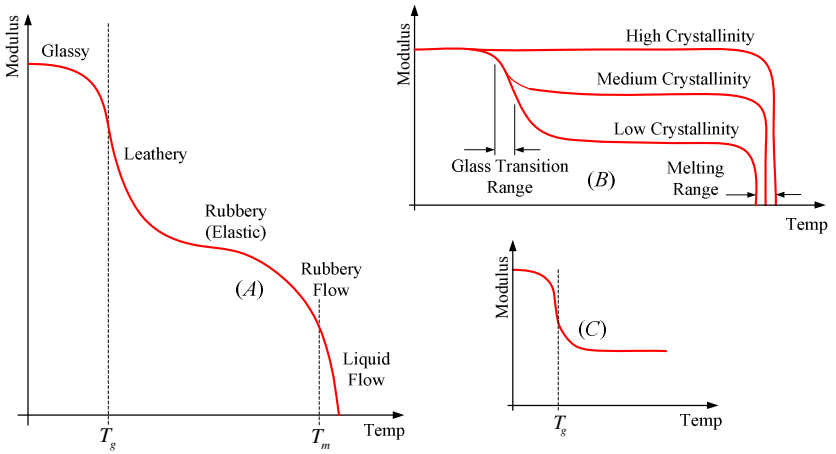

Figure 2.7: Elastic modulus versus temperature [12, 49, 54].

Figure 2.7 still illustrates the diagrams *B* and *C*, which are typical of semicrystalline and cross-linked materials, respectively. Unlike thermoplastics, the cross-linked materials, like thermosets, for example, do not become a viscous fluid when submitted to high temperatures, because their cross links restrict their molecular mobility. In this case, the material only suffers a thermal degradation, i.e., it burns. Diagram *C* of Figure 2.7 still shows that, even at high temperatures, the behavior and properties of these materials remain somewhat constant. This is a consequence of the restriction that the cross links impose on the molecular mobility. These peculiarities make that this kind of material suitable for applications at high temperatures. In practice, the diagrams of Figure 2.7 are usually obtained by means of DMA[11] tests.

As one has been defined earlier, the glass transition temperature is that, in which the molecular chains of the amorphous phase can move, i.e., can change their configurations. As semicrystalline materials have

[11] DMA stands for Dynamic Mechanical Analysis. See Attachment A (section A3) for more detail.

crystalline and amorphous regions (Figure 2.4), so these materials can or can not have a true T_g. This will depend on the percentage of amorphous phase in the material, as shows diagram *B* of Figure 2.7. As the percentage of crystalline phase increases, the material loses its ability to have a true T_g. In this diagram, one can also see that semicrystalline materials do have a true melting temperature, since this temperature is that, in which, when the material is heated, its crystalline regions disappear because the crystallites are melted. The crystalline regions remain relatively rigid at temperatures approaching T_m, whereas the amorphous regions have the same behavior at temperatures approaching T_g [12].

From Figure 2.7 and from the discussion presented previously, one may notice that the behavior and the properties of a plastic material can strongly depend on the temperature, as well as the strain rate. Figure 2.8 shows how both variables affect the behavior of a material and the shape of its stress-strain diagram. Thus, one must take a lot of care when performing tests to obtain properties of plastic materials. The temperature of the test environment must be controlled and the rate of loading must be in accordance with those described in the standards, so that the material behavior is not misunderstood. The tensile tests are usually performed by means of the ASTM D 638 or ISO 527 standards.

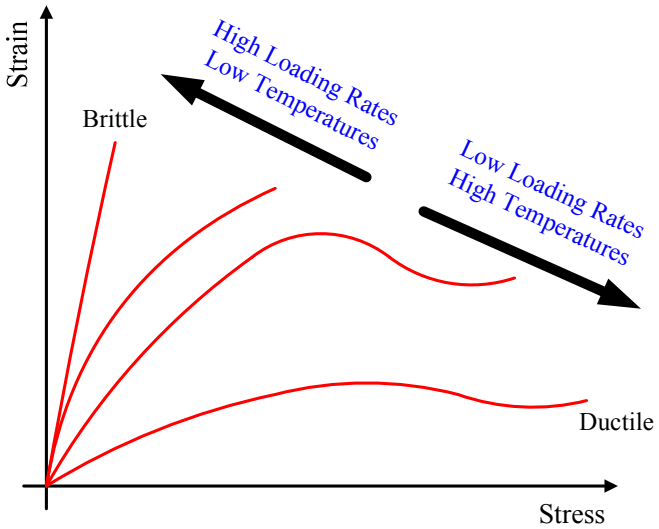

Figure 2.8: Diagrams which show the effect of the loading rate and the temperature on the behavior of plastic materials [12, 59].

2.5. FACTORS WHICH AFFECT THE STRENGTH OF PLASTIC PARTS

Besides the intrinsic characteristics of the selected material, other external influences can endanger the resistance and, even, the durability of a plastic component. In this item, one will be discussed the main factors, whose sources, be of human or environmental interferences, are able to change the functional integrity of a plastic component. Among these factors, one will be discussed: the influence of the processing, utilization of recycled material, water absorption (hygroscopy), the exposition to chemically reactive environments and to solar radiation (UV rays).

2.5.1. Processing

The inappropriate processing of a plastic material can significantly affect some of its mechanical properties, such as its impact strength and its elongation at break. If the material is improperly processed, the resulting mechanical performance of the component may differ significantly from those expected [59]. Basically, the processing can affect the resistance of a component by means of five mechanisms: voids, weld lines, residual stresses, molecular orientation and thermal degradation [12]. Voids and weld lines are defects very peculiar of the injection molding process.

Voids can be described as air bubbles which form inside the component. Its external surfaces cool and the material shrinks outwards, creating a hole in its center [51, 58, 66], as can be seen in Figure 2.9.

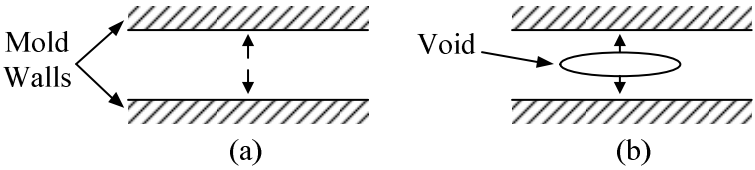

Figure 2.9: Void formation [12].

The arrows in Figure 2.9.a represent the forces acting inside the component, due to material shrinkage. Figure 2.9.b depicts the void formed inside the component due to its cooling. Voids can occur, mainly, because of the moisture in the material which has not been removed by a predrying and can contribute to the formation of crazing and, lately, nucleation of micro cracks, because this is a stress concentration area.

Weld lines are regions of the component where two or more melt flow front, after being separated, is combined. The presence of weld lines

is one of the most significant problems associated with designing plastic components for structural applications due to the potential failure in this area. According to Malloy [12] and Vianna and Cunha [67], weld lines can be caused by: (i) obstacles in the mold, like inserts; (ii) there are two or more injection points, as shows Figure 2.10; (iii) the component has variable wall thickness; and (iv) jetting[12]. Figure 2.11 exhibits details of the region where weld lines are formed, due to the presence of an obstacle (Figure 2.10.a) and presence of two injection points (Figure 2.10.b).

Weld lines reduce component strength because, during the filling of the cavity, they carry air, lubricants and other particles to the region where weld lines are formed. These particles and strange substances are introduced in the union and do not allow a good diffusion of the material, what can cause the drop in component strength. Thus, at the region where the flow fronts meet each other, two distinct regions are formed. According to Figure 2.11, one may notice both good and poor diffusion. This last area has a lack of molecular diffusion and a degree of unfavorable orientation, resulting from the fountain like flow behavior of the shocking melts fronts [12]. The degree of diffusion is maximum at the center of the component and decreases as one goes towards its surface. Rosato and Rosato [66] recommend that a surface which is submitted to loading bearing should not contain weld lines; if this is no possible the allowable working stress at weld lines regions should be kept, at least, 15% of the admissible stress of the material.

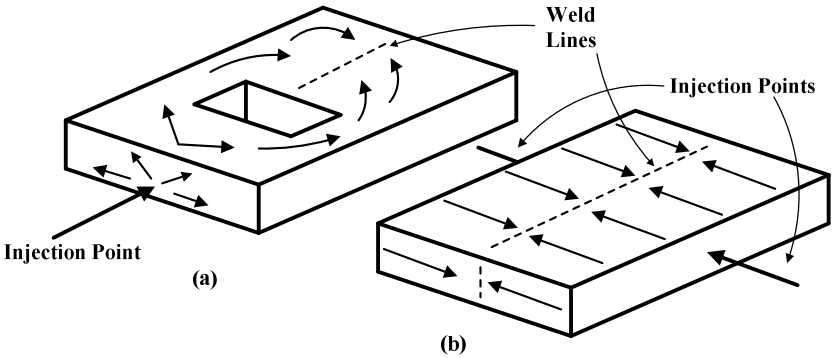

Figure 2.10: Weld lines formation [7, 12].

[12] This expression is usually used to refer to a defect which can occur in injection molded plastic components. After passing through the gate, the material expands, cools rapidly and builds a strand of relatively cold material in the cavity. After a certain time, pressure builds up in the cavity and the remaining injection volume fills the cavity normally. The initial cold strand is visibly embedded in the rest of the material and can endanger, mainly, the mechanical strength and the appearance of the component [12].

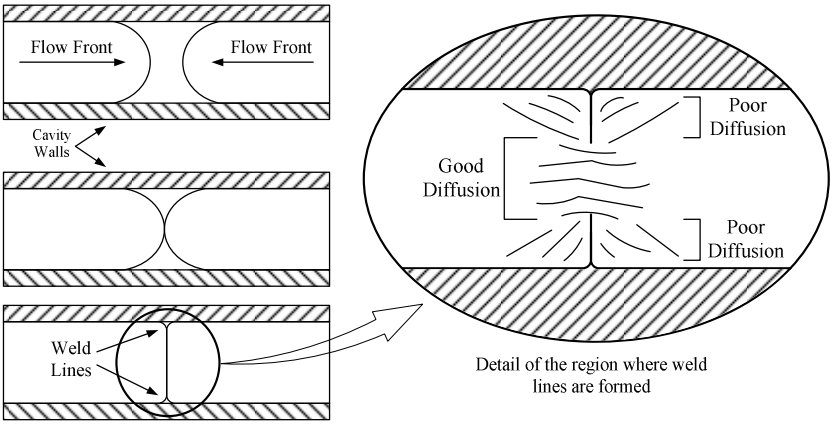

Figure 2.11: Detail of the formation of weld lines and the two distinct diffusion regions [7, 12].

Residual stresses are present in all molded plastic components to some degree. In general, high levels of residual stresses can affect some mechanical properties, as much as the chemical resistance and the dimensional stability of a plastic component. Residual stresses are usually caused by: high molding pressure, cold tool temperature, thin sections in high flow areas, fine details at the extreme of flow, sharp corners in flow path, high viscosity materials, cold metal insert in the mold, very fast cooling and cold flow front from long flow lengths [58, 59]. High levels of residual stresses may result in lack of optical clarity, acceleration of chemical attack, reduction in loading bearing capacity, warpage, inability to hold tight tolerances, reduction in impact strength and increasing in ductile-brittle failure transition temperature [58].

According to Miller [68], the distribution of residual stresses in a component can be either beneficial or harmful. The surface compressive stresses tend to improve fatigue resistance. Toughness is improved and the compressive stress reduces the harmful effect of surface notches, sharp angles and grooves, which act as stress concentrators. Thus, usually it is often desirable to introduce residual stresses intentionally.

The term **molecular orientation** means the alignment of the molecular segments in the direction of flow [61]. The degree of orientation obtained after the component is solidified depends primarily on the nature of the polymer, the shear rate stress experienced in flow and a variety of processing variables, such as injection speed, mold temperature, hold pressure and melt temperature [59, 61].

Berins [61] affirms that plastic components will be tougher in the direction of flow than perpendicular to it. This author still affirms that this

component will be prone to shrink more in the direction of flow than it will perpendicular to it, because shrinkage is a result of two factors: a normal decrease in volume due to temperature change and relaxation of the stretching caused by links between carbon atoms.

Part thickness also affects molecular orientation, because it works like a constrained flow area. Thus, the fibers near the outer surfaces freeze in the direction of the flow, because the high shear stress near these surfaces orients fibers in the molten material in the direction of the flow. As wall thickness increases, this effect is reduced because of the decreased amount of shear in the center of the flow [12].

Thermal degradation is commonly caused by high shear stresses and shear rates at the interface between the solid layer and the melt core. It usually takes place at elevated temperatures and, microscopically speaking, its initial step is the cleavage of the weakest bonds present in the material, what leads to the degradation of molecular weight and discoloring of components [12, 69].

2.5.2. Recycled Material

Due to environmental concerns, one has manufactured more and more plastic components with recycled material. Some of these components are manufactured totally with recycled materials, while others use a certain amount mixed to the virgin material.

The material to be recycled can be proceeding from several origins such as: rejected and scraped components rejected by the quality control, which are the most common cases or materials produced during the molding process, like sprues, injection runners, flashes and the like [59, 52]. The material to be recycled is milled in small pieces and blended with virgin material to produce more components and, consequently, reduce costs. Most material suppliers often suggest that 10 to 15% of regrind can be blended with virgin material without significant property loss [62].

The recycled material interferes on the mechanical properties of the virgin material, because that material has been used previously, then it exhibits a considerable degree of chemical change and thermal degradation which have taken place during previous processing. When performing the mixture, the virgin material acquires an initial wear derived from the recycled material. Based on this concern, one recommends that certain quantity of recycled material is used, in order that the components do not exhibit significant loss on their strength [12, 62].

2.5.3. Water Absorption

According to Tres [60], water absorption represents the percentage increase in weight of a material due to the absorption of water. Plastic materials can be either absorbents (hygroscopic) or non-absorbents. Water absorbed by the material after molding can degrade it by means of a process called **hydrolysis**. In this process, the water severs the polymeric chains, leading to the reduction of its molecular weight and, consequently, to the decreasing of its mechanical and electrical properties. When dealing with composite materials, the water damages the adhesion between the resin and the fibers [60].

2.5.4. Chemical Exposure

The chemical resistance of any plastic material depends primarily on the chemical composition of the material, followed by the chemical concentration, exposure time, temperature and residual stress level in the component [59, 64]. According to Ticona [51] and Michaeli [64], some substances can attack the plastic chains directly producing a progressive lowering of its molecular weight, hardness, mechanical strength and physical and electrical properties over time. The degree of changes depends on the polarity of the material and chemical substance together, like:

- Nonpolar polymers, such as PS and PE swell or dissolve in nonpolar solvents, such as gasoline and benzene, while they are resistant to polar solvents, such as water and alcohol;
- Polymers that contain polar groups, such as polyamide, are resistant to nonpolar substances, swell and dissolve in polar solvents [64].

2.5.5. Solar Radiation

In many applications, one requires that the plastic component withstands exposure to solar radiation, when used in naturally lighted areas or outdoors, because sunlight is probably the most destructive outdoor element to the integrity of plastic components. According to Fish [62], the ultraviolet (UV) radiation is the main responsible for most of the damage caused to components under its exposure.

Most natural excitation frequencies of the polymer chemical bonds correspond to the frequencies that occur in the UV range of the sunlight. Once these bonds are excited, various degradative processes, such as chain scission, can occur. The surface of the component is the first and the most damaged region, because the UV rays can only penetrate low

depths when they are absorbed. Because the rays are absorbed by a little region of the component and the exposition is incessant, its surface is thermically overloaded, leading to its degradation, which is going to be transmitted to its core, along the time.

The rate of the total degradative process is usually temperature dependent; thus, the lower frequency portion of the solar spectrum can accelerate UV degradation by heating the material. At low temperatures the material can become brittle and can shrink, so that these two processes can accelerate its degradative process. Degradation may also be accelerated by other natural elements, such as wind-born particles and man-made elements, such as air pollutants [62].

2.6. MECHANISMS OF DUCTILE FAILURE

The increasing use of plastic materials as industrial components has created a need for data that permit the designer to predict the performance of these components in service. Despite this demand, the state of the art on this subject has not been as well developed for plastic materials as it has been for metals. The main reason is that those materials have been applied in industrial mechanical components recently, due to their complex behavior [10, 70, 71]. Thus, based on these considerations, this section will provide an overview on mechanism of ductile failure of plastic materials. Basically, two modes are prone to take place: **crazing** and **shear band**.

Unlike metallic materials, plastics deform viscoelastically when subjected to a load. From the thermodynamic point of view, a fraction of the mechanical energy produced by the external loads is used to develop irreversible molecular processes, such as microscopic deformations, like crazing, shear bands, voids and micro cracks. The other part of the mechanical energy may be converted into heat within the material [72]. The gradual buildup of heat may be sufficient to cause a loss in strength and rigidity of the component [71]. This behavior is further aggravated by the low thermal conductivity of plastic materials.

The **mechanical failure** of a plastic component is characterized by initiation of a crack and its subsequent propagation. Although little detailed information is available, it seems likely that some combination of crazing and/or shear bands precedes crack initiation and propagation during the failure process [70]. Morphologically speaking, a craze is a planar defect very similar to a crack. But, as is shown in Figure 2.12, a craze differs from a crack in that it contains an interpenetrating network of voids among highly drawn plastic fibrils bridging the craze faces. As a consequence, the specimen is still able to support loads, while the cracked specimen does not [10, 73, 95].

Crazing begins in regions of the component under high triaxial tensile stresses or in regions of much localized yielding, like inclusions and surface defects, which lead to micro voids formation. After crazing has initiated, the voids increase in size and elongate along the direction of the maximum principal tensile stress. The plastic bulk material among the voids also undergoes gradual elongation to form thin fibrils. Visually, the presence of whitening regions on the component, as the result of light scattering, exposes the presence of crazing [6, 65].

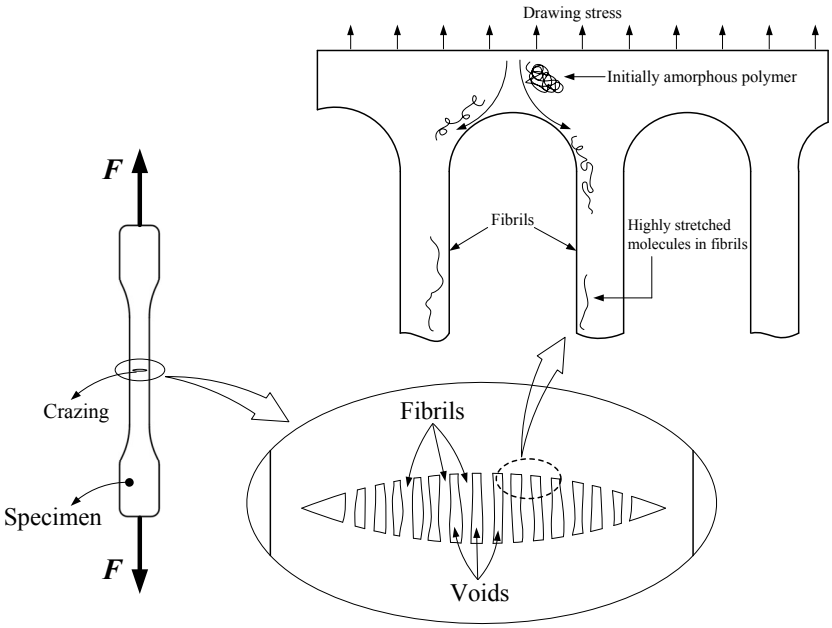

Figure 2.12: Detail of the crazed region [74, 75].

As the craze faces separate, the fibrils increase in length, while their diameters contract. When the longitudinal strain in the fibrils exceeds the maximum extensibility of the molecular network, they rupture and form a crack [76]. Figure 2.13 illustrates craze formation and its subsequent development into a crack.

Another kind of failure mode which may happen in plastic components is **shear band**. In this failure mode, the irreversible strains evolve towards the plane of maximum shear stress, i.e., 45° with respect to the direction of maximum tensile principal stress. Unlike shear band, which occurs at constant volume, crazing is a cavitation process that is accompanied by an increasing in volume. This means that under

compression, many plastic components will shear band rather than craze, as there is a contraction of volume instead of an increase [21].

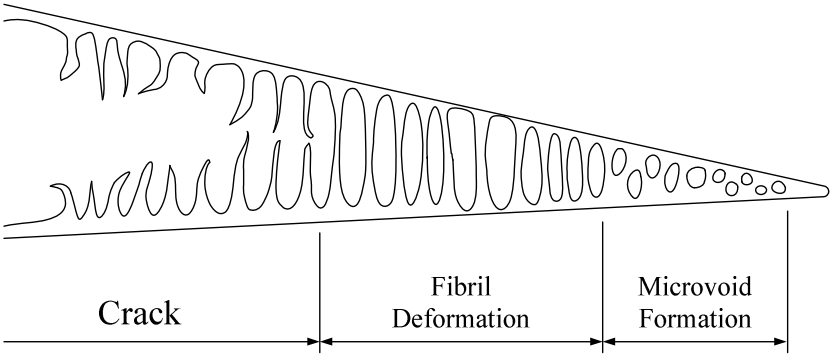

Figure 2.13: Crack formation from a craze [76].

Because plastic materials behave viscoelastically, there is the potential for having a large amount of internal friction generated within the material during mechanical deformation, as in fatigue regime. This mechanism involves the accumulation of hysteretic energy generated during each loading cycle. Because this energy is dissipated specially in the form of heat, the material experiences an associated temperature increase. As a consequence, when submitted to fatigue regime, plastic components may fail, due to excessive heating. In this case, one uses to define **thermal failure** or **thermal instability**. This kind of failure occurs when the heat transfer rate to the surroundings by conventional heat transfer mechanisms is less than the rate of heat generated by successive fatigue cycles [72, 77]. In this case, the temperature of the material increases until its properties decline to a point, at which the component can no longer withstand the loads. On the other hand, if the heat transfer rate to the surroundings equals the rate of heat generated, then the temperature of the material stabilizes and the component is able to withstand the fatigue loads without failing. In this case, one uses to say that there was a **thermal stability** [72]. Because metallic materials are very good heat conductors, these materials do not present thermal failure. Usually, this concern is not taken into account in the design of metallic components subjected to fatigue loading. In plastic components, this concern is very important and can not be neglected.

2.7. FINAL REMARKS

This chapter has introduced the most important peculiarities of plastic materials, including their main properties, behavior and failure modes. Among these characteristics, one may appoint: (i) their viscoelastic behavior, which describe their total dependence with both time and loading rate; (ii) the thermomechanical behavior, which demonstrates that their mechanical behavior and properties are very sensitive to temperature variations; (iii) the external factors, which can endanger the mechanical strength of the component and reduce its durability; and (iv) the mechanisms of ductile failure, which can occur in the form of shear bands or crazing.

In the past few years, one has observed a growing demand for eco-friendly plastic materials and products, motivated by the consequences that the traditional petroleum-based plastics have caused to the environment. In this sense, biodegradable plastics have appeared as a good alternative. Different from the fossil-fuel-based plastics, bioplastics are derived from renewable biomass sources, such as starches (corn, pea, wheat, etc.) and vegetable oil. As a consequence, one guarantees that they will not be harmful to the environment and, when decomposing, they will not contaminate the soil or the groundwater. Despite their growing demand, their application as loading bearing industrial products is still limited and needs more study and development.

The topics discussed in this chapter have provided nonspecialists in polymers and plastics a general idea on their most important peculiarities and differences when compared to other more traditional engineering materials. The background offered in this chapter will be essential, so that the reader is aware of the considerations upon which the development of the constitutive model described in the next chapters will be based.

CHAPTER 3

CONSTITUTIVE LAWS FOR DAMAGED MEDIA

For a long time, damage of materials has been modeled by damage quantities within the scope of Continuum Mechanics. Because damage, in general, results from microscopic movements, then Fremond and Nedjar [2] have proposed that the power[13] of these microscopic movements must be accounted for in a predictive theory. Thus, the authors have assumed that the power of the internal forces depended on the damage rate and on the gradient of the damage rate. This procedure leads to a nonlocal damage model that is free of spurious mesh sensitivity and able, when compared with experimental results, to predict the behavior of the material degradation [2].

The objective of this chapter is to present the basics concepts on the theory used to model the deformation and damaging phenomena of plastic materials. The development of this theory will be based on the approach proposed by Fremond and Nedjar [2], on the principle of virtual power, idealized by d'Alembert (1750), which will provide a new equation, describing the evolution of the damage quantity, β, and on the approach of the thermodynamics of the continuum medium, in order to introduce the variables related to the phenomenon in study. In this regard, the thermodynamic potentials and the method of local state will allow defining the observable and internal variables, which will naturally lead to the state equations. Additionally, the pseudo-potential of dissipation will provide the complementary laws, which will describe the irreversible processes.

Let the scalar β be defined as the **cohesion variable** with value 1 when the material is undamaged and value 0 when it is completely damaged. This variable is related with the links between material points and can be interpreted as a measure of the local cohesion state of the material. When $\beta = 1$, all the links are preserved. But, if $\beta = 0$, a local rupture is considered, since all the links between material points have been broken [2]. In this case, one considers that the variable β will develop isotropically. Because this chapter consists of a review of the concepts of the principle of virtual power and the thermodynamics of continuum media, then its reading may also be dispensable for those readers who have been familiar with the topics discussed here.

[13] In this chapter, **power** will mean the rate at which work is performed.

3.1. PRINCIPLE OF VIRTUAL POWER

According to Germain [78], the principle of virtual power consists in describing the possible movements of a mechanical system, by means of a virtual space, named **space of virtual movements**. This principle is based on two axioms: invariance of the internal loads (objectivity) and equilibrium axioms. The first one says that the virtual power of the internal loads, associated with a rigid body motion is zero, while the second axiom says that the virtual power of inertial loads, P_a, is equal to the sum of the virtual power of internal, P_i, and external loads, P_e, i.e.,

$$P_a(\vec{v},\gamma) = P_i(\vec{v},\gamma) + P_e(\vec{v},\gamma), \tag{3.1}$$

in which, $\vec{v}$ is the macroscopic velocity vector field.

In this work, one considers the approach presented by Fremond and Nedjar [2] and one chooses the power of the internal forces to depend, besides on the strain rate $\dot{\boldsymbol{\varepsilon}}$, also on the velocity of the microscopic links, γ, and its gradient, $\vec{\nabla}\gamma$. In this approach, the gradient of damage is introduced to take into account the influence of damage at a material point on the damage of its neighborhood. Thus, one assumes that the power of the internal forces is given by

$$P_i(\vec{v},\gamma) = -\int_\Omega \boldsymbol{\sigma}\cdot\dot{\boldsymbol{\varepsilon}}\, d\Omega - \int_\Omega \left(F\gamma + \vec{H}\cdot\vec{\nabla}\gamma\right) d\Omega, \tag{3.2}$$

in which, $\boldsymbol{\sigma}$ is the Cauchy stress tensor, F is the internal work of damage and $\vec{H}$ is the flux vector of internal work of damage. In addition, one assumes that the power of the external forces is given by

$$P_e(\vec{v},\gamma) = \int_\Omega \rho\vec{b}\cdot\vec{v}\, d\Omega + \int_{\partial d\Omega} \vec{t}\cdot\vec{v}\,\partial d\Omega + \int_\Omega A_v\gamma\, d\Omega + \int_{\partial d\Omega} A_s\gamma\,\partial d\Omega, \tag{3.3}$$

in which, ρ is the density, $\vec{b}$ represents the prescribed body force per unit mass, $\vec{t}$ is the prescribed external traction and A_v and A_s are, respectively, the volumetric and the surface external sources of damage work. A source of damage work can be produced by chemical (or in some cases electrical) actions, which break the bonds inside a material, without macroscopic deformations [2]. One can think, for example, of acid

reactions, solar radiation and moisture influence, which damage plastic materials. At last, one assumes that the power of the inertial forces is given by

$$P_a(\vec{v},\gamma) = \int_\Omega \rho\ddot{\vec{u}} \cdot \vec{v}\ d\Omega + \int_\Omega \rho\ddot{\beta}\gamma\ d\Omega, \tag{3.4}$$

in which, $\ddot{\vec{u}}$ is the acceleration field and $\rho\ddot{\beta}$ is the acceleration forces of the microscopic links.

Replacing Equations (3.2) to (3.4) into (3.1) and assuming that $A_v = 0$ and $A_s = 0$, one has obtained the following set of differential equations:

$$div\left[\boldsymbol{\sigma}(\vec{x},t)\right] + \rho\vec{b}(\vec{x},t) = \rho\frac{d^2\vec{u}(\vec{x},t)}{dt^2} \quad \text{in} \quad \Omega \tag{3.5}$$

and

$$div(\vec{H}) - F = \rho\ddot{\beta}(\vec{x},t) \quad \text{in} \quad \Omega. \tag{3.6}$$

This last equation governs the evolution of the damage variable. Equation (3.5) is submitted to the boundary conditions

$$\begin{cases} \boldsymbol{\sigma}(\vec{x},t)\vec{n} = \vec{t}(\vec{x},t) \quad \text{on} \quad (\vec{x},t) \in \Gamma_t \\ \vec{u}(\vec{x},t) = \overline{u} \quad \text{on} \quad (\vec{x},t) \in \Gamma_u \end{cases} \tag{3.7}$$

and to the initial conditions

$$\begin{cases} \dfrac{d\vec{u}(\vec{x},0)}{dt} = \vec{v}_o(\vec{x}) \quad \text{in} \quad \Omega \\ \vec{u}(\vec{x},0) = \vec{u}_o(\vec{x}) \quad \text{in} \quad \Omega \end{cases} \tag{3.8}$$

and

$$\begin{cases} div(\boldsymbol{\sigma}_o) = 0 \quad \text{in} \quad \Omega \\ \boldsymbol{\sigma}_o\vec{n} = 0 \quad \text{on} \quad \partial\Omega, \end{cases} \tag{3.9}$$

in order to account for the residual stress field. In this case, $\boldsymbol{\sigma}_o$ represents the initial residual stress tensor. In turn, Equation (3.6) is submitted to the following boundary and initial conditions:

$$\vec{\nabla}\beta \cdot \vec{n} = 0 \quad \text{on} \quad \partial\Omega \qquad \text{and} \qquad \beta(\vec{x},0) = 0 \quad \text{in} \quad \Omega. \tag{3.10}$$

3.2. LAWS OF THERMODYNAMICS FOR DAMAGED MEDIA

One considers the existence of four thermodynamics laws. The so-called zeroth law, which regards to the thermal equilibrium, states that if two bodies *A* and *B* are in thermal equilibrium with another body *C*, then *A* and *B* are also in equilibrium. Although it seems very obvious, this phenomenon was only checked in the 1930s, much later the first and second laws have been stated. Basically, these two laws regard, respectively, to the conservation of energy and the conditions, so that the thermodynamic transformations are able to take place. Lastly, the third law states that it is impossible, by means of a finite number of states or stages, to reach the absolute zero of temperature (zero Kelvin) or -273,15 °C. Only the first and the second laws will be discussed here.

3.2.1. First Law of Thermodynamics

Rigorously, the first law of thermodynamics only represents a statement of the principle of conservation of energy for thermodynamic systems [21]. In a thermodynamic system, a body $\mathcal{B}$ can store energy, basically, by two ways: kinetic energy (K) and internal energy (E_{int}), which represents the total capacity that a system has to perform work. Formally, the first law of thermodynamics may be stated as: "the rate of total energy of the system (kinetic and internal energies) is equal to the power of external loads (P_{ext}), applied on the body $\mathcal{B}$, added by the rate at which heat (Q) is received or released by the system". Thus, mathematically, the first principle of thermodynamics can be written as

$$\frac{d}{dt}\left(K + E_{int}\right) = P_{ext} + Q \tag{3.11}$$

in which,

$$K = \frac{1}{2}\int_{\Omega} \rho\, \dot{\vec{u}} \cdot \dot{\vec{u}}\; d\Omega + \frac{1}{2}\int_{\Omega} \rho \dot{\beta}^{2}\, d\Omega, \tag{3.12}$$

$$P_{ext} = \int_{\Omega} \boldsymbol{\sigma} \cdot \dot{\boldsymbol{\varepsilon}} \, d\Omega + \int_{\Omega} \left(F \dot{\beta} + \vec{H} \cdot \vec{\nabla} \dot{\beta} \right) d\Omega + \\ + \int_{\Omega} \rho \ddot{\vec{u}} \cdot \vec{u} \, d\Omega + \int_{\Omega} \rho \ddot{\beta} \dot{\beta} \, d\Omega, \qquad (3.13)$$

$$E_{int} = \int_{\Omega} \rho e \, d\Omega \qquad (3.14)$$

and

$$Q = \int_{\Omega} \rho \overline{r} d\Omega + \int_{\partial\Omega} \vec{q} \cdot \vec{n} d\partial\Omega. \qquad (3.15)$$

In these equations, e is the specific internal energy, $\overline{r}$ is the volumetric density of the internal heat production, $\vec{q}$ is the heat flux vector and $\vec{n}$ is the outward unit vector normal to the boundary, $\partial\Omega$, of the body $\mathcal{B}$. Replacing Equations (3.12) to (3.15) into (3.11), one obtains

$$\rho \dot{e} = \boldsymbol{\sigma} \cdot \dot{\boldsymbol{\varepsilon}} + \rho \overline{r} + F \dot{\beta} + \vec{H} \cdot \vec{\nabla} \dot{\beta} - div(\vec{q}), \qquad (3.16)$$

which, represents the first law of thermodynamics for damaged media.

3.2.2. Second Law of Thermodynamics

The second law of thermodynamics states that the energy has quality, as well quantity and the existing processes occur only if they increase the total entropy of the system [79]. In this case, one states that the rate of entropy production of a system (dS/dt) is always greater or equal to the rate of heating divided by the temperature. In other words, one can write

$$\frac{dS}{dt} \geq \int_{\Omega} \frac{\rho \overline{r}}{T} \, d\Omega + \int_{\partial\Omega} \frac{\vec{q}}{T} \cdot \vec{n} d\partial\Omega. \qquad (3.17)$$

This equation relates two new variables: the absolute temperature (T) and entropy (S), given by

$$S = \int_{\Omega} \rho s \, d\Omega, \tag{3.18}$$

in which, s is the specific entropy. Based on the first law, expressed by Equation (3.16), and introducing the Helmholtz free energy potential (Ψ), given by

$$\Psi = e - Ts, \tag{3.19}$$

one obtains

$$\boldsymbol{\sigma} \cdot \dot{\boldsymbol{\varepsilon}} + F\dot{\beta} + \vec{H} \cdot \vec{\nabla}\dot{\beta} - \rho\left(\frac{d\Psi}{dt} + s\frac{dT}{dt}\right) - \frac{\vec{q} \cdot \vec{\nabla} T}{T} \geq 0, \tag{3.20}$$

which, represents the second principle of thermodynamics for damaged media, also known as Clausius-Duhem inequality. This expression shows that a thermodynamic process is admissible if, and only if, the total dissipation of the system is positive or equal to zero.

3.2.3. Internal Constraint on the Cohesion Variable

The value of the damage quantity (β) is within the range [0;1], with β seen as the volumetric proportion of micro voids or the quotient of the modulus of the damaged material by the modulus of the undamaged material. Thus,

$$0 \leq \beta \leq 1.$$

One takes the internal constraint on β to be a physical property. Being a physical property of a state quantity, it must be taken into account by the functions which describe the whole physical properties, i.e., either the free energy, Ψ, or the dissipative forces which can be defined by a pseudo-potential of dissipation, φ.

The free energy potential, $\Psi(\circ, \beta, \vec{\nabla}\beta)$, is only defined for real processes, i.e., for processes such that $\beta \in \mathcal{K}$, where $\mathcal{K} = \{(\circ, \beta, \vec{\nabla}\beta) \mid 0 \leq \beta \leq 1\}$. In this case, $(\circ)$ represents a set of internal variables, which will be defined later. However, one may also extend Ψ for processes where $\beta \notin \mathcal{K}$ by assuming that $\Psi(\circ, \beta, \vec{\nabla}\beta) = +\infty$ for

$\beta \notin \mathcal{K}$. Moreover, one assumes Ψ to be locally sub-differentiable[14] in $\mathcal{K}$ and to be material differentiable, i.e., for $\dot{\Psi}$ to exist.

Thus, one assumes the existence of a free energy potential given by

$$\Psi(\circ, \beta, \vec{\nabla}\beta) = \Psi_1(\circ, \beta, \vec{\nabla}\beta) + I_{\mathcal{K}}(\beta), \tag{3.21}$$

in which, $\Psi_1(\circ, \beta, \vec{\nabla}\beta)$ is a smooth potential and $I_{\mathcal{K}}(\beta)$ is the indicator function of $\mathcal{K}$ given by

$$I_{\mathcal{K}}(\beta) = \begin{cases} 0, & \text{if} \quad \beta \in \mathcal{K} \\ +\infty, & \text{if} \quad \beta \notin \mathcal{K}. \end{cases} \tag{3.22}$$

The indicator function is responsible for imposing the irreversibility of the damage process. Thus, the free energy will have a physical value for any actual or physical value of β. On the other hand, the free energy is equal to $+\infty$ for any physically impossible value of β, i.e., for any $\beta \notin \mathcal{K}$.

The computation of the derivatives of the free energy in an actual evolution, that is, in an evolution such that $0 \leq \beta \leq 1$ for any point $x \in \Omega$ and any time t, allows defining the following reversible or nondissipative forces related to β and $\vec{\nabla}\beta$:

$$F^r = \rho \frac{\partial \Psi_1}{\partial \beta} \tag{3.23}$$

and

$$\vec{H}^r = \rho \frac{\partial \Psi_1}{\partial \vec{\nabla}\beta}. \tag{3.24}$$

The internal constraint is taken into account by introducing a reaction force of damage, F^{reac}, which is defined by assuming that there is a nonsmooth function[15], F^{reac}, such that

[14] For more detail on sub-differentiability, see Souza Neto *et. al.* [80].

$$F^{reac}(\vec{x},t) \in \rho \partial^{loc} I_K[\beta(\vec{x},t)], \tag{3.25}$$

in which, $\partial^{loc} I_K(\beta)$ is the sub gradient of $I_K(\beta)$, given by

$$\begin{cases} \partial^{loc} I_K(\beta) = 0 \quad \text{if} \quad 0 < \beta(\vec{x},t) < 1 \\ \partial^{loc} I_K(0) = \mathcal{R}^- \\ \partial^{loc} I_K(1) = \mathcal{R}^+ \\ \partial^{loc} I_K(\beta) = \varnothing \quad \text{if} \quad \beta(\vec{x},t) \notin \mathcal{K}. \end{cases} \tag{3.26}$$

One can notice that the relation (3.26) implies that the sub differential, $\partial^{loc} I_K(\beta)$, is not empty and, thus, that the internal constraint is satisfied. One can also say that the relation (3.26) has two meanings: the internal constraint is satisfied and there exists a reaction to the internal constraint which is zero for $0 < \beta < 1$, positive for $\beta = 1$ and negative for $\beta = 0$. If the indicator function, $I_K(\beta)$, is approximated by a smooth function, then one may compute an approximation of F^{reac} by simply computing the classical derivative of the regularized smooth function.

3.3. METHOD OF LOCAL STATE

The method of local state postulates that the thermodynamic state of a material medium can be completely defined by the knowledge of the values of a certain number of variables defined at a fixed time instant *t* [15]. This hypothesis implies that the evolution of a material medium can be considered as a succession of several equilibrium states. These variables are named **local state variables**. Thus, physical phenomena can be described with a precision which depends on the choice of the nature and the number of state variables. The process defined in this way will be thermodynamically admissible if, and only if, at any instant *t* of the evolution, the Clausius-Duhem inequality is satisfied [15]. According to Lemaitre [1] and Lemaitre and Chaboche [15], the local state variables are classified in observable and internal.

3.3.1. Observable and Internal Variables

Lemaitre and Chaboche [15] consider that the only **observable variables** which occur in elasticity, plasticity, viscoelasticity,

[15] A function is said to be **smooth** when it has continuous derivatives up to some desired order over some domain. The number of continuous derivatives necessary for a function to be considered smooth depends on the problem in study and may vary from two to infinity [80].

viscoplasticity, damage and fracture phenomena are the temperature (T) and the total strain tensor ($\boldsymbol{\varepsilon}$). The elastic or reversible phenomena depend uniquely on these variables, at any time instant t.

Lubliner [81] defines an elastic body as one in which the strain, at any point of the body, is completely determined by the current stress and temperature there, then an obvious definition of an inelastic body, characterized by exhibiting irreversible deformations when loaded, is as one in which there is something else, besides the current stress and temperature, that determines the strain. That "something else" may be thought of, for example, as the past history of the stress and the temperature at the point. An alternative way of representing the "something else" is by means of an array of variables, $(V_1, V_2, \ldots, V_k)$, such as the strain depends on these variables in addition to the stress and the temperature. These are called **internal** or **time history variables** [81]. The array of internal variables will be represented here by $\vec{V}$ and, depending on the phenomenon; their terms might be scalar, vector or tensor.

Based on the definitions discussed previously, in order to describe irreversible processes, one can introduce a set of internal variables, whose objective is to incorporate the loading history on the final response of the material. Thus, one assumes that the total strain tensor, $\boldsymbol{\varepsilon}$, is additively decomposed into an elastic, $\boldsymbol{\varepsilon}^e$, and an inelastic part, $\boldsymbol{\varepsilon}^{vp}$, named viscoplastic strain, i.e.,

$$\boldsymbol{\varepsilon} = \boldsymbol{\varepsilon}^e + \boldsymbol{\varepsilon}^{vp}. \tag{3.27}$$

Other phenomena, like hardening and damage can also be introduced into the model, through the inclusion of internal variables which are able to represent them adequately.

3.3.2. Free Energy Thermodynamic Potential

Once the state variables have been defined, one postulates the existence of a thermodynamic potential, from which the state laws can be derived. This potential has the following characteristics: (i) it is a concave function with respect to the temperature (T); and (ii) it is a convex function with respect to the other state variables V_k. For this thesis work, one has adopted the **Helmholtz free energy potential** (Ψ), which is defined as a thermodynamic potential that measures the useful work obtainable from a closed thermodynamic system at a constant temperature [15]. Thus, the Helmholtz free energy potential may be considered to

depend on the following non damage state variables $(\circ) = (\boldsymbol{\varepsilon}^e, r, \boldsymbol{\vartheta}, T, \vec{V})$. Hence, one assumes that

$$\Psi = \Psi^{vp}(\boldsymbol{\varepsilon}^e, r, \boldsymbol{\vartheta}, T, \beta, \vec{\nabla}\beta) + I_K(\beta), \tag{3.28}$$

in which, r and $\boldsymbol{\vartheta}$ are, respectively, the accumulated viscoplastic strain and the back strain tensor to account for the isotropic and the kinematic hardening processes, respectively [1].

By using the chain rule of differential calculus, one can write the temporal variation of Ψ as

$$\dot{\Psi} = \frac{\partial \Psi^{vp}}{\partial \boldsymbol{\varepsilon}^e} \cdot \dot{\boldsymbol{\varepsilon}}^e + \frac{\partial \Psi^{vp}}{\partial r}\dot{r} + \frac{\partial \Psi^{vp}}{\partial \boldsymbol{\vartheta}} \cdot \dot{\boldsymbol{\vartheta}} + \frac{\partial \Psi^{vp}}{\partial T}\dot{T} + \\ + \frac{\partial \Psi^{vp}}{\partial \beta}\dot{\beta} + \frac{\partial \Psi^{vp}}{\partial \vec{\nabla}\beta} \cdot \vec{\nabla}\dot{\beta} + \frac{1}{\rho} F^{reac}\dot{\beta}. \tag{3.29}$$

Replacing this equation into the Clausius-Duhem inequality (expression (3.20)) and accounting for expression (3.27), one obtains the following state equations:

$$\boldsymbol{\sigma} = \rho \frac{\partial \Psi^{vp}}{\partial \boldsymbol{\varepsilon}^e}, \tag{3.30}$$

$$R = \rho \frac{\partial \Psi^{vp}}{\partial r}, \tag{3.31}$$

$$F^r = \rho \frac{\partial \Psi^{vp}}{\partial \beta}, \tag{3.32}$$

$$\vec{H}^r = \rho \frac{\partial \Psi^{vp}}{\partial \vec{\nabla}\beta}, \tag{3.33}$$

$$\boldsymbol{\chi} = \rho \frac{\partial \Psi^{vp}}{\partial \boldsymbol{\vartheta}} \tag{3.34}$$

and

$$s = -\frac{\partial \Psi^{vp}}{\partial T}. \tag{3.35}$$

In these state equations, R and $\boldsymbol{\chi}$ are, respectively, the isotropic strain hardening variable and the back stress tensor, which represents the kinematic hardening [1]. From expression (3.29), one can also obtain the relation (3.25). Now, letting

$$F = F^{r} + F^{reac} + F^{i} \tag{3.36}$$

and

$$\vec{H} = \vec{H}^{r} + \vec{H}^{i} \tag{3.37}$$

in which, $F^{reac} \in \rho\partial^{loc} I_{\mathbf{K}}(\beta)$, one derives the following expression for the dissipation of energy

$$\Delta = \boldsymbol{\sigma} \cdot \dot{\boldsymbol{\varepsilon}}^{vp} - R\,\dot{r} - \boldsymbol{\chi} \cdot \dot{\boldsymbol{\vartheta}} + F^{i}\dot{\beta} + \vec{H}^{i} \cdot \vec{\nabla}\dot{\beta} \geq 0. \tag{3.38}$$

For simplicity, one assumes that there is no dissipation with respect to the gradient of the damage rate, $\vec{\nabla}\dot{\beta}$. As a result, one has only dissipative phenomena of the viscous type, for the damage rate $\dot{\beta}$. Hence, $\vec{H}^{i} = 0$, what finally yields

$$\Delta = \boldsymbol{\sigma} \cdot \dot{\boldsymbol{\varepsilon}}^{vp} - (R\,\dot{r} + \boldsymbol{\chi} \cdot \dot{\boldsymbol{\vartheta}}) + F^{i}\dot{\beta} \geq 0. \tag{3.39}$$

In this expression, the term $\boldsymbol{\sigma} \cdot \dot{\boldsymbol{\varepsilon}}^{vp}$ represents the energy dissipated by the hysteresis loop, $(R\,\dot{r} + \boldsymbol{\chi} \cdot \dot{\boldsymbol{\vartheta}})$ represents the energy stored due to the hardening processes of the material and the term $F^{i}\dot{\beta}$ represents the energy dissipated due to the damaging processes.

3.3.3. Dissipation Thermodynamic Potentials

In order to describe dissipative systems and obtain the evolution equations of the set of internal variable of a thermodynamic system, it is

necessary to introduce some complementary equations. To accomplish this, one postulates the existence of a scalar function $(\varphi(\bullet))$, called **dissipation potential** or **pseudo-potential of dissipation** and its **dual** $(\varphi^*(\bullet))$, which is a continuous and positive scalar function, convex with respect to the flux variables and zero valued at the origin of the space of the flux variables $\left(\dot{\boldsymbol{\varepsilon}}^{vp}, \dot{r}, \dot{\boldsymbol{\vartheta}}, \dot{\beta}, \vec{\nabla}\dot{\beta}, \vec{q}/T\right)$.

Additionally, one postulates a decoupling among the elasto-viscoplastic, thermal and damage dissipations, so that

$$\varphi^*(\bullet) = \varphi^*_{vp}(\boldsymbol{\sigma}, R, \boldsymbol{\chi}; \circ) + \varphi^*_T(\vec{\nabla}T; T) + \varphi^*_D(F^i; \circ), \tag{3.40}$$

in which, φ^*_{vp} and φ^*_T are differentiable functions that describe, respectively, the elasto-viscoplastic and thermal dissipations and φ^*_D is a non differentiable function that describes the damage dissipation. Thus, based on the normality hypothesis, one can derive the following evolution equations:

$$\dot{\boldsymbol{\varepsilon}}^{vp} = \dot{\lambda}\frac{\partial \varphi^*_{vp}}{\partial \boldsymbol{\sigma}}, \tag{3.41}$$

$$-\dot{r} = \dot{\lambda}\frac{\partial \varphi^*_{vp}}{\partial R}, \tag{3.42}$$

$$-\dot{\boldsymbol{\vartheta}} = \dot{\lambda}\frac{\partial \varphi^*_{vp}}{\partial \boldsymbol{\chi}}, \tag{3.43}$$

$$\dot{\beta} = \dot{\lambda}\frac{\partial \varphi^*_D}{\partial F^i} \tag{3.44}$$

and

$$-\frac{\vec{q}}{T} = \frac{\partial \varphi^*_T}{\partial \vec{\nabla}T}. \tag{3.45}$$

Equations (3.41) to (3.43) represent, respectively, the evolution equations of the viscoplastic strain, the accumulated plastic strain and the back strain, whereas Equations (3.44) and (3.45) lead, respectively, to the evolution equation of the damage variable and the Fourier's law. The parameter $\dot{\lambda}$ is named viscoplastic multiplier. Typical evolution equations for the viscoplastic multiplier, given respectively by Riande *et al.* [5], Norton [82] and Benallal [83], are

$$\dot{\lambda} = \exp\left(\frac{f(\boldsymbol{\sigma}, R, \boldsymbol{\chi}; \circ)}{K_r} \right), \tag{3.46}$$

$$\dot{\lambda} = \left(\frac{f(\boldsymbol{\sigma}, R, \boldsymbol{\chi}; \circ)}{K_n} \right)^N \tag{3.47}$$

and

$$\dot{\lambda} = \ln\left[\left(1 - \frac{f(\boldsymbol{\sigma}, R, \boldsymbol{\chi}; \circ)}{K_\infty} \right)^{-M} \right], \tag{3.48}$$

in which, K_r, K_n, K_∞, N and M are material parameters, that must be obtained experimentally, and $f(\bullet)$ is the yield function.

Basically, every modeling problem, based on the local state method, consists in determining the expressions for the free energy and dissipation thermodynamic potentials discussed previously and identifying the material parameters obtained by means of experiments. The advantage of using this approach is that one may obtain the evolution equations of the internal variables directly, from the definition of the thermodynamic potential, as show the state equations presented previously. Additionally, one guarantees that the models developed under this approach produce thermodynamically reasonable results. The underlying theory and equations presented in this chapter will be applied on the development of the damage model for plastic materials with modifications, making possible to describe some behavior specific to plastics.

CHAPTER 4

DAMAGE MODEL FOR PLASTIC MATERIALS

This chapter will present the theoretical elasto-viscoplastic coupled with a nonlocal damage model for the ductile failure analysis of plastic components, developed under the approaches presented by Lemaitre [1], Fremond and Nedjar [2] and the theory presented in Chapter 3. The discretization and solution of the models, using the finite element method, will be presented in Chapter 5. In this case, one expects that the numerical solution of these models is insensible to the mesh refinement.

According to Lemaitre [1], damage is associated with accumulation of inelastic strains in the neighborhood of defects or interfaces. In plastic materials, damage takes place by the breakage of bonds that exist between the long chains of molecules, due to accumulation of viscoplastic strains [1]. Thus, in order to develop the proposed elasto-viscoplastic coupled with the damage model, one will be introduced the free energy potential, from which one derives the state equations; the yield function, defining the elastic domain; and the pseudo-potential of dissipation, from which the evolution equations describing the irreversible processes are derived, by applying the normal dissipation criterion. For simplicity, one considers the deformation process to be isothermal and assumes an isotropic hardening law, restricting the proposed model to monotonic loadings only.

4.1. DEFINITION OF THE VISCOPLASTIC FREE ENERGY POTENTIAL

Following the ideas of Lemaitre [1], Fremond and Nedjar [2] and Mascarenhas *et al.* [84], one assumes that the viscoplastic free energy potential, $\Psi^{vp}(\boldsymbol{\varepsilon}^{\mathrm{e}}, r, \beta, \vec{\nabla}\beta)$, is given by

$$\rho\Psi^{vp}(\boldsymbol{\varepsilon}^{\mathrm{e}}, r, \beta, \vec{\nabla}\beta) = \beta\frac{1}{2}\mathbb{D}\boldsymbol{\varepsilon}^{\mathrm{e}}\cdot\boldsymbol{\varepsilon}^{\mathrm{e}} + \frac{\acute{k}}{2}\vec{\nabla}\beta\cdot\vec{\nabla}\beta + \int_0^r h(r)dr, \qquad (4.1)$$

in which, $\boldsymbol{\varepsilon}^{e}$ is the elastic strain tensor, $h(r)$ represents the function that describes the isotropic hardening curve of the material, $\acute{k}$ is a parameter that measures the influence of the damage at a material point on the damage of its neighborhood, proposed by Fremond and Nedjar [2], and $\mathbb{D}$ is the fourth order elasticity tensor, given by

$$\mathbb{D} = 2\bar{\mu}\mathbb{I} + \bar{\lambda}\ (\boldsymbol{I} \otimes \boldsymbol{I})\ , \tag{4.2}$$

in which, $\bar{\mu}$ and $\bar{\lambda}$ are the Lamé constants, given respectively by

$$2\bar{\mu} = \frac{E}{1+\nu} \tag{4.3}$$

and

$$\bar{\lambda} = \frac{\nu E}{(1+\nu)(1-2\nu)}\,, \tag{4.4}$$

so that, ν and E are the Poisson's ratio and the modulus of elasticity, respectively. Additionally, $\mathbb{I}$ and $\boldsymbol{I}$ are respectively the fourth and second order identity tensors, given by

$$\mathbb{I}_{ijrs} = \frac{\delta_{ir}\delta_{js} + \delta_{is}\delta_{jr}}{2} \tag{4.5}$$

and

$$(\boldsymbol{I} \otimes \boldsymbol{I})_{ijrs} = \delta_{ij}\delta_{rs}\,, \tag{4.6}$$

in which, δ is the Kronecker delta[16]. It is worth noticing that $\mathbb{I}$ is the identity tensor with respect only to symmetric tensors.

Considering $\rho \simeq cte$, the stress-strain constitutive equation is given by

$$\boldsymbol{\sigma} = \rho\frac{\partial \Psi^{vp}}{\partial \boldsymbol{\varepsilon}^{e}} = \beta\mathbb{D}\boldsymbol{\varepsilon}^{\mathrm{e}} \tag{4.7}$$

[16] Kronecker delta is a function of two variables, usually integers, which is 1 if they are equal and 0 otherwise. In other words, it is defined as

$$\delta_{ij} = \begin{cases} 1, & \text{if } i = j \\ 0, & \text{if } i \neq j. \end{cases}$$

and

$$R = \rho \frac{\partial \Psi^{vp}}{\partial r} = h(r). \tag{4.8}$$

From the damage variable, one obtains

$$F^r = \rho \frac{\partial \Psi^{vp}}{\partial \beta} = \frac{1}{2\beta} \boldsymbol{\sigma} \cdot \boldsymbol{\varepsilon}^e \tag{4.9}$$

and

$$\vec{H}^r = \rho \frac{\partial \Psi^{vp}}{\partial \vec{\nabla} \beta} = k \vec{\nabla} \beta. \tag{4.10}$$

4.1.1. Triaxiality Dependence of F^r

Replacing the decompositions

$$\boldsymbol{\sigma} = \boldsymbol{\sigma}^D + \sigma_H \boldsymbol{I} \tag{4.11}$$

and

$$\boldsymbol{\varepsilon}^e = \boldsymbol{\varepsilon}^{eD} + e_H^e \boldsymbol{I}. \tag{4.12}$$

into Equation (4.9), one obtains

$$F^r = \frac{1}{2\beta} \left(\boldsymbol{\sigma}^D \cdot \boldsymbol{\varepsilon}^{eD} + 3\sigma_H e_H^e \right), \tag{4.13}$$

in which, $\boldsymbol{\sigma}^D$ and σ_H are, respectively, the deviatoric and the hydrostatic part of the stress tensor, so that $\sigma_H = \frac{1}{3} tr(\boldsymbol{\sigma})$, $\boldsymbol{\varepsilon}^{eD}$ and e_H^e are, respectively, the deviatoric and the hydrostatic part of the elastic strain tensor, so that $e_H^e = \frac{1}{3} tr(\boldsymbol{\varepsilon}^e)$.

From the elastic constitutive equation and the strain equivalence principle, one obtains

$$\boldsymbol{\varepsilon}^{eD} = \frac{(1+\nu)}{E}\frac{\boldsymbol{\sigma}^{D}}{\beta} \tag{4.14}$$

and

$$e_H^e = \frac{(1-2\nu)}{E}\frac{\sigma_H}{\beta}. \tag{4.15}$$

Moreover, defining

$$\sigma_{eq}^{vm} = \left(\frac{3}{2}\boldsymbol{\sigma}^{D}\cdot\boldsymbol{\sigma}^{D}\right)^{\frac{1}{2}} \tag{4.16}$$

and replacing Equations (4.14) to (4.16) into (4.13), one obtains

$$F^r = \frac{(\sigma_{eq}^{vm})^2}{2E\beta^2}\left[\frac{2}{3}(1+\nu)+3(1-2\nu)\left(\frac{\sigma_H}{\sigma_{eq}^{vm}}\right)^2\right]. \tag{4.17}$$

The term $\left(\frac{\sigma_H}{\sigma_{eq}^{vm}}\right)$ is the triaxiality ratio, which plays a very important role in the rupture of materials.

4.2. DEFINITION OF THE YIELD FUNCTION

The first step towards the development of the damage model is the definition of the yield function. In a specific case of uniaxial loading, the yield stress (σ_y) defines what is usually named **elastic domain** in the stress space, as shown in Figure 4.1. The introduction of this concept informs that, while the uniaxial stress does not exceed σ_y there will only be elastic strains ($\varepsilon^{vp}=0$). The generalization of this concept to the multiaxial case is accomplished by introducing the concept of **yield criterion** or **function** (f), which defines, in the stress space, a domain within which any stress variation generates only variations of elastic strains [15]. Tresca, Mohr-Coulomb, Drucker-Praguer and von Mises are the most known yield criteria, so that this last one has been the most used.

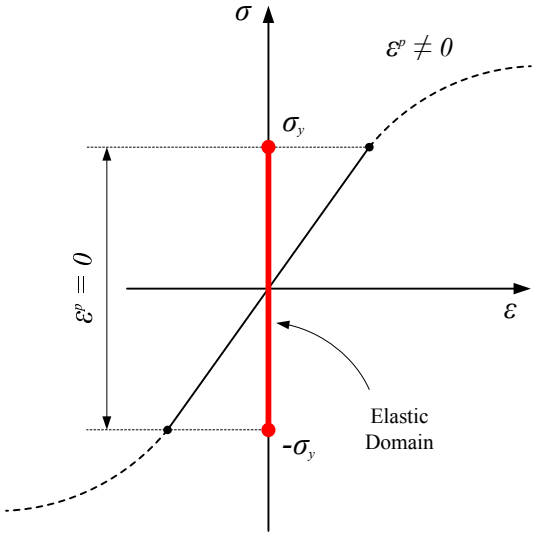

Figure 4.1: One-dimensional elastic domain [15, 80].

One knows that the yield stress for metallic materials under tensile and compressive loads is practically equal and experimental data have demonstrated that this property is not influenced by the hydrostatic part of the stress tensor. Unlike these materials, plastics demonstrate higher yield stress in compression than in tension. Moreover, some tests have demonstrated that the elastic and inelastic strains are sensitive to the hydrostatic part of the stress tensor [85]. These strains imply molecular entanglement and this mechanism is reduced under high pressures, because the molecules are compressed against each other, increasing the cohesive forces among the molecular chains and, consequently, reducing their mobility. The direct consequence is that the response of the material under tensile and compression loads is different. Under compression load, where there is high hydrostatic pressure, the material becomes tougher and its yield strength becomes higher than in tension. Therefore, one uses to say that plastic materials are much more sensitive to compressive loads than metals. Because of that, when dealing with design of plastic components, one recommends to use yield functions which take into account the influence of the hydrostatic part of the stress tensor.

The von Mises criterion, also known as J_2 [17] criterion, does not take the hydrostatic stress into account and it has been extensively used to

[17] J_2 is the second invariant of the deviatoric stress tensor.

model, for example, metallic materials. When dealing with plastic materials, this criterion has to be modified in order to account for the influence of the hydrostatic stress. Based on this idea, a class of yield criteria, named **modified von Mises criterion**, has been proposed in the literature. Among them, one may highlight Riande *et al.* [5], Quinson *et al.* [16], Goldberg *et al.* [17], Rottler and Robbins [18] and propositions. In this work, one has defined the following yield function:

$$f(\boldsymbol{\sigma}, R, \beta; \circ) = (q + \mu\, p) - \left(1 + \frac{\mu}{3}\right)(\sigma_{yo} + R) \tag{4.18}$$

in which,

$$p = \tilde{\sigma}_H\,, \tag{4.19}$$

$$q = \left(\frac{3}{2}\tilde{\boldsymbol{\sigma}}^D \cdot \tilde{\boldsymbol{\sigma}}^D\right)^{\frac{1}{2}} \tag{4.20}$$

so that, the effective stress, $\tilde{\boldsymbol{\sigma}}$, is given by

$$\tilde{\boldsymbol{\sigma}} = \frac{\boldsymbol{\sigma}}{\beta}. \tag{4.21}$$

Additionally, μ is the variable that incorporates the effect of the hydrostatic stress, σ_{yo} is the initial yield stress and R is the isotropic strain hardening variable.

4.3. PLASTIC FLOW RULE AND HARDENING LAW

In order to describe a dissipative process, one needs to introduce complementary kinetic laws. Therefore, to completely characterize the proposed viscoplastic with damage model, by defining the evolution laws for the internal variables, one assumes the existence of a pseudo-potential of dissipation, $\varphi^*(\sigma, R, F^i; \circ)$, that is a scalar continuous function, convex with respect to the dual/associate variables (σ, R, F^i), and compute the evolution equations by

$$(\dot{\boldsymbol{\varepsilon}}^{vp}, -\dot{r}, \dot{\beta}) \in \dot{\lambda}\partial\varphi^{*}(\boldsymbol{\sigma}, R, F^{i}; \circ) \tag{4.22}$$

in which, $(\circ)$ denotes the set $(\boldsymbol{\varepsilon}^{e}, r, \beta, \vec{\nabla}\beta)$ and

$$\dot{\lambda} = \begin{cases} \Im(\boldsymbol{\sigma}, R, F^{i}; \circ), & \text{if} \quad f(\boldsymbol{\sigma}, R; \circ) \geq 0 \\ 0 \qquad\quad , & \text{if} \quad f(\boldsymbol{\sigma}, R; \circ) < 0 \end{cases} \tag{4.23}$$

Moreover, one postulates a decoupling between the damage and the viscoplastic mechanical dissipation so that,

$$\varphi^{*}(\circ) = \varphi^{*}_{vp}(\boldsymbol{\sigma}, R; \circ) + \varphi^{*}_{D}(F^{i}; \circ)\ , \tag{4.24}$$

in which, $\varphi^{*}_{vp}(\boldsymbol{\sigma}, R; \circ)$ is a differentiable function that describes the elasto-viscoplastic dissipation, $\varphi^{*}_{D}(F^{i}; \circ)$ is a non differentiable function that describes the damage dissipation and $\varphi^{*}_{T} = 0$. As a result of the normality hypothesis, one may derive the following evolution equations:

1. Viscoplastic and hardening evolution equations:

$$\dot{\boldsymbol{\varepsilon}}^{vp} = \dot{\lambda}\frac{\partial\varphi^{*}_{vp}}{\partial\boldsymbol{\sigma}} \tag{4.25}$$

and

$$\dot{r} = -\dot{\lambda}\frac{\partial\varphi^{*}_{vp}}{\partial R}. \tag{4.26}$$

2. Damage evolution equations:

$$\dot{\beta} = \dot{\lambda}\frac{\partial\varphi^{*}_{D}}{\partial F^{i}}\ , \tag{4.27}$$

in which, $\dot{\lambda}$, given by expression (4.23), is a known prescribed constitutive evolution equation.

4.3.1. Definition of the Elasto-Viscoplastic Potential

In this work, one assumes an associative flow rule, i.e., the elasto-viscoplastic potential equals the yield function, that is, $\varphi_{vp}^{*}(\boldsymbol{\sigma}, R, \beta; \circ) = f(\boldsymbol{\sigma}, R, \beta; \circ)$. Thus, one can write

$$\varphi_{vp}^{*}(\boldsymbol{\sigma}, R, \beta; \circ) = (q + \mu\, p) - \left(1 + \frac{\mu}{3}\right)(\sigma_{yo} + R). \tag{4.28}$$

Replacing the given elasto-viscoplastic potential into the evolution equation (4.25), one yields

$$\dot{\boldsymbol{\varepsilon}}^{vp} = \dot{\lambda}\frac{\partial \varphi_{vp}^{*}(\boldsymbol{\sigma}, R, \beta; \circ)}{\partial \boldsymbol{\sigma}} = \frac{\dot{\lambda}}{\beta}\left(\frac{3}{2}\frac{\tilde{\boldsymbol{\sigma}}}{q} + \frac{\mu}{3}\boldsymbol{I}\right). \tag{4.29}$$

In turn, the evolution of the isotropic hardening may be similarly obtained by replacing the potential (4.28) into Equation (4.26), what yields

$$\dot{r} = -\dot{\lambda}\frac{\partial \varphi_{vp}^{*}(\boldsymbol{\sigma}, R, \beta; \circ)}{\partial R} = \left(1 + \frac{\mu}{3}\right)\dot{\lambda}. \tag{4.30}$$

At this point, in order to define the effective viscoplastic strain, e_{ef}^{vp}, whose evolution equation will define the evolution of the viscoplastic multiplier, $\dot{\lambda}$, one needs to define the effective stress measure, σ_{ef}, which is defined as

$$\sigma_{ef} = q + \mu\, p. \tag{4.31}$$

Following the ideas of Goldberg *et al* [17], to determine the effective inelastic strain rate, $\dot{e}_{ef}^{vp}$, the principle of the equivalence of the inelastic work rate is employed. The effective inelastic work rate, $\dot{W}^{vp}$, is given by

$$\dot{W}^{vp} = \tilde{\boldsymbol{\sigma}} \cdot \dot{\boldsymbol{\varepsilon}}^{vp} = \sigma_{ef}\ \dot{e}_{ef}^{vp}\ , \tag{4.32}$$

which allows us to conclude that

$$\dot{e}_{ef}^{vp} = \frac{\dot{\lambda}}{\beta}. \tag{4.33}$$

Based on the work of Benallal [83], one proposes the following evolution law for the rate of the effective inelastic strain:

$$\dot{e}_{ef}^{vp} = \ln\left[\left(1 - \frac{f(\boldsymbol{\sigma}, R, \beta; \circ)}{K_{\infty}}\right)^{-M}\right]. \tag{4.34}$$

in which, $f(\boldsymbol{\sigma}, R, \beta; \circ)$ represents the yielding function. Thus, from expression (4.33), one obtains the following evolution law for the viscoplastic multiplier:

$$\dot{\lambda} = \beta \ln\left[\left(1 - \frac{f(\boldsymbol{\sigma}, R, \beta; \circ)}{K_{\infty}}\right)^{-M}\right]. \tag{4.35}$$

Defining for $f(\boldsymbol{\sigma}, R, \beta; \circ) \geq 0$ the overstress stress function as

$$\sigma^{vp}(\dot{e}_{ef}^{vp}) = f(\boldsymbol{\sigma}, R, \beta; \circ) \geq 0\ , \tag{4.36}$$

one obtains

$$\sigma^{vp}(\dot{e}_{ef}^{vp}) = K_{\infty}\left[1 - \exp\left(\frac{-\dot{e}_{ef}^{vp}}{M}\right)\right]. \tag{4.37}$$

It is worth emphasizing that this proposed evolution equation imposes a saturation limit for the overstress term, which represents the rate of deformation sensitivity effect.

4.3.2. Definition of the Damage Potential

One may build the damage potential $\varphi_D^*(F^i;\circ)$ from its conjugate function $\varphi_D(\dot{\beta};\circ)$, given in terms of the flux variable $\dot{\beta}$, by computing the Legendre-Fenchel transform of $\varphi_D(\dot{\beta};\circ)$, which is given by

$$\varphi_D^*(F^i;\circ) = \sup_{\dot{\beta}} \left\{ F^i \dot{\beta} - \varphi_D(\dot{\beta};\circ) \right\}. \tag{4.38}$$

In this work, one considers the conjugate function $\varphi_D(\dot{\beta};\circ)$ to be decomposed as the sum of a smooth function $\varphi_D^S(\dot{\beta};\circ)$ and a nonsmooth potential $I_-(\dot{\beta})$ as

$$\varphi_D(\dot{\beta};\circ) = \varphi_D^S(\dot{\beta};\circ) + I_-(\dot{\beta}), \tag{4.39}$$

in which, $I_-(\dot{\beta})$ is the indicator function of the interval $(-\infty, 0]$, so that

$$I_-(\dot{\beta}) = \begin{cases} 0, & \text{if} \quad \dot{\beta} \le 0 \\ +\infty, & \text{if} \quad \dot{\beta} > 0. \end{cases} \tag{4.40}$$

The indicator function $I_-(\dot{\beta})$ is responsible for imposing the irreversibility of the damage process, i.e., for imposing the constraint $\dot{\beta} \le 0$, which must be satisfied for all physical admissible processes. In addition, based on Lemaitre [1] proposition, one assumes that

$$\varphi_D^S(\dot{\beta};\circ) = \frac{1}{2} \beta S_o \dot{\beta}^2, \tag{4.41}$$

in which, S_o is a material parameter that measures the damage strength of the material. As a result, the damage potential becomes

$$\varphi_D(\dot{\beta};\circ) = \tfrac{1}{2} \beta S_o \dot{\beta}^2 + I_-(\dot{\beta}). \tag{4.42}$$

Therefore, from the Legendre-Fenchel transform (4.38), one obtains

$$\varphi_D^*\left(F^i;\circ\right)=\begin{cases}\dfrac{1}{2}\beta S_o\left(\dfrac{F^i}{\beta S_o}\right)^2, & \text{if} \quad F^i\le 0\\ 0 \qquad\qquad , & \text{if} \quad F^i>0.\end{cases} \tag{4.43}$$

At this point one may calculate $\dot{\beta}$ by means of expression (4.27), what yields

$$\dot{\beta}=\begin{cases}\dot{\lambda}\left(\dfrac{F^i}{\beta S_o}\right), & \text{if} \quad F^i\le 0\\ 0 \qquad , & \text{if} \quad F^i>0.\end{cases} \tag{4.44}$$

According to Lemaitre [1], as the effective viscoplastic strain, e_{ef}^{vp}, increases from zero, the damage remains equal to zero up to the onset of nucleation of micro cracks or voids. Thus, the rate of damage must be rewritten as

$$\dot{\beta}\in\dot{\lambda}\partial\varphi_D^*(F^i;\circ)\,\overline{H}\left(e_{ef}^{vp}-e_{ef_{th}}^{vp}\right) \tag{4.45}$$

in which, one has introduced the step function, known as Heaviside function $\overline{H}(\circ)$, given by

$$\overline{H}\left(e_{ef}^{vp}-e_{ef_{th}}^{vp}\right)=\begin{cases}1, & \text{if} \quad e_{ef}^{vp}\ge e_{ef_{th}}^{vp}\\ 0, & \text{if} \quad e_{ef}^{vp}<e_{ef_{th}}^{vp}\end{cases} \tag{4.46}$$

in which, $e_{ef_{th}}^{vp}$ is named threshold effective viscoplastic strain. The threshold viscoplastic strain corresponds to a nucleation of micro cracks or micro voids which does not produce any change in the mechanical properties. It is related to the amount of energy, which is stored in the material. This stored energy is the result of micro stress concentration which develops in the neighborhood of micro cracks or micro voids.

Thus, based on this physical observation, one may express the evolution equation for the damage variable as

$$\dot{\beta} = \begin{cases} \dot{\lambda}\left(\dfrac{F^i}{\beta S_o}\right)\bar{H}\left(e_{ef}^{vp} - e_{ef_{th}}^{vp}\right), & \text{if} \quad F^i \le 0 \\ 0 \qquad\qquad , & \text{if} \quad F^i > 0. \end{cases} \tag{4.47}$$

Moreover, the sub gradient of $I_{-}(\dot{\beta})$, denoted as $\partial I_{-}(\dot{\beta})$, is given by

$$\partial I_{-}(\dot{\beta}) = \begin{cases} 0, & \text{if} \quad \dot{\beta} < 0 \\ [0, +\infty), & \text{if} \quad \dot{\beta} = 0 \\ \varnothing, & \text{if} \quad \dot{\beta} > 0. \end{cases} \tag{4.48}$$

4.4. DIFFERENTIAL EQUATION FOR THE DAMAGE EVOLUTION

The differential equation for the damage evolution is given by Equation (3.6). Restricting now to quasi-static processes, in which $\rho\ddot{\beta} = 0$, and replacing Equations (3.36) and (4.10), one obtains

$$\acute{k} div(\vec{\nabla}\beta) = F^r + F^{reac} + F^i, \tag{4.49}$$

and, consequently,

$$F^i = \acute{k} div(\vec{\nabla}\beta) - (F^r + F^{reac}). \tag{4.50}$$

One observes that F^i is related to $\dot{\beta}$ by means of Equation (4.47). Combining the above results, one may write

$$\beta S_o \dot{\beta} = \dot{\lambda}\, \bar{H}\left(e_{ef}^{vp} - e_{ef_{th}}^{vp}\right)\, H(F^i)\left[\acute{k} div(\vec{\nabla}\beta) - (F^r + F^{reac})\right], \tag{4.51}$$

in which, $\bar{H}\left(e_{ef}^{vp} - e_{ef_{th}}^{vp}\right)$ is given by expression (4.46) and

$$H(F^i) = \begin{cases} 1, & \text{if} \quad F^i \leq 0 \\ 0, & \text{if} \quad F^i > 0. \end{cases} \tag{4.52}$$

4.5. REGULARIZATION OF THE FREE ENERGY POTENTIAL

Due to the presence of the indicator function, $I_{\boldsymbol{K}}(\beta)$, the Helmholtz free energy potential given by

$$\Psi(\boldsymbol{\varepsilon}^e, r, \beta, \vec{\nabla}\beta) = \Psi^{vp}(\boldsymbol{\varepsilon}^e, r, \beta, \vec{\nabla}\beta) + I_{\boldsymbol{K}}(\beta) \tag{4.53}$$

is a nondifferentiable function. As a consequence, its numerical implementation becomes more difficult. In order to circumvent this problem, so that one could apply well known algorithms, one has employed the regularization process[18]. Thus, the regularized Helmholtz free energy potential, $\Psi_{\bar{\eta}}(\boldsymbol{\varepsilon}^e, r, \beta, \vec{\nabla}\beta)$, is such that

$$\lim_{\bar{\eta}\to 0} \Psi_{\bar{\eta}}(\boldsymbol{\varepsilon}^e, r, \beta, \vec{\nabla}\beta) = \Psi(\boldsymbol{\varepsilon}^e, r, \beta, \vec{\nabla}\beta). \tag{4.54}$$

Since Ψ^{vp} is a smooth function, then one has only needed to regularize the indicator function of the set $\mathcal{K}$, defined as $\mathcal{K} = \{(\circ, \beta, \vec{\nabla}\beta) \,|\, 0 \leq \beta \leq 1\}$, by applying internal and external penalty methods. In this case, one considers a differentiable approximation, $I_K^{\bar{\eta}}(\beta)$, such that

$$\lim_{\eta\to 0} I_K^{\bar{\eta}}(\beta) = I_K(\beta). \tag{4.55}$$

In this work, one considers the regularized function $I_K^{\bar{\eta}}(\beta)$ to be given by

$$I_{\boldsymbol{K}}^{\bar{\eta}}(\beta) = \frac{\bar{\eta}_a}{\beta} + \frac{1}{2\bar{\eta}_b}\left(\langle \beta - 1 \rangle^+\right)^2, \tag{4.56}$$

[18] **Regularization** is a process of making a function more regular or smooth. It involves the introduction of additional information in order to solve an ill-posed problem. This information is usually of the form of a penalty for complexity, such as restriction for smoothness or bounds on the vector space norm [21, 80].

in which, $\bar{\eta}_a$ and $\bar{\eta}_b$ are adequate penalty regularization parameters usually taken, so that $\bar{\eta}_a$ and $\bar{\eta}_b \in [10^{-6}, 10^{-9}]$. Thus, combining Equations (4.53) and (4.56), one finally obtains

$$\Psi(\boldsymbol{\varepsilon}^e, r, \beta, \vec{\nabla}\beta) = \Psi^{vp}(\boldsymbol{\varepsilon}^e, r, \beta, \vec{\nabla}\beta) + \frac{\bar{\eta}_a}{\beta} + \frac{1}{2\bar{\eta}_b}\left(\left\langle \beta - 1 \right\rangle^+\right)^2. \qquad (4.57)$$

In this equation, the notation $\langle \bullet \rangle^+$ is known as Macaulay bracket[19]. Because the indicator function has been regularized, the approximate reaction force of damage, F^{reac}, is then given by

$$F^{reac} = \frac{\partial I_K^{\bar{\eta}}(\beta)}{\partial \beta} = -\frac{\bar{\eta}_a}{\beta^2} + \frac{1}{\bar{\eta}_b}\left\langle (\beta - 1) \right\rangle^+. \qquad (4.58)$$

Notice that, the actual value of F^{reac} is only obtained when $\bar{\eta}_b \to 0$. In practice, the limit is not taken so one only uses a sufficiently small positive value for $\bar{\eta}_b$.

Minak *et al.* [86] recommends that it is more appropriate to use D instead of β as damage variable, because the definition of that variable is closer to the one usually adopted in the traditional works of continuum damage mechanics. Thus, replacing $\beta = (1 - D)$ into Equation (4.47) yields

$$\dot{D} = \begin{cases} \dot{\lambda}\left[\dfrac{F_D^i}{(1-D)S_o}\right]\bar{H}(e_{ef}^{vp} - e_{ef_{th}}^{vp})H(F_D^i), & \text{if} \quad F_D^i \le 0 \\ 0 \qquad\qquad\qquad\qquad\qquad\quad , & \text{if} \quad F_D^i > 0, \end{cases} \qquad (4.59)$$

in which,

$$F_D^i = k\,div(\vec{\nabla}\beta) - (F_D^r + F_D^{reac}), \qquad (4.60)$$

[19] Macaulay bracket is a notation, which represents the positive part of the function inside it. Consider a generic function $f(x)$, then its positive part, represented by $\langle f(x) \rangle^+$, is given by

$$\langle f(x) \rangle^+ = \max\{0, f(x)\} = \begin{cases} 0, & \text{if} \quad f(x) < 0 \\ f(x), & \text{if} \quad f(x) \ge 0. \end{cases}$$

$$F_D^r = \frac{(\sigma_{eq}^{vm})^2}{2E(1-D)^2}\left[\frac{2}{3}(1+\nu)+3(1-2\nu)\left(\frac{\sigma_H}{\sigma_{eq}^{vm}}\right)^2\right] \tag{4.61}$$

and

$$F_D^{reac} = -\frac{\bar{\eta}_a}{(1-D)^2}+\frac{1}{\bar{\eta}_b}\langle(-D)\rangle^+ \tag{4.62}$$

with

$$\langle(-D)\rangle^+ = \begin{cases} -D, \text{ if } D \le 0 \\ 0, \text{ if } D > 0. \end{cases} \tag{4.63}$$

4.6. ANALYSIS OF THE COLD DRAWING PROCESS

When a ductile plastic material, like polypropylene or polyethylene, is submitted to a tensile load, its stress-strain diagram looks similar to that illustrated in Figure 4.2. The objective of this section is to improve the viscoplastic model in order to be capable of modeling the cold drawing process. In order to do so, one will initially investigate Figure 4.2 and propose some simplifications. Based on these simplifications, one will make some considerations into the proposed model.

According to Ghorbel [4], the isotropic hardening, which is related to the growth of the elastic domain, can be associated with the increase in the covalent bonds, with the entanglements density and with the change of the conformation of molecular links inside the amorphous phase, which increase under deformation. In a quasistatic process, like that illustrated in Figure 4.2, the entanglements density will not be reduced. In fact, they will increase. Therefore, under these considerations, the function $h(r)$ must be a non-decreasing function on r. So, considering the load path AB of Figure 4.2, $R = h(r)$ can be responsible for the nonlinear hardening but, since it can not decrease, it is not able to represent the softening behavior. Hence, the softening behavior must be accounted for the damage variable. Considering the load path BC of Figure 4.2, representing the cold drawing process, one may assume

$$\frac{dh}{dr} = 0. \tag{4.64}$$

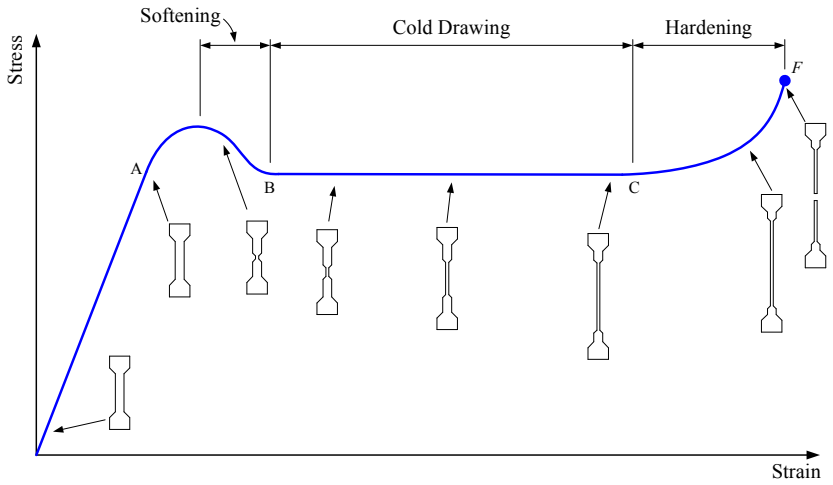

Figure 4.2: Analysis of the cold drawing process.

Considering now the load path *CF* of Figure 4.2, one observes an increase in strength of the material. So, the damage variable is not able to represent the increase in strength. Thus, the increase of strength in the load path *CF* must be taken into account by the isotropic hardening process again. Thus, based on the above considerations, one may assume a functional relation for the isotropic hardening stress (R), in terms of e_{ef}^{vp} as illustrated in Figure 4.3.a. In addition, one assumes the evolution of the damage, D, in terms of e_{ef}^{vp} to be given as illustrated in Figure 4.3.b, as well. Notice that the damage, D, in the load path *CF* may increase, causing a small decrease in the material strength. However, since the material is actually increasing its strength, then the increase in strength caused by the isotropic hardening must be larger than the decrease of strength caused by the evolution of damage in the load path *CF*. As a fracture criterion, one may assume the existence of a admissible effective viscoplastic strain, $e_{ef_{adm}}^{vp} = \Im(\dot{e}_{ef}^{vp})$, so that $e_{ef}^{vp} \leq e_{ef_{adm}}^{vp}$.

It is important to notice that the damage is responsible for describing the softening behavior of the nominal stress. The reduction of area, due to the necking, gives rise to a larger effective Cauchy stress, represented by $\tilde{\boldsymbol{\sigma}} = \boldsymbol{\sigma}/(1-D)$.

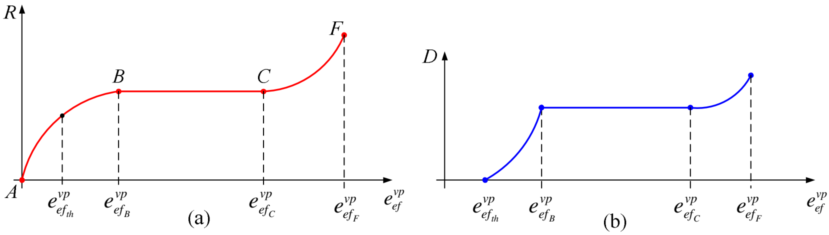

Figure 4.3: Diagrams isotropic hardening and damage *versus* effective viscoplastic strain.

In the load path *BC*, illustrated in Figure 4.2, representing a cold drawing process, one may assume once $D = D_{cd} = cte$, with $D_{cd} \in (0,1)$ so that $\dot{D} = 0$. Here, $D_{cd} \in (0,1)$ represents the critical damage value at which the necking process is interrupted. This value can be computed from the specimen data, as one can measure the reduced area at which the necking process is interrupted. In fact, as can be noticed in the cold drawing process, defined by the load path *BC* illustrated in Figure 4.2, the reduced cross section at the necking point remains approximately constant throughout the entire load path *BC*. Thus, the consideration of $\dot{D} = 0$ is a good approximation for the damage process in this stage, once the critical damage $D = D_{cd} = cte$ is reached. Thus, in order to impose the locking constraint $\dot{D} = 0$ that must be satisfied in the load path *BC*, one considers the damage evolution equation

$$\dot{D} = \begin{cases} \dot{\lambda}\left[\dfrac{F_D^i}{(1-D)S_o}\right]\bar{H}(e_{ef}^{vp} - e_{ef_{th}}^{vp})H(F_D^i), & \text{if } F_D^i \le 0 \\ 0, & \text{if } F_D^i > 0, \end{cases} \tag{4.65}$$

in which,

$$F_D^i = \not{k}\, div(\vec{\nabla} D) + (F_D^r + F_D^{reac}) \tag{4.66}$$

Notice that, at points in which $e_{ef}^{vp}(\vec{x},t)$ is in the interior of the interval $(e_{ef_B}^{vp}, e_{ef_C}^{vp})$, i.e., undergoing a cold drawing deformation process, the cross section in the specimen is kept constant, so $\vec{\nabla} D(\vec{x},t) = 0$.

Moreover, since the cross section is smaller than the initial cross section, but is not zero, then one may conclude that $D(\vec{x},t) = D_{cd} = cte$, with $D_{cd} \in (0,1)$, which implies $F^{reac} = 0$. So, for $e_{ef}^{vp}(\vec{x},t) > e_{ef_B}^{vp}$, the damage evolution equation reduces to

$$\dot{D} = \dot{\lambda}\left[\frac{F_D^r}{(1 - D_{cd})\, S_o}\right], \tag{4.67}$$

in which, F_D^r is given by

$$F_D^r = \frac{(\sigma_{eq}^{vm})^2}{2E(1-D)^2}\left[\frac{2}{3}(1+\nu) + 3(1-2\nu)\left(\frac{\sigma_H}{\sigma_{eq}^{vm}}\right)^2\right].$$

Observing the Figure 4.2, one can notice that the nominal stress is also kept constant, one may conclude that $R_v \simeq cte$ and $\sigma_{eq}^{vm} \simeq cte$, during the cold drawing process. As a result, the only form to impose the condition of locking constraint, $\dot{D} = 0$, is to suppose that the material parameter, S_o, is not a constant, i.e., that it depends on e_{ef}^{vp}. Hence, one assumes that $S_o = S_o(e_{ef}^{vp})$. Moreover, in order to implicitly impose $\dot{D} = 0$, one assumes that

$$S_o(e_{ef}^{vp}) = \begin{cases} cte, & \text{if } e_{ef}^{vp} < e_{ef_B}^{vp} \\ +\infty, & \text{if } e_{ef}^{vp} > e_{ef_B}^{vp}. \end{cases} \tag{4.68}$$

The proposed material parameter, S_o, which now depends on e_{ef}^{vp}, is able to implicitly impose the internal or locking constraint in the load path *BF*. However, $S_o(e_{ef}^{vp})$ is non differentiable. In order to circumvent this nondifferentiability and to allow a small and controllable variation of the damage rate, $\dot{D}$, in the load path *BF*, one applies the external penalty method. Thus, one defines a smooth material function, $S_{\bar{\eta}_s}(e_{ef}^{vp})$, so that

$$\lim_{\bar{\eta}_s \to 0} S_{\bar{\eta}_s}(e_{ef}^{vp}) = S_o(e_{ef}^{vp}). \tag{4.69}$$

Here, one considers for simplicity $\bar{\eta}_s$ to be a positive sufficiently small parameter, which may be identified from experimental data, so that

$$S_{\bar{\eta}_s}(e_{ef}^{vp}) = S_o + \frac{1}{2\bar{\eta}_s}\left[\left\langle\left(e_{ef}^{vp} - e_{ef_B}^{vp}\right)\right\rangle^{+}\right]^2. \tag{4.70}$$

Since $S_{\bar{\eta}_s}(e_{ef}^{vp}) < \infty$, one will have $\dot{D} \neq 0$. But, by selecting $\bar{\eta}_s$ sufficiently small, one may be able to control the increase of the damage in the load path *BF* and recover the failure criterion

$$D \leq D_{cd}. \tag{4.71}$$

Replacing the fracture criterion, previously proposed, given in terms of the total effective threshold viscoplastic strain, $e_{ef_{adm}}^{vp} = \Im(\dot{e}_{ef}^{vp})$, so that $e_{ef}^{vp} \leq e_{ef_{adm}}^{vp}$. Thus, the regularization removes this problem and since it is controllable, it may be a more realistic approach in order to properly model the real behavior of the material. Moreover, the regularized material function allows, by consequence, the proposition of a hardening function $h(r)$, whose derivative in the load path *BC* may be nonzero, i.e.,

$$\frac{dR}{dr} = \frac{dh}{dr} > 0, \tag{4.72}$$

obtained by interpolation from the available experimental data. Based on the previous assumptions, one can state now the strong form of the elasto-viscoplastic model with coupled damage.

4.6.1. Strong Form of the Elasto-Viscoplastic Model with Coupled Damage

According to Cook *et al.* [87] and Assan [88], the **strong form** of a problem, usually represented by a differential equation or a set of differential equations, is defined as that in which the conditions established to characterize the problem in study are satisfied at all points

of the domain (continuous solution). In other words, this means that the problem has an analytical solution for its equation. This possibility can restrict the admissible solution space to the point at which only one function is solution of the problem. Due to this "strong" restriction, which must be imposed on the admissible solution space for the existence of an analytical solution to the problem, the formulation is then named **strong**.

The strong formulation of the elasto-viscoplastic model coupled with damage, for quasistatic processes, without residual stresses ($\boldsymbol{\sigma}_o = 0$) and free of initial defects, may be stated as: find the displacement and damage fields, $(\vec{u}, D)$, that solve

$$div\left[\boldsymbol{\sigma}(\vec{x},t)\right] + \rho\vec{b}(\vec{x},t) = 0, \tag{4.73}$$

subjected to the boundary conditions $\vec{u} = \bar{\vec{u}}$ on Γ_u and $\boldsymbol{\sigma}\vec{n} = \vec{t}$ on Γ_t, and

$$S_{\bar{\eta}_s}\dot{D} = \frac{\dot{\lambda}}{(1-D)} F_D^i \;\; \bar{H}(e_{ef}^{vp} - e_{ef_{th}}^{vp}) H(F_D^i) \tag{4.74}$$

subjected to the boundary condition $\vec{\nabla}D \cdot \vec{n} = 0$ and to the initial condition $D(x,0) = 0$, in which

$$F_D^i = \acute{k} div(\vec{\nabla}D) + (F_D^r + F_D^{reac}),$$

$$H(F_D^i) = \begin{cases} 1, & \text{if} \quad F_D^i \le 0 \\ 0, & \text{if} \quad F_D^i > 0 \end{cases}$$

and

$$\bar{H}(e_{ef}^{vp} - e_{ef_{th}}^{vp}) = \begin{cases} 1, & \text{if} \quad e_{ef}^{vp} \ge e_{ef_B}^{vp} \\ 0, & \text{if} \quad e_{ef}^{vp} < e_{ef_B}^{vp} \end{cases}$$

in which, $S_{\bar{\eta}_s}$ is given by expression (4.70) and F_D^r and F_D^{reac} are given respectively by

$$F_D^r = \frac{(\sigma_{eq}^{vm})^2}{2E(1-D)^2}\left[\frac{2}{3}(1+\nu)+3(1-2\nu)\left(\frac{\sigma_H}{\sigma_{eq}^{vm}}\right)^2\right]$$

and

$$F_D^{reac} = -\frac{\overline{\eta}_a}{(1-D)^2}+\frac{1}{\overline{\eta}_b}\langle(-D)\rangle^+ .$$

From Equation (4.33), one knows that

$$\dot{e}_{ef}^{vp} = \frac{\dot{\lambda}}{(1-D)}. \tag{4.75}$$

Thus, one may rewrite the damage initial value problem, Equation (4.74), as

$$S_{\overline{\eta}_s}\dot{D} = \dot{e}_{ef}^{vp}\; F_D^i\; \overline{H}(e_{ef}^{vp}-e_{ef_{th}}^{vp})H(F_D^i) \tag{4.76}$$

in which, $\dot{e}_{ef}^{vp}$ is given by

$$\dot{e}_{ef}^{vp} = -M\,\ln\left(1-\frac{f(\boldsymbol{\sigma},R,D;\circ)}{K_\infty}\right) \tag{4.77}$$

for $f(\boldsymbol{\sigma},R,D;\circ)\geq 0$, subjected to the boundary condition $\vec{\nabla}D\cdot\vec{n}=0$ and to the initial condition $D(\vec{x},0)=0$. Finally, Table 4.1 summarizes the set of equations, which describes the proposed elasto-viscoplastic model coupled with damage without thermomechanical coupling, which can be used for the analysis of the ductile failure of plastic components. The discretization of these equations will be presented in Chapter 5.

Table 4.1: Set of constitutive equations of the elasto-viscoplastic model with damage.

- **Linear Momentum Equation:**

$$div\left[\boldsymbol{\sigma}(\vec{x},t)\right] + \rho\vec{b}(\vec{x},t) = 0$$

- **Elastic Stress-Strain Response:**

$$\boldsymbol{\sigma} = (1-D)\mathbb{D}\boldsymbol{\varepsilon}^{\mathrm{e}} \quad \text{with} \quad \boldsymbol{\varepsilon} = \boldsymbol{\varepsilon}^{e} + \boldsymbol{\varepsilon}^{vp}$$

- **Flow Rule and Hardening Evolution Law:**

$$\dot{\boldsymbol{\varepsilon}}^{vp} = \frac{\dot{\lambda}}{(1-D)}\left[\frac{3}{2(1-D)}\frac{\boldsymbol{\sigma}^{D}}{\sigma_{eq}^{vm}} + \frac{\mu}{3}\boldsymbol{I}\right] \quad \text{and} \quad R = h(r), \text{ in which}$$

$$\dot{e}_{ef}^{vp} = -M\ln\left(1 - \frac{f(\boldsymbol{\sigma}, R, D; \circ)}{K_{\infty}}\right)$$

with $\dot{r} = \left(1 + \frac{\mu}{3}\right)\dot{\lambda}$ and $\dot{\lambda} = (1-D)\dot{e}_{ef}^{vp}$

- **Yield Condition:**

$$f\left(\boldsymbol{\sigma}, R\right) = \frac{1}{(1-D)}\left[\left(\frac{3}{2}\boldsymbol{\sigma}^{D}\cdot\boldsymbol{\sigma}^{D}\right)^{1/2} + \mu\sigma_{H}\right] - \left(1 + \frac{\mu}{3}\right)\left(\sigma_{y_o} + R\right)$$

- **Damage Evolution Law:**

$$\dot{D} = \begin{cases} \dot{\lambda}\left[\dfrac{F_D^{i}}{(1-D)S_{\overline{\eta}_s}}\right]\overline{H}(e_{ef}^{vp} - e_{ef_{th}}^{vp})H(F_D^{i}), & \text{if} \quad F_D^{i} \le 0 \\ 0 \qquad\qquad\qquad\qquad\qquad\quad , & \text{if} \quad F_D^{i} > 0 \end{cases}$$

with

$$F_D^i = \overline{k} div(\vec{\nabla} D) + (F_D^r + F_D^{reac}),$$

$$F_D^r = \frac{(\sigma_{eq}^{vm})^2}{2E(1-D)^2}\left[\frac{2}{3}(1+\nu) + 3(1-2\nu)\left(\frac{\sigma_H}{\sigma_{eq}^{vm}}\right)^2\right],$$

$$F_D^{reac} = -\frac{\overline{\eta}_a}{(1-D)^2} + \frac{1}{\overline{\eta}_b}\left\langle(-D)\right\rangle^+$$

and

$$S_{\overline{\eta}_s}(e_{ef}^{vp}) = S_o + \frac{1}{2\overline{\eta}_s}\left[\left\langle\left(e_{ef}^{vp} - e_{ef_{th}}^{vp}\right)\right\rangle^+\right]^2,$$

in which,

$$H(F_D^i) = \begin{cases} 1, \text{ if } F_D^i \le 0 \\ 0, \text{ if } F_D^i > 0 \end{cases} \quad \text{and} \quad \left\langle(-D)\right\rangle^+ = \begin{cases} -D, \text{ if } D \le 0 \\ 0, \text{ if } D > 0. \end{cases}$$

CHAPTER 5

NUMERICAL SOLUTION OF THE MODEL

This chapter will present the numerical solution (discretization) of the set of constitutive equations given Table 4.1. As usual, the solution will be performed in **space** and in **time**. The **spatial discretization** is performed at the **global** (structural) level by means of the Galerkin Finite Element Method. In turn, the **time discretization** subdivides the time of interest [0,*t*] into a sequence of non-overlapping time steps $[t_n, t_{n+1}]$ and is performed by means of the fully implicit finite difference method, also named the **Fully Implicit Backward Euler Method** for finite difference.

According to Valoroso [89], the constitutive equations of viscoplasticity lead to a nonlinear problem of evolution, in which the most general case is not amenable to an exact solution. Accordingly, one has to suitably approximate the exact evolution by replacing time derivatives with finite differences and choose a characteristic value $t_a \in [t_n, t_{n+1}]$. A typical choice is that of taking $t_a = t_{n+1}$, which corresponds to the **fully implicit** (Backward Euler difference) scheme [89]. In addition, the hypothesis of elasticity and homogeneity will also be considered in this chapter.

Thus, in order to apply Euler's method, one performs an uniform partition of the time domain $[0, t_f]$, t_f denoting the final time of the analysis, in intervals $[t_n, t_{n+1}]$, with a constant time increment, given by $\Delta t = t_{n+1} - t_n$. Thus, for the fully implicit Euler's method, one assumes the state variables to be known at t_n and the problem consists then in the determination of the state variables at time t_{n+1}, considering the initial conditions known. This procedure leads to a constitutive initial value problem. The method employed for the integration of the constitutive initial value problem is the **operator split method**.

5.1. OPERATOR SPLIT ALGORITHM

The numerical implementation of an operator split scheme relies upon the view of the discrete evolution equations as strain driven. This problem is solved with a three steps algorithm by first computing a trial elastic state. If the hypothesis of an elastic increment is violated, then a fully elasto-viscoplastic coupled with damage corrector scheme is solved, so that the updated variables are computed by restoring consistency [80,

89]. The three steps of this technique are: the **trial elastic state**, **verification of the yielding condition** and the **elasto-viscoplastic coupled with damage corrector**.

In the trial elastic state step, the problem is assumed to be purely elastic between times t_n and t_{n+1}. In turn, in the elasto-viscoplastic coupled with damage corrector step, a discrete system of equations comprising the elasticity law; the viscoplastic flow and viscoplastic multiplier evolution equations and the hardening laws are solved, employing as initial condition the results computed in the trial elastic step. From a physical standpoint, the trial elastic state is obtained by freezing the viscoplastic variables at their values at the beginning of the time step [80, 89].

5.1.1. Trial Elastic State

Here, the problem is assumed as purely elastic between t_n and t_{n+1}, then the elastic predictor problem may be stated as: given the history of the strain and damage, $\{\boldsymbol{\varepsilon}(t), D(t)\} \in [t_n, t_{n+1}]$, find $\boldsymbol{\varepsilon}_{n+1}^{e\ trial}$ and $\vec{V}_{n+1}^{trial}$, in which $\vec{V}_{n+1}^{trial} = (\boldsymbol{\varepsilon}_{n+1}^{vp\ trial}, r_{n+1}^{trial}, e_{ef_{n+1}}^{vp\ trial})$, so that

$$\dot{\boldsymbol{\varepsilon}}^{vp\ trial} = 0 \tag{5.1}$$

and

$$\dot{\vec{V}}^{trial} = 0. \tag{5.2}$$

Thus, in the trial elastic state phase, one assumes that the response of the material in the increment from t_n to t_{n+1} is elastic. The initial condition, for this constitutive initial value problem is given by the state at t_n, i.e.,

$$\boldsymbol{\varepsilon}^{vp\ trial}(t_n) = \boldsymbol{\varepsilon}_n^{vp} \tag{5.3}$$

and

$$\vec{V}^{trial}(t_n) = \vec{V}_n. \tag{5.4}$$

Thus, integrating (5.1) and using (5.3), one obtains

$$\boldsymbol{\varepsilon}_{n+1}^{e\ trial} = \boldsymbol{\varepsilon}_{n+1} - \boldsymbol{\varepsilon}_{n}^{vp}, \tag{5.5}$$

in which, $\boldsymbol{\varepsilon}_{n+1}^{e\ trial}$ is the trial elastic strain at t_{n+1}, $\boldsymbol{\varepsilon}_{n}^{vp}$ is the viscoplastic strain at t_n and $\vec{V}_{n+1}^{trial}$ is the array of trial internal variables at t_{n+1}. From Equations (4.12) and (5.5), one may write the deviatoric part of the trial elastic strain tensor, $\boldsymbol{\varepsilon}_{n+1}^{e\,D\,trial}$, as

$$\boldsymbol{\varepsilon}_{n+1}^{e\,D\,trial} = \boldsymbol{\varepsilon}_{n+1}^{e\,trial} - e_{H}^{e\,trial}\boldsymbol{I}, \tag{5.6}$$

in which, the hydrostatic part of the trial elastic strain tensor is given by

$$e_{H_{n+1}}^{e\ trial} = \frac{1}{3} tr\left(\boldsymbol{\varepsilon}_{n+1}^{e^{trial}}\right). \tag{5.7}$$

As a consequence, one may write

$$q_{n+1}^{trial} = \left(\frac{3}{2}\tilde{\boldsymbol{\sigma}}_{n+1}^{D\ trial} \cdot \tilde{\boldsymbol{\sigma}}_{n+1}^{D\ trial}\right)^{\frac{1}{2}}, \tag{5.8}$$

$$p_{n+1}^{trial} = \frac{E}{(1-2\nu)} e_{H_{n+1}}^{e\ trial}, \tag{5.9}$$

$$\sigma_{H_{n+1}}^{trial} = (1-D_{n+1})\, p_{n+1}^{trial} \tag{5.10}$$

and

$$\boldsymbol{\sigma}_{n+1}^{D\,trial} = 2G(1-D_{n+1})\boldsymbol{\varepsilon}_{n+1}^{e\,D\,trial}, \tag{5.11}$$

in which, G is the shear modulus. Moreover, one has

$$\vec{V}_{n+1}^{trial} = \vec{V}_{n}, \tag{5.12}$$

what gives

$$\boldsymbol{\varepsilon}_{n+1}^{vp\ trial} = \boldsymbol{\varepsilon}_{n}^{vp}, \qquad e_{ef_{n+1}}^{vp\ trial} = e_{ef_n}^{vp} \qquad \text{and} \qquad r_{n+1}^{trial} = r_n,$$

so that,

$$R_{n+1}^{trial} = h(r_{n+1}^{trial}). \tag{5.13}$$

5.1.2. Verification of the Yielding Condition

Once the trial elastic state is determined, one must verify if the assumption of an elastic step increment, in the interval $[t_n, t_{n+1}]$, has in fact occurred. Otherwise, a projection procedure must be applied in order to determine the elasto-viscoplastic with damage state.

Here, one employs a strain driven projection procedure, based on the so called elasto-viscoplastic coupled with damage operator split class of algorithms. The procedure is strain driven since it enforces the total deformation, $\boldsymbol{\varepsilon}_{n+1}$, and damage, D_{n+1}, and then determines the elasto-viscoplastic with damage state. Thus, if $f(\bullet) < 0$, then the state at t_{n+1} is in fact elastic. In this case, one sets

$$\sigma_{H_{n+1}} = \sigma_{H_{n+1}}^{trial}, \quad \boldsymbol{\sigma}_{n+1}^{D} = \boldsymbol{\sigma}_{n+1}^{D\ trial}, \quad \boldsymbol{\varepsilon}_{n+1}^{vp} = \boldsymbol{\varepsilon}_{n}^{vp}, \quad e_{ef_{n+1}}^{vp} = e_{ef_n}^{vp} \quad \text{and} \quad r_{n+1} = r_n,$$

in which, the Cauchy stress tensor is given by

$$\boldsymbol{\sigma}_{n+1} = \boldsymbol{\sigma}_{n+1}^{D} + \sigma_{H_{n+1}} \boldsymbol{I}. \tag{5.14}$$

Otherwise, i.e., if $f(\bullet) \geq 0$ one must solve the elasto-viscoplastic with damage corrector scheme.

5.1.3. Elasto-Viscoplastic Coupled with Damage Corrector

The elasto-viscoplastic correction algorithm just must be executed if the trial state yields a stress, which is not inside the set of stresses defined by the yield function. In the fully implicit backward Euler's scheme, one has: given $(\boldsymbol{\varepsilon}_{n+1}, D_{n+1})$, determine the state variables at t_{n+1} satisfying the following system of nonlinear equations:

$$\boldsymbol{\varepsilon}_{n+1}^{e} = \boldsymbol{\varepsilon}_{n+1} - \boldsymbol{\varepsilon}_{n+1}^{vp}, \tag{5.15}$$

which may be written as

$$\boldsymbol{\varepsilon}_{n+1}^{e} = \boldsymbol{\varepsilon}_{n+1}^{e\ trial} - \Delta\boldsymbol{\varepsilon}_{n+1}^{vp}, \tag{5.16}$$

so that,

$$\Delta\boldsymbol{\varepsilon}_{n+1}^{vp} = \boldsymbol{\varepsilon}_{n+1}^{vp} - \boldsymbol{\varepsilon}_{n}^{vp}. \tag{5.17}$$

From the viscoplastic flow rule given by Equation (4.29), by applying the backward Euler's method, one derives

$$\boldsymbol{\varepsilon}_{n+1}^{e} = \boldsymbol{\varepsilon}_{n+1}^{e\ trial} - \frac{\Delta\lambda}{(1-D_{n+1})}\left(\frac{3}{2}\frac{\tilde{\boldsymbol{\sigma}}_{n+1}^{D}}{q_{n+1}} + \frac{\mu}{3}\boldsymbol{I}\right). \tag{5.18}$$

Taking the trace of expression (5.16), replacing Equations (4.14) and (4.15) and performing some mathematical manipulations, one obtains

$$p_{n+1} + \frac{E}{3(1-2\nu)}\frac{\mu\Delta\lambda}{(1-D_{n+1})} = p_{n+1}^{trial} \tag{5.19}$$

and

$$\left[1 + \frac{3G\Delta\lambda}{(1-D_{n+1})q_{n+1}}\right]\tilde{\boldsymbol{\sigma}}_{n+1}^{D} = \tilde{\boldsymbol{\sigma}}_{n+1}^{D\ trial}, \tag{5.20}$$

in which,

$$p_{n+1}^{trial} = \frac{E}{(1-2\nu)}e_{H_{n+1}}^{e\ trial} \tag{5.21}$$

and

$$\tilde{\boldsymbol{\sigma}}_{n+1}^{D\ trial} = 2G\boldsymbol{\varepsilon}_{n+1}^{e\ D\ trial}. \tag{5.22}$$

Moreover, from the definition of q_{n+1}, one also obtains

$$q_{n+1} + \frac{3G\Delta\lambda}{(1 - D_{n+1})} = q_{n+1}^{trial} \tag{5.23}$$

with

$$q_{n+1}^{trial} = \sqrt{\frac{3}{2}\tilde{\boldsymbol{\sigma}}_{n+1}^{D\,trial} \cdot \tilde{\boldsymbol{\sigma}}_{n+1}^{D\,trial}}. \tag{5.24}$$

From the isotropic hardening law given by Equation (4.30), by applying the backward Euler's method, one derives

$$r_{n+1} - r_n = \left(1 + \frac{\mu}{3}\right)\Delta\lambda. \tag{5.25}$$

In turn, from the evolution equation of the viscoplastic multiplier given in (4.34), by applying the backward Euler's method, one also derives

$$\frac{\Delta\lambda}{(1 - D_{n+1})} = -M \ln\left[1 - \frac{f\left(p, q, R, D\right)_{n+1}}{K_\infty}\right]\Delta t, \tag{5.26}$$

in which, $\Delta\lambda$ is the increment of the viscoplastic multiplier. In this case, the yield function can be rewritten as

$$f\left(p, q, R, D\right)_{n+1} = \left(q_{n+1} + \mu\, p_{n+1}\right) - \left(1 + \frac{\mu}{3}\right)(\sigma_{yo} + R_{n+1}). \tag{5.27}$$

At this point, by combining the results obtained from Equations (5.15) to (5.27) and performing some simplifications, one may derive a reduced set of non linear equations, which comprises the elasto-viscoplastic coupled with damage corrector problem. Thus, the elasto-viscoplastic corrector problem may be formulated as: given $(\varepsilon_{n+1}, D_{n+1})$, determine $(\Delta\lambda, p_{n+1}, q_{n+1})$, in order to satisfy

$$\begin{cases} R_1 = \dfrac{\Delta\lambda\sigma_{yo}}{(1-D_{n+1})} + \sigma_{yo} M \ln\left[1 - \dfrac{f\left(p,q,R,D\right)_{n+1}}{K_\infty}\right]\Delta t = 0 \\ R_2 = p_{n+1} + \dfrac{E}{3(1-2\nu)}\dfrac{\mu\Delta\lambda}{(1-D_{n+1})} - p_{n+1}^{trial} = 0 \\ R_3 = q_{n+1} + \dfrac{3G\Delta\lambda}{(1-D_{n+1})} - q_{n+1}^{trial} = 0. \end{cases} \tag{5.28}$$

Once the set $(\Delta\lambda, p_{n+1}, q_{n+1})$ is computed, the Cauchy stress tensor (Equation (5.14)) may also be determined from

$$\boldsymbol{\sigma}_{n+1}^{D} = \boldsymbol{\sigma}_{n+1}^{D\ trial}\left[1 + \frac{3G\Delta\lambda}{(1-D_{n+1})}\right]^{-1} \tag{5.29}$$

and

$$\sigma_{H_{n+1}} = (1-D_{n+1})\, p_{n+1}. \tag{5.30}$$

In addition, one can also determine

$$\boldsymbol{\varepsilon}_{n+1}^{vp} = \boldsymbol{\varepsilon}_{n}^{vp} + \frac{\Delta\lambda}{(1-D_{n+1})}\left[\frac{3}{2}\frac{\boldsymbol{\sigma}_{n+1}^{D}}{(1-D_{n+1})q_{n+1}} + \frac{\mu}{3}\boldsymbol{I}\right], \tag{5.31}$$

$$r_{n+1} = r_n + \left(1 + \frac{\mu}{3}\right)\Delta\lambda \tag{5.32}$$

and

$$e_{ef_{n+1}}^{vp} = e_{ef_n}^{vp} + \frac{\Delta\lambda}{(1-D_{n+1})}, \tag{5.33}$$

in which, r is the accumulated viscoplastic strain and e_{ef}^{vp} is the effective viscoplastic strain.

In order to solve the system of nonlinear equations (5.28), one applies Newton-Raphson method. This procedure requires the determination of the local tangent stiffness matrix $\mathbf{K}^T$, whose components are given by

$$\mathrm{K}_{ij}^{T} = \frac{\partial R_i}{\partial a_j}, \tag{5.34}$$

in which, $\vec{a} = (\Delta\lambda, p_{n+1}, q_{n+1})$ and the indexes i and j range from 1 to 3.

5.2. DISCRETIZATION OF THE ELASTO-VISCOPLASTIC MODEL

Here, one considers the solution to be known in the interval $[0, t_n]$ and imposes the equilibrium equations at t_{n+1}. As a result, accounting for a quasistatic process, one has

$$div(\boldsymbol{\sigma}_{n+1}) + \rho\vec{b}_{n+1} = 0, \tag{5.35}$$

subjected to the boundary conditions

$$\vec{u}_{n+1} = \vec{\bar{u}}_{n+1} \quad \text{on} \quad \Gamma_u \tag{5.36}$$

and

$$\boldsymbol{\sigma}_{n+1}\vec{n} = \vec{t}_{n+1} \quad \text{on} \quad \Gamma_t\,. \tag{5.37}$$

From the damage initial value problem, one has

$$(S_{\bar{\eta}_s})\,\dot{D} = \dot{e}_{ef}^{vp}\left[k div(\vec{\nabla}D) + (F_D^r + F_D^{reac})\right]\bar{H}(e_{ef}^{vp} - e_{ef_D}^{vp})\,H(F_D^i). \tag{5.38}$$

Integrating both sides of this expression and assuming the approximations

$$\int_{t_n}^{t_{n+1}} (S_{\overline{\eta}_s})\,\dot{D}\,dt \simeq (S_{\overline{\eta}_s})\int_{t_n}^{t_{n+1}} \dot{D}\,dt = (S_{\overline{\eta}_s})\left(D_{n+1} - D_n\right),$$

$$\int_{t_n}^{t_{n+1}} \dot{e}_{ef}^{vp}\left[k div(\vec{\nabla} D) + (F_D^r + F_D^{reac})\right]\overline{H}(e_{ef}^{vp} - e_{ef_D}^{vp})\,H(F_D^i)\,dt$$
$$\simeq \left[k div(\vec{\nabla} D_{n+1}) + (F_{D_{n+1}}^r + F_{D_{n+1}}^{reac})\right]\overline{H}(e_{ef}^{vp} - e_{ef_D}^{vp})\,H(F_{D_{n+1}}^i)\int_{t_n}^{t_{n+1}} \dot{e}_{ef}^{vp}\,dt$$

and

$$\int_{t_n}^{t_{n+1}} \dot{e}_{ef}^{vp}\,dt = \int_{t_n}^{t_{n+1}} \frac{\dot{\lambda}}{(1-D)}\,dt \simeq \frac{\Delta\lambda}{(1-D_{n+1})}$$

one derives

$$S_{\overline{\eta}_{s_{n+1}}}(D_{n+1} - D_n) = \frac{\Delta\lambda}{(1-D_{n+1})}\Big[k div(\vec{\nabla} D_{n+1}) +$$
$$+(F_{D_{n+1}}^r + F_{D_{n+1}}^{reac})\Big]\overline{H}\left(e_{ef_{n+1}}^{vp} - e_{ef_{th}}^{vp}\right)H\left(F_{D_{n+1}}^i\right), \quad (5.39)$$

subjected to the initial condition

$$D(\vec{x}, 0) = 0. \quad (5.40)$$

Additionally, in Equation (5.39), one also has

$$F_{D_{n+1}}^i = k div(\vec{\nabla} D_{n+1}) + (F_{D_{n+1}}^r + F_{D_{n+1}}^{reac}), \quad (5.41)$$

$$F_{D_{n+1}}^r = \frac{1}{2E}\left[\frac{2}{3}(1+\nu)q_{n+1}^2 + 3(1-2\nu)p_{n+1}^2\right], \quad (5.42)$$

$$F_{D_{n+1}}^{reac} = -\frac{\overline{\eta}_a}{(1-D_{n+1})^2} + \frac{1}{\overline{\eta}_b}\left\langle(-D_{n+1})\right\rangle^+ \quad (5.43)$$

and

$$S_{\bar{\eta}_{s_{n+1}}} = S_o + \frac{1}{2\bar{\eta}_s}\left[\left\langle\left(e^{vp}_{ef_{n+1}} - e^{vp}_{ef_B}\right)\right\rangle^+\right]^2. \tag{5.44}$$

5.2.1. Weak Formulation of the Elasto-Viscoplastic Model

Once one has defined the constitutive equations and the strategy for updating the internal variables at t_{n+1}, what defines the so-called local problem, it is possible to solve the global boundary value problem associated with the displacement and with the damage, i.e., $(\vec{u}, D)$. In this case, one employs the incremental formulation, which considers that, between t_n and t_{n+1} the displacement and damage fields are given, respectively, by

$$\vec{u}_{n+1} = \vec{u}_n + \Delta\vec{u}_n \tag{5.45}$$

and

$$D_{n+1} = D_n + \Delta D_n. \tag{5.46}$$

While the strong formulation is characterized by a continuous solution throughout the domain, in the **weak formulation**, the conditions are only satisfied at discrete points of the domain (discrete solution) [87, 88]. Compared to the strong form, one requires less attributes to the functions, which are potential solutions of the problem. In this case, one considers that the solution of the problem has been weakened. Although the terminologies strong and weak may suggest inferiority of the weak form, both are valid statements of a problem [87].

Thus, at t_{n+1}, the weak formulation of the elasto-viscoplastic with coupled damage model may be stated as: determine the displacement and damage fields, $\left(\vec{u}_{n+1}, D_{n+1}\right) \in \bar{\mathcal{K}}$, so that

$$F_1(\vec{u}_{n+1}, D_{n+1}; \vec{w}) = \int_\Omega \boldsymbol{\sigma}_{n+1} \cdot \varepsilon(\vec{w}) d\Omega - \int_\Omega \rho\vec{b}_{n+1} \cdot \vec{w} d\Omega - \\ - \int_{\Gamma_t} \vec{t}_{n+1} \cdot \vec{w} dA = 0, \quad \forall \vec{w} \in \mathcal{V}_u \tag{5.47}$$

and

$$F_2(\vec{u}_{n+1}, D_{n+1}; \gamma) = \int_\Omega S_{\bar{\eta}_{s_{n+1}}} (D_{n+1} - D_n)\gamma d\Omega + \\ + \int_\Omega k\, \phi_{n+1} \vec{\nabla} D_{n+1} \cdot \vec{\nabla}\gamma d\Omega - \\ - \int_\Omega (F^{r}_{D_{n+1}} + F^{reac}_{D_{n+1}})\phi_{n+1}\gamma d\Omega = 0, \quad \forall \gamma \in \mathcal{V}_D \qquad (5.48)$$

in which,

$$\phi_{n+1} = \frac{\Delta\lambda}{(1 - D_{n+1})} \bar{H}(e^{vp}_{ef_{n+1}} - e^{vp}_{ef_{th}}) H(F^{i}_{D_{n+1}}) \qquad (5.49)$$

and $F^{r}_{D_{n+1}}$, $F^{reac}_{D_{n+1}}$ and $S_{\bar{\eta}_{s_{n+1}}}$ are given, respectively, by expressions (5.42) to (5.44). Here, $\bar{\mathcal{K}}$ denotes the set of admissible displacements and damage, $\bar{\mathcal{K}} = \bar{\mathcal{K}}_u \times \bar{\mathcal{K}}_D$, with

$$\bar{\mathcal{K}} = \left\{ (\vec{u}_{n+1}, D_{n+1}) \;\middle|\; (\vec{u}_{n+1}, D_{n+1}) \text{ is sufficiently regular, } \vec{u}_{n+1} = \bar{\vec{u}}_{n+1} \text{ on } \Gamma_u \right\}$$

and $\mathcal{V}$ denotes the set of admissible variations, $\mathcal{V} = \mathcal{V}_u \times \mathcal{V}_D$, with

$$\mathcal{V} = \left\{ (\vec{w}, \gamma) \;\middle|\; (\vec{w}, \gamma) \text{ is sufficiently regular, } \vec{w} = \vec{0} \text{ on } \Gamma_u \right\}.$$

Since the above problem is nonlinear, one has applied Newton-Raphson method to solve it.

5.2.2. Application of the Newton-Raphson Method

The Newton-Raphson method is a numerical tool largely used to find approximated roots of real valued functions. Thus, based on this method, let $\vec{u}^0_{n+1} = \vec{u}_n$ and $D^0_{n+1} = D_n$ be, respectively, the values of the displacement and damage at the beginning of the Newton-Raphson iteration scheme, in which the upper index represents the iteration number. Then, at the *k-th* iteration, one has

$$\vec{u}_{n+1}^{\,k+1} = \vec{u}_{n+1}^{\,k} + \Delta\vec{u}_{n+1}^{\,k} \tag{5.50}$$

and

$$D_{n+1}^{k+1} = D_{n+1}^{k} + \Delta D_{n+1}^{k}. \tag{5.51}$$

In order to obtain $\Delta\vec{u}_{n+1}^{\,k}$ and ΔD_{n+1}^{k}, one imposes that

$$\begin{cases} F_1(\vec{u}_{n+1}^{\,k} + \Delta\vec{u}_{n+1}^{\,k}, D_{n+1}^{k} + \Delta D_{n+1}^{k}; \vec{w}) = 0, \quad \forall \vec{w} \in \mathcal{V}_u \\ \\ F_2(\vec{u}_{n+1}^{\,k} + \Delta\vec{u}_{n+1}^{\,k}, D_{n+1}^{k} + \Delta D_{n+1}^{k}; \gamma) = 0, \quad \forall \gamma \in \mathcal{V}_D. \end{cases} \tag{5.52}$$

Considering F_1 and F_2 as being smooth and expanding them in a Taylor series, one derives, for a first order approximation,

$$\begin{bmatrix} \partial_{uu}F_1(\vec{u}_{n+1}^{\,k}, D_{n+1}^{k}; \vec{w}) & \partial_{ud}F_1(\vec{u}_{n+1}^{\,k}, D_{n+1}^{k}; \vec{w}) \\ \partial_{du}F_2(\vec{u}_{n+1}^{\,k}, D_{n+1}^{k}; \gamma) & \partial_{dd}F_2(\vec{u}_{n+1}^{\,k}, D_{n+1}^{k}; \gamma) \end{bmatrix} \begin{Bmatrix} \Delta\vec{u}_{n+1}^{\,k} \\ \Delta D_{n+1}^{k} \end{Bmatrix} = -\begin{Bmatrix} F_1 \\ F_2 \end{Bmatrix}. \tag{5.53}$$

In this case, one has:

- **Determination of** $\partial_{uu}F_1\left(\vec{u}_{n+1}^{\,k}, D_{n+1}^{k}; \vec{w}\right)\left[\Delta\vec{u}_{n+1}^{\,k}\right]$:

$$\partial_{uu}F_1\left(\vec{u}_{n+1}^{\,k}, D_{n+1}^{k}; \vec{w}\right)\left[\Delta\vec{u}_{n+1}^{\,k}\right] = \lim_{\varepsilon\to 0} \frac{F_1\left(\vec{u}_{n+1}^{\,k} + \varepsilon\Delta\vec{u}_{n+1}^{\,k}, D_{n+1}^{k}; \vec{w}\right) - F_1\left(\vec{u}_{n+1}^{\,k}, D_{n+1}^{k}; \vec{w}\right)}{\varepsilon}$$

$$= \frac{d}{d\varepsilon}\left[F_1\left(\vec{u}_{n+1}^{\,k} + \varepsilon\Delta\vec{u}_{n+1}^{\,k}, D_{n+1}^{k}; \vec{w}\right)\right]_{\varepsilon=0} \tag{5.54}$$

in which,

$$\partial_{uu}F_1\left(\vec{u}_{n+1}^{\,k}, D_{n+1}^{k}; \vec{w}\right)\left[\Delta\vec{u}_{n+1}^{\,k}\right] = \int_{\Omega}\left[\mathbb{D}_{n+1}^{uu}\right]\boldsymbol{\varepsilon}(\Delta\vec{u}_{n+1}^{\,k})\cdot\boldsymbol{\varepsilon}(\vec{w})\, d\Omega, \tag{5.55}$$

so that,

$$\left[\mathbb{D}^{uu}_{n+1}\right] = \frac{\partial \boldsymbol{\sigma}_{n+1}}{\partial \boldsymbol{\varepsilon}^{e\ trial}_{n+1}} \tag{5.56}$$

is the consistent[20] displacement tangent modulus.

- **Determination of** $\partial_{ud} F_1(\vec{u}^k_{n+1}, D^k_{n+1}; \vec{w})\left[\Delta D^k_{n+1}\right]$:

$$\partial_{ud} F_1\left(\vec{u}^k_{n+1}, D^k_{n+1}; \vec{w}\right)\left[\Delta D^k_{n+1}\right] = \lim_{\varepsilon \to 0} \frac{F_1\left(\vec{u}^k_{n+1}, D^k_{n+1} + \varepsilon \Delta D^k_{n+1}; \vec{w}\right) - F_1\left(\vec{u}^k_{n+1}, D^k_{n+1}; \vec{w}\right)}{\varepsilon}$$

$$= \frac{d}{d\varepsilon}\left[F_1\left(\vec{u}^k_{n+1}, D^k_{n+1} + \varepsilon \Delta D^k_{n+1}; \vec{w}\right)\right]_{\varepsilon=0} \tag{5.57}$$

in which,

$$\partial_{ud} F_1(\vec{u}^k_{n+1}, D^k_{n+1}; \vec{w})\left[\Delta D^k_{n+1}\right] = \int_{\Omega} \left[\boldsymbol{D}^{ud}_{n+1}\right] \Delta D^k_{n+1} \cdot \boldsymbol{\varepsilon}(\vec{w})\ d\Omega, \tag{5.58}$$

so that,

$$\left[\boldsymbol{D}^{ud}_{n+1}\right] = \frac{\partial \boldsymbol{\sigma}_{n+1}}{\partial D} \tag{5.59}$$

is the consistent displacement-damage tangent modulus.

- **Determination of** $\partial_{du} F_2(\vec{u}^k_{n+1}, D^k_{n+1}; \gamma)\left[\Delta \vec{u}^k_{n+1}\right]$:

$$\partial_{du} F_2\left(\vec{u}^k_{n+1}, D^k_{n+1}; \gamma\right)\left[\Delta \vec{u}^k_{n+1}\right] = \lim_{\varepsilon \to 0} \frac{F_2\left(\vec{u}^k_{n+1} + \varepsilon \Delta \vec{u}^k_{n+1}, D^k_{n+1}; \gamma\right) - F_2\left(\vec{u}^k_{n+1}, D^k_{n+1}; \gamma\right)}{\varepsilon}$$

[20] **Consistent** means coherent with the numerical time-integration method used to solve the local problems, which is typically the Backward Euler scheme or the Midpoint Rule [70, 83].

$$= \frac{d}{d\varepsilon}\left[F_2\left(\vec{u}^{\,k}_{n+1} + \varepsilon\Delta\vec{u}^{\,k}_{n+1}, D^k_{n+1}; \gamma\right)\right]_{\varepsilon=0} \qquad (5.60)$$

in which,

$$\begin{aligned}\partial_{du} F_2(\vec{u}^{\,k}_{n+1}, D^k_{n+1}; \gamma)\left[\Delta\vec{u}^{\,k}_{n+1}\right] = &\int_\Omega \frac{d}{de}\left(S_{\bar{\eta}_{s_{n+1}}}\right)\Big|_{e=0} (D_{n+1} - D_n)\gamma \, d\Omega \\ &- \int_\Omega \boldsymbol{P}^{ud}_{n+1}\boldsymbol{\varepsilon}(\Delta\vec{u}^{\,k}_{n+1})\gamma \, d\Omega \\ &+ \int_\Omega k\left[\boldsymbol{H}^{ud}_{n+1}\boldsymbol{\varepsilon}(\Delta\vec{u}^{\,k}_{n+1})\right](\vec{\nabla} D_{n+1}\cdot\vec{\nabla}\gamma)\, d\Omega - \\ &- \int_\Omega \left(F^{\,r}_{D_{n+1}} + F^{\,reac}_{D_{n+1}}\right)\left[\boldsymbol{H}^{ud}_{n+1}\boldsymbol{\varepsilon}(\Delta\vec{u}^{\,k}_{n+1})\right]\gamma \, d\Omega, \qquad (5.61)\end{aligned}$$

$$\boldsymbol{H}^{ud}_{n+1} = \frac{\bar{H}(e^{vp}_{ef_{n+1}} - e^{vp}_{ef_{th}})H(F^i_{D_{n+1}})}{(1-D_{n+1})}\frac{\partial\Delta\lambda}{\partial\boldsymbol{\varepsilon}^{e\ trial}_{n+1}} \qquad (5.62)$$

and

$$\boldsymbol{P}^{ud}_{n+1} = \frac{\phi_{n+1}}{E}\left[\frac{2}{3}(1+\nu)q_{n+1}\frac{\partial q_{n+1}}{\partial\boldsymbol{\varepsilon}^{e\ trial}_{n+1}} + 3(1-2\nu)\,p_{n+1}\frac{\partial p_{n+1}}{\partial\boldsymbol{\varepsilon}^{e\ trial}_{n+1}}\right]. \qquad (5.63)$$

- **Determination of** $\partial_{dd} F_2(\vec{u}^{\,k}_{n+1}, D^k_{n+1}; \gamma)\left[\Delta D^k_{n+1}\right]$:

$$\partial_{dd} F_2\left(\vec{u}^{\,k}_{n+1}, D^k_{n+1}; \gamma\right)\left[\Delta D^k_{n+1}\right] = \lim_{\varepsilon\to 0}\frac{F_2\left(\vec{u}^{\,k}_{n+1}, D^k_{n+1} + \varepsilon\Delta D^k_{n+1}; \gamma\right) - F_2\left(\vec{u}^{\,k}_{n+1}, D^k_{n+1}; \gamma\right)}{\varepsilon}$$

$$= \frac{d}{d\varepsilon}\left[F_2\left(\vec{u}^{\,k}_{n+1}, D^k_{n+1} + \varepsilon\Delta D^k_{n+1}; \gamma\right)\right]_{\varepsilon=0} \qquad (5.64)$$

in which,

$$\partial_{dd} F_2(\vec{u}_{n+1}^k, D_{n+1}^k; \gamma)\left[\Delta D_{n+1}^k\right] = \int_\Omega \left[\alpha_s (D_{n+1}^k - D_n) + S_{\bar{\eta}_{s_{n+1}}}\right] \Delta D_{n+1}^k \gamma \, d\Omega + \\ + \int_\Omega k \phi_{n+1} \left[\vec{\nabla}\left(\Delta D_{n+1}^k\right) \cdot \vec{\nabla}\gamma\right] d\Omega - \\ - \int_\Omega (\alpha_F + \gamma_F + \eta_F) \Delta D_{n+1}^k \gamma \, d\Omega, \tag{5.65}$$

$$\alpha_s = \frac{\left\langle \left(e_{ef_{n+1}}^{vp} - e_{ef_B}^{vp}\right)\right\rangle^+}{(1 - D_{n+1}^k)\bar{\eta}_s} \left[\frac{\Delta\lambda}{(1 - D_{n+1}^k)} + \frac{\partial \Delta\lambda}{\partial D}\right], \tag{5.66}$$

$$\alpha_F = \frac{\phi_{n+1}}{E}\left[\frac{2}{3}(1+\nu) q_{n+1} \frac{\partial q_{n+1}}{\partial D} + 3(1-2\nu)\, p_{n+1} \frac{\partial p_{n+1}}{\partial D}\right], \tag{5.67}$$

$$\gamma_F = -\phi_{n+1}\left[\frac{2\bar{\eta}_a}{(1 - D_{n+1}^k)^3} + \frac{\delta(D_{n+1}^k)}{\bar{\eta}_b}\right], \tag{5.68}$$

$$\eta_F = (F_{D_{n+1}}^r + F_{D_{n+1}}^{reac}) H_{n+1}^{dd}, \tag{5.69}$$

$$H_{n+1}^{dd} = \frac{\bar{H}(e_{ef_{n+1}}^{vp} - e_{ef_{th}}^{vp}) H(F_{D_{n+1}}^i)}{(1 - D_{n+1}^k)} \left[\frac{\partial \Delta\lambda}{\partial D} + \frac{\Delta\lambda}{(1 - D_{n+1}^k)}\right], \tag{5.70}$$

$$\frac{d}{d\epsilon}\left(S_{\bar{\eta}_{s_{n+1}}}\right)\Big|_{\epsilon=0} = \frac{1}{\bar{\eta}_s} \frac{\left\langle \left(e_{ef_{n+1}}^{vp} - e_{ef_B}^{vp}\right)\right\rangle^+}{(1 - D_{n+1})} \frac{\partial \Delta\lambda}{\partial \boldsymbol{\varepsilon}_{n+1}^{e\ trial}} \boldsymbol{\varepsilon}(\Delta \vec{u}_{n+1}^k) \tag{5.71}$$

and

$$\delta(D_{n+1}^k) = \begin{cases} 1, \text{ if } D_{n+1}^k \le 0 \\ 0, \text{ if } D_{n+1}^k > 0. \end{cases} \tag{5.72}$$

In order to finally solve the system of equations (5.52), it is necessary to determine the remaining terms $\frac{\partial p_{n+1}}{\partial D}$, $\frac{\partial q_{n+1}}{\partial D}$, $\frac{\partial \Delta\lambda}{\partial D}$, $\frac{\partial p_{n+1}}{\partial \boldsymbol{\varepsilon}_{n+1}^{e\ trial}}$, $\frac{\partial q_{n+1}}{\partial \boldsymbol{\varepsilon}_{n+1}^{e\ trial}}$ and $\frac{\partial \Delta\lambda}{\partial \boldsymbol{\varepsilon}_{n+1}^{e\ trial}}$. By taking the partial derivative of (5.28) with respect to $\boldsymbol{\varepsilon}_{n+1}^{e\ trial}$, one obtains a system of linear equations that may be solved for $\frac{\partial p_{n+1}}{\partial \boldsymbol{\varepsilon}_{n+1}^{e\ trial}}$, $\frac{\partial q_{n+1}}{\partial \boldsymbol{\varepsilon}_{n+1}^{e\ trial}}$ and $\frac{\partial \Delta\lambda}{\partial \boldsymbol{\varepsilon}_{n+1}^{e\ trial}}$. In turn, by taking the partial derivative of (5.28) with respect to D_{n+1}, one obtains another system of linear equations that may be solved for obtaining $\frac{\partial p_{n+1}}{\partial D}$, $\frac{\partial q_{n+1}}{\partial D}$ and $\frac{\partial \Delta\lambda}{\partial D}$.

5.2.3. Finite Element Discretization

In order to apply the finite element method, one divides the domain, Ω, into finite elements, Ω_e, as illustrated in Figure 5.1. In this work, two finite element formulations will be applied and implemented: axisymmetric and plane strain states. The axisymmetric formulation is usually used to model solids of revolution components. In this case, one assumes that the material properties, loads and boundary conditions are independent of the angular coordinate, θ, in a cylindrical coordinate system, (r,θ,z), and the material points have only the displacement components u_r and u_z, in radial and axial directions, respectively [87].

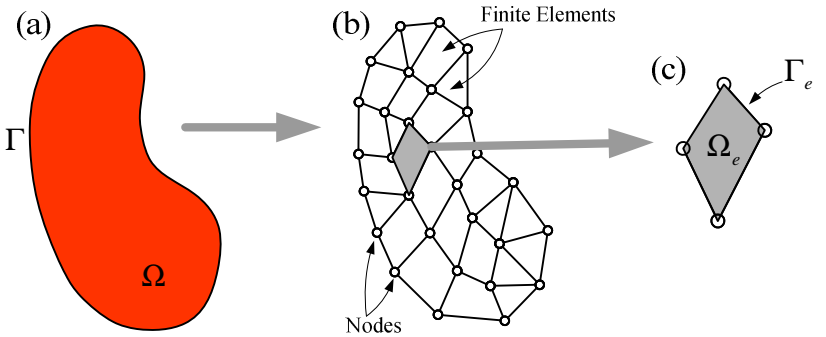

Figure 5.1: Finite element discretization of the domain.

The case of plane strain state is usually used to model components, in which its thickness is much larger than its other two dimensions. In this case, the strains in the direction of the longest dimension, ε_{zz}, and the shear strains γ_{xz} and γ_{yz} are very small compared to the cross-sectional strains, then they are usually constrained to be nearly zero [79, 87]. Only the finite element discretization of the axisymmetric case will be exposed in this chapter section, but both problems will be implemented. Since they are similar, then the discretization of the plane strain state case is obtained by applying some few changes.

For the axisymmetric problem, the displacement field is given by

$$\vec{u} = u_r \vec{e}_r + u_\theta \vec{e}_\theta + u_z \vec{e}_z, \tag{5.73}$$

in which,

$$u_r = u_r(r, z),$$

$$u_\theta = 0$$

and

$$u_z = u_z(r, z).$$

Since the problem is independent of θ, one has $d\Omega = 2\pi r dr dz$. Moreover, the stress and strain vectors are given, respectively, by $\vec{\sigma}^T = (\sigma_{rr}, \sigma_{zz}, \tau_{rz}, \sigma_{\theta\theta})$ and $\vec{\varepsilon}^T = (\varepsilon_{rr}, \varepsilon_{zz}, \gamma_{rz}, \varepsilon_{\theta\theta})$. In order to perform the integrations of Equations (5.53) in the element partition, Ω_e, one employs a change of variables, i.e., the physical elements are mapped into a reference element in the local coordinate system, (ξ,η). Thus, the components of the displacement field are interpolated in Ω_e as

$$u_r(\xi,\eta) = u_{r_i} N_i(\xi,\eta) \tag{5.74}$$

and

$$u_z(\xi,\eta) = u_{z_i} N_i(\xi,\eta), \tag{5.75}$$

in which, the index *i* ranges from one to the number of nodes in the element and $N_i(\xi,\eta)$ are the classical interpolation functions used in the finite element method.

Denoting $\vec{q}_e^{\,T} = (u_{r_1}, u_{z_1}, D_1, u_{r_2}, u_{z_2}, D_2, \ldots)$ as the element degree of freedom vector, in which (u_{r_i}, u_{z_i}, D_i) are the *i-th* nodal displacement-damage components, one may express the displacement components $\vec{u}$ in a matrix form as

$$\vec{u} = \mathbf{N}^u \vec{q}_e, \tag{5.76}$$

in which,

$$\mathbf{N}^u = \begin{bmatrix} \mathbf{N}_1^u & \mathbf{N}_2^u & \ldots & \mathbf{N}_i^u \end{bmatrix}$$

so that, $\mathbf{N}_i^u$ is given by

$$\mathbf{N}_i^u = \begin{bmatrix} N_i(\xi,\eta) & 0 & 0 \\ 0 & N_i(\xi,\eta) & 0 \end{bmatrix}. \tag{5.77}$$

The damage field, *D*, is also interpolated as

$$D = \vec{N}^d \cdot \vec{q}_e, \tag{5.78}$$

in which,

$$\vec{N}^d = \begin{Bmatrix} \mathbf{N}_1^d & \mathbf{N}_2^d & \ldots & \mathbf{N}_i^d \end{Bmatrix}, \tag{5.79}$$

so that,

$$\mathbf{N}_i^d = \begin{bmatrix} 0 & 0 & N_i(\xi,\eta) \end{bmatrix}. \tag{5.80}$$

Additionally, the virtual fields $\vec{w}$ and γ are interpolated as

$$\vec{w} = \mathbf{N}^u \delta \vec{q}_e \tag{5.81}$$

and

$$\gamma = \vec{N}^d \cdot \delta\vec{q}_e. \tag{5.82}$$

The strain vector may be expressed in a matrix form as

$$\vec{\varepsilon}(\vec{u}) = \mathbf{B}^u \vec{q}_e, \tag{5.83}$$

in which,

$$\mathbf{B}^u = \left[\mathbf{B}_1^u \quad \mathbf{B}_2^u \quad \ldots \quad \mathbf{B}_i^u \right]. \tag{5.84}$$

In turn, the components of the gradient of the damage variable may be expressed in matrix form as

$$\vec{\nabla} D = \begin{Bmatrix} \dfrac{\partial D}{\partial r} \\ \dfrac{\partial D}{\partial z} \end{Bmatrix} = \mathbf{B}^d \vec{q}_e, \tag{5.85}$$

in which,

$$\mathbf{B}^d = \left[\mathbf{B}_1^d \quad \mathbf{B}_2^d \quad \ldots \quad \mathbf{B}_i^d \right], \tag{5.86}$$

so that, $\mathbf{B}_i^u$ and $\mathbf{B}_i^d$ are given by

$$\mathbf{B}_i^u = \begin{bmatrix} N_{i,r} & 0 & 0 \\ 0 & N_{i,z} & 0 \\ N_{i,z} & N_{i,r} & 0 \\ -- & -- & -- \\ \dfrac{N_i}{r} & 0 & 0 \end{bmatrix} \tag{5.87}$$

and

$$\mathbf{B}_i^d = \begin{bmatrix} 0 & 0 & N_{i,r} \\ 0 & 0 & N_{i,z} \end{bmatrix}. \tag{5.88}$$

In these previous matrices, $N_{i,r}$ and $N_{i,z}$ are the derivatives of the interpolation functions, N_i, with respect to the coordinates *r* and *z*, given by

$$\begin{Bmatrix} N_{i,r} \\ N_{i,z} \end{Bmatrix} = \frac{1}{J} \begin{bmatrix} z_{,\eta} & -z_{,\xi} \\ -r_{,\eta} & r_{,\xi} \end{bmatrix} \begin{Bmatrix} N_{i,\xi} \\ N_{i,\eta} \end{Bmatrix}, \tag{5.89}$$

in which, $N_{i,\xi}$ and $N_{i,\eta}$ are the derivatives of the interpolation functions, N_i, with respect to the natural coordinates ξ and η and J is the determinant of the Jacobian matrix, i.e.,

$$J = r_{,\xi} z_{,\eta} - r_{,\eta} z_{,\xi}. \tag{5.90}$$

Moreover, one has

$$\vec{\varepsilon}(\vec{w}) = \mathbf{B}^u \delta \vec{q}_e, \tag{5.91}$$

$$\vec{\nabla} \gamma = \mathbf{B}^d \delta \vec{q}_e \tag{5.92}$$

and

$$div(\vec{\nabla} D) = \vec{L}^d \cdot \vec{q}_e, \tag{5.93}$$

in which,

$$\left(\vec{L}^d\right)^T = \left\{ 0 \quad 0 \quad \left(\frac{1}{r} N_{i,r} + N_{i,rr} + N_{i,zz} \right) \right\}. \tag{5.94}$$

In this case, $N_{i,rr}$ and $N_{i,zz}$ are the second derivative of N_i with respect to the coordinates *r* and *z*.

5.2.3.1. Linear Momentum Equation

Applying the finite element discretization on function $F_1(\vec{u}_{n+1}, D_{n+1}; \vec{w})$, one derives

$$\mathbf{K}^{uu} = 2\pi \int_{\xi=0}^{1} \int_{\eta=0}^{1-\xi} [\mathbf{B}^u]^T \left[\breve{\boldsymbol{D}}_{uu}^{ep} \right] [\mathbf{B}^u] J\, r\, d\xi d\eta \tag{5.95}$$

and

$$\mathbf{K}^{ud} = 2\pi \int_{\xi=0}^{1} \int_{\eta=0}^{1-\xi} \left\{ [\mathbf{B}^u]^T \{\vec{w}_{uu}\} \otimes [\vec{N}^d] \right\} J\, r\, d\xi d\eta, \tag{5.96}$$

in which, $\breve{\boldsymbol{D}}_{uu}^{ep}$ is the compact form of the consistent operator tangent $\mathbb{D}^{uu}$, the sign $\otimes$ means tensorial product and the vector $\vec{w}_{uu}$ is given by

$$\vec{w}_{uu} = \left\{ \mathbb{D}_{11}^{uu} \quad \mathbb{D}_{22}^{uu} \quad \mathbb{D}_{12}^{uu} \quad \mathbb{D}_{33}^{uu} \right\}.$$

In addition, the internal force, the body force and the prescribed traction contributions are given, respectively, by

$$\vec{F}_e^{int} = 2\pi \int_{0}^{1} \int_{0}^{1-\xi} \rho \left[\mathbf{B}^u \right]^T \vec{\sigma}\, J\, r\, d\xi d\eta \tag{5.97}$$

$$\vec{F}_e^{\vec{b}} = 2\pi \int_{0}^{1} \int_{0}^{1-\xi} \rho \left[\mathbf{N}^u \right]^T \vec{b}\, J\, r\, d\xi d\eta \tag{5.98}$$

and

$$\vec{F}_e^{\vec{t}} = 2\pi \int_{0}^{1} \rho \left[\mathbf{N}^u(\tau) \right]^T \vec{t}\, J(\tau) r(\tau) d\tau, \tag{5.99}$$

in which, the stress vector is given by $\vec{\sigma}^T = \{\sigma_{rr} \quad \sigma_{zz} \quad \tau_{rz} \quad \sigma_{\theta\theta}\}$, τ is a local variable employed in the parametrization of the boundary and

$$J(\tau) = \sqrt{\left(\frac{dx(\tau)}{d\tau}\right)^2 + \left(\frac{dy(\tau)}{d\tau}\right)^2}.$$

5.2.3.2. Damage Equation

Applying, now, the finite element discretization on the damage equation, $F_2(\vec{u}_{n+1}, D_{n+1}; \gamma)$, one has obtained the damage force

$$\vec{F}_e^{\,D} = \vec{F}_e^{\,S_\eta} + \vec{F}_e^{\,k} - \vec{F}_e^{\,F}, \tag{5.100}$$

in which,

$$\vec{F}_e^{\,S_\eta} = \int_{\Omega_e} S_{\bar{\eta}_{s_{n+1}}}(D_{n+1} - D_n)\vec{N}^d d\Omega_e, \tag{5.101}$$

$$\vec{F}_e^{\,k} = \int_{\Omega_e} k\phi_{n+1}\mathbf{B}^d \vec{\nabla} D_{n+1} d\Omega_e \tag{5.102}$$

and

$$\vec{F}_e^{\,F} = \int_{\Omega_e} \phi_{n+1}\left(F^r_{D_{n+1}} + F^{reac}_{D_{n+1}}\right)\vec{N}^d d\Omega_e. \tag{5.103}$$

Moreover, from the tangent operator (5.53), one derives the following matrices:

$$\mathbf{K}^{du} = \mathbf{K}^{du}_{S_\eta} + \mathbf{K}^{du}_{k} - \mathbf{K}^{du}_{F_1} - \mathbf{K}^{du}_{F_2} \tag{5.104}$$

and

$$\mathbf{K}^{dd} = \mathbf{K}^{dd}_{S_\eta} + \mathbf{K}^{dd}_{k_1} + \mathbf{K}^{dd}_{k_2} - \mathbf{K}^{dd}_{F}, \tag{5.105}$$

in which,

$$\mathbf{K}_{S_\eta}^{du} = \int_{\Omega_e} (D_{n+1} - D_n)\left(\vec{N}^d \otimes [\mathbf{B}^u]^T \vec{w}_\beta\right) d\Omega_e, \tag{5.106}$$

$$\mathbf{K}_{\bar{k}}^{du} = \int_{\Omega_e} \bar{k}\left([\mathbf{B}^d]^T \vec{\nabla} D_{n+1} \otimes [\mathbf{B}^u]^T \vec{w}_H\right) d\Omega_e, \tag{5.107}$$

$$\mathbf{K}_{F_1}^{du} = \int_{\Omega_e} \left(F_{D_{n+1}}^r + F_{D_{n+1}}^{reac}\right)\left(\vec{N}^d \otimes [\mathbf{B}^u]^T \vec{w}_H\right) d\Omega_e, \tag{5.108}$$

$$\mathbf{K}_{F_2}^{du} = \int_{\Omega_e} \left(\vec{N}^d \otimes [\mathbf{B}^u]^T \vec{w}_P\right) d\Omega_e, \tag{5.109}$$

$$\mathbf{K}_{S_\eta}^{dd} = \int_{\Omega_e} \left[\alpha_s (D_{n+1} - D_n) + S_{\bar{\eta}_{s_{n+1}}}\right]\left(\vec{N}^d \otimes \vec{N}^d\right) d\Omega_e, \tag{5.110}$$

$$\mathbf{K}_{\bar{k}_1}^{dd} = \int_{\Omega_e} \bar{k}\phi_{n+1}\left([\mathbf{B}^d]^T [\mathbf{B}^d]\right) d\Omega_e, \tag{5.111}$$

$$\mathbf{K}_{\bar{k}_2}^{dd} = \int_{\Omega_e} \bar{k}\, H^{dd}\left([\mathbf{B}^d]^T \vec{\nabla} D_{n+1} \otimes \vec{N}^d\right) d\Omega_e \tag{5.112}$$

and

$$\mathbf{K}_F^{dd} = \int_{\Omega_e} \left(\alpha_F + \gamma_F + \eta_F\right)\left(\vec{N}^d \otimes \vec{N}^d\right) d\Omega_e. \tag{5.113}$$

In these previous matrices, the remaining terms are given by

$$\vec{w}_\beta = \left\{\beta_{rr}^{du} \quad \beta_{zz}^{du} \quad \beta_{rz}^{du} \quad \beta_{\theta\theta}^{du}\right\} = \left\{\beta_{11}^{du} \quad \beta_{22}^{du} \quad \beta_{13}^{du} \quad \beta_{33}^{du}\right\}, \tag{5.114}$$

$$\beta_{ij}^{du} = \frac{1}{\bar{\eta}_s}\left\langle\left(e_{ef_{n+1}}^{vp} - e_{ef_B}^{vp}\right)\right\rangle^+ \frac{1}{(1 - D_{n+1})} \frac{\partial \Delta\lambda}{\partial \varepsilon_{ij}^{e\ trial}}, \tag{5.115}$$

$$\vec{w}_H = \left\{ H_{rr}^{dd} \quad H_{zz}^{dd} \quad H_{rz}^{dd} \quad H_{\theta\theta}^{dd} \right\} = \left\{ H_{11}^{dd} \quad H_{22}^{dd} \quad H_{21}^{dd} \quad H_{33}^{dd} \right\}, \tag{5.116}$$

$$H_{ij}^{ud} = \frac{\bar{H}\left(e_{ef_{n+1}}^{vp} - e_{ef_{th}}^{vp}\right) H\left(F_{D_{n+1}}^{i}\right)}{(1 - D_{n+1}^{k})} \frac{\partial \Delta\lambda}{\partial \varepsilon_{ij}^{e\ trial}} \tag{5.117}$$

and

$$\vec{w}_P = \left\{ P_{rr}^{ud} \quad P_{zz}^{ud} \quad P_{rz}^{ud} \quad P_{\theta\theta}^{ud} \right\} = \left\{ P_{11}^{ud} \quad P_{22}^{ud} \quad P_{21}^{ud} \quad P_{33}^{ud} \right\}. \tag{5.118}$$

in which, P_{ij}^{ud} is given by

$$P_{ij}^{ud} = \frac{\phi_{n+1}}{E} \left[\frac{2}{3}(1+\nu) q_{n+1} \frac{\partial q_{n+1}}{\partial \varepsilon_{ij}^{e\ trial}} + 3(1-2\nu)\, p_{n+1} \frac{\partial p_{n+1}}{\partial \varepsilon_{ij}^{e\ trial}} \right]$$

and ϕ_{n+1} is given by (5.49). In order to solve the previous integrals, one has employed the numerical integration procedure. Among the available integration methods, one has applied the Gauss quadrature rule.

5.2.3.3. Assembly of the Global Nonlinear Problem

Let $\vec{U}^{(k)}$ be the vector of all nodal degree of freedom at the *k-th* iteration of Newton-Raphson method, i.e.,

$$\vec{U}^{(k)} = \bigcup_{e=1}^{n} \left\{ \vec{q}_e^{(k)} \right\}. \tag{5.119}$$

Assume that the state is known in the interval $[0, t_n]$. The problem consists in the determination of the vector of nodal degree of freedom vector, $\vec{U}_{n+1}$, at time t_{n+1}. Then, the discrete nonlinear problem at time t_{n+1} may be formulated as shown in Table 5.1.

In Table 5.1, $\bar{R}$ is the residual error, *Tol* is the global convergence tolerance and the global consistent tangent stiffness matrix, $\mathbf{K}^G$, is given by

$$\mathbf{K}^G = \begin{bmatrix} \mathbf{K}^{uu} & \mathbf{K}^{ud} \\ \mathbf{K}^{du} & \mathbf{K}^{dd} \end{bmatrix}. \tag{5.120}$$

In turn, the global nodal force vector, $\vec{F}^G$, is given by

$$\vec{F}^G = \left(\vec{F}_e^{\text{int}} - \vec{F}_e^{\vec{b}} - \vec{F}_e^{\vec{t}} \right) + \vec{F}_e^D \tag{5.121}$$

and the vector of global nodal degree of freedom, $\Delta\vec{U}_{n+1}$, is given by $\left(\Delta\vec{U}_{n+1}\right)^T = \left\{\Delta\vec{u}_{n+1} \ \Delta D_{n+1}\right\}$. The numerical implementation of the problem stated in Table 5.1 and some numerical results will be discussed in Chapter 7.

Table 5.1: Nonlinear problem statement.

Let $\vec{U}_{n+1}^{(0)} = \vec{U}_n$ be the initial nodal degree of freedom vector, then:

Find $\vec{U}_{n+1}^{(k+1)}$, so that $\left\| \vec{R}\left(\vec{U}_{n+1}^{(k+1)}\right) \right\| \leq Tol$, in which

$$\left[\mathbf{K}^G \left(\vec{U}_{n+1}^{(k)}\right) \right] \Delta\vec{U}_{n+1}^{(k)} = -\vec{F}^G \left(\vec{U}_{n+1}^{(k)}\right),$$

so that,

$$\vec{U}_{n+1}^{(k+1)} = \vec{U}_{n+1}^{(k)} + \Delta\vec{U}_{n+1}^{(k)}.$$

CHAPTER 6

EXPERIMENTAL MEASUREMENTS

In order to implement the constitutive model presented previously, it is necessary to input it with some material properties and constants, which must be obtained and/or identified experimentally. Thus, the objective of this chapter is to present a summary of the tests performed and illustrate the results obtained from them, which will be used as inputs for the model.

In this work, only mechanical properties have been obtained to characterize the selected material. From the experimental data, one has calculated their standard deviation and mean values, which has been the value assigned as the property of the material. This is recommended by most standards. These tests have been performed at the Fibre and Polymer Technology Department of the Royal Institute of Technology (KTH), Stockholm, Sweden. Thus, the following sections will discuss the main activities and procedures followed to accomplish them and the results obtained.

6.1. THE SELECTED MATERIAL

Currently, in the automotive and aeronautics industries, for instance, one has been very common to find plastic components submitted to the most diverse loading conditions. Automotive door knobs, window cranks and snap fits, which are usually manufactured with commodities, are good examples.

In order to perform the experimental tests, one has chosen a polypropylene grade plastic due to two reasons. Firstly, a polypropylene resin was easily available at the Royal Institute of Technology (KTH). Secondly, one can find many applications of plastic components subjected to ductile failure and manufactured with this kind of material. The grade available at the department and used in the tests was the HE125MO®, supplied by Borealis.

According to Borealis, this grade is an isotactic polypropylene homopolymer[21] intended for injection molding and is characterized by good flow properties and high stiffness. Its molecular weight is 587 kg/mol and its most common applications are: house wares, thin wall packaging and articles with rather long and narrow flow lengths.

[21] Polymers that contain only a single type of monomer are known as **homopolymers**.

6.2. MECHANICAL PROPERTIES

The mechanical properties necessary to the models presented in Chapters 4 and 5 are summarized in Table 6.1. This table contains the meaning of the properties, their units and the sources from where they have been acquired. The procedure for obtaining of each property will be discussed in the following sections.

Table 6.1: Mechanical properties necessary to the mathematical models.

PROPERTIES	MEANING	UNITS	SOURCES
ρ	Density	kg/m^3	Density Test
E	Modulus of Elasticity	MPa	Tensile Test
σ_{oy}	Initial yield Stress	MPa	Tensile Test
$h(r)$	Function that describes the isotropic hardening curve of the material	MPa	-
v	Poisson's ratio	-	Tensile & DSP
μ	Material constant that determines the effect of the hydrostatic stress on the yield point	-	Brown [92]

The shape of the specimens used in the tensile and Poisson's ratio tests is shown in Figure 6.2. They have been injection molded by using a Battenfeld Plus 250® injection mould machine and their dimensions can be seen in Figure 6.1.

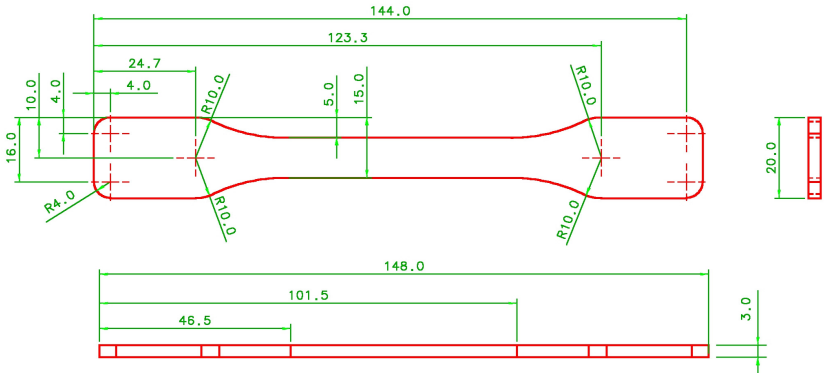

Figure 6.1: Specimen geometry and dimensions, in millimeters.

One has discussed in Chapter 2, that specimens molded under different conditions can exhibit different properties. Several factors may influence, among them one can highlight the degree of crystallinity and molecular orientation. So, in order to produce specimens as uniform as possible and, consequently, minimize those differences, they have been injection molded under specifications and recommendations of ASTM D 3641 standard. Thus, the material properties obtained in the tests will be regarded to the degree of crystallinity obtained from the injection conditions set up, which are illustrated in Table 6.2. The following items will discuss the main features and will show the mains results obtained from the mechanical tests. But, first, one will be discussed the test performed to determine the degree of crystallinity of the specimens.

Table 6.2: Processing conditions used to produce the specimens.

Mold Temperature	22.0 °C
Melt Temperature	220.0 °C
Holding Pressure	20.0 MPa
Cooling Time	35.0 s
Injection Time	1.0 s
Ejection Time	0.5 s
Closing Time	2.0 s

In short, the injection molding process begins when the mold closes and the molten material is pushed into the cavity. As soon as the cavity is filled, a holding pressure is held to compensate for material shrinkage, while the material is cooled down. Once the material is sufficiently cooled, the mold opens and the component is ejected. Following, the mold closes and the cycle starts again. The total cycle time is determined by adding twice the mold close time, the injection, cooling and ejection times. According to Table 6.2, the cycle time was 38.5 s.

Figure 6.2: Samples of the specimens used in the tensile and Poisson's ratio tests.

6.2.1. Determination of the Degree of Crystallinity of the Specimens

In Chapter 2, one has discussed that the degree of crystallinity refers to the relative percentage of crystalline areas compared to the amorphous ones. Usually, this relation can be determined by using the data obtained from DSC[22] measurements. In order to perform the tests and determine the degree of crystallinity of the specimens, one has followed the specifications and recommendations of ASTM E 1356 standard.

The tests have been accomplished by means of the Mettler DSC 820® equipment and six specimens, with masses about 15 mg, have been tested (see Figure 6.3). According to the ASTM E 1356 standard, for each specimen, one has performed an initial thermal program, with a heating rate of 10 °C/min, from -50 °C to 200 °C, to remove any previous thermal history. That has been the temperature range considered in these tests. Then, this final temperature has been held constant for 5 minutes, in order that the specimens have achieved equilibrium. Following, one has

[22] DSC stands for Differential Scanning Calorimetry. See Attachment A (section A1) for more detail.

performed a cooling program at a rate of 20 °C/min to -50 °C and, again, this final temperature has been also held constant for 5 minutes. Finally, the specimens have been heated again with a heating rate of 10 °C/min to 200 °C to close the cycle. Figure 6.4 schematically illustrates the temperature program of the DSC tests. One must emphasize that during the tests, dry nitrogen has been purged at a flow rate of 50 ml/min throughout the experiments to prevent oxidation. In the end, one has obtained the diagram illustrated in Figure 6.5. This figure shows the specific heat flow as a function of temperature of one of the specimens and some characteristics values, which can be extracted from this diagram. The curve of the first heating is not illustrated in this figure.

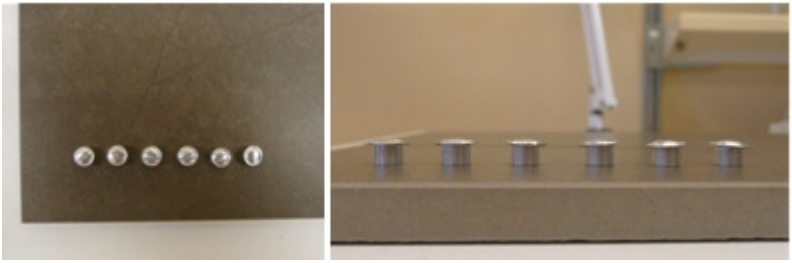

Figure 6.3: Crucibles with the samples for the DSC tests.

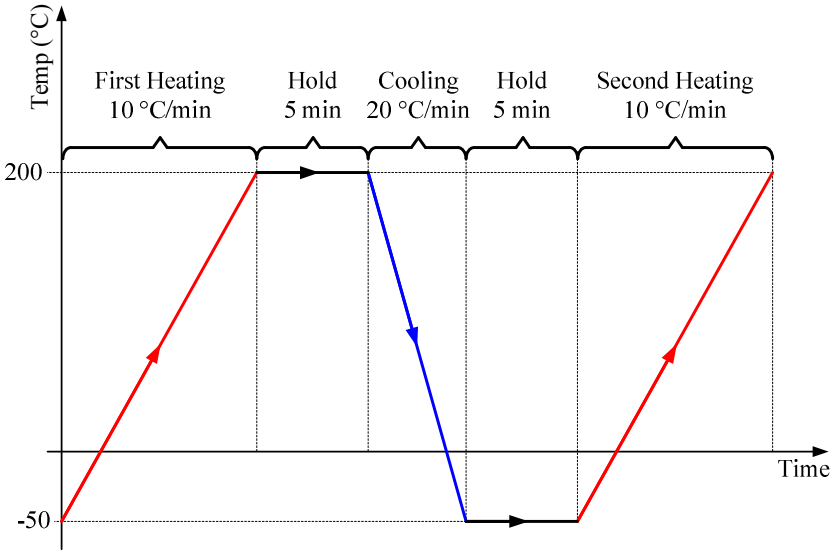

Figure 6.4: Temperature program used in the DSC tests.

In Figure 6.5, the area under the second heating peak gives the specific heat absorbed during melting (ΔH_m), whereas the area above the first cooling dip gives the specific heat released for the crystallization of the polymer (ΔH_c). Based on the standard, the degree of crystallinity, X_c , has been calculated by

$$X_c = \frac{\Delta H_m}{\Delta H_{fus}} \times 100\%, \tag{6.1}$$

in which, ΔH_{fus} is the specific heat absorbed during melting, when the material is fully crystalline. For polypropylene, $\Delta H_{fus} = 209\,\mathrm{J/g}$ [90]. The mean value and the standard deviation of the degree of crystallinity obtained in this test are shown in Table 6.3. Thus, the mechanical properties, in this work, obtained by standardized tests will be regarded to the degree of crystallinity of 41.3%.

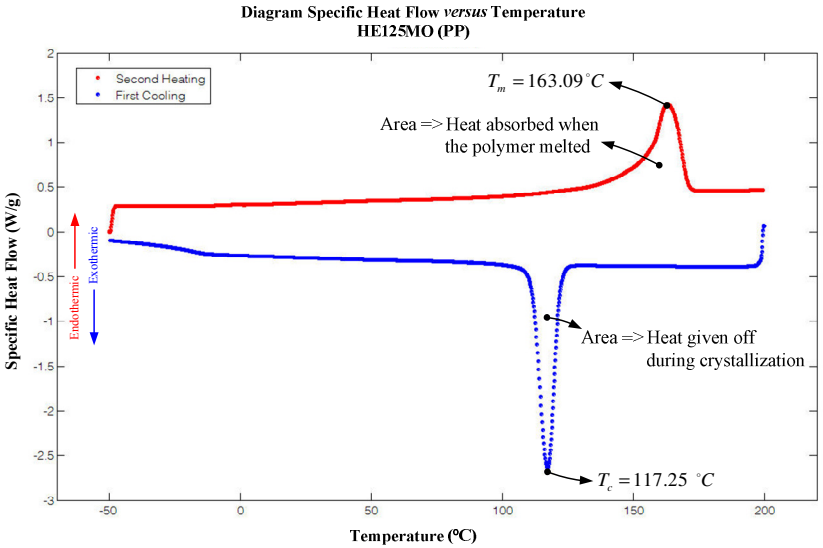

Figure 6.5: Diagram specific heat flow *versus* temperature of one of the specimens.

Table 6.3: Mean value and Standard deviation of the degree of crystallinity of the specimens.

	Mean Value	Standard Deviation
Degree of Crystallinity (%)	41.3	1.40

6.2.2. Density Test

The density of a body is a measure of how tightly the matter within it is packed together and is given by the ratio of its mass to its volume [21]. In practice, this data is usually useful for determining the weight of a component, estimating its cost and calculating its strength-weight ratio. The objective of this test is to obtain the density of the material under study, at ambient conditions[23]. In order to reach this objective, this test has been performed in accordance with method *B* of ASTM D 792 standard.

The test principle used in this method is based on the Archimedes principle, in which the mass of the specimen is determined in air. Following, it is immersed in a liquid, with known density, its apparent mass upon immersion is determined and, finally, its density is calculated. The liquid used in this test has been Limonene[24], whose density is $841.10\ \mathrm{kg/m^3}$. Five specimens, weighting about 10 g, have been cut from the tensile test specimens and tested. Table 6.4 shows the mean value and the standard deviation of the density of the selected material.

Table 6.4: Mean value and Standard deviation of the density of the selected material.

	Mean Value	Standard Deviation
Density ($\mathrm{kg/m^3}$)	9.02×10^2	0.83

6.2.3. Tensile Tests and Material Properties

The tensile test is designed to establish behavior of materials under axial stretch loading. Data from this test are usually used to determine tensile properties of the material, such as elastic limit, strain to failure,

[23] One states, from now on, that the ambient conditions are those, in which the temperature is 23 ± 2ºC and the relative humidity is 50 ± 5%, as ASTM D 792 and D 638 standards recommend.

[24] Limonene ($C_{10}H_{16}$) belongs to the group of hydrocarbons. It is a colorless liquid at room temperature with a strong smell of orange [21]. Its density value has been obtained from the supplier datasheet (Sigma Aldrich).

modulus of elasticity, yield point, tensile strength and other properties. When dealing with plastic materials, the obtainment of their tensile properties is driven by ASTM D 638 or ISO 527 standards.

The tests to obtain the tensile properties of the material in consideration have been performed at ambient conditions, using an Instron 5566® tensile test machine, equipped with a video extensometer[25] device. The tensile force has been measured by a standard load cell (1 kN). Because the tensile properties of plastic materials may vary with temperature (see section 2.4), then 10 specimens have been previously selected and conditioned to the test environment for two days. The ASTM D 638 standard assigns different speeds of testing for each kind of specimen. According to the standard, one should choose a speed, which gives rupture within 0.5 to 5 min testing time. Thus, after some preliminary tests, one has defined the speed of 50 mm/min. Then, their stress-strain diagrams have been generated and the modulus of elasticity, yield stress and strain at yielding have been obtained.

According to ISO 527 standard, the modulus of elasticity (E) is determined by

$$E = \frac{\sigma_b - \sigma_a}{\varepsilon_b - \varepsilon_a}, \tag{6.2}$$

in which, σ_a and σ_b are the stresses measured, respectively, at strains $\varepsilon_a = 0.05\ \%$ (0.0005 mm/mm) and $\varepsilon_b = 0.25\ \%$ (0.0025 mm/mm). Usually, these strain values are not recorded by the acquisition data system of the equipment. In this case, one may perform an interpolation of the data to find the stresses σ_a and σ_b. In this work, a spline interpolation has been performed, in order to obtain these stress values as precise as possible.

The yield stress (σ_y) of each test has been determined according to recommendations of ASTM D 638 standard. In this case, one recommends that the maximum load of each test be divided by the original cross-sectional area of the central length segment of the

[25] The measurement of strains during material testing has been traditionally performed, by using some form of contacting strain device, like strain gages. Presently, an alternative way for the traditional methods is the **video extensometer**, which is a device capable of measuring strains, by capturing continuous images of the specimen during the test, using a digital camera attached to a computer. Before the test, the specimen is marked with specific markers, then, it is placed in the grips of the testing machine and the distance between the marks is initially captured and measured by the digital camera. The strain is, then, calculated from the mark separation at the beginning of the test and the current mark separation. This method is more accurate because it eliminates measurement errors due, for example, to grips slip.

specimen, i.e., 30.0 mm^2 (see Figure 6.1). The strain associated with this stress has been assigned as the strain at yielding (ε_y). This method would be equivalent to take the maximum nominal stress and its corresponding strain and assign them as the yield stress and strain, respectively, as is illustrated in Figure 2.5. Finally, the mean value and the standard deviation of E, σ_y and ε_y have been calculated, as can be seen in Table 6.5. Figure 6.6 illustrates the stress-strain diagram of all samples, at ambient temperature (23 ºC), and an amplified view of the initial regions of these diagrams, in which one can observe the dispersion among their tensile behavior. In this regard, one can notice that some specimens have elongated much more than others and some have exhibited more pronounced hardening than others before fracture. In turn, Figure 6.7 illustrates the stress-strain diagram of only one sample, as well as an amplified view of the initial regions of this diagram.

Table 6.5: Mean value and Standard deviation of the tensile properties of the material, at 23 ºC.

	Modulus of Elasticity (GPa)	**Yield Stress (MPa)**	**Strain at Yielding (%)**
Mean Value	1.54	31.6	8.00
Std. Dev.	0.27	0.58	9.30×10^{-2}

During the development of the tensile tests, one could observe three aspects. First, at the beginning of each test, due to the molecular chains orientation process, the narrower section of the specimens started becoming white and thinner, characterizing a pre-neck, prior appearing the neck, which will lead to the cold drawing process. The whiteness of the narrower section has been the result of a localized change in material refractive index, caused by formation of micro voids and crazes. Because their dimensions are equal to or greater than the wavelength of light, then they scatter light, which falls on the specimen. Stress whitening is a material damage and can be the indication of complete material failure [45, 46]. The second aspect regards the remarkable ductility exhibited by the material, before failure. As a consequence, one can notice that its stress-strain diagram is strongly nonlinear and exhibits the three peculiar regions, as predicted in Figure 2.5. Lastly, one could observe that the fractured regions have occurred at the stretched end of the gauge section,

as can be seen some samples in Figure 6.8, because of the high level of triaxiality, due to stress concentration.

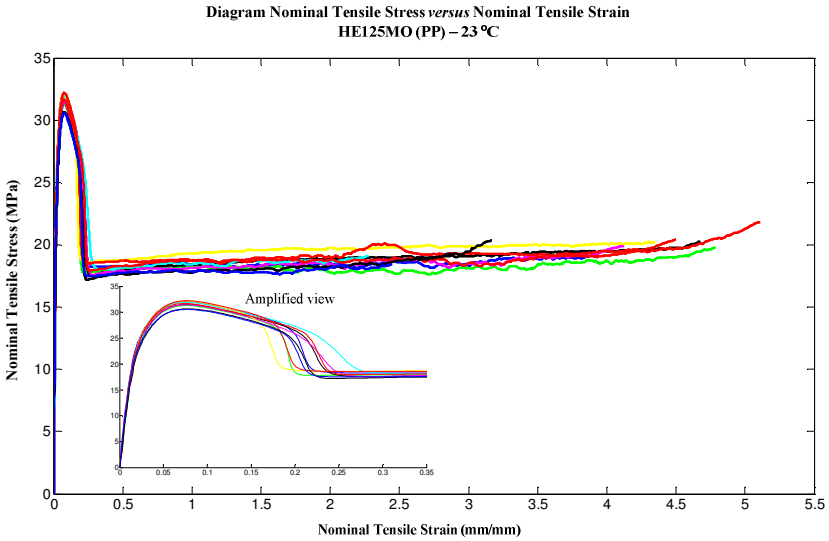

Figure 6.6: Stress-Strain diagram of all samples, at ambient conditions.

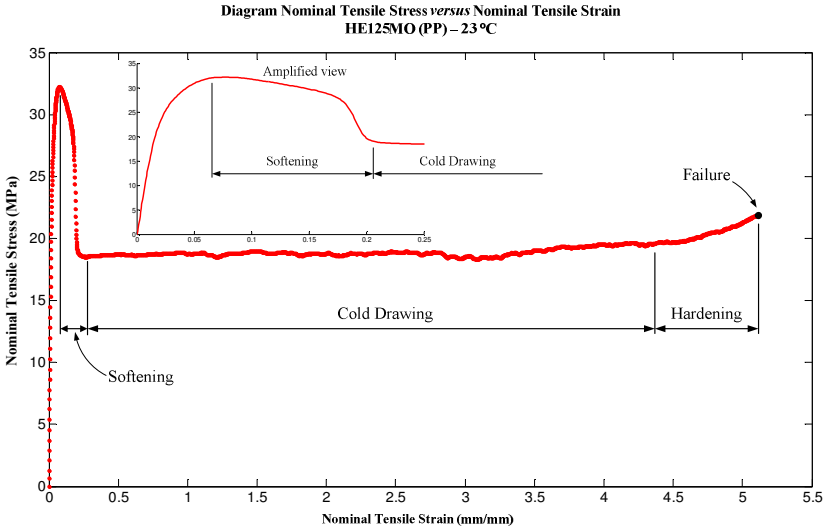

Figure 6.7: Stress-Strain diagram of one sample, at ambient conditions.

Figure 6.8: Fractured samples.

6.2.4. Determination of the Poisson's Ratio

Poisson's ratio (ν) is used for design of structures where all dimensional changes, resulting from application of external forces. The Poisson's ratio of the material in study, at ambient conditions, has been determined by means of the DSP[26] technique, along with the tensile test machine Instron 5567® and recommendations of the ASTM E 132 standard.

According to the standard, the stresses and strains must be measured within the linear region of the stress-strain curve and the Poisson's ratio is calculated as

$$\nu = -\frac{d\varepsilon_y}{d\varepsilon_x}, \tag{6.3}$$

in which, ε_x and ε_y are the longitudinal and transverse strains, respectively. Since the stresses and strains are within the linear region of the stress-strain curve, then there should be a linear relation between ε_x and ε_y. Thus, as can be seen in Equation (6.3), the Poisson's ratio represents the angular coefficient of the straight line, obtained from the fitting of the experimental data between ε_x and ε_y.

Prior to the tests, 10 specimens have been selected and conditioned to the ambient conditions for two days. In order to obtain sufficiently small speckles to render good resolution, the speckle patterns have been carefully applied, by spraying an appropriate ink on the specimens

[26] DSP stands for Digital Speckle Photography. This technique is sometimes named DIC, which stands for Digital Image Correlation. See Attachment A (section A2) for more detail.

(Belton® SpectRAL Lackspray – RAL[27] 9005), as can be seen in Figure 6.9.

Figure 6.9: Speckled specimens used in the DSP tests.

Following, the specimens have been placed in the tensile test machine, as can be seen in Figure 6.10, and the tests have been conducted at a strain rate of 5 mm/min, as recommends the standard. One has set the DSP equipment (Aramis®) to capture two frames per second and, because the stresses and strains must be within the elastic region, one has also set the tensile test machine to stop the tests as soon as the stresses reached about half of the yield stress, i.e., 16 MPa.

The DSP equipment has captured about 46 frames for each specimen. During the processing of the images, in order to obtain the results, one has drawn a rectangular area (55 mm x 10 mm) on the image of frame zero, comprising the narrow section of the specimens, so that the final results have been calculated only within this area. Among the available results, only strains have been of interest. Figure 6.11 illustrates the distribution of strain on one of the specimens during the eight first frames, so that frame zero represents the situation, in which the specimen is undeformed, i.e., it is the reference state. Since the stresses and strains are within the linear region, one can observe that the gradient of strain on the specimen is nearly constant at all frames.

[27] This abbreviation comes from the German expression ***R**eichs**a**usschuß für **L**ieferbedingungen und Gütesicherung*, which means Imperial Commission for Delivery Terms and Quality Assurance. In short, RAL is a standardized scale of color tones established in 1927 by this German committee [21].

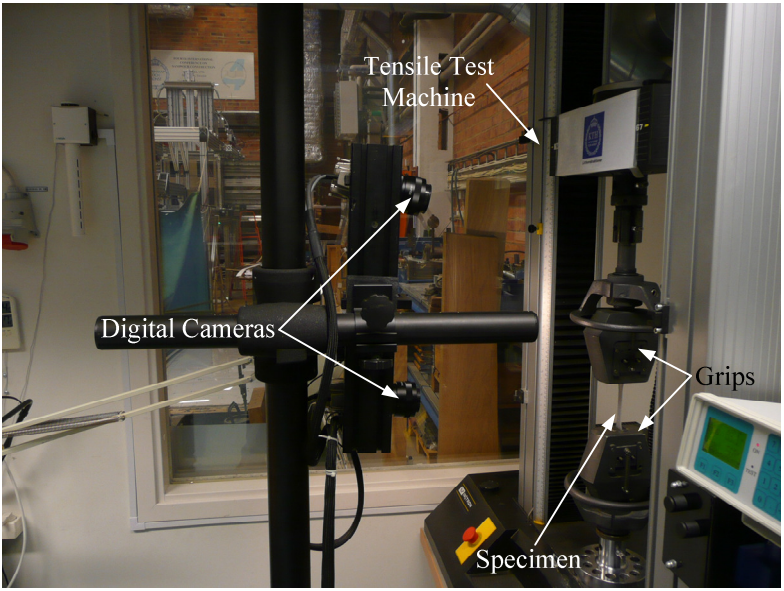

Figure 6.10: Configuration of the DSP – Tensile test.

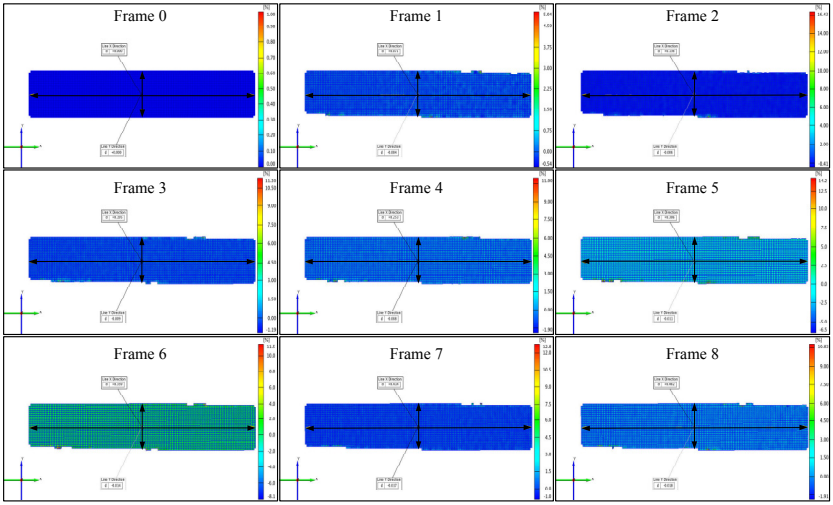

Figure 6.11: Distribution of strains in the eight first stages.

In order to determine the longitudinal and transverse strains, one has drawn two perpendicular lines at frame zero, as can be seen in Figure

6.11 (Frame 0). A line in the longitudinal direction (x-direction), comprising the whole length of the selected area, and another one in the transverse direction (y-direction), comprising the whole width of the selected area. The strains ε_x and ε_y, at each frame, have been calculated by dividing the change in length of the lines at an actual frame by their lengths at frame zero. Then, one has plotted ε_x against ε_y and performed a linear fitting through the experimental data points, as is illustrated in Figure 6.12. The Poisson's ratio is taken as the angular coefficient of the line obtained from the fitting. This procedure has been repeated for all specimens. Thus, Table 6.6 illustrates the mean value and the standard deviation of the Poisson's ration for the selected material. It is worth emphasizing that the experimental data points in Figure 6.12 represent the strains ε_x and ε_y at each frame.

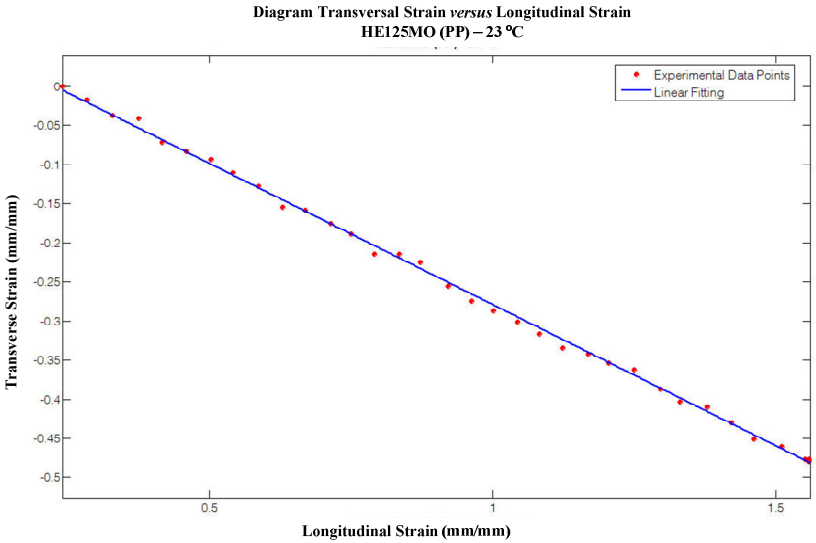

Figure 6.12: Experimental data and linear fitting of one specimen, at ambient conditions.

Table 6.6: Mean value and Standard deviation of the Poisson ratio for the selected material.

	Mean Value	Standard Deviation
Poisson Ratio	0.36	0.02

According to Bayer [59], the Poisson's ratio of polymeric materials usually falls between 0.35 and 0.42. Some rubbery materials have ratio approaching the constant-volume value of 0.5. For design purpose, when the Poisson's ratio of the material is not known, Ticona [51] recommends that one uses 0.35. Li *et al.* [91] affirm that the Poisson ration of polypropylene is about 0.36.

6.2.5. Obtainment of the Parameter μ

One knows that the yielding behavior of plastic materials is more sensitive to compressive loads than metals. Thus, when dealing with design of plastic components, one recommends using yield criteria, which also account for the influence of the hydrostatic part of the stress tensor. This is usually done by introducing the parameter μ into the criterion, as a coefficient of influence of the hydrostatic pressure on the yield stress of the material. The parameter μ for the material selected in this work (polypropylene) has been taken from Table 6.7, i.e., 0.12. This table also contains values for other materials, at 23 ºC. According to Miller [68], a value of 0.15 for μ may be considered for a plastic material, when no experimentally determined value is available.

Table 6.7: Values for the parameter μ for different materials [68, 92].

MATERIAL	PARAMETER μ
Polystyrene (PS)	0.250
Polymethyl Methacrylate (PMMA)	0.158
Polycarbonate (PC)	0.120
Polyethylene Terephthalate (PET)	0.090
High Density Polyethylene (HDPE)	0.050
Polyvinyl Chloride (PVC)	0.110
Polypropylene (PP)	0.120

6.3. REMARKS

This chapter has discussed the development of tests to obtain the mechanical properties and parameters of the model presented in Chapter 4. Initially, a plastic material has been selected, standardized specimens have been produced and, then, the necessary tests have been performed. From the results of the tests, one can highlight two aspects: (1) the standard deviations have been low, leading to a low dispersion; and (2) the numerical values of the properties, represented by the mean values of each test, have been very close to those published by the material supplier (Borealis), as can be seen in Table 6.8. This means that the test results are

reliable and consistent. At last, based on the experience obtained in the experiments, one suggests that the strain to failure data should be interpreted with care, whenever the failure of the specimens takes place near the tabs, as is illustrated in Figure 6.8. Because this is a region of high level of triaxiality, due to stress concentration, this may disguise the real value of the strain to failure data.

Table 6.8: Confrontation between tests and material supplier results.

	TESTS	**MATERIAL SUPPLIER**
Density (kg/m^3)	9.02×10^2	9.02×10^2
Modulus of Elasticity (GPa)	1.54	1.55
Yield Stress (MPa)	31.6	34.5
Yield Strain (%)	8.00	9.00
Poisson ratio	0.36	-

CHAPTER 7

NUMERICAL EXAMPLES

In this chapter section, one will be presented a set of problem cases, based on the theory developed in Chapters 4 and 5 and on the experimental results presented in Chapter 6. The proposed theory consists of a damage model for the ductile fracture analysis of plastic components. Some of the material parameters, necessary to fully characterize the material model, are given in Table 6.8. The remaining material parameters are also provided.

Most material parameters have been identified from standardized tests, while others have been estimated based on the values published by Lemaitre [1] and Ghorbel [4]. For example, the viscoplastic parameters *M* and K_∞ can be determined by means of relaxation and creep tests [1, 4]. For plastic materials, Ghorbel [4] affirms that *M* is about $2.0\ \text{s}^{-1}$ and K_∞ is usually equal to the yield stress of the material, i.e., $K_\infty = \sigma_y$. The estimated values for the remaining material parameters are given in Table 7.1, as well as the references where these values have been taken or estimated.

Table 7.1: Remaining material parameters necessary to the mathematical model.

PARAMETERS	VALUES	REFERENCES
M	$2.0\ \text{s}^{-1}$	Ghorbel [4]
K_∞	31.6 MPa	Ghorbel [4]
$\overline{\eta}_a$ $\overline{\eta}_b$	1.0×10^{-5} 1.0×10^{-9}	Lemaitre [1]
S_o	0.15 MPa	Lemaitre [1]
$\overline{\eta}_s$	1.0×10^{-9}	Lemaitre [1]
$\bar{k}$	$2.0\ \text{MPa}\cdot\text{mm}^2$	Fremond and Nedjar [2]
$e^{vp}_{ef_{th}}$	0.75	Lemaitre [1]

One starts by simulating the behavior of the material under tensile loading. In this first problem case, one compares the numerical results, obtained from a rough estimation of the material parameters, with the

results obtained from the experimental uniaxial tension test. Additionally, the numerical results of three other examples will be presented and discussed. The first example will be a mechanical component submitted to a tensile load. The second example considers a plastic pulley, submitted to a radial compressive load and modeled as an axisymmetric problem. At last, the performance of an automotive snap fit, resulting from the assembly of an additional component, will be numerically investigated. The first and the third examples will be modeled under the assumption of plane strain state problem and all examples have run on a Pentium® 5 AMD Athlon™ 64 processor. One has looked for considering components with irregular geometries, with fillets and other stress concentrator features, in order to truly attest the robustness of the proposed numerical scheme.

A six-node triangular finite element (Tri6) with six integration points has been implemented for both problems (axisymmetric and plane strain state), as illustrated in Figure 7.1. One assumes that each node of the finite element has three degrees of freedom, which are the nodal values of: the damage field, *D*, and the in-plane translations components u_r and u_z for the axisymmetric problem and u_x and u_y for the plane strain state. Consequently, this element will have 18 degrees of freedom. Moreover, both the displacement components and the damage field are interpolated by quadratic functions within each finite element domain, according to the following expressions:

$$N_1(\xi,\eta) = \xi(2\xi - 1)\,, \tag{7.1}$$

$$N_2(\xi,\eta) = \eta(2\eta - 1)\,, \tag{7.2}$$

$$N_3(\xi,\eta) = \varsigma(2\varsigma - 1)\,, \tag{7.3}$$

$$N_4(\xi,\eta) = 4\xi\eta\,, \tag{7.4}$$

$$N_5(\xi,\eta) = 4\eta\varsigma \tag{7.5}$$

and

$$N_6(\xi,\eta) = 4\xi\varsigma\,, \tag{7.6}$$

in which, ξ and η are the local coordinate system of the element, as can be seen in Figure 7.1, and ς is given by

$$\varsigma = (1 - \xi - \eta) \, . \tag{7.7}$$

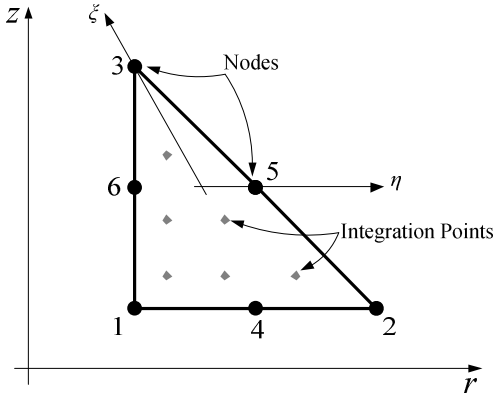

Figure 7.1: Tri6 finite element in an axisymmetric coordinate system.

7.1. UNIAXIAL TENSILE TEST SIMULATION

In this initial section, the uniaxial tensile test is simulated, in order to show the approximation employed in the identification of the material parameters. This is done by comparing the numerical solution, obtained by a rough identification procedure of the required material parameters, with the experimental response of the material obtained by performing a uniaxial tensile test. The estimated material parameters employed in the mathematical model are given in Table 7.1. Additionally, the required estimation of the isotropic hardening curve of the material, *h(r)*, is given in Table 7.2. The material parameters given in Tables 7.1 and 7.2 will be employed for all the problem cases considered in this chapter.

Table 7.2: Hardening curve data points [1].

h(*r*) (MPa)	0.0	1.0	2.0	2.5
r (mm/mm)	0.0	0.2	0.4	2.0

In the uniaxial tensile test simulation, the problem has been considered as axisymmetric and subjected to a prescribed displacement

on the upper edge, as illustrated in Figure 7.2. Additionally, one can see the boundary conditions applied. The final value for the prescribed displacement on the upper edge was $\overline{u}_z = 60$ mm, representing the displacement of the moving crosshead of the tensile machine. The domain shown in Figure 7.2 has a radius of 30 mm and a height of 50 mm.

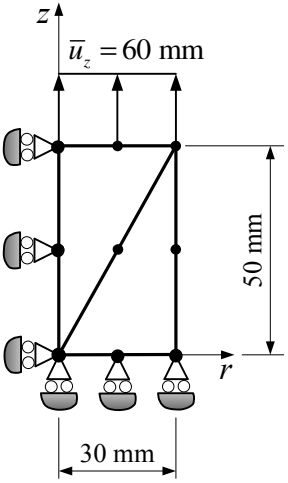

Figure 7.2: Mesh and boundary conditions for the tensile test simulation.

Figure 7.3 illustrates the comparison between both the experimental and numerical stress-strain diagrams for the tensile test. In order to reduce the processing time, one has considered the total time of the analysis is equal to 60 seconds, which has been a sufficient time to reach the cold drawing region. In addition, one has also considered 1000 load steps and a global convergence tolerance of 10^{-5}. The hardening curve, $h(r)$, has been obtained by interpolation, using spline functions and the given data in Table 7.2.

The maximum error between the experimental and numerical results has been about 22%. This difference has taken place in the softening region, where the neck appears and evolves to the cold drawing region. Post-yield behavior is usually associated with molecular instabilities and its modeling is generally very challenging. As a consequence, the cold drawing and the post-yield behaviors can not be predicted by any conventional model using J_2 flow theory with some viscoelastic generalization. In this case, one requires a more sophisticated model, similar to that which has been proposed in this work. This error

may be reduced considerably by performing an adequate identification of the material parameters. This can be obtained by using, for example, a genetic algorithm scheme, in order to compute an approximation to the global minimum of a least square optimization problem.

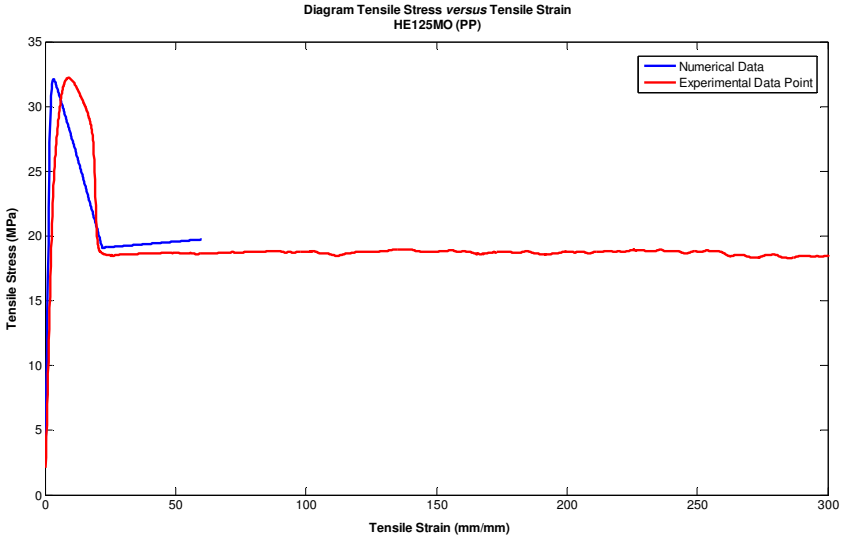

Figure 7.3: Stress-strain diagram for the tensile simulation.

Providing that several material parameters have been taken or estimated from literature, one considers that the error between experimental data and numerical prediction, observed in the softening region of Figure 7.3, is encouraging. Along with the genetic algorithm scheme, the assumption of finite strain deformation might also help to reduce the error, because the necking process would be modeled more effectively.

The evolution of the damage variable, as a function of "time" (loading parameter), is illustrated in Figure 7.4, in which one can see the action of the locking restriction on the damage variable, making the value of the damage approximately constant once the applied effective viscoplastic strain, e_{ef}^{vp}, becomes larger than the critical value $e_{ef_{th}}^{vp}$. Notice that, since the mathematical model considers the deformation to be homogeneous, the above distribution holds for every point in the domain.

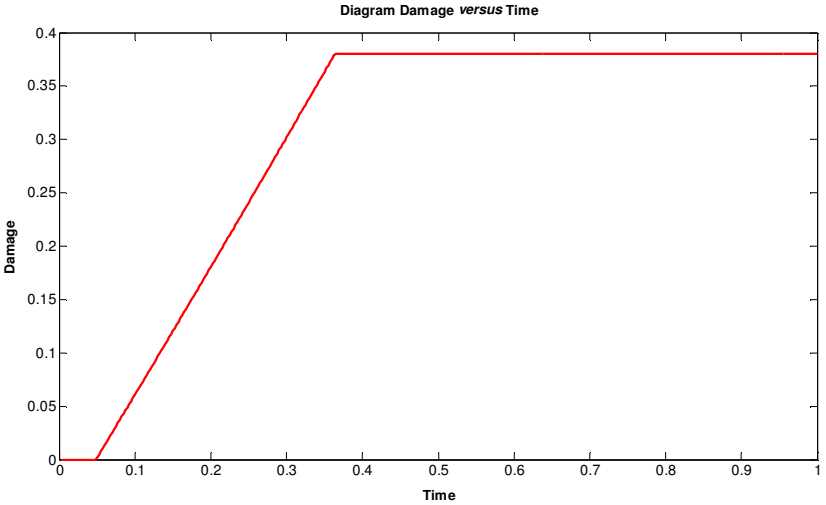

Figure 7.4: Evolution of the damage field as a function of "time".

The evolution of the viscoplastic strain, ε_{zz}^{vp}, at a generic point in the domain, as a function of "time", is illustrated in Figure 7.5 and Figure 7.6 illustrates the evolution of the stress component, σ_{zz}, at a generic point in the domain, as a function of "time". Additionally, the distribution of the displacement component u_z and damage within the domain of the model at $\overline{u}_z = 60$ mm, i.e., the final value of the prescribed displacement on the upper edge, is illustrated in Figure 7.7. One can notice that the damage is evenly distributed all over the component. This has taken place because of the implementation strategy adopted in this work and discussed in section 4.2.2.

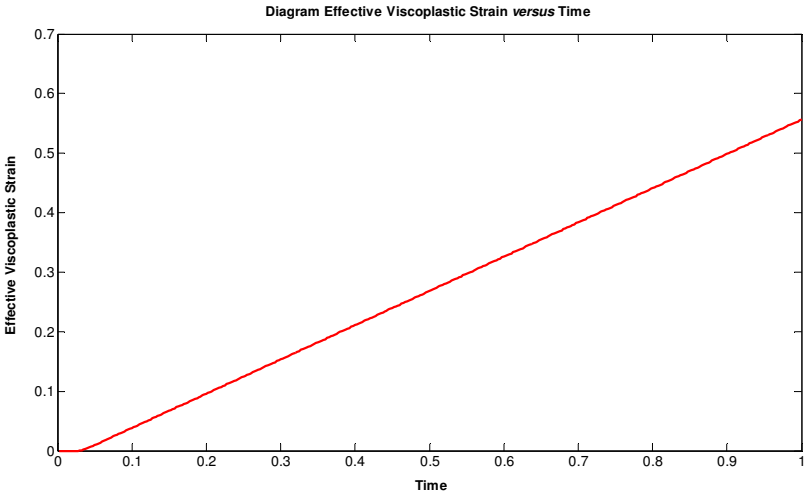

Figure 7.5: Evolution of the viscoplastic strain component ε_{zz}^{vp} as a function of "time".

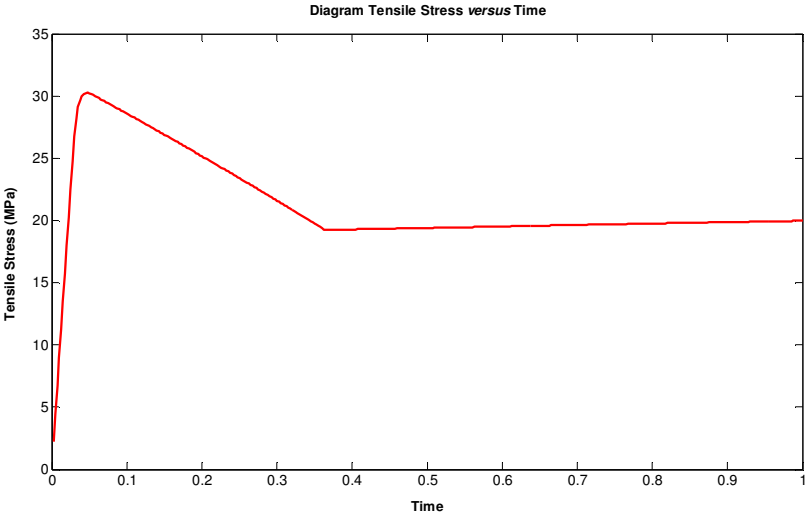

Figure 7.6: Evolution of the stress component σ_{zz} as a function of "time".

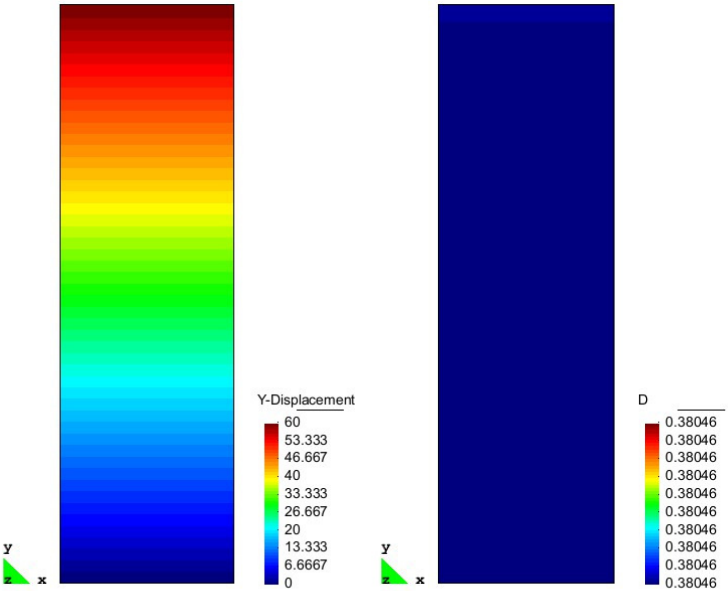

Figure 7.7: Distribution of the displacement component u_z and damage at $\overline{u}_z = 60$ mm, prescribed displacement applied on the upper edge.

Notice that, when the material reaches the cold drawing region, the reduced cross section of the necking remains approximately constant in this stage, i.e., the evolution of the damage variable is $\dot{D} \simeq 0$, which implies $D \simeq cte$.

7.2. EXAMPLE 1 – MECHANICAL COMPONENT

This second example illustrates the performance of a small plastic slab, submitted to a tensile prescribed displacement condition. Its geometry and dimensions are illustrated in Figure 7.8. Since its shape is prismatic and it has two planes of symmetry, then quarter of its geometry has been modeled as a plane strain problem, as can be seen the mesh in Figure 7.9. In this figure, one also observes that on the right edge, one has applied a tensile prescribed displacement in the x-direction, varying linearly up to $\overline{u}_x = 2.0$ mm. Additionally, the left and the lower edges have been constrained in the x and y-directions, respectively, in order to simulate the symmetry conditions.

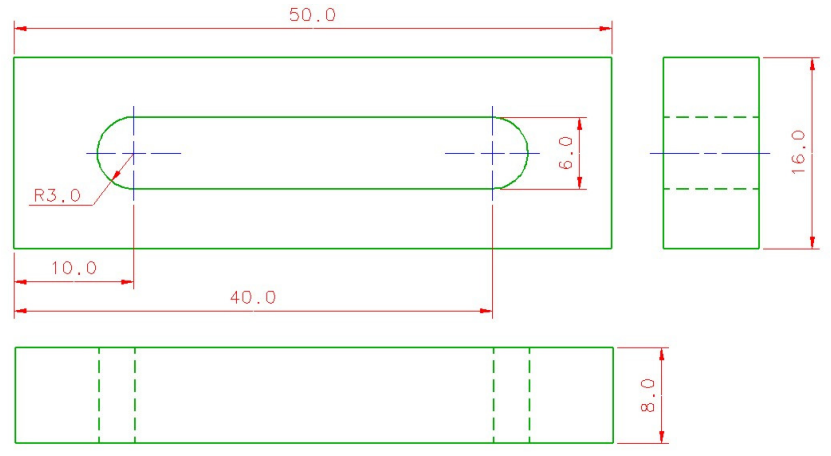

Figure 7.8: Mechanical component geometry and dimensions, in millimeters.

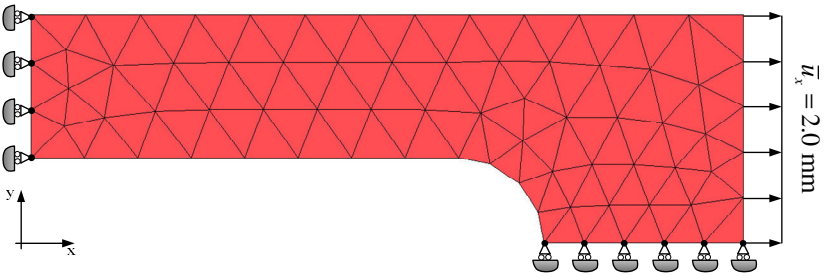

Figure 7.9: Mechanical component mesh and boundary conditions.

The distribution of the displacement in the x-direction, u_x, for a prescribed displacement at the right edge of $\overline{u}_x = 1.935$ mm, is illustrated in Figure 7.10. In turn, Figure 7.11 illustrates the distribution of the equivalent viscoplastic strain. Additionally, Figure 7.12 illustrates the distribution of the damage variable at the end of the analysis. In this figure, one may observe the approximately homogeneous distribution of the damage variable at the bottom edge of the left side of the component. Here, one can verify the effect of the cold drawing deformation process occurring at the middle of the component. In the case of a metal alloy model, with no damage locking constraint, one would only see a localization of the damage field in the vicinity of the stress concentration point, located close to the radius of the component.

Figure 7.10: Displacement in the *x*-direction at the end of the analysis, in millimeters.

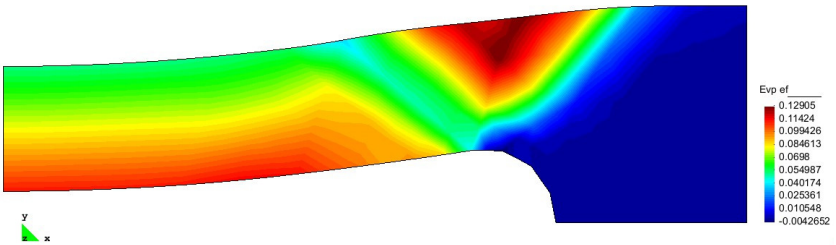

Figure 7.11: Distribution of the equivalent viscoplastic strain at the end of the analysis.

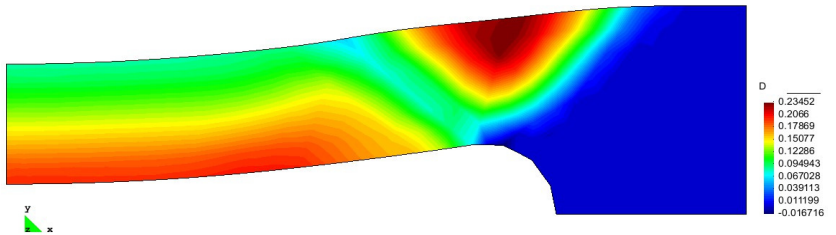

Figure 7.12: Distribution of damage at the end of the analysis.

7.3. EXAMPLE 2 – PLASTIC PULLEY

In this example, one will illustrate the performance of a V-belt generic plastic pulley, submitted to a compressive prescribed displacement condition, representing the load from the belt. Figure 7.13 illustrates two practical examples of application of plastic pulleys. In Figure 7.13.a, the bicycle pulley is made of metal, but it may be replaced by a plastic one, while in Figure 7.13.b, one illustrates the application of plastic pulleys as moving elements of engines. In this case, one requires

that the material of the pulley is selected, so that it withstands the wear and high temperatures.

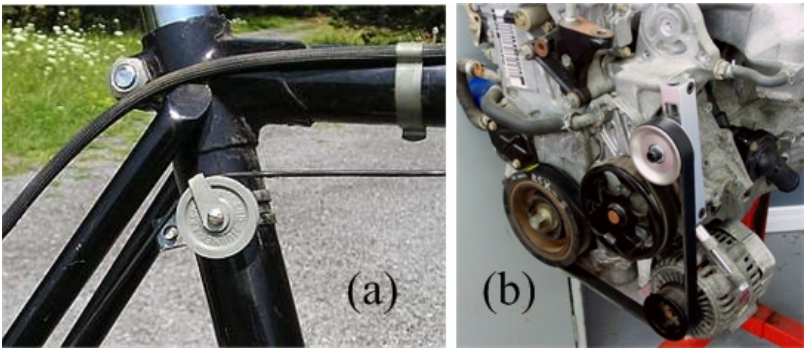

Figure 7.13: Some practical examples of application of plastic pulleys.

Because the pulley is a solid of revolution, then one has approximated the analysis by considering the problem to be axisymmetric. The diameter of its central hole is 30 mm and its cross-section dimensions are illustrated in Figure 7.14. The mesh and the boundary conditions are illustrated in Figure 7.15. In this figure, one observes that on the right end, one has applied a uniform compressive prescribed displacement in the radial direction, varying linearly up to $\overline{u}_r = -3.5$ mm and the left end has been fully constrained, in order to simulate the assembly of the pulley on a rigid axle and assuming a non slip condition in the interface pulley-axle.

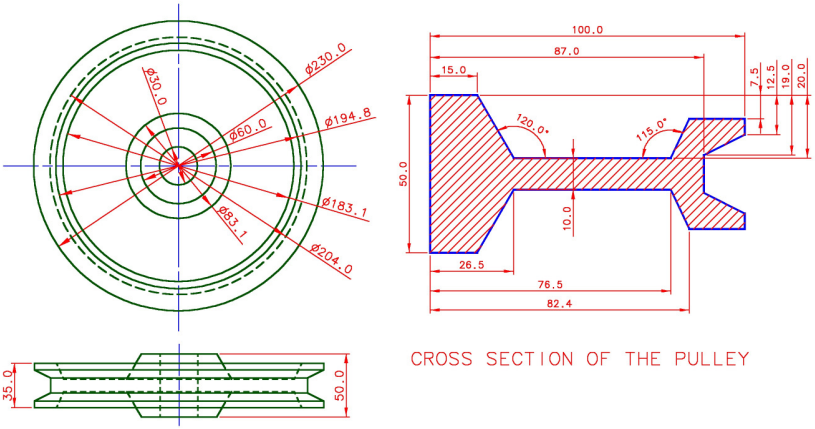

Figure 7.14: Plastic pulley geometry and dimensions, in millimeters.

The region with a finer mesh in Figure 7.15 is a consequence of some preliminary analyses, in which one has observed that the highest values of damage, stresses and equivalent plastic strain have taken place in this region, due to variation of geometry, which generates stress concentration. Thus, one has decided to refine it, in order to obtain better results.

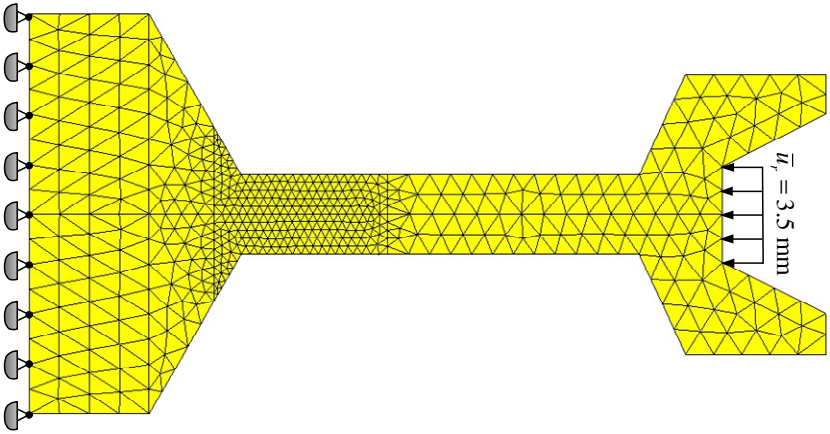

Figure 7.15: Plastic pulley mesh and boundary conditions.

This analysis has run with 10000 load steps and global tolerance for convergence of 10^{-5}. Figure 7.16 illustrates the distribution of the norm of the displacement at the end of the analysis, in millimeters, and Figure 7.17 illustrates the distribution of equivalent plastic strain. The distribution of the damage variable at the end of the analysis, i.e., for a prescribed displacement of $\bar{u}_r = -3.5$ mm, is depicted in Figure 7.18. One can observe that the region with higher concentration of viscoplastic strains looks much like a "X" letter, in which each of its leg is inclined about 45° with respect to the radial direction. This peculiarity strongly suggests the formation of shear bands, which is a characteristic failure mode of plastic components under compressive loads, as has been discussed in section 2.6. Additionally, one also observes that the maximum value for the effective viscoplastic strain occurs at the intersection of the shear bands.

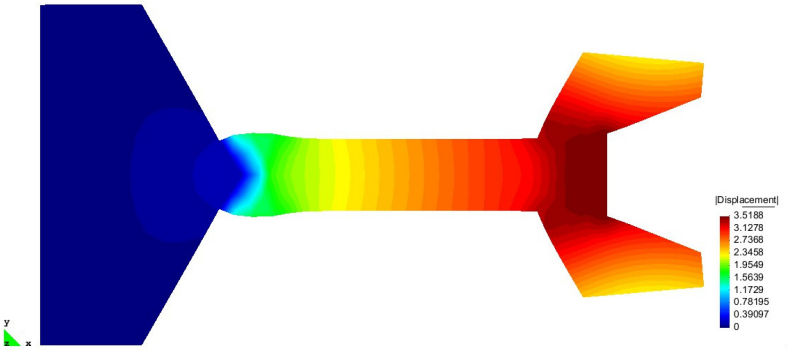

Figure 7.16: Displacement field at the end of the analysis, in millimeters.

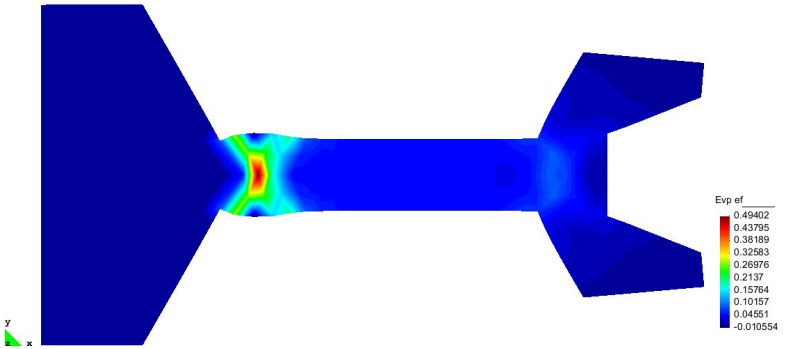

Figure 7.17: Distribution of equivalent viscoplastic strain, in mm/mm.

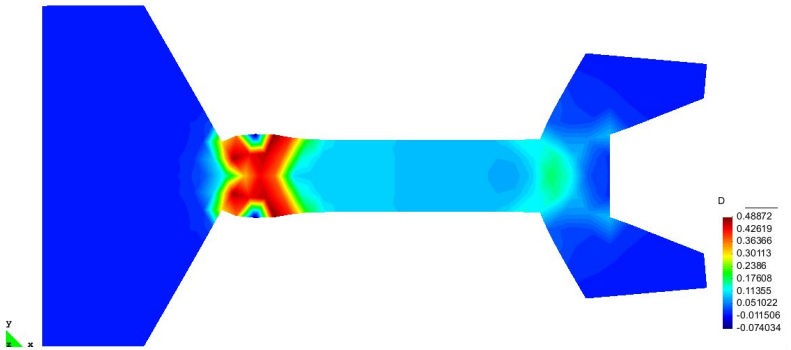

Figure 7.18: Distribution of damage.

7.4. EXAMPLE 3 – AUTOMOTIVE SNAP FIT

This third example will illustrate the performance of an automotive snap fit[28], submitted to a prescribed displacement, relative to the displacement necessary for installation of an additional component. The snap fit has been produced by means of the extrusion process and, due to industrial confidentiality reasons; its shape has been slightly modificated from the original geometry. The new geometry and its dimensions are illustrated in Figure 7.19 and the problem has been modeled as a plane strain problem, since this component is very thick. The mesh and the boundary conditions are illustrated in Figure 7.20, where one can see the application of a displacement of 4.0 mm, in the *x*-direction, in order to simulate the assemblage of an additional component, and the application of a fully clamped constraint on the left edges, in order to simulate the fixing of the snap fit on the vehicle structure.

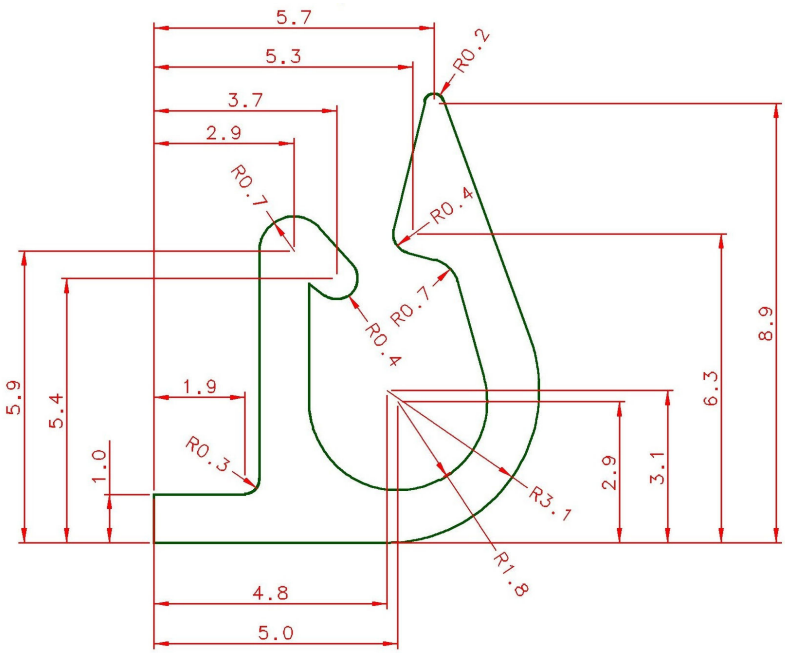

Figure 7.19: Snap fit geometry and dimensions, in millimeters.

[28] Snap fits are mechanical joint systems, used to assembly components. The attachment is accomplished by means of a protruding part of one component, such as a hook, stud or bead, which is briefly deflected during the joint operation and is caught in a depression in the mating component. After the joining operation, the joint should return to a stress free condition [12].

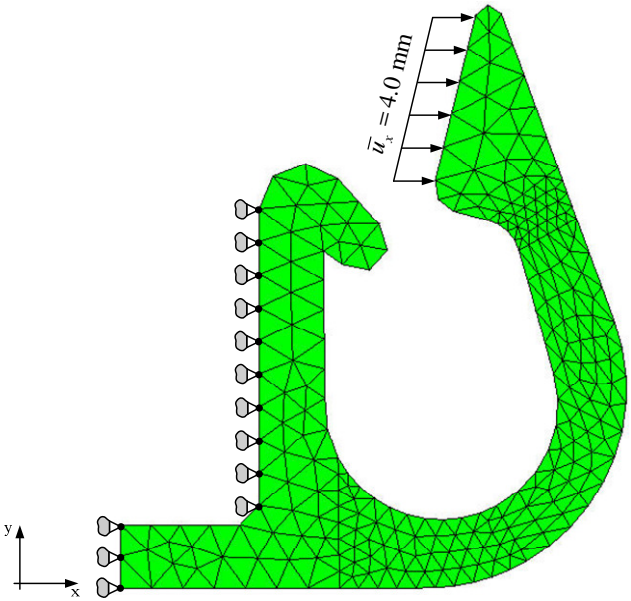

Figure 7.20: Mesh and boundary conditions of the snap fit.

Figure 7.21 illustrates the distribution of the norm of the displacement field of the snap fit, in millimeters. A total of 5000 load steps has been applied in the analysis of the component and one has employed a global convergence tolerance of 10^{-5}.

The distribution of the effective viscoplastic strain, at the end of the analysis, i.e., for a prescribed displacement of $\bar{u}_x = 1.94$ mm, is depicted in Figure 7.22. These results demonstrate that, despite the assembly displacement is small (1.94 mm), it is sufficient to produce irreversible strains and, consequently, a very small amount of damage, as can be seen in Figure 7.23. From the boundary conditions illustrated in Figure 7.20, one can conclude that the most damaged area, illustrated in Figure 7.21, will be submitted to tensile stresses, due to its bending. As a consequence, on the opposite side, there will be compressive stresses. Therefore, crazing formation will be the most likely failure mode for this component.

Notice that even after unloading the snap fit, an irreversible damage does occur, due to its irreversibility nature. This might cause premature failure of this component, by means of aging, elevated temperatures, since it will be located close to the engine block, and due to other environmental factors. It is worth emphasizing that, in practice, the

design of this component has been performed empirically, as has been accordingly discussed in section 1.2, and the above simplified analysis has not accounted for the influence of variation of temperature.

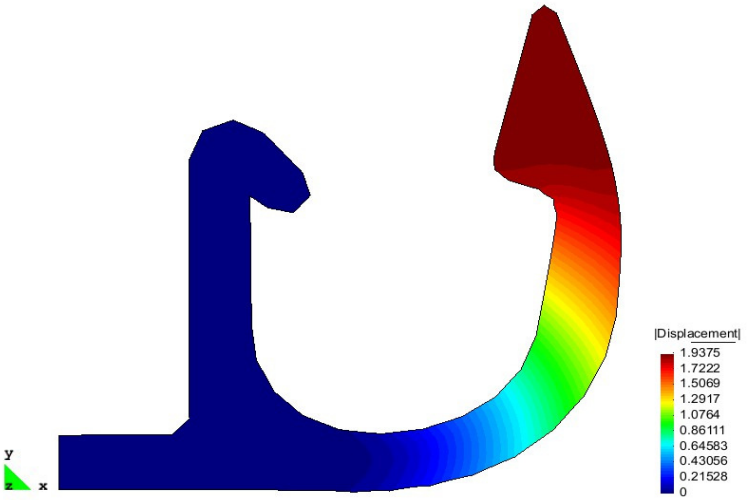

Figure 7.21: Displacement field of the snap fit at the end of the analysis, in millimeters.

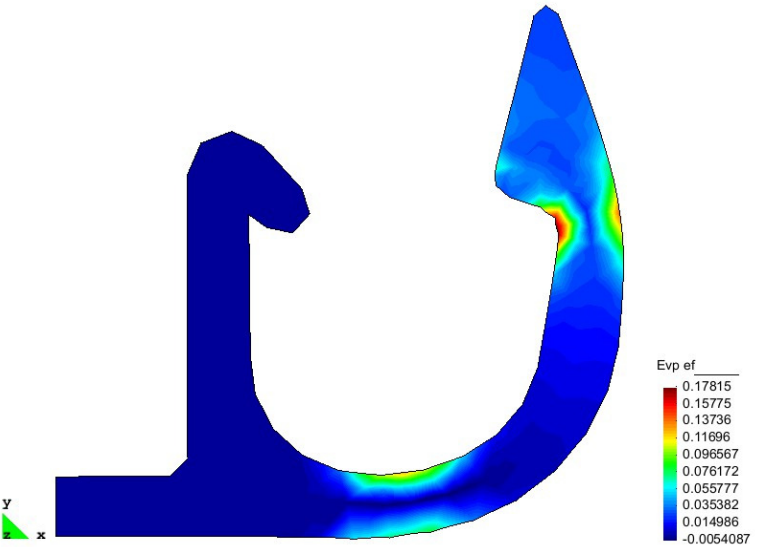

Figure 7.22: Distribution of the equivalent viscoplastic strain, in mm/mm.

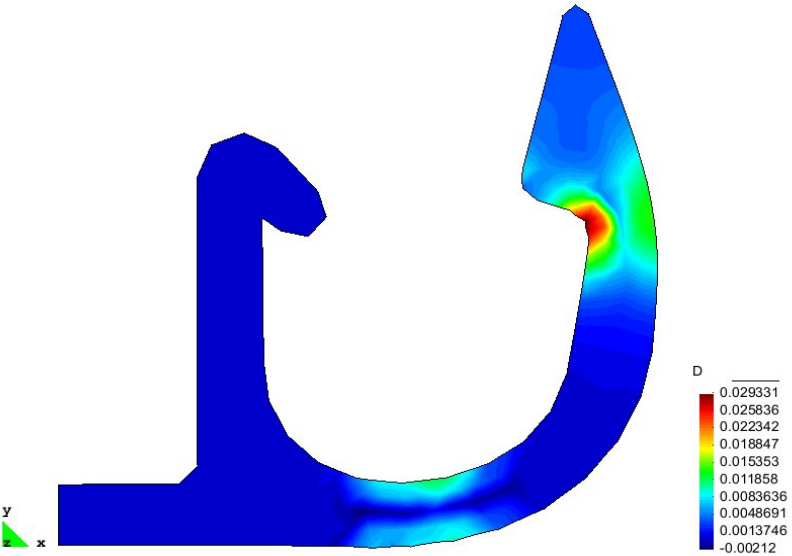

Figure 7.23: Distribution of damage of the snap fit.

CHAPTER 8

FINAL CONSIDERATIONS

The accomplishment of this work has been motivated by the empiricism, in which the design of plastic components is performed, which, in many cases, leads to the production of over-dimensioned components, and by the absence of consistent numerical tools capable of simulating the damaging processes of plastic components, when submitted to mechanical loading. Thus, based on these deficiencies, this work has aimed at proposing an elasto-viscoplastic with coupled damage model, to be used to analyze the mechanical behavior of plastic components and the development of experimental tests, in order to obtain the material properties required by the model. This chapter section will be addressed to discuss the final remarks of this work. In this regard, one will be presented the conclusions and some suggestions for future works, within this same line of research.

8.1. CONCLUSIONS

During the accomplishment of this work, one could notice that plastics are very complex materials and many different approaches have been applied to model their mechanical behavior. Also, one could notice that their thermal, mechanical and electrical behaviors are strongly influenced by factors, like: composition, kind of molecular arrangement and structure (linear, branched, cross-linked and network), degree of crystallinity, presence of additives, temperature, loading rate and other environmental influences, such as moisture and sunlight. Even so, these materials have been extensively used as structural elements or as replacement of metallic materials in many load bearing industrial applications, due to their low cost, when compared with the most traditional engineering materials, versatility, lightness, durability and corrosion resistance.

This present work can be didactically subdivided as: the theoretical development of the proposed model; the part associated with the discretization of the derived mathematical model and, finally, the part describing the experimental tests performed in order to identify the material parameters, which has been performed at the Fibre and Polymer Technology Department of the Royal Institute of Technology, in Stockholm, Sweden.

When working with material modeling, it is very common to consider some assumptions and hypotheses, so that their equations are

readily obtained, solved and implemented. Among the hypotheses regarded in this work (see section 1.4), one considers that isotropy and homogeneity, infinitesimal strain regime and isotropy of the damage measure deserve to be highlighted, because these hypotheses can strongly influence the final results of the modeling, although their application has led to good results.

A rough calibration of the model has been attempted by using the data of a uniaxial tensile test, from which one has obtained the experimental stress-strain diagram. By comparing the numerical response associated with a given set of material parameters with the response obtained from the experimental test one could determine, by a trial and error procedure, an approximate identification of the material parameters that yielded a maximum error of about 22%. This maximum error occurred in the softening response phase, which leads to the formation of the necking and cold drawing process.

In this work, the softening behavior has been accounted for by the damage variable, which is responsible for describing the reduction of the cross section that occurs in the necking formation. Since, in the cold drawing process, the cross section remains approximately constant, at each point with the reduced cross section area, the damage variable should be approximately constant as has been enforced by the damage locking constraint. Thus, the proposed approach has led to a constant damage distribution in the tensile specimen of the numerical simulation.

The consideration of a finite deformation model may be more adequate to simulate the necking formation and the cold drawing process, since, physically, the reduction of area of the cross section is a large deformation process. As a result, the damage variable would need to describe only the nucleation of micro voids or micro cracks, which would give a better fit of the numerical response with the available experimental data. A better determination of the isotropic hardening parameters could be obtained by solving a least square optimization process, using, for example, a genetic algorithm. Notice that the identification of parameters may be formulated as an inverse problem, which can be formulated as a least square minimization problems. Moreover, by using a genetic algorithm one may compute an approximation to the global minimum, resulting in this way in an improved identification for the material parameters.

Due to the coupling of the problem, the implementation of the model has been relatively tough. In order to prevent volumetric locking, one has employed a six-node triangular finite element, as can be seen in Figure 7.1. Thus, both the displacement and the damage fields have been interpolated by quadratic polynomial functions.

The modeling proposed in this work is most addressed to model geometries, which yield non-homogeneous deformation, resulting from the deformation of components with some kind of stress concentrators, like fillets, notches or variation of thickness. Thus, one has sought for simulating components with such peculiarities. One can notice that the last numerical example of Chapter 7 has not reached the whole initial prescribed displacement, i.e., there has been some convergence failure. Although other investigations with smaller load step have been attempted, no convergence has been reached. In this case, a strategy based on arc-length algorithms with variable load steps may give a more robust strategy. Despite the elevated error between numerical and experimental data (about 22%), one considers that the model is appropriated to represent the mechanical behavior and the degradation processes of plastic components under mechanical loads, because, qualitatively speaking, the proposed three numerical examples have provided very consistent results and an improvement in the identification process may decrease considerably the mentioned error.

Since this work has been developed, based on the damage approach proposed by Fremond and Nedjar [2], in which one accounts for the gradient of damage, then one expects that the results are mesh insensitive. At last, the extension of the work to plane stress problems may broaden the applicability of the proposed theory and may be used to solve other important problem cases that could be compared with experimental data.

The second part of this work refers to the development of mechanical tests, performed in order to obtain the material properties required to fully characterize the material model. Initially, a plastic material (polypropylene resin), commonly used to manufacture load bearing components similar to those used in the numerical examples chapter, has been selected and its main mechanical properties have been obtained. The tests have been conducted following ASTM standards recommendations and two aspects have been observed: the standard deviations have been low, what has led to a low scattering; and a good agreement between the test results and the data published by the material supplier (Borealis), what means that the test results are reliable and consistent.

The possibility of implementing this work on commercial codes, such as Abaqus, Ansys or LS-Dyna may also be considered as a future goal, which would enable the modeling proposed in this work to be used to analyze the mechanical performance and the damaging processes of industrial components, as currently most commercial codes are not able to support such analysis procedure. In the context of product development,

its use may be introduced in the stress-strain analysis step of the preliminary design phase, as has been illustrate in Figure 1.1.

The modeling proposed in this work might not be useful for practical applications, unless one guarantees that the components under analysis are free of defects derived from the manufacturing process, because these defects may drastically reduce their strength and, consequently, provoke their premature failure. Moreover, the theory proposed in this work assumes that the components will be free of defects, which means that the initial damage equals zero, i.e., $D(x,0)=0$. Therefore, it is extremely important to assure that plastic components are dimensioned, so that they fulfill either the mechanical or the manufacturing requirements, which require a reliable analysis of the behavior of the component. In practice, these precautions may help to reduce costs related to maintenance and even from casual replacements of those components which have failed precociously. For injection molded components, the occurrence of manufacturing defects can be checked by means of a rheological analysis.

8.2. PROPOSALS FOR FUTURE WORKS

The increasing use of plastic materials in many load bearing industrial products, during the last decades, has motivated the development of this work, in which one has proposed a constitutive model to describe the inelastic behavior and damaging process of plastic components submitted to mechanical loads. Certainly, this work might also motivate the development of future ones, within this same research line. Thus, some suggestions for future works will be discussed following.

In this work, one has attempted to calibrate the model by addressing the numerical tensile test simulation with the experimental tensile test data and a considerable difference has been obtained. Such difference has been verified in the softening region of the diagram, where the specimen necks and, then, evolves to the cold drawing region. In order to improve the modeling of the softening region and, thus, decrease that error, one suggests the **development of this model by assuming finite strain deformation**.

When working with mathematical modeling, one should bearing in mind that the input variables are subject to many sources of uncertainty, including error of measurement, absence of information and poor or partial understanding of the problem. In order to reduce the influence of those uncertainties on the outputs of the model, one suggests the **development of a sensitivity analysis investigation**, in which the model

inputs will be ordered by importance and their influence on the outputs will be measured and optimized.

The model proposed in this work may also be solved by means of other numerical methods, other than the finite element method, and their results may be compared. Among the available alternatives, one suggests the **application of the meshfree Galerkin method**, due to its noticeable versatility. Moreover, one also suggests the **implementation of a variable load step strategy**, based on arc-length algorithms, in order to become the code more robust.

One knows that plastic materials are neither isotropic nor homogeneous. The arrangements of molecular chains become the material inhomogeneous and with mechanical and thermal behaviors depending on the direction. In this case, the damaging process will develop anisotropically. Thus, one proposes the **development of this model, accounting for anisotropic damage**. This work might also be developed by using the approaches proposed by Lemaitre [1] and Fremond and Nedjar [2].

According to Gotham [10], about 70% of premature failure of plastic components is regarded to the fatigue phenomenon. Because this is a very representative number and because plastic components have been increasingly used as structural elements, then one suggests the **development of a model to be used to analyze plastic components under both low and high cycle fatigue loading**. This model might be obtained by only modifying the model proposed in this present work, so that it can describe the degradation processes of the component. In this regard, a kinematic hardening variable will have to be introduced as state variable, fatigue tests might be performed, the micro crack closure effect may also be considered and the effect of temperature must be introduced, in order to predict the possibility of thermal failure.

REFERENCES

[1] LEMAITRE, J. **A Course on Damage Mechanics**. Springer, Berlin, Germany, 1996. 228 p.

[2] FREMOND M.; NEDJAR B. **Damage, Gradient of Damage and Principle of Virtual Power**. International Journal of Solids Structures, Vol. 33, n°. 8, 1996. p. 1083 – 1103.

[3] LEE, K. **Principles of CAD/CAM/CAE Systems**. Addison-Wesley Longman, Inc., Harlow, England, 1999. 263 p.

[4] GHORBEL, E. **A Viscoplastic Constitutive Model for Polymeric Materials**. International Journal of Plasticity. Vol. 24, n°. 11, 2008. p. 2032 – 2058.

[5] RIANDE, E.; DIAZ-CALLEJA, R.; PROLONGO, M. G.; MASEGOSA, R. M.; SALOM, C. **Polymer Viscoelasticity: Stress and Strain in Practice**. Marcel Dekker. 2000. 879 p.

[6] LEMAITRE, J.; DESMORAT, R. **Engineering Damage Mechanics: Ductile, Creep, Fatigue and Brittle Failures**. Springer-Verlag, Berlin, Germany, 2005. 380 p.

[7] MASCARENHAS, W. N. **Systematization of the Obtainment Process of the Dimensional Layout of Injection Molded Plastic Components**. M.Sc. Dissertation (In Portuguese), Mechanical Engineering Department, Federal University of Santa Catarina (UFSC), Florianópolis, SC, Brazil, 2002. 218 p.

[8] OGLIARI, A. **Systematization of the Product Conception Aided by Computer Applied to the Injection Molded Components Design**. Ph.D. Thesis (in Portuguese). Mechanical Engineering Department, Federal University of Santa Catarina (UFSC), Florianópolis, SC, Brazil, 1999. 349 p.

[9] DARÉ, G. **Proposition of a Reference Model for the Integrated Development of Injection Molded Components**. M.Sc. Dissertation (in Portuguese). Mechanical Engineering Department, Federal University of Santa Catarina (UFSC), Florianópolis, SC, Brazil, 2001. 219 p.

[10] GOTHAM, K. V. **Fatigue and Long-Term Strength of Thermoplastics**. Development in Plastics Technology – 3, Elsevier Applied Science Publishers, London, UK, 1985. 321p.

[11] KRISHNA, A. **Stress Analysis of Instrumental Panel Knob**. SAE Paper, 2000.

[12] MALLOY, R. A. **Plastic Part Design for Injection Molding: An Introduction**. Carl Hanser Verlag, Munich, Germany, 1995. 237p.

[13] KRISHNAMACHARI, S. I. **Recommended Factors of Safety and Related Considerations**. SPE Annual Technical Conference – ANTEC, San Francisco, USA, 2002.

[14] MASCARENHAS, W. N.; AHRENS, C. H.; OGLIARI, A. **Design Criteria and Safety Factors for Plastic Components Design**. Materials & Design, Vol. 25, n°. 3, 2004. p. 257 – 261.

[15] LEMAITRE, J.; CHABOCHE, J. L. **Mechanics of Solid Materials**. Cambridge University Press, Cambridge, UK, 1990. 556p.

[16] QUINSON, R.; PEREZ, J.; RINK, M.; PAVAN, A. **Yield Criteria for Amorphous Glassy Polymers**. Journal of Materials Science, Vol. 32, n°. 5, 1997. p. 1371 – 1379.

[17] GOLDBERG, R. K.; ROBERTS, G. D.; GILAT, A. **Implementation of an Associative Flow Rule Including Hydrostatic Stress Effect Into the High Strain Rate Deformation Analysis of Polymer Matrix Composites**. NASA

Center for Aerospace Information. Report Number 2003-212382, 2003.

[18] ROTTLER, J.; ROBBINS, M. O. **Yield Conditions for Deformation of Amorphous Polymer Glasses**. Physical Review E, Vol. 64, n°. 5, 2001. p. 1 – 9.

[19] ALTENBACH, H.; TUSHTEV, K. **A New Static Failure Criterion for Isotropic Polymers**. Mechanics of Composite Materials. Vol. 37, n°. 5-6, 2001. p. 475 – 482.

[20] KREMPL, E.; HO, K. **Inelastic Compressive and Incompressible, Isotropic, Small Strain Viscoplasticity Based on Overstress (VBO)**. In Lemaitre Handbook of Materials Behavior Models. Academic Press, New York, p. 336 – 348. 2001.

[21] Wikipedia Web Site. Available from: http://en.wikipedia.org/wiki/Main_Page.

[22] KREMPL, E.; HO, K. **An Overstress Model for Solid Polymer Deformation Behavior Applied to Nylon 66**. ASTM STP. N°. 1357, 2000. p. 118 – 137.

[23] COLAK, O. U.; DUSUNCELI, N. **Modeling Viscoelastic and Viscoplastic Behavior of High Density Polyethylene (HDPE)**. Journal of Engineering Materials and Technology, Vol. 128, n°. 4, 2006. p. 572 – 578.

[24] COLAK, O. U. **Modeling Deformation Behavior of Polymers with Viscoplasticity Theory Based on Overstress**. International Journal of Plasticity. Vol. 21, n°. 1, 2005. p. 145 – 160.

[25] FRANK, G. J.; BROCKMAN, R. A. **A Viscoelastic-Viscoplastic Constitutive Model for Glassy Polymers**. International Journal of Solid Structures, Vol. 38, n°. 30/31, 2001. p. 5149 – 5164.

[26] RIESEN, R.; SCHAWE, J. **The Glass Transition Temperature Measured by Different TA Techniques. Part 1: Overview**. UserCom Publication, n°. 17, 2003. p. 1 – 4.

[27] DROZDOV, A. D. **Viscoelasticity and Viscoplasticity of Glassy Polymers in the Vicinity of the Yield Point**. Mechanics Research Communication, Vol. 28, n°. 3, 2001. p. 247 – 254.

[28] DROZDOV, A. D. **A Model for the Viscoelastic and Viscoplastic Response of Glassy Polymers**. International Journal of Solid Structures, Vol. 38, n°. 46/47, 2001. p. 8285 – 8304.

[29] DROZDOV, A. D.; YUAN, Q. **The Viscoelastic and Viscoplastic Behavior of Low-Density Polyethylene**. International Journal of Solid Structures, Vol. 40, n°. 10, 2003. p. 2321 – 2342.

[30] DROZDOV, A. D.; GUPTA, R. K. **Non-Linear Viscoelasticity and Viscoplasticity of Isotactic Polypropylene**. International Journal of Engineering Science, Vol. 41, n°. 20, 2003. p. 2335 – 2361.

[31] DROZDOV, A. D.; CHRISTIANSEN, J. C. **Modeling the Viscoplastic Response of Polyethylene in Uniaxial Loading-Unloading Tests**. Mechanics Research Communication, Vol. 30, n°. 5, 2003. p. 431 – 442.

[32] LEE, Y. K.; GHOSH, J. **The Significance of J_3 to the Prediction of Shear Bands**. International Journal of Plasticity. Vol. 12, n°. 9, 1996. p. 1179 – 1197.

[33] HALL, R. B. **A Thermodynamic Framework for Viscoplasticity Based on Overstress (VBO)**. Journal of Engineering Materials and Technology, Vol. 127, n°. 4, 2005. p. 369 – 373.

[34] FATEMI, A.; YANG, L. **Cumulative Fatigue Damage and Life prediction Theories: a Survey of the State of the Art for**

Homogeneous Materials. International Journal of Fatigue. Vol. 20, n°. 1, 1998. p. 9 – 34.

[35] GAMSTEDT, E. K.; SJÖGREN, B. A. **Micromechanisms in Tension-Compression Fatigue of Composites Laminates Containing Transverse Plies**. Composites Science and Technology. Vol. 59, n°. 2, 1999. p. 167 – 178.

[36] GAMSTEDT, E. K.; SJÖGREN, B. A. **An Experimental Investigation of the Sequence Effect in Block Amplitude Loading of Cross-Ply Composite Laminates**. International Journal of Fatigue. Vol. 24, n°. 2 – 4, 2002. p. 437 – 446.

[37] TANG, C. Y.; LEE, W. B. **Damage Mechanics Applied to Elastic Properties of Polymers**. Engineering Fracture Mechanics, Vol. 52, n°. 4, 1995. p. 717 – 729.

[38] TANG, C. Y.; PLUMTREE, A. **Damage Mechanics Applied to Polymers**. Engineering Fracture Mechanics, Vol. 49, n°. 4, 1994. p. 499 – 508.

[39] JIE, M.; TANG, C. Y.; LI, Y. P.; LI, C. C. **Damage Evolution and Energy Dissipation of Polymers with Crazes**. Theoretical and Applied Fracture Mechanics, Vol. 28, n°. 3, 1998. p. 165 – 174.

[40] VINOGRADOV, A.; RASSI, E. **Modeling of Cyclic Damage Evolution in Polymers**. Proceedings of the 41st Annual SES Technical Meeting, Lincoln, Nebraska, USA, 2004.

[41] TANG, C. Y.; TAI, W.H.; LEE, W. B. **Modeling of Damage Behaviors of High Impact Polystyrene**. Engineering Fracture Mechanics, Vol. 55, n°. 4, 1996. p. 583 – 591.

[42] ZAÏRI, F.; ABDELAZIZ, M. N.; GLOAGUEN, J. M.; LEFEBVRE, J. M. **Modeling of the Elasto-Viscoplastic Damage Behavior of Glassy Polymer**. International Journal of Plasticity, Vol. 24, n°. 4, 2008. p. 945 – 965.

[43] DROZDOV, A. D. **Modeling Nonlinear Viscoelasticity and Damage in Amorphous Glassy Polymers**. Mathematical and Computer Modeling, Vol. 33, n°. 4, 2001. p. 883 – 893.

[44] ISAKSSON, P.; HÄGGLUND, R.; GRADIN, P. **Continuum Damage Mechanics Applied to Papers**. International Journal of Solids and Structures. Vol. 41, n°. 16 - 17, 2004. p. 4731 – 4755.

[45] ISAKSSON, P.; HÄGGLUND, R. **Analysis of the Strain Field in the Vicinity of a Crack-Tip in an In-Plane Isotropic Paper**

Material. International Journal of Solids and Structures. Vol. 44, n°. 2, 2007. p. 659 – 671.

[46] CHALLAMEL, N.; LANOS, C.; CASANDJIAN, C. **Creep Damage Modeling for Quasi-Brittle Materials**. European Journal of Mechanics – A/Solids. Vol. 24, n°. 4, 2005. p. 593 – 613.

[47] COSTA MATOS, H. S.; SAMPAIO, RUBENS. **Analysis of the Fracture of Brittle Elastic Materials Using a Continuum Damage Model**. Structural Engineering and Mechanics. Vol. 3, n°. 5, 1995. p. 411 – 427.

[48] HÄGGLUND, R.; ISAKSSON, P. **Influence of Damage in the Vicinity of a Crack-Tip in Embossed Low-Basis-Weight Paper**. Engineering Fracture Mechanics. Vol. 74, n°. 11, 2007. p. 1758 – 1769.

[49] CANEVAROLO JR., S. V. **Polymers Science** (in Portuguese). Artliber Press, São Paulo, SP, Brazil, 2002. 183 p.

[50] GORNI, A. A. **Introduction to Plastics**. Available from: http://www.gorni.e.ng.br/.

[51] TICONA. **Designing With Plastics**. Available from: http://www.ticona.com/.

[52] PÖSTSCH, G.; MICHAELI, W. **Injection Molding: An Introduction**. Carl Hanser Verlag, Munich, Germany, 1995. 195p.

[53] McCHESNEY, C. E. **Liquid Crystal Polymers (LCP)**. Engineering Materials Handbook: Engineering Plastics, Volume 2. ASM International™, Ohio, USA, 1997. 883p.

[54] HUANG, J. C. **Mechanical Properties**. Engineering Materials Handbook: Engineering Plastics, Volume 2. ASM International™, Ohio, USA, 1997. 883p.

[55] WARD, I. M.; HADLEY, D. W. **An Introduction to the Mechanical Properties of Solid Polymers**. John Wiley & Sons, Chichester, UK, 1993. 334 p.

[56] THRONE, J. L.; PROGELHOF, R. C. **Creep and Stress Relaxation**. Engineering Materials Handbook: Engineering Plastics, Volume 2. ASM International™, Ohio, USA, 1997. 883p.

[57] RIETVELD, J. **Viscoelasticity**. Engineering Materials Handbook: Engineering Plastics, Volume 2. ASM International™, Ohio, USA, 1997. 883p.

[58] GE PLASTIC. **Design Guide**. Available from: http://www.geplastic.com/.

[59] BAYER. **Bayer's Manual**. Available from: www.plastics.bayer.com.

[60] TRES, P. A. **Designing Plastic Parts for Assembly, 3rd Edition**. Carl Hanser Verlag, Munich, Germany, 1998. 258 p.

[61] BERINS, M. L. **Plastics Engineering Handbook of the Society of the Plastic Industry, Inc.**, 5th Edition. Chapman & Hall, New York, NY, USA, 1991. 869 p.

[62] FISH, F. A. **Design Approach for Engineering Plastic**. Engineering Materials Handbook: Engineering Plastics, Volume 2. ASM International™, Ohio, USA, 1997. 883p.

[63] KENNEDY, P. **Flow Analysis of Injection Molds**. Carl Hanser Verlag, Munich, Germany, 1995. 237 p.

[64] MICHAELI, W. **Plastics Processing: An Introduction**. Carl Hanser Verlag, Munich, Germany, 1995. 211 p.

[65] RUBIN, I. I. **Injection Moulding: Theory and Practice**. John Wiley and Sons, Inc., New York, NY, USA, 1992. 657 p.

[66] ROSATO, D. V.; ROSATO, D. V. **Injection Moulding Handbook**. Von Nostradamus Reinhold, Inc., New York, NY, USA, 1986. 899p.

[67] VIANA, J. C.; CUNHA, A. M. The **Impact Behavior of Weld Lines in Injection Molding**. Journal of Injection Molding Technology, December 2002, Vol. 6, n° 4.

[68] MILLER, E. **Introduction to Plastic and Composite: Mechanical Properties and Engineering Applications**. Marcel Dekker, Inc., New York, NY, USA, 1996. 434 p.

[69] SEYMOUR, R. B. **Determination of Chemical Susceptibility**. Engineering Materials Handbook: Engineering Plastics, Volume 2. ASM International™, Ohio, USA, 1997. 883p.

[70] HERTZBERG, R. W.; MANSON, J. A. **Fatigue of Engineering Plastics**. Academic Press, New York, NY, USA, 1980. 293p.

[71] YELLE, H. J. M.; ESTABROOK, F. R. **Fatigue Loading**. Engineering Materials Handbook: Engineering Plastics, Volume 2. ASM International™, Ohio, USA, 1997. 883p.

[72] MOET, A.; AGLAN, H. **Fatigue Failure**. Engineering Materials Handbook: Engineering Plastics, Volume 2. ASM International™, Ohio, USA, 1997. 883p.

[73] DAO, K. C.; DICKEN, D. J. **Fatigue Failure in Polymers**. Polymer Engineering and Science, Vol. 27, n°. 4, 1987. p. 271 – 276.

[74] TIJSSENS, M. G. A.; VAN DER GIESSEN, E.; SLUYS, L. J. **Modeling of Crazing Using a Cohesive Surface Methodology**. Mechanics of Materials. Vol. 32, n°. 1, 2000. p. 19 – 35.

[75] PETRIE, S. P. **Crazing and Fracture**. Engineering Materials Handbook: Engineering Plastics, Volume 2. ASM International™, Ohio, USA, 1997. 883p.

[76] SO, P. K. **Fractography**. Engineering Materials Handbook: Engineering Plastics, Volume 2. ASM International™, Ohio, USA, 1997. 883p.

[77] CONSTABLE, I.; WILLIAMS, J. G.; BURNS, D. J. **Fatigue and Cyclic Thermal Softening of Thermoplastics**. Journal of Mechanical Engineering Science, Vol. 12, n°. 1, 1970. p. 20 – 29.

[78] GERMAIN, P. ***Cours de Mécanique des Milieux Continus***. Masson & Cie, Paris, France, 1973.

[79] MALVERN, L. E. **Introduction to the Mechanics of a Continuous Medium**. Prentice Hall, New Jersey, NY, USA, 1969. 713 p.

[80] SOUZA NETO, E. A.; PERIĆ, D.; OWEN, D. R. J. **Computational Methods for Plasticity: Theory and Applications**. John Wiley Ltd., London, UK, 2008. 783 p.

[81] LUBLINER, J. **Plasticity Theory**. Macmillan Publishing Company, New York, NY, USA, 1990. 495 p.

[82] NORTON, L. H. **The Creep of Steel at High Temperatures**. MacGraw-Hill, New York, USA, 1929. 108 p.

[83] BENALLAL, A. **Thermoviscoplasticity and Structural Damage**. Ph.D. Thesis (in French). University Pierre and Marie Curie, Paris 6, France, 1989.

[84] MASCARENHAS, W. N.; ALVES, M. K.; GAMSTEDT, E. K. **A First Order Damage Model for Low Cycle Fatigue of Polymer Matrix Composite Materials**. In 2nd Thematic Conference on the Mechanical Response of Composites (ECCOMAS), London, England, April/2009.

[85] EHRENSTEIN, G. W.; ERHARD, G. **Designing With Plastics: A Report on the State of the Art**. Carl Hanser Verlag, Munich, Germany, 1984. 135p.

[86] MINAK, G.; CHIMISSO, F. E. G.; COSTA MATTOS, H. S. da. **Cyclic Plasticity and Damage of Metals by a Gradient-Enhanced CDM Model**. 1st International Symposium on Solid Mechanics, USP, São Paulo - Brazil, March/2007.

[87] COOK, R. D.; MALKUS, D. S.; PLESHA, M. E.; WITT, R. J. **Concepts and Applications of Finite Element Analysis**. John Wiley & Sons, Inc., New York, NY, USA, 2004. 719 p.

[88] ASSAN, A. E. **Finite Elements Method: First Steps** (in Portuguese). Unicamp Press, Campinas, SP, Brazil, 2003. 298 p.

[89] VALOROSO, N. **Theory and Implementation of Plasticity and Viscoplasticity**. ITC – CNR Institute publication, Rome, Italy. 2002.

[90] ONO, M.; WASHIYAMA, J.; NAKAJIMA, K.; NISHI, T. **Anisotropic Thermal Expansion in Polypropylene/Poly(ethylene-co-octane) Binary Blends: Influence of Arrays of Elastomers Domain**. Polymer. Vol. 46, n°. 13, 2005. p. 4899 – 4908.

[91] LI, H.; JIA, Y.; MANTIMIN, G.; JIANG, W.; AN, L. **Stress Transfer and Damage Evolution Simulations of Fiber-Reinforced Polymer-Matrix Composites**. Materials Science and Engineering A. Vol. 425, n°. 1-2, 2006. p. 178 – 184.

[92] BROWN, N. **A Theory of Yielding of Amorphous Polymers at Low Temperature – A Molecular Viewpoint**. Journal of Materials Science. Vol. 18, n°. 8, 1983. p. 2241 – 2254.

[93] RIESEN, R. **Simple Determination of the Thermal Conductivity of Polymers by DSC**. UserCom Publication, n°. 22, 2005. p. 19 – 23.

[94] ANDRÉS, N.; RECUERO, S.; ARROY, M. P.; BONA, M. T.; ANDRÉS, J. M.; ANGUREL, L. A. **Fast Visualization of Corrosion Processes Using Digital Speckle Photography**. Corrosion Science. Vol. 50, n°. 10, 2008. p. 2965 – 2971.

[95] FOGUET, A. P.; FERRAN, A. R.; HUERTA, A. **Consistent Tangent Matrices for Substepping Schemes**. Computer Methods in Applied Mechanics and Engineering. Vol. 190, n°. 35, 2001. p. 4627 – 4647.

CHAPTER 9

RESUMO ESTENDIDO

Este capítulo adicional tem como objetivo apresentar este trabalho de tese redigido na língua portuguesa, de forma resumida, visto que o mesmo foi escrito na sua totalidade na língua inglesa. As referências citadas neste capítulo estão também descritas na seção anterior (Referências).

9.1. INTRODUÇÃO – CAPÍTULO 1

Neste capítulo introdutório, são definidas e traçadas as principais diretrizes do trabalho. Inicialmente, será apresentado o enfoque, a fim de que os objetivos do trabalho fiquem claramente delimitados e entendidos. Em seguida, serão apresentadas as razões que motivaram a sua realização, o objetivo que se pretende alcançar e uma revisão bibliográfica. Adicionalmente, as principais hipóteses, que suportaram o desenvolvimento deste trabalho, também serão apresentadas. Por fim, será apresentado o conteúdo do trabalho.

9.1.1. Enfoque do Trabalho

Atualmente, têm-se notado que poucos trabalhos sobre modelamento dos processos degradativos e falha de componentes têm sido desenvolvidos. Estes trabalhos são necessários, pois componentes de plástico têm sido bastante utilizados em aplicações industriais; pois, espera-se que estes componentes também apresentem a mesma confiabilidade dos componentes metálicos. Assim, baseado nestas considerações, este trabalho está focado no estudo e no modelamento matemático dos processos inelásticos e degradativos de componentes de plástico, devido a esforços mecânicos.

9.1.2. Motivações

Considera-se que as motivações deste trabalho estão baseadas no empiricismo em que o projeto de componentes de plástico é realizado e na ausência de ferramentas numéricas capazes de simular os processos degradativos de materiais plástico, quando submetidos a carregamentos mecânicos. Assim, este trabalho pode ser especialmente útil para auxiliar a análise estrutural de componentes industriais.

9.1.3. Objetivos do Trabalho

Baseado no enfoque e nas motivações apresentadas anteriormente, os principais objetivos deste trabalho são:

- Proposição de um modelo teórico e um sistema numérico baseado no Método de Elementos Finitos de Galerkin, o qual poderá ser utilizado para analisar componentes mecânicos fabricados com materiais plásticos, submetidos a carregamentos mecânicos monotônicos que promovam a falha dúctil do componente. O modelo matemático proposto é composto por um modelo viscoelastoplástico acoplado a uma teoria de dano não local. A utilização desta teoria não local é fundamental, a fim de reduzir a sensibilidade à malha, que ocorre quando teorias locais são empregadas.
- Descrever e realizar uma série de ensaios experimentais, os quais são necessários a fim de identificar os parâmetros materiais utilizados para descrever o modelo proposto.

9.1.4. Hipóteses e Considerações Básicas

O modelo matemático deste trabalho foi desenvolvido, assumindo que o comportamento inelástico e os processos de degradação de materiais plásticos podem ser também tratados dentro da estrutura básica padrão utilizadas para descrever o comportamento de materiais de engenharia. O desenvolvimento utilizado é o mesmo daquele geralmente aplicado para modelar metais e suas ligas com algumas modificações, que tornam possível descrever alguns fenômenos inerentes aos materiais plásticos. Neste sentido, a diferença mais notável origina-se da expressão da função de escoamento utilizada e da estratégia de travamento para a variável de dano. Além disso, algumas hipóteses também foram consideradas, que, basicamente, são:

- **Deformações Infinitesimais:** Assume que, em qualquer instante de tempo *t*, o tensor deformação total, $\boldsymbol{\varepsilon}$, é aditivamente decomposto em uma parte elástica (reversível), $\boldsymbol{\varepsilon}^{e}$, e uma inelástica (irreversível), $\boldsymbol{\varepsilon}^{vp}$, também conhecida como deformação viscoplástica, devido a sua dependência com o tempo.
- **Variáveis Termodinâmicas:** O formalismo termodinâmico clássico considerado neste trabalho está baseado na hipótese das variáveis de estado local, as quais requerem o conhecimento das variáveis de estado do material. Estas variáveis são decompostas em observáveis e internas.

- **Potencial de Energia Livre (Ψ):** O formalismo termodinâmico está também baseado na hipótese da existência de um potencial de energia livre, Ψ, de onde as equações de estado da viscoplasticidade são derivadas.
- **Potencial de Dissipação (φ):** Assume-se a existência de um potencial de dissipação definido como uma função escalar convexa e contínua e nula na origem das variáveis. Do potencial de dissipação, derivam-se as equações complementares, necessárias para descrever os processos dissipativos, aplicando o critério de dissipação normal.
- **Hipótese da Normalidade:** A hipótese da normalidade considera que o vetor de fluxo viscoplástico ($\dot{\boldsymbol{\varepsilon}}^{vp}$) é normal à superfície de escoamento. A hipótese da normalidade generalizada associada com os fenômenos dissipativos é também considerada, permitindo expressar a evolução das equações complementares das variáveis internas.
- **Isotropia e Homogeneidade:** Estritamente falando, materiais plásticos não são isotrópicos e nem totalmente homogêneos. Diferentes disposições das cadeias moleculares podem ser obtidas, o que torna o material não-homogêneo e com comportamento térmico e mecânico dependendo bastante da direção. Neste trabalho, a hipótese isotropia and homogeneidade serão considerados.
- **Sem Dependência da Temperatura:** Sabe-se que o comportamento mecânico de materiais plásticos é muito sensível a variações de temperatura. Por simplicidade, será considerado que o processo de deformação seja isotérmico. Já que o processo de deformação é dissipativo, esta consideração requer que o processo de carregamento mude vagarosamente ao longo do tempo.
- **Processo Quasiestatico:** Um processo quasiestático é aquele em que um sistema evolui sob uma seqüência de estados que são infinitamente próximas do equilíbrio. Na Mecânica dos Sólidos, um processo é considerado quasiestático quando a taxa de carregamento é tão lenta, que as acelerações produzidas podem ser negligenciadas.
- **Livre de Tensões Residuais:** Tensões residuais indesejáveis estão presentes em todos os componentes de plástico moldados e suas principais causas são: resfriamento desigual e empenamento diferencial. Segundo Lemaitre [1], um campo de tensão residual pode ser introduzido como uma condição inicial do problema. Neste trabalho, será considerado que os componentes estarão livres de tensões residuais.
- **Livre de Defeitos:** Defeitos, como linhas de solda e vazios, derivados do processo de fabricação, são comuns de acontecer. Neste caso, estes

defeitos podem ser considerados como um dano inicial para o problema, ou seja, $D(x,0) \neq 0$. Neste trabalho, será considerado que os componentes estarão livres de defeitos, ou seja, será considerado $D(x,0) = 0$ como condição inicial do problema, em que *D* é o dano.

- **Sem Efeito de Fechamento de Trinca:** Para a maioria dos materiais sob certas condições de carregamento, os micros defeitos podem fechar durante a compressão. O fenômeno de fechamento de trinca aumenta a área que efetivamente suporta as cargas de compressão e a resistência pode ser parcialmente ou totalmente recuperada neste momento [6]. Pelo fato deste trabalho tratará do modelamento da falha dúctil de materiais plásticos sob cargas estáticas, então, o efeito de fechamento de trinca não será considerado.
- **Dano Isotrópico:** Devido à natureza anisotrópica dos materiais plásticos, o processo de danificação dos componentes, quando submetidos a carregamentos mecânicos, não se desenvolve de forma isotrópica, ou seja, a resistência resultante, depois da nucleação de micro vazios e trincas, é dependente da direção [6]. Portanto, em muitos casos práticos, a anisotropia induzida pelo processo de danificação pode ser negligenciada, resultando em bons resultados quando comparados aos dados experimentais.

9.1.5. Revisão Bibliográfica

A fim de melhorar o entendimento da revisão bibliográfica, este item foi subdividido em três partes. Na primeira, foram discutidas as referências existentes relacionadas ao projeto de componentes. Na seqüência, foram apresentadas as principais referências, relacionadas ao modelamento viscoplástico de materiais plástico propostos na literatura. Por fim, foram introduzidos os modelos de dano mais relevantes na literatura, para descrever o processo de degradação de materiais plástico.

De forma similar com o que acontecem com os produtos industriais, os componentes de plástico também passam por uma seqüência de processos relacionados às etapas do seu desenvolvimento, que vai desde a sua concepção até seu lançamento no mercado [7]. Embora haja várias propostas de metodologias de projeto, cada uma com suas próprias peculiaridades, nota-se que todas têm elementos similares: **projeto informacional**, **conceitual**, **preliminar** e **detalhado**.

Atualmente, a maioria das referências sobre análises de tensões e deformações de componentes de plástico está relacionada à fadiga, pois, de acordo com Gotham [10], 70% de falhas prematura são atribuídas a este fenômeno. Em geral, estas referências têm sido baseadas em:

recomendações de projeto, práticas empíricas e proposição de modelos, baseado na abordagem da mecânica da fratura.

Qualquer que seja a abordagem utilizada, geralmente têm se negligenciado a fase de nucleação de trinca, a qual representa, aproximadamente, 95% da vida do componente [10]. Neste caso, é realizada uma avaliação de baixa confiabilidade sobre a vida do componente sob fadiga. Devido a sua importância, recomenda-se que a fase de nucleação de trinca não seja desprezada. Isto pode ser contornado através do desenvolvimento e proposição de modelos apropriados, que descrevam os processos de degradação do material.

Em muitos casos, a forma empírica com que o projeto de componentes de plástico é realizado conduz à produção de componentes superdimensionados com, consequentemente, alto custo e peso excessivo. É importante enfatizar que, atualmente, esta é uma prática bastante comum na empresas dos setores aeronáuticos e automobilísticos, embora estas empresas possuam poderosas ferramentas computacionais.

Em projetos de engenharia, é muito comum a utilização de coeficientes de segurança. Informalmente falando, Krishnamachari [13] define coeficientes de segurança como "coeficientes de ignorância" e eles são definidos proporcionalmente ao medo que se tem da influência das variáveis desconhecidas do problema. Estes coeficientes de segurança protegem o projeto do espaço existente entre a vida real e os modelos de analise idealizados, bem como dos vários fatores de projeto não quantificáveis [7].

De acordo com Krishnamachari [13] e Mascarenhas *et al.* [14], a escolha dos coeficientes de segurança devem estar baseados no comportamento do material, custos, condições de trabalho e do estado da arte de projeto, análise e processamento. Estes coeficientes podem ser diferentemente definidos para diferentes produtos, materiais, bem como modos de falha. Assim, baseado nestes aspectos Mascarenhas *et al.* [14] fornecem alguns coeficientes de segurança para o projeto de componentes de plástico.

Segundo Lemaitre and Chaboche [15], viscoelasticidade é a teoria responsável por descrever o comportamento inelástico de materiais sensíveis à taxa de deformação, como os plásticos. Na prática, esta teoria pode ser utilizada para calcular deformações permanentes and prever colapso plástico de estruturas, investigar estabilidade ou calcular forças necessárias para realizar operações de forjamento, como termoformagem e forjamento a vácuo. A fim de que esta teoria seja aplicada, é necessário definir uma função de escoamento, que será responsável por estabelecer o início do comportamento inelástico. Para materiais plásticos, que são bastante sensíveis a esforços de compressão, recomenda-se utilizar funções de escoamento que considerem a influência do tensor tensão

hidrostática. Neste sentido, Quinson *et al.* [16], Goldberg *et al.* [17] e Rottler e Robbins [18] propuseram funções de escoamento baseados na proposta de Drucker-Praguer, também conhecido como von Mises modificado.

A literatura sobre modelos elasto-viscoplástico é muito extensa. Estes trabalhos têm sido desenvolvidos sob as mais variadas considerações ou, em alguns casos, desenvolvido para um tipo específico de material, devido a sua grande demanda ou importância no meio industrial. A abordagem mais comum é baseada na termodinâmica dos meios contínuos com variáveis de estado, em que se postula a existência de um potencial termodinâmico, de onde se derivam as equações de estado. Outras teorias, como viscoplasticidade baseada na sobre tensão (VBO) e regiões cooperativamente rearranjadas (CRR) são os principais exemplos.

Os modelos desenvolvidos sob os preceitos da VBO não possuem critério de escoamento e condição de carregamento/descarregamento. Ela é composta de dois tensores variáveis de estado: os tensores de equilíbrio e o de tensão cinemática e dois escalares: tensões isotrópicas e de arrasto [20]. Esta abordagem foi inicialmente introduzida por Krempl and Ho [20] para modelar materiais metálicos e, mais tarde, foi modificado por Krempl and Ho [22] para melhorar a capacidade de modelamento da VBO para analisar materiais plásticos. Neste caso, esta teoria recebeu o nome específico de **viscoplasticidade baseada na sobre tensão para polímeros** (VBOP). Assim, sob as abordagens da VBOP, pode-se destacar: Krempl e Ho [22], Colak e Dusunceli [23] e Colak [24].

Na abordagem do CRR, a malha entre as cadeias poliméricas limitam a taxa com que os segmentos podem se mover sob a influência de uma carga externa [25]. A fim de ilustrar este mecanismo, Riesen and Schawe [26] o associam a um ônibus cheio. Durante a viagem, os passageiros estão próximos um do outro e não podem se mover. Se alguém tiver de sair do ônibus e esteja carregando uma bagagem grande, então alguns passageiros terão de se mover, ou seja, cooperativamente, para que outro consiga sair – provavelmente, alguém próximo à porta terá de sair do ônibus. Assim, os passageiros do ônibus experimentam uma série de rearranjos cooperativos. Sob esta teoria, pode-se destacar Frank e Brockman [25], Drozdov [27] e [28], Drozdov e Yuan [29] e Drozdov e Gupta [30].

Desenvolvido sob a abordagem da termodinâmica dos meios contínuos com variáveis de estado, Ghorbel [4] propôs um modelo viscoplástico, baseado em uma nova função de escoamento. Esta nova proposta é derivada do critério de Drucker-Praguer, em que se inclui o primeiro invariante do tensor tensão (I_1) e o segundo (J_2) e terceiro (J_3) invariantes do tensor tensão deviatórico. De acordo com este autor,

a introdução de J_3 significa que as forces necessárias para ativar mobilidades inter and intramoleculares são mais importantes em tensão e/ou compressão do que em cisalhamento, já que a tensão, necessária para ativar deformações plásticas, é menor em cisalhamento do que em tensão e/ou compressão.

A importância de incluir J_3 na função de escoamento é discutida por Lee e Ghosh [32]. Estes autores afirmam que se o material plástico estiver submetido a uma torção, então a deformação envolve cisalhamento puro e rotação. Portanto, três mecanismos básicos de deformação ocorrem: dilatação, caracterizado por I_1, cisalhamento puro, caracterizado por J_2, e rotação, caracterizado por J_3. Assim, os autores recomendam que estes três invariantes sejam introduzidos no modelo.
De acordo com Fatemi e Yang [34], as teorias de dano podem ser classificadas em seis grupos: dano linear, curva não-linear de dano, métodos de modificação da curve de vida, abordagens baseadas nas teorias de crescimento de trinca, modelos baseados na mecânica do dano e teorias baseadas na energia. No meio industrial, o modelo de dano mais utilizado é a regra linear de Palmgren-Miner.

O modelamento proposto neste trabalho baseou-se na abordagem da mecânica do dano. Segundo Lemaitre [1], esta abordagem estuda os mecanismos envolvidos na deterioração do material, por meio de variáveis mecânicas, quando o material estiver submetido a carregamentos externos. O desenvolvimento desta abordagem iniciou-se em 1958, quando Kachanov publicou o primeiro trabalho sobre falha de materiais metálicos sob fluência. Desde então, a mecânica do dano tem estado em pleno desenvolvimento e aplicado para descrever os processos de degradação de vários tipos de materiais [1].

Atualmente, a maioria dos modelos de dano propostos para materiais plásticos tem tido como objetivo, descrever os processos de degradação ou determinar a vida do componente quando o mesmo estiver submetido a carregamento de fadiga, devido a sua freqüente incidência. Neste sentido, pode-se destacar os trabalhos de Tang e Lee [37], Tang e Plumtree [38], Jie *et al.* [39], Vinogradov e Rassi [40] e Tang *et al.* [41].

Esta revisão bibliográfica revelou que a maioria dos modelos propostos na literatura não apresenta acoplamento entre viscoplasticidade e dano e entre os poucos modelos acoplados, nenhum dá atenção especial ao fenômeno, como o estiramento a frio (*cold-drawing*). Em muitos casos, isto pode conduzir a uma avaliação de baixa confiabilidade dos processos de degradação do material. Neste trabalho, através da análise do desempenho de componentes de plástico submetidos a carregamentos monotônicos até a sua falha dúctil, foi proposto um modelo viscoplástico acoplado a uma teoria de dano não-local. Como conseqüência, um

sistema com duas equações diferenciais acopladas foi estabelecido, em que uma destas equações é responsável por descrever a evolução dos processos de degradação do material, por meio da variável de dano, e a outra é a equação de conservação do momento linear. Na prática, este modelo pode ser utilizado para auxiliar a atividade de análise estrutural de componentes de plástico and, assim, fazer com que seja possível produzir componentes mais baratos e mais leves.

9.2. MATERIAIS PLÁSTICOS: UMA VISÃO GERAL – CAPÍTULO 2

O objetivo deste capítulo é fornecer a não especialistas em polímeros e plásticos uma visão geral sobre suas mais importantes peculiaridades. Neste sentido, este capítulo abordará suas classificações, principais propriedades, comportamento e particularidades sobre seus modos de falha.

9.2.1. Definição de Polímeros

Os materiais plásticos pertencem ao grupo de materiais orgânicos denominados de **polímeros**. Esta denominação origina-se da junção das palavras Gregas *πολυ* (*polu* - muitos) e *μέρος* (*meros* – partes) e é utilizada para se referir aos compostos químicos de alta massa molecular relativa. Em outras palavras, um polímero é uma macromolécula composta por milhares de *meros*, unidos por ligações covalentes formadas através de reações químicas conhecidas como **polimerização** [21, 49].

9.2.2. Classificação

Há diversas maneiras de se classificar os polímeros. A classificação conforme suas características mecânicas talvez sejam a mais importante e as mais comum. Sob este aspecto, os materiais poliméricos podem ser classificados, basicamente, em: **termoplásticos**, **termofixos** e **elastômeros**. Baseados na conformação ou morfologia das cadeias poliméricas, os materiais termoplásticos podem ser classificados como: **amorfos, cristalinos** ou **líquido cristalinos** [12, 50, 51].

Os **termoplásticos** são polímeros de cadeias lineares, ramificadas ou não, que podem ser fundidos diversas vezes, ou seja, podem ser recicladas várias vezes. Estruturalmente, as cadeias moleculares dos materiais termoplásticos podem ser imaginadas como uma série de linhas independentes e entrelaçadas entre si, semelhante a espaguete. Os materiais **termofixos** são polímeros que, quando sujeitos a aplicação de temperatura e pressão, amolecem e fluem adquirindo a forma do molde,

reagem quimicamente, num processo de cura, formando uma estrutura molecular na forma de uma complexa rede tridimensional insolúvel e infusível, ligada fisicamente entre si pelas ligações cruzadas.

Define-se um material termoplástico como **amorfo**, se suas cadeias moleculares estiverem dispostas de forma desordenada ou emaranhada. Quando as cadeias poliméricas de um material apresentam-se de forma ordenada, costuma-se designá-lo como sendo **cristalino**. Mas, sabe-se que o grau de cristalinidade de um material nunca alcança 100%. Desta forma, é mais adequado denominar o material de **semicristalino**. Os polímeros **líquidos cristalinos** caracterizam-se por possuírem uma estrutura molecular ordenada e rígida, disposta em forma de haste.

9.2.3. Principais Propriedades dos Materiais Plásticos

As propriedades mecânicas de um material são caracterizadas pela forma com que estes materiais respondem aos esforços mecânicos aplicados, que podem ser tanto tensões ou deformações. Basicamente, a natureza desta resposta depende da estrutura química, temperatura, tempo de aplicação do esforço e as condições de processamento [49].

A estrutura molecular de um polímero proporciona aos materiais plásticos um comportamento viscoso, como os líquidos, superposto com um comportamento elástico, como os sólidos Hookeanos. Este fenômeno é denominado de **viscoelasticidade** e ocorre tanto nos termoplásticos quanto nos termofixos. Os elastômeros, em particular, apresentam um outro fenômeno mais peculiar, denominado de **elasticidade da borracha**, a qual envolve o desenvolvimento de grandes deformações [49].

Quando uma carga constante é aplicada a um componente de plástico, o mesmo apresenta uma deformação inicial semelhante a um sólido Hookeano, ou seja, o componente deforma-se elasticamente. Após esta deformação inicial, o componente continua a deformar-se e rompe-se após um determinado tempo. A deformação que ocorre após a parte elástica e a subseqüente falha são denominadas de **fluência** e **falha por fluência**, respectivamente [56]. Além da fluência, outro fenômeno conseqüência da viscoelasticidade é a **relaxação de tensão**, que é definido como um gradual decréscimo na tensão quando um corpo de prova é mantido sob uma deformação constante.

Comparado aos metais, a resposta dos materiais plásticos a estímulos termomecânicos é mais complexa. Devido a sua natureza viscoelástica, o diagrama tensão-deformação dos materiais plásticos não possui verdadeiramente um limite de proporcionalidade e nem se comportam de forma linear. Seu formato é fortemente influenciado pela taxa com que a tensão é aplicada e pela temperatura [77]. Um material dúctil é caracterizado por apresentar uma grande deformação antes da

falha, a qual ocorre devido ao movimento relativo entre suas cadeias moleculares. Por outro lado, um material frágil caracteriza-se por apresentar uma baixa deformação antes da falha, que ocorre devido à quebra das ligações moleculares.

Em geral, os materiais plásticos apresentam, pelo menos, três temperaturas de transição, que caracterizam a mudança de comportamento do material, são elas: temperatura de transição vítrea, temperatura de fusão cristalina e temperatura de cristalização. Além destas temperaturas, outras propriedades térmicas mais importantes são: coeficiente de dilação térmica, condutividade térmica, calor específico e temperatura de amolecimento *Vicat*.

A **temperatura de transição vítrea** (T_g) é definida como o valor médio da faixa de temperatura que, durante o aquecimento de um material plástico, de uma temperatura muito baixa para valores altos, permite que as cadeias poliméricas da fase amorfa adquiram mobilidade, ou seja, possibilidade de mudança de conformação. A **temperatura de fusão cristalina** (T_m) é definida como o valor médio da faixa de temperatura, no qual durante o aquecimento do material as regiões cristalinas desaparecem com a fusão dos cristalitos. Neste ponto, a energia do sistema atinge o nível necessário para superar as forças intermoleculares secundárias entre as cadeias da fase cristalina destruindo a estrutura regular de empacotamento, mudando o comportamento do material de borrachoso para o estado viscoso. Por fim, tem-se a **temperatura de cristalização** (T_c), que é definida como a temperatura na qual se tem a máxima taxa de conversão de cristalização no material.

9.2.4. Comportamento Termo-Mecânico dos Materiais Plásticos

Comparado à maioria dos metais, as propriedades dos materiais plásticos são muito sensíveis a variações de temperatura. Um mesmo material pode ter desempenhos totalmente distintos sob faixas de temperatura diferentes. Segundo Malloy [12], materiais plásticos com boa estabilidade térmica são aqueles que possuem baixo coeficiente de dilatação térmica e bom desempenho mecânico ao longo da faixa de temperatura associada com a aplicação, ou seja, são materiais capazes de manter suas tolerâncias dimensionais quando solicitados termicamente e apresentam pouca variação nas suas propriedades mecânicas.

Este é um assunto muito importante e que exige bastante cuidado e atenção dos projetistas, principalmente no momento de selecionar o material para uma aplicação que possa envolver mudança de propriedades devido à variação de temperatura. Uma das grandes conseqüências atribuídas a este comportamento foi a tragédia do ônibus espacial

Challenger em 1986, que explodiu 73 segundos após seu lançamento devido à falha de um anel de vedação do sistema de combustível [21]. Ao alcançar uma elevada altitude, onde a temperatura ambiente estava abaixo da T_g do material, este mudou de comportamento tornando-se frágil. Os esforços a que o componente estava submetido foi suficiente para causar sua falha e, conseqüentemente, a tragédia.

9.2.5. Fatores que Afetam a Resistência de Peças Plásticas

Além de características inerentes ao material utilizado, outras influências externas, quer seja de interferência humana ou ambiental, são capazes de alterar a integridade funcional de um componente de plástico, podem comprometer sua resistência e, até mesmo, sua durabilidade. Dentre estas influências externas destacam-se: a influência do processamento, a utilização de material reciclado, a absorção de água (higroscopia), a influência da exposição a ambientes quimicamente reativos e à radiação solar.

Basicamente, o processamento pode afetar a resistência do componente através de quatro mecanismos: pela formação de vazios, linhas de solda, surgimento de tensões residuais e pela orientação molecular [12].

O material reaproveitado interfere nas propriedades mecânicas do material virgem, porque aquele material, por já ter sido utilizado antes, apresenta um nível considerável de degradação térmica proveniente do processo de moldagem. Ao realizar a mistura, o material virgem adquire um desgaste inicial proveniente do material misturado.

De acordo com Tres [60], a absorção de água refere-se ao aumento em porcentagem de peso do material devido à absorção de umidade. Os materiais plásticos tanto podem ser absorventes (higroscópicos) quanto não absorvente. A água absorvida pelo material polimérico pode degradar quimicamente um material com ou sem preenchimento reduzindo o seu peso molecular através da hidrólise, resultando em perdas principalmente nas propriedades físicas e elétricas.

Em muitas aplicações de materiais plásticos, necessita-se que o material suporte a exposição da radiação solar quando utilizado em ambientes abertos, pois a radiação constitui-se no elemento ambiental mais prejudicial à integridade estrutural dos componentes de plástico. A maioria das freqüências naturais das ligações químicas existentes nas cadeias poliméricas corresponde às freqüências que ocorrem na faixa ultravioleta da luz solar. A degradação de um material plástico também pode ser acelerada por outros elementos, como água, partículas transportadas pelo vento e elementos produzidos pelo homem, como poluentes [62].

9.2.6. Mecanismos de Falha Dúctil

Basicamente, os materiais plásticos podem falhar por dois modos: **fibrilamento** e **bandas de cisalhamento**. Diferentemente dos materiais metálicos, os plásticos se deformam viscoelasticamente quando submetidos a um carregamento. Neste caso, uma fração da energia mecânica produzida por cargas externas é utilizada para desenvolver processos moleculares irreversíveis, tais como deformações microscópicas do tipo fibrilamento, bandas de cisalhamento, vazios e micro trincas. A outra parte da energia mecânica pode ser convertida em calor dentro do material [72]. O crescimento gradual de calor pode ser suficiente para causar a perda de resistência e rigidez do componente [71]. Este comportamento é agravado pela baixa condutividade térmica dos materiais plásticos.

A falha mecânica de componentes de plástico é caracterizada pela formação de uma trinca e sua subseqüente propagação. Embora, poucas informações detalhadas estejam disponíveis, parece provável que alguma combinação de fibrilamento e/ou bandas de cisalhamento precedam a fase de nucleação da trinca e propagação durante o processo de falha [70]. Morfologicamente falando, o fibrilamento é um defeito plano muito parecido a uma trinca. Mas, aquele se diferencia de uma trinca, porque ele possui uma rede de vazios entre umas pontes de material altamente estirado que ligam as faces das superfícies fibriladas [10, 73, 74].

O fibrilamento inicia-se em regiões do componente sob alta triaxialidade ou em regiões de escoamento muito localizado, como inclusões e defeitos superficiais, que conduzem à formação de micro vazios. Depois de iniciar o fibrilamento, os vazios aumentam em tamanho e se alongam na direção da tensão de tração máxima. O volume de material entre os vazios também sofrem uma gradual elongação para formar fibras finas [10, 75]. Conforme as faces do fibrilamento se separam, as fibras aumentam de comprimento, enquanto seus diâmetros contraem. Quando a deformação longitudinal na fibra excede a máxima extensibilidade da rede molecular, eles rompem e formam a trinca [76].

Outro tipo de modo de falha comum aos componentes de plástico é a **banda de cisalhamento**. Neste modo de falha, as deformações irreversíveis evoluem ao longo do plano de tensões de cisalhamento máximas, ou seja, 45° em relação à direção da máxima tensão principal.

Pelo fato de os materiais plásticos se comportarem viscoelasticamente, há uma possibilidade de haver uma grande quantidade de atrito interno gerado dentro do material durante a deformação mecânica. Este mecanismo envolve a acumulação de energia histerética gerada durante cada ciclo de carga. Pelo fato de esta energia ser dissipada especialmente na forma de calor, o material experimenta um

aumento de temperatura. Como conseqüência, os componentes de plástico podem falhar, devido ao aquecimento excessivo. Neste caso, costuma-se definir **falha** ou **instabilidade térmica**. Este tipo de falha ocorre quando a taxa de calor transferido para a vizinhança é menor do que a taxa de calor gerado pelos sucessivos ciclos de carregamento [72, 77]. Neste caso, a temperatura do material aumenta até que suas propriedades decresçam até o ponto em que o componente não consiga mais suportar os carregamentos. Por outro lado, se o calor transferido for igual à taxa de calor gerado, então a temperatura se estabiliza e o componente não falhará. Neste caso, costuma-se dizer que houve uma **estabilidade térmica** [72].

9.3. LEIS CONSTITUTIVAS PARA MEIOS DANIFICADOS – CAPÍTULO 3

O objetivo deste capítulo é apresentar os conceitos básicos sobre a teoria utilizada para modelar os fenômenos de degradação e deformação de materiais plásticos. O desenvolvimento desta teoria foi baseada na abordagem proposta por Fremond and Nedjar [2], no princípio das potências virtuais, idealizado por d'Alembert (1750), que fornecerá uma nova equação, descrevendo a evolução da variável de dano, β, e na abordagem da termodinâmica dos meios contínuos, a fim de introduzir as variáveis relacionadas ao fen6omeno em estudo.

Considere o escalar β definido como **variável de coesão** com valor 1 quando o material está sem dano e valor 0 quando estiver completamente danificado. Esta variável está relacionada com os ligamentos entre pontos materiais e pode ser interpretada como uma medida do estado de coesão local do material. Quando $\beta = 1$, todas as ligações estão preservadas. Mas, se $\beta = 0$, uma ruptura local é considerada, já que todas as ligações entre pontos materiais foram quebradas [2].

9.3.1. Princípio das Potências Virtuais

De acordo com Germain [78], o princípio das potências virtuais consiste em descrever os possíveis movimentos de um sistema mecânico, por meio de um espaço virtual, denominado **espaço dos movimentos virtuais**. Este princípio é baseado em dois axiomas: invariância das cargas internas (objetividade) e equilíbrio. Desta forma, baseado no princípio dos trabalhos virtuais, obtêm-se o seguinte sistema de equações diferenciais:

$$div\left[\boldsymbol{\sigma}(\vec{x},t)\right] + \rho\vec{b}(\vec{x},t) = \rho\frac{d^2\vec{u}(\vec{x},t)}{dt^2} \quad \text{em} \quad \Omega \tag{9.1}$$

e

$$div(\vec{H}) - F = \rho\ddot{\beta}(\vec{x},t) \quad \text{em} \quad \Omega. \tag{9.2}$$

A Equação (9.1) está submetida às condições de contorno

$$\begin{cases} \boldsymbol{\sigma}(\vec{x},t)\vec{n} = \vec{t}(\vec{x},t) \quad \text{em} \quad (\vec{x},t) \in \Gamma_t \\ \vec{u}(\vec{x},t) = \overline{u} \quad \text{em} \quad (\vec{x},t) \in \Gamma_u \end{cases} \tag{9.3}$$

e às condições iniciais

$$\begin{cases} \dfrac{d\vec{u}(\vec{x},0)}{dt} = \vec{v}_o(\vec{x}) \quad \text{em} \quad \Omega \\ \vec{u}(\vec{x},0) = \vec{u}_o(\vec{x}) \quad \text{em} \quad \Omega, \end{cases} \tag{9.4}$$

e

$$\begin{cases} div(\boldsymbol{\sigma}_o) = 0 \quad \text{em} \quad \Omega \\ \boldsymbol{\sigma}_o\vec{n} = 0 \quad \text{em} \quad \partial\Omega, \end{cases} \tag{9.5}$$

em que, $\boldsymbol{\sigma}_o$ representa o tensor tensão residual inicial. Por sua vez, a Equação (9.2) está submetida às seguintes condições de contorno e iniciais:

$$\vec{\nabla}\beta \cdot \vec{n} = 0 \quad \text{em} \quad \partial\Omega \quad \text{e} \quad \beta(\vec{x},0) = 0 \quad \text{em} \quad \Omega. \tag{9.6}$$

9.3.2. Leis da Termodinâmica para Meios Danificados

Formalmente, a **primeira lei da termodinâmica** pode ser postulada como: "a taxa de variação da energia total do sistema (energia cinética e interna) é igual à potência dos esforços externos, aplicado no corpo $\mathcal{B}$, adicionado pelo fluxo de energia térmica que o sistema recebe ou dissipa". Matematicamente, esta lei é representada por

$$\rho\dot{e} = \boldsymbol{\sigma} \cdot \dot{\boldsymbol{\varepsilon}} + \rho\overline{r} + F\dot{\beta} + \vec{H} \cdot \vec{\nabla}\dot{\beta} - div(\vec{q}). \tag{9.7}$$

A segunda lei da termodinâmica pode ser escrita como

$$\boldsymbol{\sigma} \cdot \dot{\boldsymbol{\varepsilon}} + F\dot{\beta} + \vec{H} \cdot \vec{\nabla}\dot{\beta} - \rho\left(\frac{d\Psi}{dt} + s\frac{dT}{dt}\right) - \frac{\vec{q} \cdot \vec{\nabla} T}{T} \geq 0, \tag{9.8}$$

que é denominada de inequação de Clausius-Duhem. Esta expressão demonstra que um processo termodinâmico é admissível se, e somente se, a dissipação total do sistema é positiva ou igual à zero.

O valor da variável (β) está dentro da faixa [0;1], com β visto como a proporção volumétrica de micro vazios ou o quociente do módulo elástico do material danificado pelo módulo do material não danificado. Assim, $0 \leq \beta \leq 1$.

O potencial de energia livre, $\Psi(\circ, \beta, \vec{\nabla}\beta)$, é apenas definido para processos reais, ou seja, para processos tais que $\beta \in \mathcal{K}$, em que $\mathcal{K} = \{(\circ, \beta, \vec{\nabla}\beta) \mid 0 \leq \beta \leq 1\}$. Portanto, pode-se também estender Ψ para processos onde $\beta \notin \mathcal{K}$ assumindo que $\Psi(\circ, \beta, \vec{\nabla}\beta) = +\infty$ para $\beta \notin \mathcal{K}$. Além disso, assume-se Ψ ser localmente subdiferenciável em $\mathcal{K}$, a fim de que $\dot{\Psi}$ exista. Portanto, assume-se a existência de um potencial de energia livre dado por

$$\Psi(\circ, \beta, \vec{\nabla}\beta) = \Psi_1(\circ, \beta, \vec{\nabla}\beta) + I_{\boldsymbol{K}}(\beta), \tag{9.9}$$

em que, ($\circ$) representa um conjunto de variáveis internas, que serão definidas posteriormente, $\Psi_1(\circ, \beta, \vec{\nabla}\beta)$ é um potencial suave e $I_{\boldsymbol{K}}(\beta)$ é a função indicadora de $\mathcal{K}$ dado por

$$I_{\boldsymbol{K}}(\beta) = \begin{cases} 0, & \text{se} \quad \beta \in \mathcal{K} \\ +\infty, & \text{se} \quad \beta \notin \mathcal{K}. \end{cases} \tag{9.10}$$

Assim, a energia livre possui um valor físico para qualquer valor físico de β. Por outro lado, a energia livre é igual a $+\infty$ para qualquer valor fisicamente impossível de β, ou seja, para qualquer $\beta \notin \mathcal{K}$.

A determinação das derivadas da energia livre na evolução atual, ou seja, numa evolução tal que $0 \leq \beta \leq 1$ para qualquer ponto $x \in \Omega$ e qualquer tempo *t*, permite definir as seguintes forças reversíveis e não-dissipativas relacionadas a β e $\vec{\nabla}\beta$:

$$F^r = \rho \frac{\partial \Psi_1}{\partial \beta} \tag{9.11}$$

e

$$\vec{H}^r = \rho \frac{\partial \Psi_1}{\partial \vec{\nabla} \beta}. \tag{9.12}$$

A restrição interna é levada em consideração pela introdução de uma força de reação, F^{reac}, que é definida assumindo que há uma função, F^{reac}, tal que

$$F^{reac}(\vec{x},t) \in \rho \partial^{loc} I_K[\beta(\vec{x},t)], \tag{9.13}$$

em que, $\partial^{loc} I_K(\beta)$ é o subgradiente de $I_K(\beta)$, dado por

$$\begin{cases} \partial^{loc} I_K(\beta) = 0 \quad \text{se} \quad 0 < \beta(\vec{x},t) < 1 \\ \partial^{loc} I_K(0) = \mathcal{R}^- \\ \partial^{loc} I_K(1) = \mathcal{R}^+ \\ \partial^{loc} I_K(\beta) = \varnothing \quad \text{se} \quad \beta(\vec{x},t) \notin \mathcal{K}. \end{cases} \tag{9.14}$$

9.3.3. Método do Estado Local

O axioma do método do estado local postula que o estado termodinâmico de um meio material pode ser definido pelo conhecimento dos valores de certo número de variáveis definidas em um instante de tempo *t* fixo [15]. Esta hipótese implica que a evolução de um meio contínuo pode ser considerada como a sucessão de vários estados de equilíbrio ou termoestáticos. Estas variáveis são denominadas **variáveis de estado local**. Segundo Lemaitre [1] e Lemaitre e Chaboche [15], as variáveis de estado local são classificadas em variáveis observáveis e variáveis internas.

Lemaitre and Chaboche [15] consideram que as únicas **variáveis observáveis** que ocorrem nos fenômenos da elasticidade, plasticidade, viscoplasticidade, dano e ruptura dos materiais são a temperatura (*T*) e a deformação total ($\boldsymbol{\varepsilon}$). Os fenômenos elásticos ou reversíveis dependem unicamente destas variáveis, em qualquer instante de tempo *t*.

Lubliner [81] define um corpo elástico com sendo aquele em que a deformação em qualquer ponto é completamente determinada pela tensão e temperatura que atuam naquele ponto. Então, torna-se obvio perceber que um corpo inelástico, caracterizado por apresentar deformações irreversíveis, quando submetidos a um carregamento, é definido como aquele em que há algo mais que determina o nível de deformação de um ponto do corpo, além da tensão e temperatura atuantes neste ponto. Este "algo mais" pode ser imaginado como sendo, por exemplo, o histórico da evolução da tensão e da temperatura no referido ponto. Uma forma alternativa de representar este "algo mais" é através de um vetor de variáveis, $(V_1, V_2, \dots, V_k)$, de tal forma que a deformação no ponto seja função destas variáveis, bem como da tensão e da temperatura. Estas variáveis são denominadas de **variáveis internas** [81]. Este vetor será representado aqui por $\vec{V}$ e, dependendo do fenômeno, seus termos poderão ser de natureza escalar, vetorial ou tensorial.

Assume-se que o tensor deformação total, $\boldsymbol{\varepsilon}$, é aditivamente decomposto em uma parcela elástica, $\boldsymbol{\varepsilon}^e$, e uma inelástica, $\boldsymbol{\varepsilon}^{vp}$, denominada deformação viscoplástica, ou seja,

$$\boldsymbol{\varepsilon} = \boldsymbol{\varepsilon}^e + \boldsymbol{\varepsilon}^{vp}. \tag{9.15}$$

Para este trabalho, adotou-se o **potencial de energia livre de Helmholtz** (Ψ), que é definido como um potencial termodinâmico que mede o trabalho útil obtido de um sistema termodinâmico fechado a uma temperatura constante [15]. Assim, potencial de energia livre de Helmholtz pode ser considerado depender das seguintes variáveis de estado não-danificáveis $(\circ) = (\boldsymbol{\varepsilon}^e, r, \boldsymbol{\vartheta}, T, \vec{V})$. Portanto, assume-se que

$$\Psi = \Psi^{vp}(\boldsymbol{\varepsilon}^e, r, \boldsymbol{\vartheta}, T, \beta, \vec{\nabla}\beta) + I_K(\beta), \tag{9.16}$$

em que, r e $\boldsymbol{\vartheta}$ são, respectivamente, a deformação viscoplástica acumulada e o tensor *back strain* para considerar os processos de encruamento isotrópico e cinemático, respectivamente [1].

Apartir da desigualdade de Clausius-Duhem (expressão (9.8)) e da expressão (9.15), obtêm-se as seguintes equações de estado:

$$\boldsymbol{\sigma} = \rho \frac{\partial \Psi^{vp}}{\partial \boldsymbol{\varepsilon}^e}, \tag{9.17}$$

$$R = \rho \frac{\partial \Psi^{vp}}{\partial r}, \tag{9.18}$$

$$F^{r} = \rho \frac{\partial \Psi^{vp}}{\partial \beta}, \tag{9.19}$$

$$\vec{H}^{r} = \rho \frac{\partial \Psi^{vp}}{\partial \vec{\nabla} \beta}, \tag{9.20}$$

$$\boldsymbol{\chi} = \rho \frac{\partial \Psi^{vp}}{\partial \boldsymbol{\vartheta}} \tag{9.21}$$

e

$$s = -\frac{\partial \Psi^{vp}}{\partial T}. \tag{9.22}$$

Nestas equações, R e $\boldsymbol{\chi}$ são, respectivamente, a variável de encruamento isotrópico e o tensor *back stress* que representa o encruamento cinemático [1]. Considerando

$$F = F^{r} + F^{reac} + F^{i} \tag{9.23}$$

e

$$\vec{H} = \vec{H}^{r} + \vec{H}^{i} \tag{9.24}$$

em que, $F^{reac} \in \rho \partial^{loc} I_{\mathbf{K}}(\beta)$, não havendo dissipação com relação ao gradiente da taxa de dano, $\vec{\nabla}\dot{\beta}$ e $\vec{H}^{i} = 0$, obtêm-se

$$\Delta = \boldsymbol{\sigma} \cdot \dot{\boldsymbol{\varepsilon}}^{vp} - (R\,\dot{r} + \boldsymbol{\chi} \cdot \dot{\boldsymbol{\vartheta}}) + F^{i}\dot{\beta} \geq 0. \tag{9.25}$$

A fim de obter as equações de evolução do conjunto de variáveis internas de um sistema termodinâmico, defini-se a existência de uma função escalar $(\varphi(\bullet))$, denominado de **potencial de dissipação** e seu

dual $(\varphi^*(\bullet))$, que são funções escalares contínuas e positivas, convexas com relação às variáveis de fluxo e nula na origem dos espaços destas variáveis. Adicionalmente, postula-se o desacoplamento entre as dissipações viscoelastoplástica, térmica e de dano, de forma que

$$\varphi^*(\bullet) = \varphi^*_{vp}(\boldsymbol{\sigma}, R, \boldsymbol{\chi}; \circ) + \varphi^*_T(\vec{\nabla} T; T) + \varphi^*_D(F^i; \circ), \tag{9.26}$$

em que, φ^*_{vp} e φ^*_T são funções diferenciáveis que descrevem, respectivamente, as dissipações viscoelastoplástica e térmica e φ^*_D é uma função não diferenciável que descreve a dissipação do dano. Assim, baseado na hipótese da normalidade, pode-se obter as seguintes equações de evolução:

$$\dot{\boldsymbol{\varepsilon}}^{vp} = \dot{\lambda} \frac{\partial \varphi^*_{vp}}{\partial \boldsymbol{\sigma}}, \tag{9.27}$$

$$-\dot{r} = \dot{\lambda} \frac{\partial \varphi^*_{vp}}{\partial R}, \tag{9.28}$$

$$-\dot{\boldsymbol{\vartheta}} = \dot{\lambda} \frac{\partial \varphi^*_{vp}}{\partial \boldsymbol{\chi}}, \tag{9.29}$$

$$\dot{\beta} = \dot{\lambda} \frac{\partial \varphi^*_D}{\partial F^i} \tag{9.30}$$

e

$$-\frac{\vec{q}}{T} = \frac{\partial \varphi^*_T}{\partial \vec{\nabla} T}. \tag{9.31}$$

O parâmetro $\dot{\lambda}$ é denominado de multiplicador plástico. Equações de evolução típicas para o multiplicador viscoplástico, dados respectivamente por Riande *et al.* [5], Norton [82] e Benallal [83], são

$$\dot{\lambda} = \exp\left(\frac{f(\boldsymbol{\sigma}, R, \boldsymbol{\chi}; \circ)}{K_r} \right), \tag{9.32}$$

$$\dot{\lambda} = \left(\frac{f(\boldsymbol{\sigma}, R, \boldsymbol{\chi}; \circ)}{K_n} \right)^N \tag{9.33}$$

e

$$\dot{\lambda} = \ln\left[\left(1 - \frac{f(\boldsymbol{\sigma}, R, \boldsymbol{\chi}; \circ)}{K_\infty} \right)^{-M} \right], \tag{9.34}$$

em que, K_r, K_n, K_∞, N e M são parâmetros materiais, que devem ser obtidas experimentalmente, e $f(\bullet)$ é a função de escoamento.

9.4. MODELO DE DANO PARA MATERIAIS PLÁSTICOS – CAPÍTULO 4

A fim de desenvolver o modelo proposto de elasto-viscoplasticidade acoplado ao dano, inicialmente, foi definido o potencial de energia livre. Seguindo as idéias de Lemaitre [1], Fremond e Nedjar [2] e Mascarenhas *et al.* [84], assume-se que o potencial de energia livre viscoplástico, $\Psi^{vp}(\boldsymbol{\varepsilon}^{\mathrm{e}}, r, \beta, \vec{\nabla}\beta)$, é dado por

$$\rho\Psi^{vp}(\boldsymbol{\varepsilon}^{\mathrm{e}}, r, \beta, \vec{\nabla}\beta) = \beta\frac{1}{2}\mathbb{D}\boldsymbol{\varepsilon}^{\mathrm{e}} \cdot \boldsymbol{\varepsilon}^{\mathrm{e}} + \frac{k}{2}\vec{\nabla}\beta \cdot \vec{\nabla}\beta + \int_0^r h(r)dr. \tag{9.35}$$

Em seguida, definiu-se a função de escoamento baseado nas propostas apresentadas por Riande *et al.* [5], Quinson *et al.* [16], Goldberg *et al.* [17], Rottler e Robbins [18] e outros. Neste trabalho, definiu-se a seguinte função de escoamento:

$$f\left(\boldsymbol{\sigma}, R, \beta; \circ\right) = (q + \mu\ p) - \left(1 + \frac{\mu}{3}\right)(\sigma_{yo} + R) \tag{9.36}$$

em que,

$$p = \tilde{\sigma}_H \,, \tag{9.37}$$

$$q = \left(\frac{3}{2} \tilde{\boldsymbol{\sigma}}^D \cdot \tilde{\boldsymbol{\sigma}}^D \right)^{\frac{1}{2}} \tag{9.38}$$

de forma que, a tensão efetiva, $\tilde{\boldsymbol{\sigma}}$, é dada por

$$\tilde{\boldsymbol{\sigma}} = \frac{\boldsymbol{\sigma}}{\beta}. \tag{9.39}$$

Para o potencial de dissipação viscoplástico, assumiu-se uma regra de fluxo associativo, ou seja, o potencial viscoplástico é dado por

$$\varphi_{vp}^*(\boldsymbol{\sigma}, R, \beta; \circ) = (q + \mu\ p) - \left(1 + \frac{\mu}{3}\right)(\sigma_{yo} + R). \tag{9.40}$$

Por sua vez, baseado na proposição de Lemaitre [1], defini-se o potencial de dissipação do dano como

$$\varphi_D^*\left(F^i; \circ\right) = \frac{1}{2} \beta S_o \left(\frac{F^i}{\beta S_o} \right)^2 . \tag{9.41}$$

A Tabela 9.1 ilustra o conjunto de equações que compõe o modelo teórico elasto-viscoplástico acoplado ao dano sem acoplamento termomecânico. A discretização destas equações será resumida no Capítulo 5.

Tabela 9.1: Conjunto de equações que compõe o modelo elasto-viscoplástico acoplado ao dano.

- **Equação da Conservação de Movimento:**

  $div\left[\boldsymbol{\sigma}(\vec{x}, t)\right] + \rho \vec{b}(\vec{x}, t) = 0$

- **Resposta Tensão-Deformação Elástica:**

  $\boldsymbol{\sigma} = (1 - D)\mathbb{D}\boldsymbol{\varepsilon}^{\mathrm{e}} \quad \text{com} \quad \boldsymbol{\varepsilon} = \boldsymbol{\varepsilon}^e + \boldsymbol{\varepsilon}^{vp}$

- **Leis de Fluxo Viscoplástico e de Encruamento:**

$$\dot{\boldsymbol{\varepsilon}}^{vp} = \frac{\dot{\lambda}}{(1-D)}\left[\frac{3}{2(1-D)}\frac{\boldsymbol{\sigma}^{D}}{\sigma_{eq}^{vm}} + \frac{\mu}{3}\boldsymbol{I}\right] \quad \text{e} \quad R = h(r), \text{ em que}$$

$$\dot{e}_{ef}^{vp} = -M \ln\left(1 - \frac{f(\boldsymbol{\sigma}, R, D; \circ)}{K_{\infty}}\right)$$

com $\dot{r} = \left(1 + \frac{\mu}{3}\right)\dot{\lambda}$ e $\dot{\lambda} = (1-D)\dot{e}_{ef}^{vp}$

- **Condição de Escoamento:**

$$f\left(\boldsymbol{\sigma}, R\right) = \frac{1}{(1-D)}\left[\left(\frac{3}{2}\boldsymbol{\sigma}^{D}\cdot\boldsymbol{\sigma}^{D}\right)^{1/2} + \mu\sigma_{H}\right] - \left(1 + \frac{\mu}{3}\right)(\sigma_{yo} + R)$$

- **Equação de Evolução do Dano:**

$$\dot{D} = \begin{cases} \dot{\lambda}\left[\dfrac{F_D^i}{(1-D)S_{\bar{\eta}_s}}\right]\bar{H}(e_{ef}^{vp} - e_{ef_D}^{vp})H(F_D^i), & \text{se} \quad F_D^i \le 0 \\ 0 \qquad\qquad\qquad\qquad\qquad\qquad\qquad\qquad , & \text{se} \quad F_D^i > 0 \end{cases}$$

com

$$F_D^i = \cancel{k} div(\vec{\nabla} D) + (F_D^r + F_D^{reac}),$$

$$F_D^r = \frac{(\sigma_{eq}^{vm})^2}{2E(1-D)^2}\left[\frac{2}{3}(1+\nu) + 3(1-2\nu)\left(\frac{\sigma_H}{\sigma_{eq}^{vm}}\right)^2\right],$$

$$F_D^{reac} = -\frac{\bar{\eta}_a}{(1-D)^2} + \frac{1}{\bar{\eta}_b}\langle(-D)\rangle^{+}$$

e

$$S_{\bar{\eta}_s}(e_{ef}^{vp}) = S_o + \frac{1}{2\bar{\eta}_s}\left[\left\langle \left(e_{ef}^{vp} - e_{ef_{th}}^{vp}\right)\right\rangle^{+}\right]^2,$$

em que,

$$H(F_D^i) = \begin{cases} 1, \text{ se } F_D^i \le 0 \\ 0, \text{ se } F_D^i > 0 \end{cases} \quad \text{e} \quad \langle(-D)\rangle^{+} = \begin{cases} -D, \text{ se } D \le 0 \\ 0, \text{ se } D > 0. \end{cases}$$

9.5. SOLUÇÃO NUMÉRICA DO MODELO – CAPÍTULO 5

A solução do conjunto de equações ilustrada na Tabela 9.1 foi iniciada com a solução do problema local por meio da técnica de implementação *operator split*. Os três passos desta estratégia são: **predição elástica**, **verificação da condição de escoamento** e **corretor elasto-viscoplástico com dano acoplado**.

Na etapa de predição elástica, o problema é considerado ser puramente elástico entre t_n e t_{n+1}, então o problema de predição elástica pode ser declarada como: dado a história de deformação e dano $\{\boldsymbol{\varepsilon}(t), D(t)\} \in [t_n, t_{n+1}]$, encontre $\boldsymbol{\varepsilon}_{n+1}^{e\ trial}$ e $\vec{V}_{n+1}^{trial}$, em que $\vec{V}_{n+1}^{trial} = (\boldsymbol{\varepsilon}_{n+1}^{vp\ trial}, r_{n+1}^{trial}, e_{ef_{n+1}}^{vp\ trial})$, de forma que

$$\dot{\boldsymbol{\varepsilon}}^{e\ trial} = 0 \tag{9.42}$$

e

$$\vec{V}^{trial}(t_n) = \vec{V}_n. \tag{9.43}$$

Assim, na etapa de predição elástica, assume-se que a resposta do material no incremento de t_n a t_{n+1} é elástico.

Assim que o estado de predição elástica esteja determinado, deve-se verificar a consideração de um incremento elástico, no intervalo $[t_n, t_{n+1}]$, de fato ocorreu. Caso contrário, um procedimento de projeção deve ser utilizado a fim de determinar o estado viscoplástico. Assim, se $f(\bullet) < 0$, então o estado no tempo t_{n+1} é de fato elástico. Neste caso, aplica-se

$$\boldsymbol{\sigma}_{H_{n+1}} = \boldsymbol{\sigma}_{H_{n+1}}^{trial}, \quad \boldsymbol{\sigma}_{n+1}^{D} = \boldsymbol{\sigma}_{n+1}^{D\ trial}, \quad \boldsymbol{\varepsilon}_{n+1}^{vp} = \boldsymbol{\varepsilon}_{n}^{vp}, \quad e_{ef_{n+1}}^{vp} = e_{ef_n}^{vp} \quad \text{and} \quad r_{n+1} = r_n,$$

em que,

$$\boldsymbol{\sigma}_{n+1} = \boldsymbol{\sigma}^{D}_{n+1} + \sigma_{H_{n+1}} \boldsymbol{I}. \tag{9.44}$$

Caso contrário, ou seja, se $f(\bullet) \geq 0$ deve-se resolver as equações viscoplástica.

A correção viscoplástica deve ser executada apenas se o estado teste fornecer uma tensão, que não esteja dentro do conjunto de tensões definidas pela função de escoamento. Assim, o problema de correção viscoplástica pode ser formulada como: dado $(\boldsymbol{\varepsilon}_{n+1}, D_{n+1})$, determine $(\Delta\lambda, p_{n+1}, q_{n+1})$, a fim de satisfazer

$$\begin{cases} R_1 = \dfrac{\Delta\lambda\sigma_{yo}}{(1-D_{n+1})} + \sigma_{yo} M \ln\left[1 - \dfrac{f(p,q,R,D)_{n+1}}{K_\infty}\right]\Delta t = 0 \\ R_2 = p_{n+1} + \dfrac{E}{3(1-2\nu)}\dfrac{\mu\Delta\lambda}{(1-D_{n+1})} - p^{trial}_{n+1} = 0 \\ R_3 = q_{n+1} + \dfrac{3G\Delta\lambda}{(1-D_{n+1})} - q^{trial}_{n+1} = 0. \end{cases} \tag{9.45}$$

Uma vez que o conjunto $(\Delta\lambda, p_{n+1}, q_{n+1})$ seja determinado, o tensor tensão de Cauchy $(\boldsymbol{\sigma})$ pode também ser determinado apartir de

$$\boldsymbol{\sigma}^{D}_{n+1} = \boldsymbol{\sigma}^{D\ trial}_{n+1}\left[1 + \frac{3G\Delta\lambda}{(1-D_{n+1})}\right]^{-1} \tag{9.46}$$

e

$$\sigma_{H_{n+1}} = (1-D_{n+1})\, p_{n+1}. \tag{9.47}$$

A fim de resolver o sistema de equações não-lineares (9.45), aplica-se o método de Newton-Raphson. Este procedimento requer a determinação da matriz de rigidez tangente local $\mathbf{K}^T$, cujas componentes são dadas por

$$\mathrm{K}_{ij}^{T} = \frac{\partial R_i}{\partial a_j}, \tag{9.48}$$

em que, $\vec{a} = (\Delta\lambda, p_{n+1}, q_{n+1})$ e os índices *i* e *j* variam de 1 a 3.

No instante t_{n+1}, a formulação fraca do modelo viscoelastoplástico com dano acoplado pode ser declarado como: determine os campos de deslocamento e dano, $(\vec{u}_{n+1}, D_{n+1}) \in \bar{\mathcal{K}}$, de forma que

$$F_1(\vec{u}_{n+1}, D_{n+1}; \vec{w}) = \int_\Omega \boldsymbol{\sigma}_{n+1} \cdot \varepsilon(\vec{w}) d\Omega - \int_\Omega \rho \vec{b}_{n+1} \cdot \vec{w} d\Omega - \\ - \int_{\Gamma_t} \vec{t}_{n+1} \cdot \vec{w} dA = 0, \quad \forall \vec{w} \in \mathcal{V}_u \tag{9.49}$$

e

$$F_2(\vec{u}_{n+1}, D_{n+1}; \gamma) = \int_\Omega S_{\bar{\eta}_{s_{n+1}}} (D_{n+1} - D_n)\gamma d\Omega + \\ + \int_\Omega k \phi_{n+1} \vec{\nabla} D_{n+1} \cdot \vec{\nabla} \gamma d\Omega - \\ - \int_\Omega (F^{r}_{D_{n+1}} + F^{reac}_{D_{n+1}}) \phi_{n+1} \gamma d\Omega = 0, \quad \forall \gamma \in \mathcal{V}_D \tag{9.50}$$

em que,

$$\phi_{n+1} = \frac{\Delta\lambda}{(1 - D_{n+1})} \bar{H}(e^{vp}_{ef_{n+1}} - e^{vp}_{ef_{th}}) H(F^{i}_{D_{n+1}}). \tag{9.51}$$

Já que o problema acima é não-linear, aplica-se o método de Newton-Raphson para resolvê-lo.

Baseado no método de Newton-Raphson, considere $\vec{u}^0_{n+1} = \vec{u}_n$ e $D^0_{n+1} = D_n$ como sendo, respectivamente, os valores do deslocamento e dano no início do processo de iterações do método de Newton-Raphson. Então, na *k*-ésima iteração, tem-se

$$\vec{u}^{\,k+1}_{n+1} = \vec{u}^{\,k}_{n+1} + \Delta\vec{u}^{\,k}_{n+1} \tag{9.52}$$

e

$$D_{n+1}^{k+1} = D_{n+1}^{k} + \Delta D_{n+1}^{k}. \tag{9.53}$$

A fim de obter $\Delta\vec{u}_{n+1}^{k}$ e ΔD_{n+1}^{k}, impõe-se que

$$\begin{cases} F_1(\vec{u}_{n+1}^{k} + \Delta\vec{u}_{n+1}^{k}, D_{n+1}^{k} + \Delta D_{n+1}^{k}; \vec{w}) = 0, \quad \forall \vec{w} \in \mathcal{V}_u \\ \\ F_2(\vec{u}_{n+1}^{k} + \Delta\vec{u}_{n+1}^{k}, D_{n+1}^{k} + \Delta D_{n+1}^{k}; \gamma) = 0, \quad \forall \gamma \in \mathcal{V}_D. \end{cases} \tag{9.54}$$

Considerando F_1 e F_2 como sendo funções suaves e expandindo-as em série de Taylor, deriva-se, para uma aproximação de primeira ordem,

$$\begin{bmatrix} \partial_{uu} F_1(\vec{u}_{n+1}^{k}, D_{n+1}^{k}; \vec{w}) & \partial_{ud} F_1(\vec{u}_{n+1}^{k}, D_{n+1}^{k}; \vec{w}) \\ \partial_{du} F_2(\vec{u}_{n+1}^{k}, D_{n+1}^{k}; \gamma) & \partial_{dd} F_2(\vec{u}_{n+1}^{k}, D_{n+1}^{k}; \gamma) \end{bmatrix} \begin{Bmatrix} \Delta\vec{u}_{n+1}^{k} \\ \Delta D_{n+1}^{k} \end{Bmatrix} = -\begin{Bmatrix} F_1 \\ F_2 \end{Bmatrix}. \tag{9.55}$$

Neste caso, tem-se:

$$\partial_{uu} F_1\left(\vec{u}_{n+1}^{k}, D_{n+1}^{k}; \vec{w}\right)\left[\Delta\vec{u}_{n+1}^{k}\right] = \int_{\Omega} \left[\mathbb{D}_{n+1}^{uu}\right] \boldsymbol{\varepsilon}(\Delta\vec{u}_{n+1}^{k}) \cdot \boldsymbol{\varepsilon}(\vec{w})\, d\Omega, \tag{9.56}$$

em que,

$$\left[\mathbb{D}_{n+1}^{uu}\right] = \frac{\partial \boldsymbol{\sigma}_{n+1}}{\partial \boldsymbol{\varepsilon}_{n+1}^{e\ trial}} \tag{9.57}$$

é o modulo tangente consistente de deslocamento. Além disso, tem-se

$$\partial_{ud} F_1(\vec{u}_{n+1}^{k}, D_{n+1}^{k}; \vec{w})\left[\Delta D_{n+1}^{k}\right] = \int_{\Omega} \left[\boldsymbol{D}_{n+1}^{ud}\right] \Delta D_{n+1}^{k} \cdot \boldsymbol{\varepsilon}(\vec{w})\, d\Omega, \tag{9.58}$$

em que,

$$\left[\boldsymbol{D}_{n+1}^{ud}\right] = \frac{\partial \boldsymbol{\sigma}_{n+1}}{\partial D} \tag{9.59}$$

é o modulo tangente consistente de deslocamento-dano. Além disso, têm-se

$$\begin{aligned}\partial_{du}F_2(\vec{u}^k_{n+1},D^k_{n+1};\gamma)\left[\Delta\vec{u}^k_{n+1}\right] = &\int_\Omega \frac{d}{de}\left(S_{\bar{\eta}_{s_{n+1}}}\right)\Big|_{\epsilon=0}(D_{n+1}-D_n)\gamma\, d\Omega - \\ &-\int_\Omega \boldsymbol{P}^{ud}_{n+1}\boldsymbol{\varepsilon}(\Delta\vec{u}^k_{n+1})\gamma\, d\Omega \\ &+\int_\Omega k\left[\boldsymbol{H}^{ud}_{n+1}\boldsymbol{\varepsilon}(\Delta\vec{u}^k_{n+1})\right](\vec{\nabla}D_{n+1}\cdot\vec{\nabla}\gamma)\, d\Omega - \\ &-\int_\Omega \left(F^r_{D_{n+1}}+F^{reac}_{D_{n+1}}\right)\left[\boldsymbol{H}^{ud}_{n+1}\boldsymbol{\varepsilon}(\Delta\vec{u}^k_{n+1})\right]\gamma\, d\Omega, \end{aligned} \tag{9.60}$$

$$\boldsymbol{H}^{ud}_{n+1} = \frac{\bar{H}(e^{vp}_{ef_{n+1}}-e^{vp}_{ef_{th}})H(F^i_{D_{n+1}})}{(1-D_{n+1})}\frac{\partial\Delta\lambda}{\partial\boldsymbol{\varepsilon}^{e\ trial}_{n+1}} \tag{9.61}$$

e

$$\boldsymbol{P}^{ud}_{n+1} = \frac{\phi_{n+1}}{E}\left[\frac{2}{3}(1+\nu)q_{n+1}\frac{\partial q_{n+1}}{\partial\boldsymbol{\varepsilon}^{e\ trial}_{n+1}} + 3(1-2\nu)p_{n+1}\frac{\partial p_{n+1}}{\partial\boldsymbol{\varepsilon}^{e\ trial}_{n+1}}\right]. \tag{9.62}$$

e

$$\begin{aligned}\partial_{dd}F_2(\vec{u}^k_{n+1},D^k_{n+1};\gamma)\left[\Delta D^k_{n+1}\right] = &\int_\Omega\left[\alpha_s(D^k_{n+1}-D_n)+S_{\bar{\eta}_{s_{n+1}}}\right]\Delta D^k_{n+1}\gamma\, d\Omega + \\ &+\int_\Omega k\phi_{n+1}\left[\vec{\nabla}\left(\Delta D^k_{n+1}\right)\cdot\vec{\nabla}\gamma\right]\, d\Omega - \\ &-\int_\Omega(\alpha_F+\gamma_F+\eta_F)\Delta D^k_{n+1}\gamma\, d\Omega, \end{aligned} \tag{9.63}$$

A fim de aplicar o método dos elementos finitos, divide-se o domínio, Ω, em elementos finitos, Ω_e. Neste trabalho, dois elementos finitos foram aplicados e implementados: axissimétrico e estado plano de deformação. Para o problema axissimétrico, o campo de deslocamento é dado por

$$\vec{u} = u_r\vec{e}_r + u_\theta\vec{e}_\theta + u_z\vec{e}_z, \tag{9.64}$$

em que,

$$u_r = u_r(r,z),$$

$$u_\theta = 0$$

e

$$u_z = u_z(r,z).$$

Já que o problema é independente de θ, tem-se $d\Omega = 2\pi r dr dz$. Além disso, os vetores de tensão e deformação são dados, respectivamente, por $\vec{\sigma}^T = (\sigma_{rr}, \sigma_{zz}, \tau_{rz}, \sigma_{\theta\theta})$ e $\vec{\varepsilon}^T = (\varepsilon_{rr}, \varepsilon_{zz}, \gamma_{rz}, \varepsilon_{\theta\theta})$. Assim, as componentes do campo de deslocamento são interpolados no elemento Ω_e como

$$u_r(\xi,\eta) = u_{r_i} N_i(\xi,\eta) \tag{9.65}$$

e

$$u_z(\xi,\eta) = u_{z_i} N_i(\xi,\eta), \tag{9.66}$$

em que, o índice *i* varia de um ao número de nós no elemento e $N_i(\xi,\eta)$ são as funções de interpolação clássicas utilizadas no método dos elementos finitos. Aplicando a discretização na função $F_1(\vec{u}_{n+1}, D_{n+1}; \vec{w})$, obtêm-se

$$\mathbf{K}^{uu} = 2\pi \int_{\xi=0}^{1} \int_{\eta=0}^{1-\xi} [\mathbf{B}^u]^T \left[\breve{\boldsymbol{D}}_{uu}^{ep} \right] [\mathbf{B}^u] J\, r\, d\xi d\eta \tag{9.67}$$

e

$$\mathbf{K}^{ud} = 2\pi \int_{\xi=0}^{1} \int_{\eta=0}^{1-\xi} \left\{ [\mathbf{B}^u]^T \{\vec{w}_{uu}\} \otimes [\vec{N}^d] \right\} J\, r\, d\xi d\eta, \tag{9.68}$$

em que, $\breve{\boldsymbol{D}}_{uu}^{ep}$ é a forma compacta do operador tangente $\mathbb{D}^{uu}$, a notação $\otimes$ significa produto tensorial e o vetor $\vec{w}_{uu}$ é dado por

$$\vec{w}_{uu} = \left\{ \mathbb{D}_{11}^{uu} \quad \mathbb{D}_{22}^{uu} \quad \mathbb{D}_{12}^{uu} \quad \mathbb{D}_{33}^{uu} \right\}.$$

Além disso, a força interna, a força de corpo e a contribuição da tração prescrita são dadas, respectivamente, por

$$\vec{F}_e^{int} = 2\pi \int_0^1 \int_0^{1-\xi} \rho \left[\mathbf{B}^u \right]^T \vec{\sigma}\, J\, r\, d\xi d\eta \tag{9.69}$$

$$\vec{F}_e^{\vec{b}} = 2\pi \int_0^1 \int_0^{1-\xi} \rho \left[\mathbf{N}^u \right]^T \vec{b}\, J\, r\, d\xi d\eta \tag{9.70}$$

e

$$\vec{F}_e^{\vec{t}} = 2\pi \int_0^1 \rho \left[\mathbf{N}^u(\tau) \right]^T \vec{t}\, J(\tau) r(\tau) d\tau, \tag{9.71}$$

Aplicando agora a discretização na equação de dano, $F_2(\vec{u}_{n+1}, D_{n+1}; \gamma)$, obteve-se as forças de dano

$$\vec{F}_e^{\,D} = \vec{F}_e^{\,S_\eta} + \vec{F}_e^{\,\bar{k}} - \vec{F}_e^{\,F}, \tag{9.72}$$

em que,

$$\vec{F}_e^{\,S_\eta} = \int_{\Omega_e} S_{\bar{\eta}_{s_{n+1}}} (D_{n+1} - D_n) \vec{N}^d d\Omega_e, \tag{9.73}$$

$$\vec{F}_e^{\,\bar{k}} = \int_{\Omega_e} \bar{k} \phi_{n+1} \mathbf{B}^d \vec{\nabla} D_{n+1} d\Omega_e \tag{9.74}$$

e

$$\vec{F}_e^{\,F} = \int_{\Omega_e} \phi_{n+1} \left(F_{D_{n+1}}^r + F_{D_{n+1}}^{reac} \right) \vec{N}^d d\Omega_e. \tag{9.75}$$

Além disso, do operador tangente (5.53), deriva-se as seguintes matrizes:

$$\mathbf{K}^{du} = \mathbf{K}_{S_\eta}^{du} + \mathbf{K}_{\bar{k}}^{du} - \mathbf{K}_{F_1}^{du} - \mathbf{K}_{F_2}^{du} \tag{9.76}$$

e

$$\mathbf{K}^{dd} = \mathbf{K}^{dd}_{S_\eta} + \mathbf{K}^{dd}_{k_1} + \mathbf{K}^{dd}_{k_2} - \mathbf{K}^{dd}_{F}, \tag{9.77}$$

em que,

$$\mathbf{K}^{du}_{S_\eta} = \int_{\Omega_e} (D_{n+1} - D_n)\left(\vec{N}^d \otimes [\mathbf{B}^u]^T \vec{w}_\beta\right) d\Omega_e, \tag{9.78}$$

$$\mathbf{K}^{du}_{k} = \int_{\Omega_e} k\left([\mathbf{B}^d]^T \vec{\nabla} D_{n+1} \otimes [\mathbf{B}^u]^T \vec{w}_H\right) d\Omega_e, \tag{9.79}$$

$$\mathbf{K}^{du}_{F_1} = \int_{\Omega_e} \left(F^r_{D_{n+1}} + F^{reac}_{D_{n+1}}\right)\left(\vec{N}^d \otimes [\mathbf{B}^u]^T \vec{w}_H\right) d\Omega_e, \tag{9.80}$$

$$\mathbf{K}^{du}_{F_2} = \int_{\Omega_e} \left(\vec{N}^d \otimes [\mathbf{B}^u]^T \vec{w}_P\right) d\Omega_e, \tag{9.81}$$

$$\mathbf{K}^{dd}_{S_\eta} = \int_{\Omega_e} \left[\alpha_s (D_{n+1} - D_n) + S_{\bar{\eta}_{s_{n+1}}}\right]\left(\vec{N}^d \otimes \vec{N}^d\right) d\Omega_e, \tag{9.82}$$

$$\mathbf{K}^{dd}_{k_1} = \int_{\Omega_e} k\phi_{n+1}\left([\mathbf{B}^d]^T [\mathbf{B}^d]\right) d\Omega_e, \tag{9.83}$$

$$\mathbf{K}^{dd}_{k_2} = \int_{\Omega_e} k\ H^{dd}\left([\mathbf{B}^d]^T \vec{\nabla} D_{n+1} \otimes \vec{N}^d\right) d\Omega_e \tag{9.84}$$

em que

$$\mathbf{K}^{dd}_{F} = \int_{\Omega_e} (\alpha_F + \gamma_F + \eta_F)\left(\vec{N}^d \otimes \vec{N}^d\right) d\Omega_e. \tag{9.85}$$

A fim de resolver as integrais anteriores, aplica-se um procedimento numérico. Dentre os métodos disponíveis, utilizou-se a regra de quadratura de Gauss.

Considere, então, o vetor $\vec{U}^{(k)}$ como sendo o vetor de todos os graus de liberdade na k-ésima iteração do método de Newton-Raphson, ou seja,

$$\vec{U}^{(k)} = \bigcup_{e=1}^{n} \left\{ \vec{q}_e^{(k)} \right\}. \tag{9.86}$$

Assume-se que o estado é conhecido no intervalo $[0, t_n]$. O problema consiste na determinação do vetor de graus de liberdade nodal, $\vec{U}_{n+1}$, no instante de tempo t_{n+1}. O problema não-linear discreto no instante t_{n+1} pode ser formulado como ilustrado na Tabela 9.2.

Tabela 9.2: Declaração do problema não-linear.

Considere $\vec{U}_{n+1}^{(0)} = \vec{U}_n$ como sendo o vetor de graus de liberdade nodal, então:

Encontre $\vec{U}_{n+1}^{(k+1)}$, de forma que $\left\| \vec{R}\left(\vec{U}_{n+1}^{(k+1)}\right) \right\| \leq Tol$, em que

$$\left[\mathbf{K}^G \left(\vec{U}_{n+1}^{(k)} \right) \right] \Delta \vec{U}_{n+1}^{(k)} = -\vec{F}^G \left(\vec{U}_{n+1}^{(k)} \right),$$

de forma que,

$$\vec{U}_{n+1}^{(k+1)} = \vec{U}_{n+1}^{(k)} + \Delta \vec{U}_{n+1}^{(k)}.$$

Na Tabela 9.2, $\vec{R}$ é o erro residual, *Tol* é a tolerância de convergência global e a matriz de rigidez consistente tangente global, $\mathbf{K}^G$, é dada por

$$\mathbf{K}^G = \begin{bmatrix} \mathbf{K}^{uu} & \mathbf{K}^{ud} \\ \mathbf{K}^{du} & \mathbf{K}^{dd} \end{bmatrix}. \tag{9.87}$$

Por sua vez, o vetor de força nodal global, $\vec{F}^G$, é dado por

$$\vec{F}^G = \left(\vec{F}_e^{\text{int}} - \vec{F}_e^{\vec{b}} - \vec{F}_e^{\vec{t}} \right) + \vec{F}_e^D \tag{9.88}$$

e o vetor graus de liberdade global é dado por $(\Delta \vec{U}_{n+1})^T = \left\{ \Delta \vec{u}_{n+1} \ \Delta D_{n+1} \right\}$.

9.6. MEDIÇÕES EXPERIMENTAIS – CAPÍTULO 6

A fim de implementar o modelo constitutivo apresentado anteriormente, é necessário fornecê-lo algumas constantes e propriedades materiais, que devem ser obtidas e/ou identificadas experimentalmente. Assim, o objetivo desta seção é apresentar um resumo dos ensaios realizados e ilustrar os resultados obtidos apartir deles.

9.6.1. O Material Selecionado

A fim de realizar os ensaios, escolheu-se uma resina de polipropileno devido a duas razões. Primeiro, uma resina de polipropileno estava facilmente disponível no Instituto Real de Tecnologia (KTH), onde os ensaios foram realizados. Segundo, podem-se encontrar muitas aplicações de componentes de plástico sujeitas à falha dúctil e fabricados com este material. O material disponível no KTH e utilizado nos testes foi o HE125MO®, fornecido pela Borealis.

9.6.2. Propriedades Mecânicas

As propriedades mecânicas necessárias ao modelo apresentado nos capítulos anteriores foram, basicamente: densidade, módulo de elasticidade, tensão de escoamento, coeficiente de Poisson e a constante material que introduz o efeito das tensões hidrostáticas.

A geometria e as dimensões dos corpos de prova utilizados nos ensaios de tração e de obtenção do coeficiente de Poisson estão ilustradas na Figura 9.2. Os corpos de prova foram produzidos pelo processo de moldagem por injeção por meio do equipamento Battenfeld Plus 250® e sob as recomendações da norma ASTM D 3641, a fim de obter corpos de prova uniformes.

Inicialmente, foram realizados ensaios para determinar o grau de cristalinidade dos corpos de prova, visto que este fator exerce forte influência no desempenho mecânico dos componentes, e associaram-se as propriedades mecânicas do material a este grau de cristalinidade. Os ensaios foram realizados por meio da técnica DSC, utilizando o equipamento Mettler DSC 820® e sob as recomendações e especificação da norma ASTM E 1356. Seis corpos de prova, com massas de aproximadamente 15 gramas, foram testados. No final, obteve-se o valor de grau de cristalinidade ilustrado na Tabela 9.3.

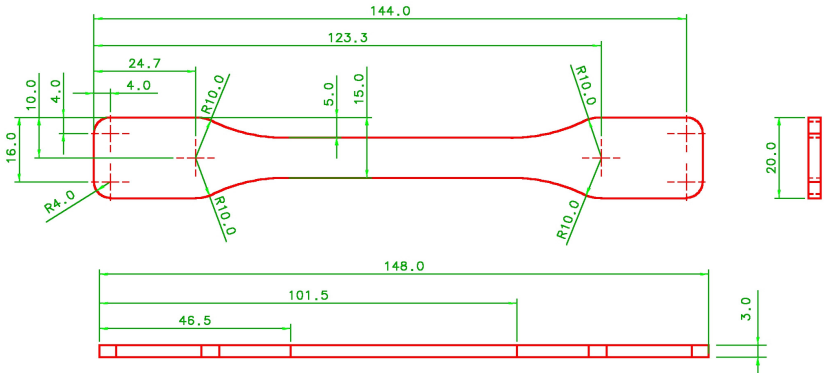

Figura 9.2: Geometria de dimensões dos corpos de prova, em milímetros.

Tabela 9.3: Valor médio e Desvio Padrão do grau de cristalinidade dos corpos de prova.

	Valor Médio	**Desvio Padrão**
Grau de Cristalinidade (%)	41.3	1.40

Os ensaios para obtenção da densidade do material foram realizados segundo o método *B* da norma ASTM D 792. Cinco corpos de prova, pesando cerca de 10 gramas foram cortados dos corpos de prova do teste de tração e testados. A Tabela 9.4 ilustra o valor médio e o desvio padrão da densidade do material selecionado.

Tabela 9.4: Valor médio e Desvio Padrão da densidade do material.

	Valor Médio	**Desvio Padrão**
Densidade (kg/m^3)	9.02×10^2	0.83

Os ensaios de tração foram realizados segundo as normas ASTM D 638 e ISO 527, sob condições ambientais e utilizou-se a máquina de tração Instron 5566®, equipado com um aparelho de extensômetro por vídeo e uma célula de carga de 1 kN. Apartir dos dados experimentais do teste de tração, foram calculados os valores médios e os desvios padrões de E, σ_y and ε_y, como estão ilustrados na Tabela 9.5.

Tabela 9.5: Valor médio e Desvio Padrão das propriedades trativas do material.

	Módulo de Elasticidade (GPa)	**Tensão de Escoamento (MPa)**	**Deformação no Escoamento (%)**
Valor Médio	1.54	31.6	8.00
Desv. Pad	0.27	0.58	9.30×10^{-2}

O coeficiente de Poisson do material em estudo, em condições ambientais, foi determinado por meio da técnica DSP em conjunto da máquina de ensaios de tração Instron 5567® e das recomendações da norma ASTM E 132. De acordo com esta norma, as tensões e deformações devem ser medidas dentro da região linear da curva tensão-deformação e o coeficiente de Poisson é, então, calculado como

$$\nu = -\frac{d\varepsilon_y}{d\varepsilon_x}, \tag{9.89}$$

em que, ε_x e ε_y são as deformações longitudinal e transversal. Assim, verifica-se que o coeficiente de Poisson representa o coeficiente angular da linha reta, obtida do ajuste de curva dos resultados experimentais entre ε_x e ε_y. Para o material em estudo, obteve-se o valor de coeficiente de Poisson ilustrado na Tabela 9.6. Li *et al.* [91] afirma que o coeficiente de Poisson do polipropileno é cerca de 0,36.

Tabela 9.6: Valor médio e Desvio padrão do coeficiente de Poisson.

	Valor Médio	**Desvio Padrão**
Coeficiente de Poisson	0.36	0.02

Pelo fato de os materiais plásticos serem sensíveis a esforços de compressão, recomenda-se utilizar critérios de escoamento, que considerem a influência do tensor hidrostático. Isto é geralmente feito pela introdução do parâmetro μ no critério. Este parâmetro para o material selecionado foi obtido da Tabela 9.7, que contém também o valor para outros materiais, à temperatura de 23 ºC. De acordo com Miller [68], um valor de 0,15 para μ pode ser utilizado, quando não houver um valor determinado experimentalmente.

Tabela 9.7: Valores para o parâmetro μ para diferentes materiais [68, 92].

MATERIAL	PARÂMETRO μ
Polystyrene (PS)	0.250
Polymethyl Methacrylate (PMMA)	0.158
Polycarbonate (PC)	0.120
Polyethylene Terephthalate (PET)	0.090
High Density Polyethylene (HDPE)	0.050
Polyvinyl Chloride (PVC)	0.110
Polypropylene (PP)	0.120

Durante a realização dos ensaios, foram observados dois aspectos: (1) os desvios padrões foram baixos, o que produziu baixa dispersão; e (2) os valores numéricos das propriedades estão muito próximos daqueles publicados pelo fornecedor do material (Borealis), como pode ser visto na Tabela 9.8. Isto significa que os resultados dos testes são confiáveis e consistentes.

Tabela 9.8: Comparação entre os resultados dos ensaios e do fornecedor do material.

	ENSAIOS	FORNECEDOR DO MATERIAL
Densidade (kg/m^3)	9.02×10^2	9.02×10^2
Módulo de Elasticidade (GPa)	1.54	1.55
Tensão de Escoamento (MPa)	31.6	34.5
Deformação Escoamento (%)	8.00	9.00
Coeficiente de Poisson	0.36	-

9.7. EXEMPLOS NUMÉRICOS – CAPÍTULO 7

Este item apresentará alguns exemplos numéricos, baseado na teoria desenvolvida nos Capítulos 4 e 5 e nos resultados experimentais apresentados no Capítulo 6. A teoria proposta consiste de um modelo de dano para a análise da fratura dúctil de componentes de plástico. Dentre os parâmetros e propriedades materiais, alguns deles foram identificados apartir de ensaios padronizados, enquanto que outros foram estimados, tendo como base os valores publicados por Lemaitre [1] e Ghorbel [4]. Os valores estimados para os outros parâmetros materiais são dados na Tabela 9.9, bem como as referências de onde os mesmo foram tirados ou estimados.

Tabela 9.9: Parâmetros materiais remanescentes necessários ao modelo matemático.

PARÂMETROS	VALORES	REFERÊNCIAS
M	2.0 s^{-1}	Ghorbel [4]
K_∞	31.6 MPa	Ghorbel [4]
$\overline{\eta}_a$ $\overline{\eta}_b$	1.0×10^{-5} 1.0×10^{-9}	Lemaitre [1]
S_o	0.15 MPa	Lemaitre [1]
$\overline{\eta}_s$	1.0×10^{-9}	Lemaitre [1]
$\bar{k}$	2.0 MPa · mm^2	Fremond and Nedjar [2]
$e^{vp}_{ef_{th}}$	0.75	Lemaitre [1]

No primeiro exemplo, simulou-se o comportamento do material sob carregamento de tração. Aqui, comparam-se os resultados numéricos, obtidos de uma estimativa dos parâmetros materiais, com os resultados obtidos do ensaio de tração uniaxial. Os parâmetros materiais estimados em utilizados no modelo matemático são dados na Tabela 9.9. Adicionalmente, uma estimativa para a curva da variável de encruamento isotrópico do material é dada na Tabela 9.10.

Tabela 9.10: Pontos da curva de encruamento [1].

$h(r)$ (MPa)	0,0	1,0	2,0	2,5
r (mm/mm)	0,0	0,2	0,4	2,0

A Figura 9.3 ilustra uma comparação entre os diagramas experimentais e numéricos do teste de tração. A fim de reduzir o tempo de processamento, considerou-se o tempo total de análise igual a 60 segundos, que foi o tempo suficiente para alcançar a região de estiramento. Além disso, considerou-se também 1000 incrementos de carga e tolerância de convergência global de 10^{-5}. A curva de encruamento foi obtida por interpolação, usando funções *spline* e os dados da Tabela 9.10.

O erro máximo entre os resultados experimentais e numéricos foi de aproximadamente 22%. Esta diferença ocorreu na região de amolecimento, onde a estricção surge e evolui para a região de estiramento. Este erro pode ser consideravelmente reduzido, realizando uma identificação mais adequada dos parâmetros materiais. Isto pode ser

obtido, usando, por exemplo, um esquema de algoritmo genético, a fim de computar uma aproximação do mínimo global de um problema de otimização por mínimo quadrado.

O Segundo exemplo ilustra o desempenho de um pequeno componente mecânico genérico, submetido a uma condição de deslocamento prescrito. Sua geometria e dimensões estão ilustradas na Figura 9.4. Já que este componente possui formato prismático e tem dois planos de simetria, então se modelou apenas um quarto da sua geometria como estado plano de deformação, como pode ser visto na Figura 9.5. Nesta figura, pode-se observar também que na extremidade direita, aplicou-se um deslocamento prescrito na direção *x*, variando linearmente até $\overline{u}_x = 2.0$ mm. Além disso, as extremidades esquerda e direita foram restringidas nas direções *x* e *y*, respectivamente, a fim de simular a condição de simetria.

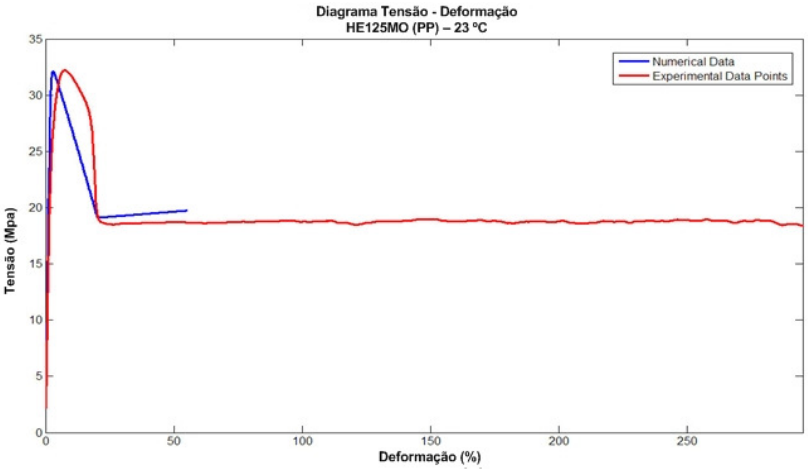

Figura 9.3: Diagrama tensão-deformação para a simulação do teste de tração.

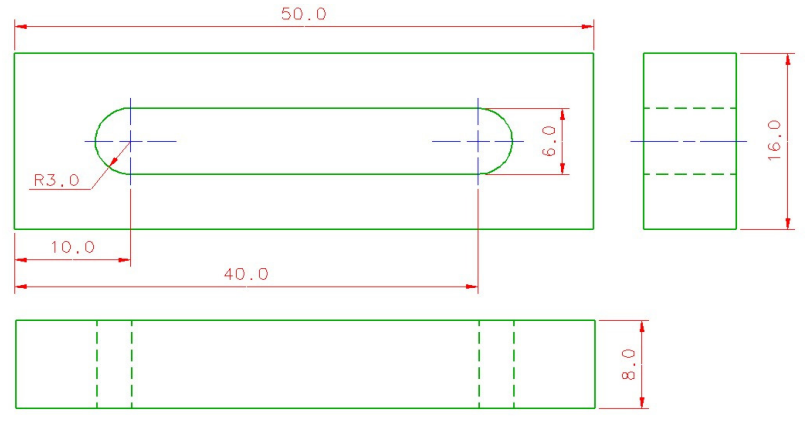

Figura 9.4: Geometria e dimensões do componente mecânico, em milímetros.

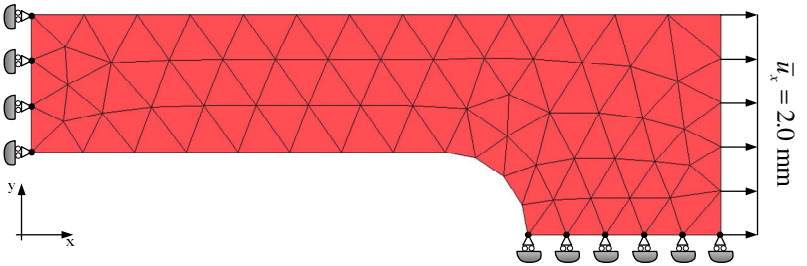

Figura 9.5: Malha e condições de contorno do componente mecânico.

A distribuição dos deslocamentos na direção x, u_x, está ilustrada na Figura 9.6. Por sua vez, a Figura 9.7 ilustra a distribuição da deformação viscoplástica equivalente. Adicionalmente, a Figura 9.8 ilustra a distribuição da variável de dano no final da análise.

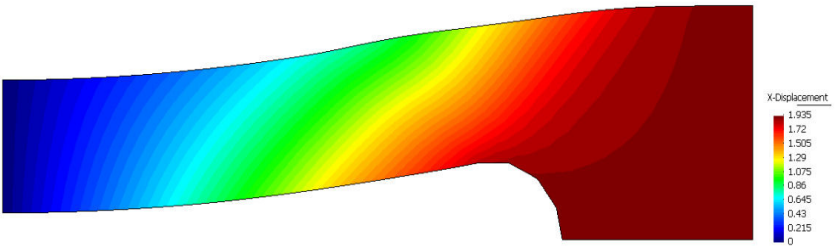

Figura 9.6: Deslocamento na direção x no final da análise, em milímetros.

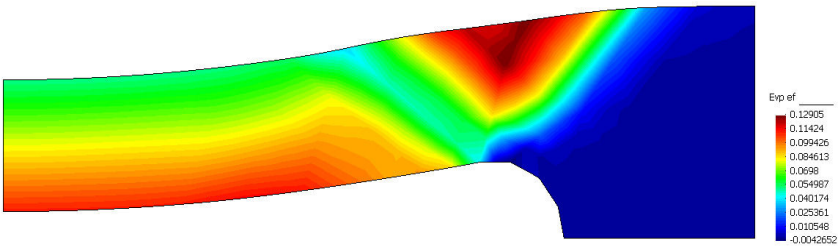

Figura 9.7: Distribuição da deformação viscoplástica equivalente no final da análise.

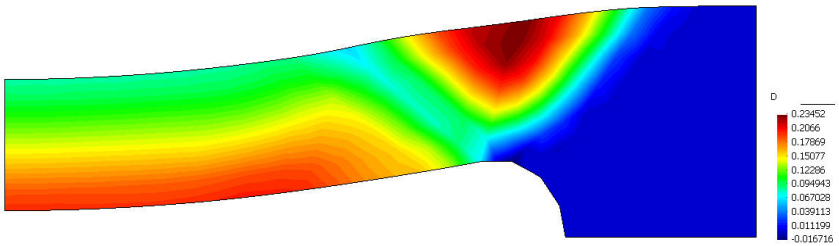

Figura 9.8: Distribuição do dano no final da análise.

O terceiro exemplo ilustra o desempenho de uma polia de plástico, submetida a uma condição de deslocamento prescrito, representando a carga proveniente da correia. Pelo fato de a polia é um sólido de revolução, então se decidiu modelá-la como sendo um problema axissimétrico. Suas dimensões estão ilustradas na Figura 9.9. A malha e as condições de contorno estão ilustradas na Figura 9.10.

A Figura 9.11 ilustra a distribuição da norma do deslocamento no final da análise, em milímetros, e a Figura 9.12 ilustra a distribuição da deformação equivalente. A distribuição da variável de dano no final da análise está ilustrada na Figura 9.13. Pode-se observar que a região de dano assemelha-se muito com uma letra "X", em que cada uma de suas pernas está inclinada, aproximadamente, 45° em relação à direção radial. Esta peculiaridade sugere a formação de bandas de cisalhamento, que é o modo de falha mais característica de componentes de plástico sob cargas compressivas. Adicionalmente, pode-se observar que o valor máximo para a deformação viscoplástica efetiva ocorre na intersecção das bandas de cisalhamento.

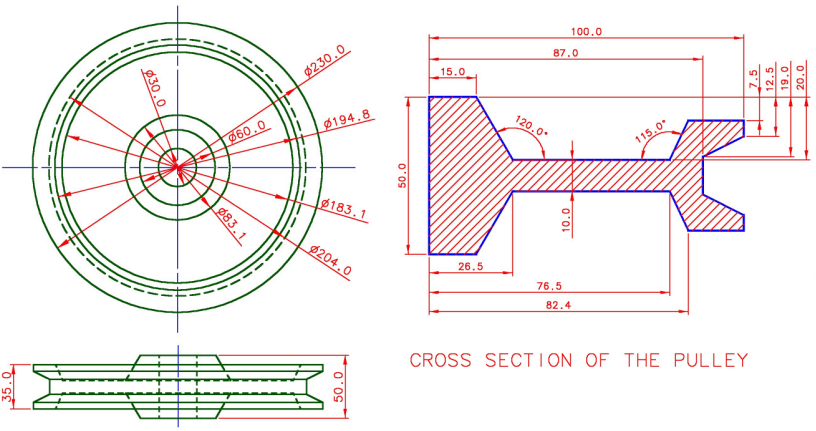

Figura 9.9: Geometria e dimensões da polia de plástico, em milímetros.

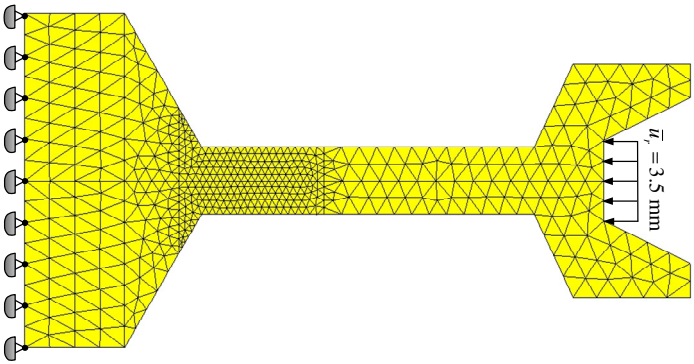

Figura 9.10: Malha e condições de contorno da polia de plástico.

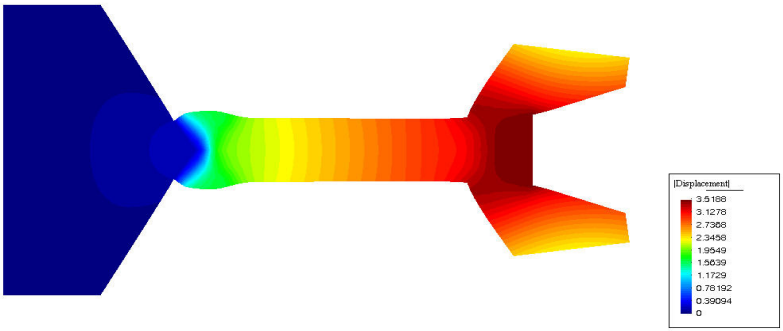

Figura 9.11: Campo de deslocamento no final da análise, em milímetros.

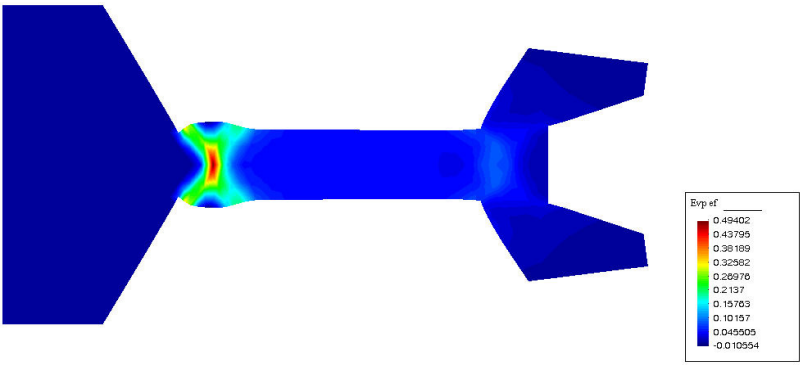

Figura 9.12: Distribuição da deformação plástica equivalente, em mm/mm.

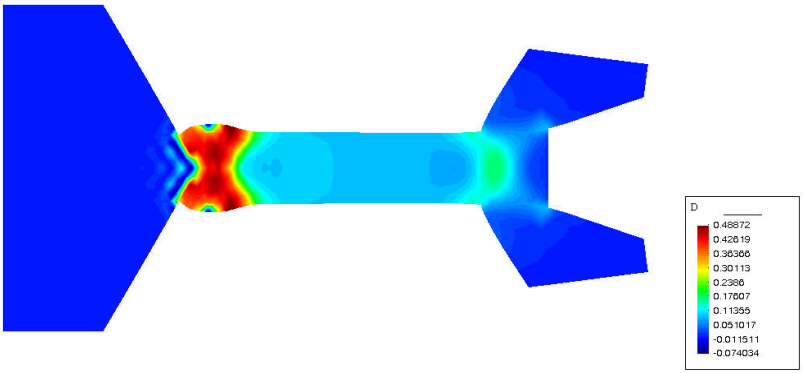

Figura 9.13: Distribuição do dano.

O último exemplo ilustra o desempenho de um *snap fit* utilizado em aplicações automotivas, submetido a um deslocamento prescrito, relativo ao deslocamento necessário para instalação de um componente adicional. A geometria e as dimensões estão ilustradas na Figura 9.14 e o problema foi modelado como sendo de estado plano de deformação, já que e o componente é bastante comprido. A malha de elementos finitos e as condições de contorno estão ilustradas na Figura 9.15, em que se pode ver a aplicação de um deslocamento de 4.0 mm, na direção x, a fim de simular a montagem de um componente adicional, e a aplicação das restrições, a fim de simular a fixação do componente na estrutura do veículo.

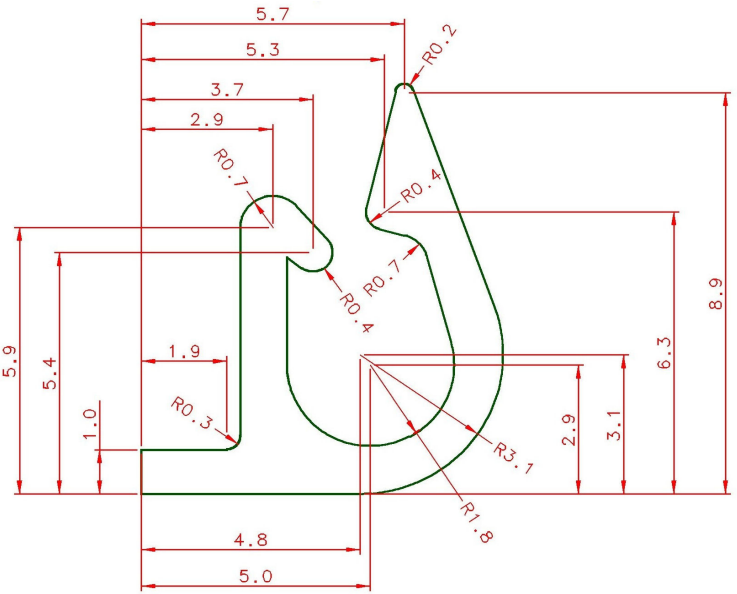

Figura 9.14: Geometria e dimensões do *snap fit*, em milímetros.

A Figura 9.16 ilustra a distribuição da norma do campo de deslocamento no componente, em milímetros. A distribuição da deformação viscoplástica efetiva, no final da análise, está ilustrada na Figura 9.17. Esses resultados demonstram que, apesar de o deslocamento de montagem ser pequeno, ele é suficiente para produzir deformações irreversíveis e, consequentemente, uma pequena quantidade de dano, como pode ser observado na Figura 9.18.

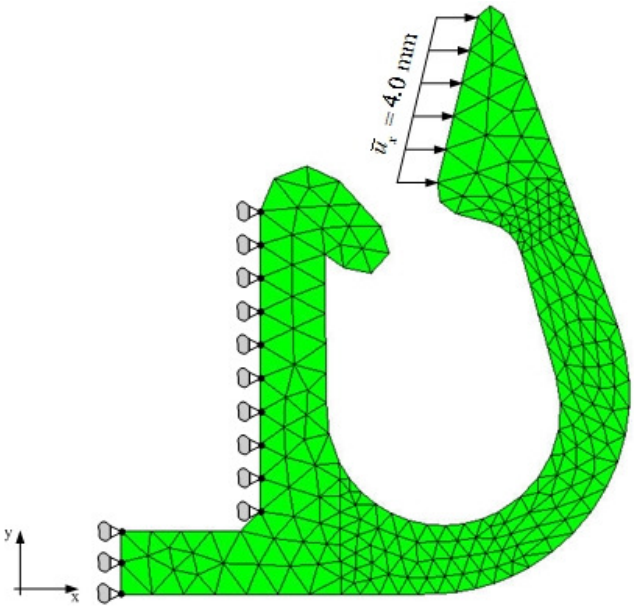

Figura 9.15: Malha e condições de contorno do *snap fit*.

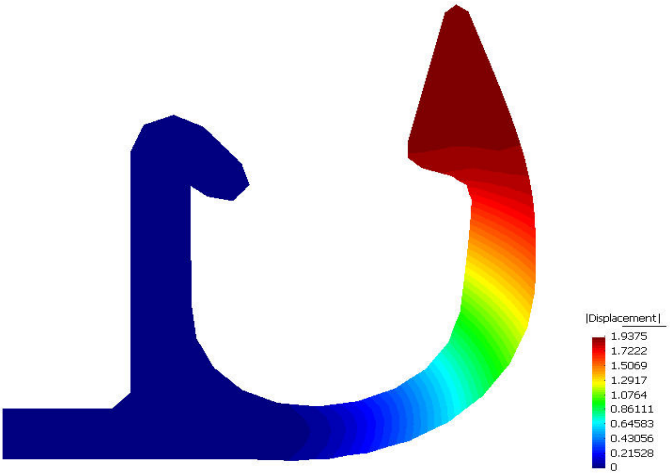

Figura 9.16: Campo de deslocamento, em milímetros.

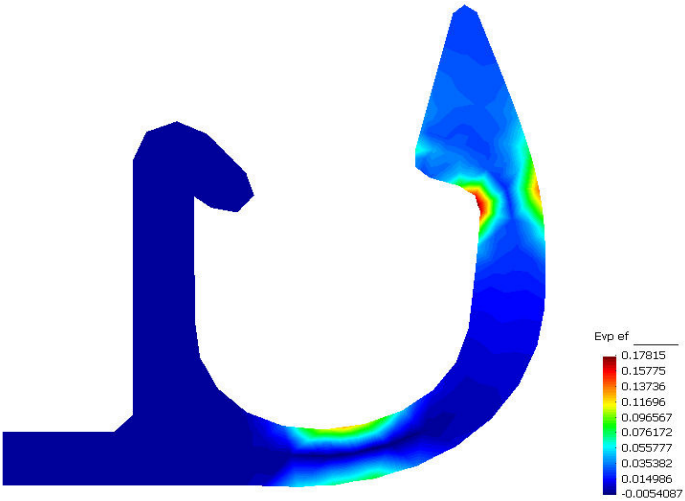

Figura 9.17: Distribuição da deformação viscoplástica, em mm/mm.

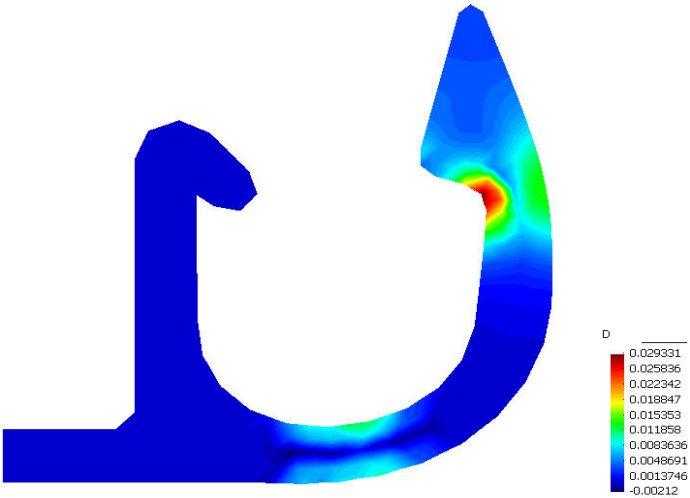

Figura 9.18: Distribuição do dano no *snap fit*.

9.8. CONSIDERAÇÕES FINAIS – CAPÍTULO 8

Este trabalho teve como objetivo propor um modelo elasto-viscoplástico acoplado ao dano, para ser utilizado para analisar o comportamento mecânico de componentes de plástico e o desenvolvimento

de ensaios experimentais, a fim de obter as propriedades do material necessárias ao modelo.

9.8.1. Conclusões

Este trabalho foi didaticamente subdividido em: desenvolvimento teórico do modelo proposto; a parte associada com a discretização do modelo matemático e, finalmente, a parte que descreve os ensaios experimentais realizados para identificar os parâmetros materiais.

Uma calibração do modelo foi tentada através dos dados de um ensaio de tração uniaxial, de onde se obteve o diagrama tensão-deformação experimental. Pela comparação dos resultados numéricos e experimentais, obteve-se um erro máximo de 22%, que ocorreu na região de amolecimento, que, em seguida, conduz ao processo de estiramento e estricção.

Neste trabalho, o amolecimento foi considerado pela variável de dano, que é responsável por descrever a redução da seção transversal que ocorre na formação da estricção. Já que, no processo de estiramento, a seção transversal permanece aproximadamente constante, a variável de dano deve ser aproximadamente constante como foi forçado pela restrição.

A consideração de modelamento por deformações finitas pode ser mais adequada para simular a formação da estricção e do processo de estiramento, já que a redução de área da seção transversal é um processo com grandes deformações. Como resultado, a variável de dano seria necessário apenas para descrever apenas a nucleação de micro vazios e micro trincas, que daria uma melhor aproximação da resposta numérica com relação aos dados experimentais. Uma melhor determinação do parâmetro de encruamento isotrópico poderia ser obtida, implementando-se um processo de otimização por mínimos quadrados, utilizando algoritmo genético. Neste caso, a identificação dos parâmetros pode ser formulada como um problema inverso.

O modelamento proposto neste trabalho é mais apropriado para modelar geometrias, que produzam deformações não homogêneas, resultante da deformação de componentes com algum tipo de concentrador de tensão. Assim, procurou-se por simular componentes com tais peculiaridades. Apesar do elevado erro entre os dados numéricos e experimentais (aproximadamente 22%), considera-se que o modelo representa apropriadamente o comportamento mecânico e os processos de degradação de componentes de plástico submetido a cargas mecânicas, pois, qualitativamente falando, os três exemplos numéricos produziram resultados bastante consistentes.

A segunda parte do trabalho refere-se ao desenvolvimento de ensaios mecânicos, realizados a fim de obter as propriedades materiais requeridas para caracterizar o material modelado. Inicialmente, um material plástico (resina de polipropileno) foi selecionado e suas principais propriedades mecânicas foram obtidas. Os testes foram conduzidos por meio das normas ASTM e dois aspectos foram observados: os desvios padrões foram baixos, que conduziu a uma baixa dispersão dos resultados; e boa concordância entre os resultados e os dados publicados pelo fornecedor do material (Borealis), o que significa que os resultados dos ensaios são confiáveis e consistentes.

O modelamento proposto neste trabalho pode não ser útil para aplicações práticas, a menos que se garanta que os componentes em análise estejam livres de defeitos originados dos processos de fabricação, pois estes defeitos podem reduzir drasticamente sua resistência e, consequentemente, causar sua falha prematura. Portanto, é extremamente importante garantir que os componentes de plástico sejam dimensionados, de forma que eles cumpram tanto os requisitos de resistência mecânica quanto os de manufatura. Na prática, esta precaução pode ajudar a reduzir custos relacionados a manutenção e até de uma substituição destes componentes que tenham falhado prematuramente.

9.8.2. Sugestões para Trabalhos Futuros

Este trabalho pode servir de base para o desenvolvimento de novas pesquisas na área de modelamento do comportamento mecânico e térmico de materiais plásticos. Algumas sugestões para trabalhos futuros desenvolvidos nesta mesma linha de pesquisa são apresentadas a seguir:

- Desenvolvimento deste modelo, considerando a formulação de grandes deformações;
- Desenvolvimento de uma análise de sensibilidade;
- Discretização das equações pelo Método de Elementos Livres de Galerkin;
- Implementação de um algoritmo de incrementação de carga variável;
- Desenvolvimento deste modelo, considerando dano isotrópico; e
- Desenvolvimento de um modelo para analisar componentes sob fadiga de baixo e alto ciclo.

ATTACHMENT A - EXPERIMENTAL TECHNIQUES

The objective of this section is to present a brief description of the main experimental techniques used to develop the tests described in Chapter 6. Some of these techniques, like DSC and DMA, are not often practiced in the mechanical engineering field and others, like DSP, are new techniques and not much diffused, yet. Thus, these will be the main techniques discussed here.

A.1. DSC TECHNIQUE

Differential Scanning Calorimetry (DSC) is a thermo analytical technique, in which the difference in amount of heat required to increase the temperature of a sample and a reference crucible is measured as a function of temperature. Both the sample and reference crucibles are maintained at nearly the same temperature throughout the experiment [93]. Figure A.1 illustrates a simplified view of the elements of a DSC equipment, whereas Figure A.2 illustrates the measuring device of the equipment used in the tests described in Chapter 6. In one crucible, one places the sample and the other is left empty (reference crucible). The computer controls the heaters, so that they heat the two crucibles at a same specific rate.

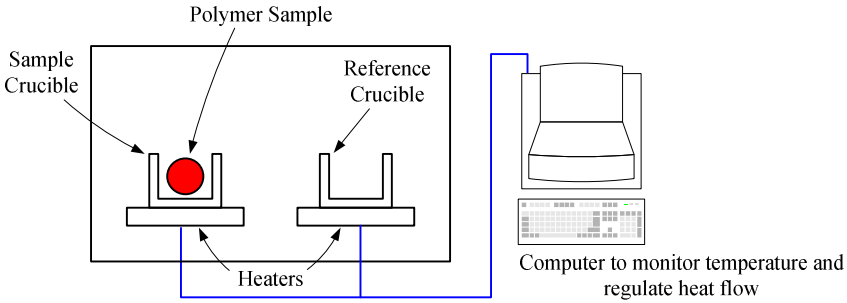

Figure A.1: Simplified illustration of the DSC device [93].

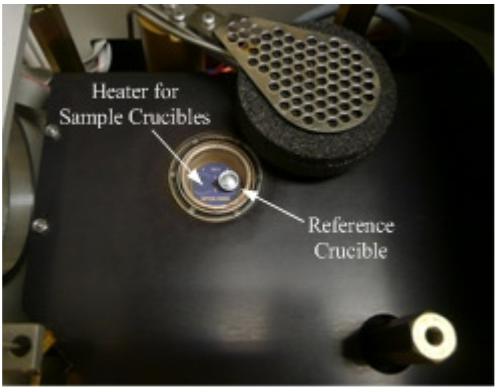

Figure A.2: Device of the DSC equipment used in the tests.

Because the sample crucible contains an amount of material, it will require more heat to keep its temperature increasing at the same rate as the reference crucible. Thus, the heater beneath the sample crucible will have to transfer more heat to it. A DSC test measures how much more heat is necessary to give to the sample crucible, so that it keeps heating at the same rate as the reference crucible.

The result of a DSC test is a curve of heat flow *versus* temperature or *versus* time, similar to that of Figure A.3. This technique can be used to measure a number of characteristic properties of a material, like: glass transition temperature, enthalpies of transitions, melting temperature, specific heat, crystallization temperature and degree of crystallization. In addition, it is possible to study oxidation, as well as other chemical reactions.

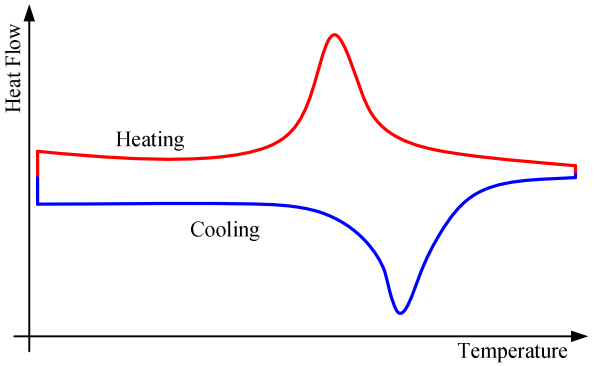

Figure A.3: Typical diagram obtained from DSC measurements.

A.2. DIGITAL SPECKLE PHOTOGRAPHY - DSP

There is a group of characterization techniques that are based on the fact that when a surface is illuminated with a coherent light, the recorded images exhibit a granularity named **speckle**. Because this granularity comes from the interference of the light scattered by different points at the surface, the microscopic properties of the surface are transferred to the speckle pattern and can be used as its fingerprints. Any changes in the surface shape or structure are reflected by a related change in the scattered speckle field, i.e., displacement or decorralation. Thus, surface changes can be inferred from a comparison of speckle patterns obtained at different object states [94]. The two most used techniques are: **speckle photography** and **speckle interferometry**.

In digital speckle photography (DSP) technique, the light scattered by the sample surface, after having been illuminated with a laser beam, is recorded on a digital camera, as can be seen in the configuration of Figure A.4. The objective of the experiment is to compare two different speckle patterns of the object. The first one, considered as the reference image of the undeformed state, is recorded prior the object modification process starts and compared with that of a deformed state [94], as can be seen in Figure A.5. This technique allows determination of 3D coordinates and displacements, 3D speeds and accelerations, plane strain tensor and plane strain rate and material characteristics.

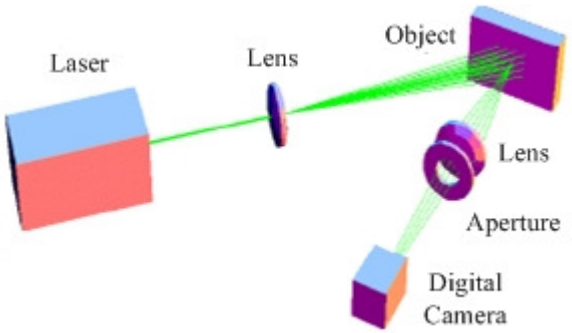

Figure A.4: Configuration of the digital speckle photography technique.

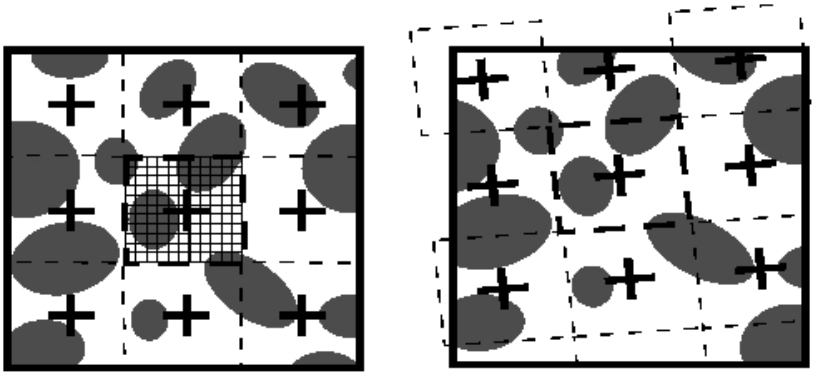

Figure A.5: Schematic illustration of undeformed and deformed speckle surfaces.

A.3. DMA TECHNIQUE

When a specimen is submitted, for example, to a sinusoidal stress regime, a steady state will eventually be reached, in which the resulting strain is also sinusoidal, having the same frequency of the stress, but retarded in phase by an angle δ. If $\delta = 0°$ or $\delta = 90°$, the material of the sample is classed as **elastic** or **viscous**, respectively. Many materials, like plastics, are classified as viscoelastic, i.e., the phase angle (δ) is between 0° and 90°.

In a general case, the stress-strain functions can be written as

$$\varepsilon = \varepsilon_o \cos(\omega t) \tag{A.1}$$

and

$$\sigma = \sigma_o \cos(\omega t + \delta), \tag{A.2}$$

in which, σ_o and ε_o are the stress and strain amplitudes, respectively, and ω is the frequency of excitation. Equation (A.2) may be conveniently written as

$$\sigma^* = \sigma_o' \cos(\omega t) + i\sigma_o'' \sin(\omega t). \tag{A.3}$$

In this equation, σ^* is the complex stress, $i = \sqrt{-1}$, $\sigma'_o = \sigma_o \cos(\delta)$ and $\sigma''_o = \sigma_o \sin(\delta)$. Dividing both sides of Equation (A.3) by ε_o, one obtains

$$E^* = E' + iE'', \tag{A.4}$$

in which, E^*, E' and E'' are, respectively, the complex, storage and the loss moduli. The loss factor (tan δ) is determined by

$$\tan(\delta) = \frac{E''}{E'}. \tag{A.5}$$

An ideal elastic material stores the entire mechanical energy responsible for the deformation. When the load is removed, this energy is liberated. The modulus is independent of frequency; stress and strain are in phase. In this case, $E^* = E'$. In an ideal liquid, the applied stress and strain are phase-shifted by 90°. Because the molecules are free to move, no mechanical energy is stored, i.e., the energy is completely converted into heat. In this case, $E^* = iE''$. The imaginary number, $i = \sqrt{-1}$, is a mathematical expression that represents the fact that the mechanical energy is converted into heat. In plastic materials, the reaction to an external load is accompanied by molecular rearrangements that take place over a wide frequency range. Their properties lie between those of an ideal liquid and an ideal elastic solid. Because they have both elastic and viscous properties, these materials are said to be **viscoelastic**. Thus, their mechanical behavior is described mathematically by the complex modulus of Equation (A.4).

The DMA technique measures the mechanical properties of materials as a function of time, temperature and frequency. In this test, a sample is submitted to a sinusoidal mechanical force and the corresponding deformations are measured. Depending on the characteristics of the sample, it can be mounted in the DMA equipment by means of one of the six different modes illustrated in Figure A.6. In case of viscoelastic materials, the test yields a diagram similar to that of Figure A.7, showing the variation of the storage and loss moduli and loss factor, as a function of temperature. The shape of these curves can vary, depending on the degree of crystallinity of the material, as is illustrated in Figure 2.7. Among other information, this diagram allows obtaining: glass transition and melting temperatures.

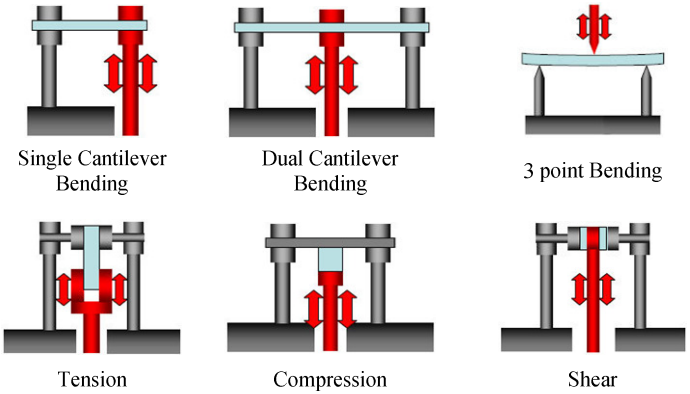

Figure A.6: DMA measurement modes [26].

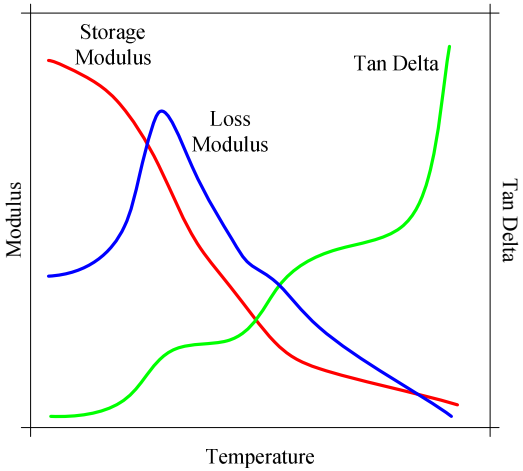

Figure A.7: Typical curves obtained from DMA measurements.

INDEX

A

B

C

D

F

G

H

I

J

K

N

O

P

Q

R

S

T

U

V